SUPERCRITICAL WATER GASIFICATION OF BIOMASS

An Experimental Study of Model Compounds And Potential Biomass Feeds

Anand Gupta Chakinala

Supercritical Water Gasification of Biomass

An experimental study of model compounds and potential biomass feeds

Members of the committee

Chairman/Secretary:	Prof.dr. G. van der Steenhoven	University of Twente
Promoters:	Prof.dr. S.R.A. Kersten	University of Twente
	Prof.dr.ir. W.P.M. van Swaaij	University of Twente
Assistant Promoter:	Dr.ir. D.W.F. Brilman	University of Twente
Members:	Prof. A. Kruse	University of Hohenheim
	Prof.dr. K. Seshan	University of Twente
	Prof.dr.ir. D.C. Nijmeijer	University of Twente
	Prof.dr.ir. G. Brem	University of Twente
	Dr.ir. R.H. Venderbosch	BTG, The Netherlands

The research described in this Thesis was financially supported by Senter Novem as part of the EOS-LT program project 05020: "*Vergassing van natte biomassa in superkritiek water*".

Supercritical water gasification of biomass

An experimental study of model compounds and potential biomass feeds

By Anand Gupta Chakinala

Ph.D. Thesis, University of Twente
Cover page design: Veeranna Chakinala and Veera Alluri
Printed by Ipskamp Drukkers B.V. Enschede, The Netherlands.

ISBN 978-90-365-3583-0
9 789036 535830 >
DOI: 10.3990/1.9789036535830

SUPERCRITICAL WATER GASIFICATION OF BIOMASS

AN EXPERIMENTAL STUDY OF MODEL COMPOUNDS AND POTENTIAL BIOMASS FEEDS

PROEFSCHRIFT

ter verkrijging van,
de graad van doctor aan de Universiteit Twente,
op gezag van de rector magnificus,
Prof.dr. H.Brinksma,
volgens besluit van het College voor Promoties
in het openbaar te verdedigen
op vrijdag 06 December 2013 om 12.45 uur

door

Anand Gupta Chakinala
geboren op 29 Juni 1979
te Jangaon, INDIA

This dissertation has been approved by:

Prof.dr. S.R.A. Kersten (Promotor)

Prof.dr.ir. W.P.M. van Swaaij (Promotor)

Dr.ir. D.W.F. Brilman (Assistant Promotor)

To my family

TABLE OF CONTENTS

SUMMARY

Gasification of biomass in supercritical water is a complex process. In supercritical water ideally the biomass structure and the larger molecules are broken down into smaller, gaseous components under the influence of radicals. However, the biomass is normally fed to the system at low temperature and, hence, should traverse a large temperature range before the supercritical conditions are met. During this warming-up (mostly ionic-) reactions may occur leading to the formation of intermediate compounds which are difficult to gasify, but lead to *e.g.* carbon formation that can cause blockage of process equipment. In case of uncatalyzed gasification the required temperatures are often above 650 °C and thus far above the supercritical temperature for water (374 °C). Together with the required high operating pressures (above 221 bar), this leads to high demands for the materials of construction and, hence, high costs. Reducing the operating temperature to below 600 °C is, next to maximizing gasification efficiency and minimizing carbon formation, an important target for catalyst development.

In this thesis, attractive and relevant biomass feed streams have been used; like (crude) glycerine, a by-product from the biodiesel production, algae slurries and aqueous phases produced during the fast pyrolysis of lignocellulosic biomass as well as the aqueous phase produced during upgrading (by hydrogenation) of the primary pyrolysis oil. Results for these raw materials are presented for both the uncatalyzed gasification as well as for gasification in the presence of existing (commercial-) and newly developed (in this project) catalysts. For the model compounds chosen, glycerol and ethylene glycol, significant progress is made in the area of catalyst development and deduction of the prevailing reaction mechanisms. Additionally, a more fundamental study into the effect of the molecular structure of n-alcohols and n-carboxylic acids on the gasification performance is performed.

Initial studies were carried with algae and glycerol gasification experiments using quartz and continuous flow reactor respectively (Chapter 2). For algae slurries, experiments using quartz capillaries showed that complete gasification is not realistic without catalyst addition. Even at 700 °C the uncatalyzed degree of conversion was only 80%. A hypothesis that protein material in algae would hinder gasification was tested by adding amine acids to a reference experiment of glycerol gasification in the continuous setup. The addition of L-Proline was found to decrease the glycerol gasification efficiency. This is most likely related to the radical-scavenging effect of L-Proline (which is part of the natural defence mechanism of plants). Moreover, the colourless aqueous effluent from glycerol gasification coloured to 'chocolate-brown' upon addition of L-Proline and some other amino-acids, which is most likely due to Maillard-type

reactions. With catalysts (among which the construction material Inconel) a high degree of conversion for the algae slurries seems possible at temperatures of about 600 °C.

In a more fundamental study into the effect of the (alkyl-) chain length on the gasification efficiency for n-alcohols and n-carboxylic acids for a fixed set of reaction conditions (uncatalyzed, 600 °C, 10 minutes reaction time). A remarkable oscillation was noticed in the mole fraction of methane and CO_2 in the product gas, when plotted as function of the carbon number. Using a new proposed reaction scheme, based on initial breakage of the acidic O-H bond followed by decarboxylation and β-scissioning, these oscillations can be understood. Also the gasification efficiency itself is a function of the alkyl chain length; acids with an even carbon number show a higher (carbon-based) gasification efficiency that the adjacent odd-numbered carboxylic acids. From data-analysis it was further found that with increasing alkyl chain length (from n=3 onwards), there is a net consumption of water and hence additional hydrogen production. For alcohols, the gasification efficiency is independent of the reactant (alcohol) concentration, whereas, for acids this decreases strongly with increasing concentration. This supports the suggestion of the above-mentioned ionic-reactions during heating-up, leading to compounds which are difficult to gasify. Furthermore, indications are obtained about the effect of chain-branching and having more –OH groups inside the molecule was found to be beneficial for the gasification efficiency.

Catalyst development was done using ethylene glycol as model compound (see Chapter 4). It was found that a Pt-Ni bimetallic catalyst was able to achieve complete conversion at temperatures as low as 400-450 °C and short contact times (5-10 s), without char formation and with a high selectivity towards hydrogen gas (H_2). The product gas contained around 70% of H_2, significantly higher than predicted by thermodynamic equilibrium. Ni and Pt enhance the production of H_2 and CO_2. CO formed in high yields during uncatalyzed conversion, is only found in minor amounts in the product gas for catalyzed conversion, in accordance with chemical equilibrium for the water-gas shift reaction.

For the uncatalyzed (except possible catalytic effects by the material of construction) gasification of glycerol a distinct difference in the product gas composition for crude- (from a biodiesel process) and pure glycerol was shown in Chapter 5. For the crude glycerol and in case of higher conversion levels (above 50%) a significant lower CO yield was found, by increased water-gas shift activity (turning CO and H_2O into CO_2 and H_2), due to the presence of alkali. For diluted glycerol feed (below 30 wt%) no significant difference was found. From the product gas composition and the compounds identified in the aqueous effluent, as function of temperature and conversion, reaction schemes are composed which can able to

explain the observed trends. Long term catalysts stability was conducted for 85 h showing no decay of either activity or selectivity.

For the aqueous phase of pyrolysis oil (either directly from a pyrolysis process after phase separation or obtained after hydrogenation of the primary pyrolysis oil) it was found that the catalysts used show significant deactivation after several hours on stream, due to coke formation. Duration tests showed that catalyst regeneration was able to restore the initial activity and accompanying selectivity profile, after which a new deactivation cycle starts. Managing the competition between the coke formation and gasification of coke precursors is crucial to determine the catalyst lifetime. This is supported by the higher gasification efficiency and lower deactivation obtained for the less reactive aqueous phases obtained from pyrolysis oil upgrading and pyrolysis condenser fractions.

Summary

SAMENVATTING

Vergassing van biomassa in superkritiek water is een complex proces. Idealiter wordt in superkritiek water bij hoge druk en temperatuur de biomassa structuur afgebroken en worden onder invloed van radicalen grotere moleculen omgezet in kleinere, gasvormige componenten. De biomassa wordt veelal op lage temperatuur aangeleverd en moet derhalve een groot temperatuurtraject doorlopen, voordat het zich in het superkritieke regime bevindt. Gedurende deze opwarming kunnen (veelal ionische-) reacties optreden, waardoor tijdens de omzetting tussenproducten worden gevormd die later moeilijk te vergassen zijn, en welke leiden tot koolvorming dat verstopping van procesapparatuur kan veroorzaken. Voor de niet gekatalyseerde vergassing in superkritiek water zijn veelal temperaturen boven de 650 °C en dus ver boven de superkritische temperatuur van water (374 °C) nodig. Mede door de hoge procesdruk (boven 221 bar), leidt dit tot hoge eisen aan de constructiematerialen en daarmee tot hoge kosten. Reduceren van de werktemperatuur tot beneden 600 °C is, naast maximaliseren van de vergassing en minimaliseren van koolvorming, dan ook een belangrijke doelstelling voor de gekatalyseerde vergassing van biomassa in superkritiek water.

In dit proefschrift is de toepassing van deze technologie op mogelijk geschikte- en relevante biomassa stromen onderzocht, te weten (ruwe) glycerine, een bijproduct uit de biodiesel productie, algen slurries, de waterfase geproduceerd tijdens pyrolyse van lignocellulose biomassa en de waterfase geproduceerd bij de hydrogenering van pyrolyse-olie. Resultaten voor deze grondstoffen zijn gepresenteerd voor zowel de niet gekatalyseerde vergassing als voor de vergassing in de aanwezigheid van bestaande en nieuwe, in dit project ontwikkelde-, katalysatoren. Voor de modelstoffen methanol, glycerol en ethyleenglycol is veel werk verzet op het gebied van katalysator ontwikkeling en ontrafeling van het reactiemechanisme. Daarnaast is een meer fundamentele studie uitgevoerd naar het effect van de moleculaire structuur van lineaire alcoholen en carbonzuren op de vergassings-efficiëntie.

Voor algen en glycerol als grondstof zijn verkennende vergassingsexperimenten uitgevoerd, zowel met kwartsglazen capillairen als batch reactor als met een continu bedreven reactor (hoofdstuk 2). Voor algenslurries is uit experimenten met kwartsglazen capillairen gebleken dat volledige vergassing niet realiseerbaar was zonder toepassing van een (relatief grote hoeveelheid-) katalysator; zelfs bij 700 °C bedroeg de niet gekatalyseerde conversie nog maar 80%. Een hypothese dat het proteine-materiaal uit algen de vergassing bemoeilijkt, is daarna getest door modelcomponenten (aminozuren) toe te voegen aan een gestandaardiseerde vergassingstest van glycerol. De toevoeging van onder andere L-Proline (een radicaalvanger en onderdeel van een natuurlijk beschermingssysteem van planten) gaf een duidelijke verlaging van de vergassingsefficiëntie te zien en een sterke verkleuring van het waterige effluent van

nagenoeg kleurloos naar 'chocolade-bruin' (mogelijk als gevolg van zgh. Maillard-reacties). Mét katalysatoren (waaronder het constructie materiaal Inconel) lijkt, zelfs bij temperaturen van rond 600 °C, wél een hoge conversie van algenslurries mogelijk.

In een meer fundamentele studie naar het effect van de (alkyl-)ketenlengte op de vergassingsefficiëntie voor n-alcoholen en n-alkaanzuren is voor een vaste set van procescondities voor niet gekatalyseerde vergassing (600 °C, 10 minuten reactietijd) een opmerkelijke oscillatie van de molfracties methaan, CO_2 en C2-componenten in het productgas waargenomen, wanneer deze wordt uitgezet tegen het aantal koolstofatomen in het molecuul. Nadere analyse toonde aan dat deze oscillatie goed konden worden begrepen uit een, op radicaal-chemie gebaseerd, kraakreactie schema waarbij als eerste stap de O-H binding wordt aangepakt, CO_2 wordt afgesplitst en vervolgens de alkylketen stapsgewijs wordt afgebroken via zgh. "β-scissioning". Ook blijkt de (koolstof gebaseerde-) vergassingsefficiëntie zelf een functie van de alkyl-ketenlengte te zijn; voor zuren met even aantal koolstofatomen is deze hoger dan voor de naastgelegen n-carbonzuren met een oneven aantal koolstofatomen. Uit data-analyse is verder vastgesteld dat bij langere ketenlengtes (vanaf drie koolstofatomen) er netto water wordt verbruikt bij de vergassing en er dus extra H_2 wordt gevormd. De vergassingsefficiëntie zelf is voor alcoholen onafhankelijk van de initiële reactant (alcohol-)concentratie, maar voor de n-alkaanzuren neemt de vergassingsefficiëntie sterk af met een toename van de initiële zuurconcentratie, hetgeen wijst op de eerdergenoemde (ionische-) reacties gedurende het opwarmtraject die leiden tot moeilijker te vergassen componenten. Verder is er gekeken naar alcoholen met een vertakte-, in plaats van lineaire-, molecuulstructuur. Voor een vergelijkbare molecuulstructuur leidt een vergroting van het aantal -OH groepen tot een hogere conversiegraad.

Katalysator ontwikkeling, gebruikmakend van ethyleenglycol als modelcomponent (zie hoofdstuk 4), toonde aan dat een Ni/Pt bimetallische katalysator in staat was om nagenoeg volledige conversie te bereiken bij een temperatuur van niet meer dan 450 °C, zonder koolvorming, en waarbij het gasvormig product een hoge fractie (70%) waterstof gas bevat, veel meer dan men op basis van de thermodynamische evenwichtssamenstelling zou verwachten. Nikkel (Ni) en Platina (Pt) als actief katalysator metaal bevorderen de productie van H_2 en CO_2. Naast H_2 (rond 35%) en CO_2 (rond 50- 55%) zijn methaan (rond 10%) en C2-componenten (5-10%) de belangrijkste componenten in het productgas. Koolmonoxide, in ruime hoeveelheid gevormd bij ongekatalyseerde vergassing, wordt alleen in lage hoeveelheden aangetroffen, overeenkomstig thermodynamisch evenwicht in de gasfase. Dit betekent dat de gebruikte katalysator ook actief is voor de water-gas schift reactie.

Summary

Voor niet gekatalyseerde vergassing van glycerol (uitgezonderd evt. effecten van de reactorwand) werd een duidelijk verschil gevonden, zie hoofdstuk 5, tussen de productgas samenstelling voor zuiver glycerine en voor glycerine verkregen uit een biodiesel proces. In het laatste geval werd bij hogere glycerol concentraties (boven 50%) een lagere CO opbrengst gevonden door een verhoogde watergas-schuif activiteit (van CO naar CO_2, daarbij extra H_2 producerend uit water) door de aanwezigheid van alkali. Voor verdunde glycerol voeding (minder dan 30 wt%) was er geen noemenswaardig verschil. Uit de productgas samenstelling en de aangetoonde producten in het waterige effluent, als functie van temperatuur en conversie, zijn reactieschema's opgesteld die de gevonden productspectra kunnen verklaren (op basis van dehydrogenering, dehydratatie en vervolgens hydrogenering) en is tevens een reactiekinetiek beschrijving afgeleid. Een duurtest gedurende 85 uur voor evaluatie van de katalysator stabiliteit liet geen verval van activiteit noch van selectiviteit zien.

Voor de waterfractie van pyrolyse-olie is gevonden dat de gebruikte katalysatoren na verloop van tijd achteruitgaan in prestatie als gevolg van koolvorming. Dit gold zowel voor de waterfase verkregen uit pyrolyse olie direct uit een pyrolyse plant als ook voor de waterfase verkregen na stabilisatie van de pyrolyse-olie door hydrogenering. Duurtesten hebben laten zien dat de katalysator-activiteit na deactivering door koolvorming kan worden hersteld door een waterstofbehandeling, waarna een nieuwe cyclus start. Beheer van de competitie tussen cokesvorming en vergassing van gevormde cokesprecursors is cruciaal voor de levensduur van de katalysator. Dit wordt ondersteund door de waargenomen hogere efficiëntie bij vergassing en verlaagde katalysator deactivering in het geval van minder reactieve waterige fasen, zoals die verkregen uit met waterstofgas behandelde pyrolyse-olie en voor pyrolyse condensor fracties.

Summary

Chapter 1

Introduction

Chapter 1

1.1 MOTIVATION – POTENTIAL OF BIOMASS AS A SUSTAINABLE ENERGY SOURCE

Conventional energy resources like coal, oil and natural gas, have already proven to be effective drivers of the world economy, providing about 84% of the world's energy demands.[1] Worldwide concerns about increasing population and consumption of fossil fuels, both leading to the depletion of fossil fuels, to socio-economic and political stresses associated with imported oil (partly relieved by the shale gas exploitation) and environmental issues surrounding emissions of carbon dioxide have led to increased interest in exploring alternative energy sources that are CO_2 neutral, renewable, more sustainable and can meet today's energy demands. It is therefore imperative to develop economical and energy efficient renewable technologies for the sustainable generation of fuels and chemicals.

Currently, there are several sustainable energy sources considered such as wind, solar, hydro, wave power, geothermal energy and biomass. Each of these energy resources has its own pro's and con's and their abundance depends on the geographical location. Biomass is considered to be one of the most sought after energy resource that has the potential to replace/to meet some extent of the today's global energy supply due to its abundant, widespread availability.[1-2] It is foreseen that, over the decades to come, the replacement of fossil energy sources by sustainable energy resources is likely to continue as their costs could decline compared to the oil and gas price fluctuation.

The term biomass in general identifies all non-fossilized organic matter, and mainly constitutes of organic matter originated from trees, agricultural crops and other living or dead plant material to human waste. Among the sustainable energy sources as mentioned earlier, biomass is the only one to have the potential of directly producing liquid fuels for the transportation sector. Therefore it is of utmost important to integrate with the existing fossil-based refineries, because it reduces the capital investment costs and offers guaranteed markets for the products in the transition towards a completely sustainable society.[3] On the long run, (residual) biomass can be utilized for the optimal production of fuels and chemicals, while other renewable energy sources can be used for heat and power generation.

1.2 AVAILABLE TECHNOLOGIES FOR BIOMASS

The bio-fuel industry is still in its infancy compared to fossil fuels. Currently, there are several technologies, in varying stages of their development, available for the conversion of biomass feedstocks to either gaseous or liquid fuels. The performance of these processing technologies still depends significantly on the type of biomass feedstock used. Typically, these biomass conversion technologies are classified into two types, thermochemical conversion and

biological conversion. A simplified overview of the most prominent biomass conversion techniques is shown in Figure 1.1.

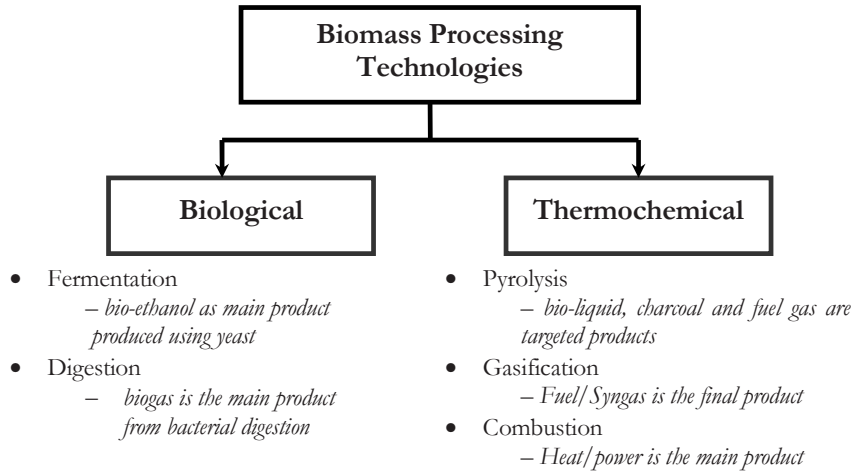

Figure 1.1: Simplified classification of biomass processing technologies.[4]

1.2.1 BIOLOGICAL CONVERSION

Fermentation is a biological process in which ethanol is produced by fermentation of carbohydrates, often using yeast (*Saccharomyces Cerevisiae*), and it is currently the most used technology that is available for the generation of liquid fuels from biomass. The yields of ethanol from sugarcane are reported to be in the range of 160–190 L/metric ton.[5]

Anaerobic digestion is another biological process, in which micro-organisms, in the absence of oxygen, convert the biodegradable organics to produce methane. It is a proven technology for the conversion of wet biomass to biogas. Typically, very long residence times of 10–30 days are required to achieve a reasonable biomass conversion (30–60% to gas and the rest remain as a solid residue), limiting its use to small scale and decentralized applications.[4-5] This thesis is mainly focussed on thermochemical conversion process therefore the biological conversion technologies are not further discussed in detail here.

1.2.2 THERMOCHEMICAL CONVERSION

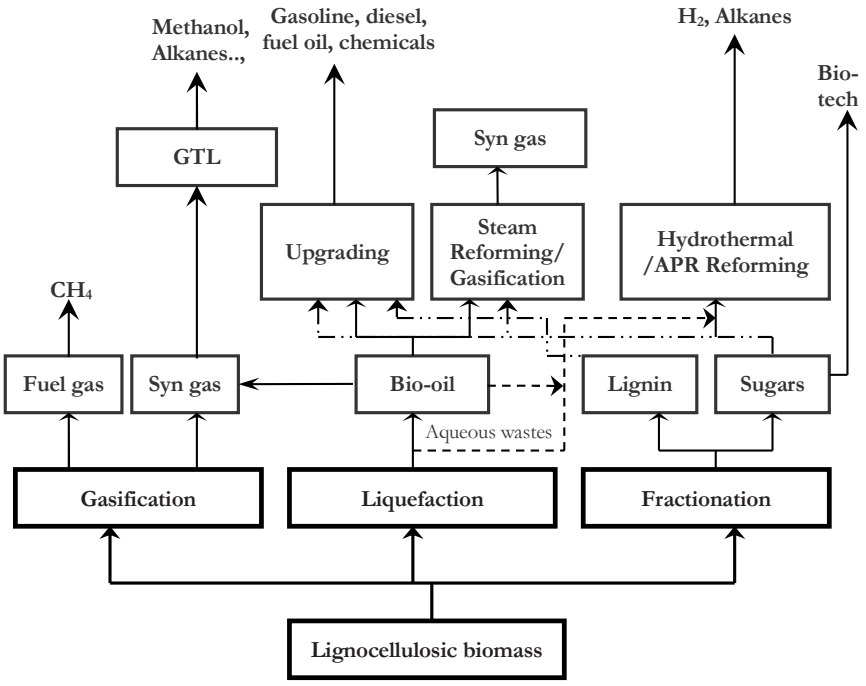

Figure 1.2: Strategies for the production of liquid and gaseous fuels and chemicals from lignocellulosic biomass via thermochemical routes (dotted arrows indicate the sources of aqueous waste streams from different processing units that can be used as a feedstock for another unit to produce fuel gases).[5]

The tree of available options for the production of fuels/chemicals from thermochemical conversion of lignocellulosic biomass is presented in Figure 1.2. There are three main routes for the conversion of dry biomass as shown in Figure 1.2; syngas production by high temperature gasification, bio-oil production by fast pyrolysis or hydrothermal liquefaction (HTL), fractionation of biomass (*e.g.* organosolv)to produce aqueous sugars and its derivatives and lignin, which can be converted into gaseous and liquid fuels via aqueous phase reforming.

High temperature gasification is an option for dry feedstocks such as coal, biomass, solid or liquid carbonaceous material which react with air/steam/oxygen at temperatures in the range of 800–1300 °C to produce a product gas called syngas or producer gas that contains CO, CO_2, H_2, CH_4, and N_2 in varying ratios. The actual outlet gas distribution from the gasification process is dependent on several factors such as biomass composition, reactor choice, catalyst

used and operating conditions.[5] Producer gas contains higher levels of N_2 and is combusted to generate heat or electricity. A syngas conversion unit (*e.g.* a Fischer-Tropsch, Methanol production or Methanation unit) can be added for the production of fuels and chemicals.

Pyrolysis is a versatile liquefaction process in which dry biomass is rapidly heated to temperatures in the range of 350–550 °C in the absence of oxygen for very short residence times (below 2s), forming a gaseous product, which upon condensation forms a dark brown coloured liquid, called bio-oil or pyrolysis oil.[6] At present, several applications of these bio-oils are being explored; like direct usage in boilers/burners, as a source of chemicals, upgraded bio-oil having less oxygen content to be processed in a standard refinery for the production of diesel and gasoline fuels[3] and syngas production via steam reforming process[7] which can then be utilized for several applications as mentioned earlier.

Hydrolysis of biomass is a fractionation process for the conversion of biomass to sugars and lignin as target products.[5] The aqueous sugars obtained can be either biologically fermented to produce bio-ethanol or, depending on the aqueous phase sugar concentration, thermochemically converted by either steam reforming to produce syngas or it can be used as feedstock for aqueous phase processing to liquid fuels or be used in supercritical water gasification for the production of gaseous fuels. The lignin rich fraction can be further upgraded via hydrodeoxygenation to produce fuels and chemicals or it can also be directly gasified or steam reformed to produce syngas.

Aqueous waste streams, containing 10–40 wt% of organics, obtained from different condenser fractions of pyrolysis process[6], as well as from the bio-oil upgrading[3] process can be used as feedstock for the hydrothermal reforming/supercritical water gasification process to generate methane, or hydrogen, depending on the severity of the process conditions and catalysts used.

The focus of this thesis is to completely convert aqueous waste streams available in bio-refinery systems to gaseous fuels via supercritical water gasification.

1.3 OPTIONS AVAILABLE FOR THERMOCHEMICAL CONVERSION OF WET BIOMASS

Conventional gasification technologies are not suitable for processing aqueous biomass streams having 60% moisture or more (on dry weight basis) due to the negative overall process thermal efficiency.[4, 7] Thermal drying or similar means in other processing approaches, to remove the aqueous medium leads to energy losses, exceeding the energy content of the biomass. Conversion technologies for wet biomass, avoiding evaporation of water are therefore very attractive. By operating at high pressure, the phase change (evaporation) of

water can be avoided, allowing heat exchange between the feed and reactor effluent heat as a result of which high efficiency can be obtained even with very wet streams.[4, 8]

Biomass conversion in hot-compressed water is divided into three categories, depending on the operating conditions (pressure, temperature); liquefaction, low temperature catalytic gasification and high temperature gasification. Hydrothermal liquefaction occurs at sub-critical conditions of water (200–370 °C and 40–200 bar).[5] At lower temperatures in the range of 350–500 °C, complete gasification of feedstock is very difficult. Through, the use of active metal catalysts complete gasification of biomass with high levels of methane, as dictated by thermodynamics, can be accomplished.[4-5, 8] Operation in this regime is also referred to as aqueous phase reforming.

Aqueous phase reforming is a process developed at the University of Wisconsin, in which the aqueous wastes streams are reformed catalytically on a noble metal catalyst and relatively mild operating conditions, in the range of 250 – 300 °C and 30 – 50 bar, into gaseous or liquid fuels, depending on the catalyst of choice.[5, 9-10] The research reported so far is mostly based on the exploratory research carried out with biomass model compounds, rather than with real biomass, and only at low feed concentrations and very long residence times. This process was technically demonstrated on lab scale with model compounds. Based on this process, Virent announced to have a demonstration plant capable of producing 10,000 gallons per year of biogasoline.[11]

Supercritical water gasification (SCWG) is a promising technology, in early stage of development for the conversion of aqueous biomass streams. Unlike anaerobic digestion and aqueous phase reforming, very high feedstock concentrations of real biomass[4, 12-13] and model compounds[14] (up to 30 wt%) were successfully gasified at very short residence times. An ancillary advantage of the supercritical gasification is that the gaseous products are produced at high pressure (typically 250 bar) and the aqueous product stream leaving the process is virtually clean, sterilized with respect to any possible pathogens (biotoxins, bacteria, virus) and can be fed directly to any municipal wastewater treatment plant without further purification.[15] The nutrients present in the solid waste streams can often be recovered and reused as fertilizer.[4, 16]

Temperatures in the range of 500–800 °C are employed in high temperature supercritical water gasification to achieve complete carbon to gas conversion and in the absence of any catalyst, due to the high reactivity of biomass at these conditions.[8, 17-19] However, in practice, it is more desirable to operate closer to the critical conditions of water (below 600 °C, preferably below 500 °C) in order to minimize the investment costs needed for the reactor (material of construction), for energy efficiency and enhanced process safety.

The primary gas produced by the SCWG process differs significantly from the syngas that is produced in other common thermal, dry biomass gasifiers:

- The product gas is obtained at high pressure
- No dilution by nitrogen
- High content of H_2 and CO_2 or CH_4 and CO_2, depending on conditions

Based on the process characteristics three main applications of the SCWG processes are identified:

- Hydrogen production (maximise H_2)
- Synthesis gas production (minimise CH_4)
- Synthetic natural gas (maximise CH_4 and minimise CO)

Considering the high pressure at which the synthesis gas is produced, the syn gas can be used without additional pressurization step for the production of renewable transportation fuels like F-T diesel, methanol, dimethyl ether etc.

1.4 FEEDSTOCKS FOR SCWG

Delivering feedstocks to the high pressure and high temperature conditions prevailing in the reactor (at supercritical conditions) is a technological challenge. Typically, feedstocks for supercritical water gasification (SCWG) should be pumpable so that they can be pressurized to very high pressures. At present, feeding of real biomass, having different particle sizes, to such high pressures (250 bar) is very difficult. It is thus essential to pre-treat the biomass slurries to make them pumpable and enable pressurization. Two types of feedstocks such as real biomass and biomass based model compounds are studied in SCW. Real biomass feedstocks provide practical/realistic information related to gasification behaviour. While, biomass based model compounds are mainly used for the sake of fundamental studies to mimic the gasification behaviour of realistic feedstocks. A wide range of pumpable feedstocks are available for the SCWG which include pulp and paper mill effluents[20-21], saw dust[12], chicken manure[22-23], oil refinery wastewater, distillery wastewater, food industry wastes[12, 24-25], leather industries[26], municipal/sewage sludge[27-29], aqueous wastewater from pyrolysis and from upgrading of bio-oils in a bio-refinery[30-34], algae slurries[13, 35-37], and water hyacinth[38]. Feedstocks with high inorganic content are less favourable as they will lead to lower gas yields, resulting in a low overall thermal efficiency of the process.

In this study, we have investigated three different feedstocks namely microalgae, glycerol and aqueous fraction of bio-oil. Study of other biomass or biomass model compounds other than those described earlier fall beyond the scope of this study.

1.5 PHYSICAL PROPERTIES OF WATER AT SUPERCRITICAL CONDITIONS

A supercritical fluid is any substance at a temperature and pressure above its critical point. It can diffuse through solids like a gas, and dissolve materials like a liquid. In addition, close to the critical point, minor changes in the pressure or temperature result in large deviations in physical properties, allowing the properties to be fine-tuned. Supercritical fluids are suitable as a substitute for organic solvents in a wide range of industrial and laboratory processes. Supercritical water and carbon dioxide are the most commonly used supercritical fluids applied *e.g.* for power generation, decaffeination, extraction of lipids.

The phase behaviour of pure water is shown in Figure 1.3. Supercritical water exists at temperature and pressure above the critical point water (374 °C, 221 bar). Above the critical point, supercritical water becomes an environmentally benign non-polar solvent, capable of dissolving and breaking down organics by radical reactions and hydrolysis.

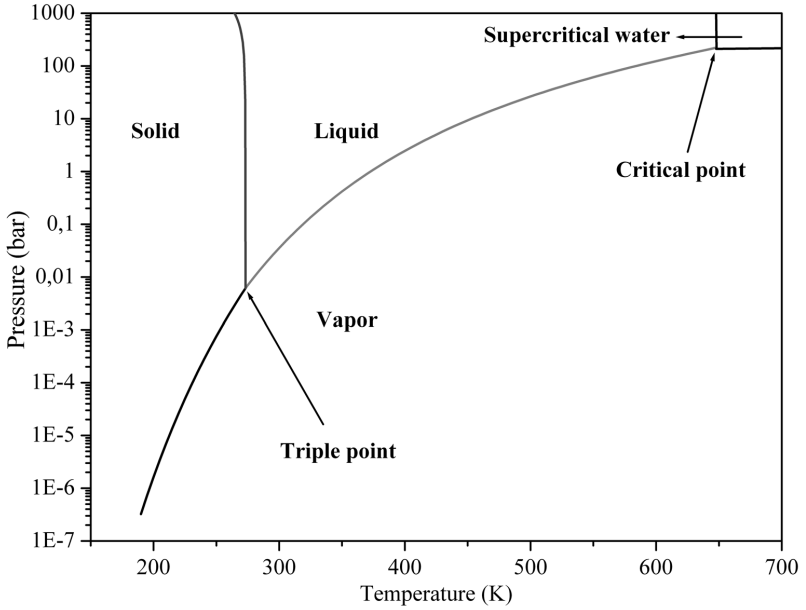

Figure 1.3: Phase diagram of water.[39]

Generally, two different types of reactions mechanisms are proposed at near-critical and supercritical conditions of water ionic reactions and free radical reactions. Ionic reactions are more prevalent at subcritical conditions, at higher pressures and low temperatures (below 600 °C) whereas, free radical reactions are dominant at lower pressures and higher temperatures (above 600 °C). The change of mechanism is probably related to the change in dielectric constant (relative permittivity, ε_r) of water.[40] As the temperature and pressure increases the dielectric constant of water declines sharply. At ambient temperature and pressure (20 °C, 1 atm), the dielectric constant is comparatively large because of strong effect of hydrogen bonds in water and it decreases specifically from 80 at 25 °C to 2 at 450 °C.[15, 41]

Other interesting properties, such as the ionic product for water dissociation $\left(K_w \equiv [H_3O^+][OH^-]\right)$, initially increases with increasing temperature from ambient up to the critical point from 10^{-14} to around 10^{-11} and beyond the critical temperature, it rapidly declines again to below 10^{-20} $(mole/L)^2$. This indicates the availability of large number of H^+ and OH^- ions at near critical conditions. At further increase of temperature above the critical point, the ionic product of water declines drastically. This supports the dominant roles of ionic reactions around the critical point and of free radical reaction mechanisms under supercritical conditions of water.

Therefore, a lot of reactions catalyzed by protons or hydroxyl ions occur at near- supercritical water without the addition of acids or bases, simply because of the ionic product of the water under this condition.

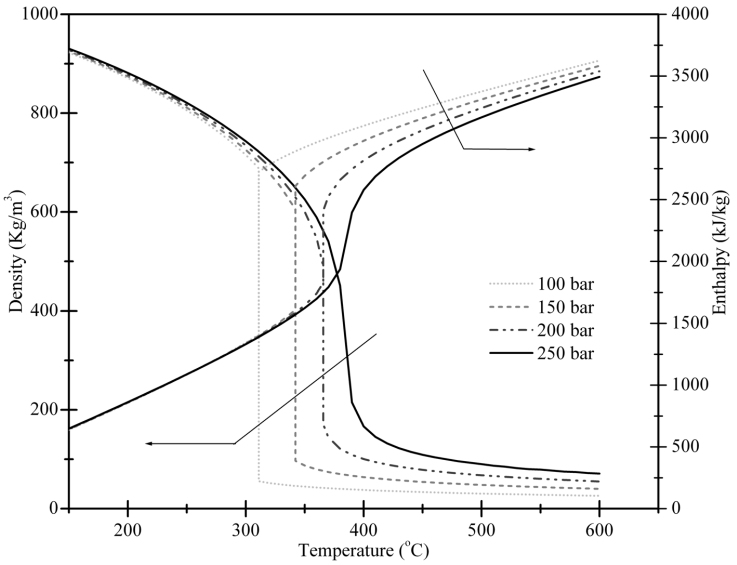

Figure 1.4: Influence of pressure and temperature on the density and enthalpy of water.

The density and enthalpy of water at different pressures as a function of temperature is displayed in Figure 1.4. The density of water can be tuned both by changing the temperature or pressure. The density decreases drastically, nearly two orders of magnitude above 350 °C, from typical liquid-like values (about 600 kg/m^3) to gas like densities (100 kg/m^3). These changes in density correlate with other properties, such as dissolving power, degree of hydrogen bonding, polarity, dielectric strength, molecular diffusivity and viscosity, all reflecting the changes at the molecular level. There is neither evaporation nor condensation above the critical point. These notable changes in the water properties at critical conditions of water have led to a great deal of research interest for various applications such as chemical reactions[42-44], hydrothermal synthesis[45], waste oxidation[46-48], biomass conversion[46-47] and synthesis of nanoparticles[49].

1.6 THESIS OUTLINE

Supercritical water is a promising milieu for reforming biomass and its constituents in a continuous flow reactor. However, some of the technological challenges that need to be addressed are the low biomass conversion and (accumulating) coke formation during long duration tests, due to refractory intermediate formation during the heating up of feed, leads to catalyst deactivation and frequent reactor plugging in a continuous flow operation.

Chapter 1

This thesis reports on the experimental studies of model compounds and potential biomass feedstocks using batch and continuous flow reactors aimed for studying long durations runs and different operating conditions like feed concentrations, temperature effects, space velocities and catalyst positioning. The problem of coke formation is approached by a combination of chemistry, catalysis and process engineering studies. Chemistry of model compounds was studied at fundamental level to gain insight into gasification mechanisms. All the studies were carried out in the supercritical regime of water therefore here after we refer to as supercritical water gasification or supercritical water reforming.

In Chapter 2, both catalytic and non-catalytic gasification of microalgae (*Chlorella Vulgaris*) and glycerol in supercritical water was studied using batch and continuous flow tubular reactors respectively. This initial work, clearly illustrates the potential and the complexity of the topic. High carbon to gas conversions of micro algae under non-catalytic conditions was obtained at low feed concentrations, high temperatures and long reaction times. To elucidate part of the difficulties related to the supercritical water gasification of algae, reforming of glycerol as a model compound was carried out in a continuous flow reactor in the presence of additives representing biomass building blocks like amino acids. Gasification of real biomass (here: micro algae) at low temperatures leads to char formation and incomplete conversion in the absence of any catalysts. Therefore, the need to study the chemistry and catalyst development for minimizing char formation and steering the product selectivities towards desired gases is underlined. These are investigated in the subsequent chapters.

In Chapter 3 the chemistry aspects of the influence of molecular structure and functional groups on the gasification behaviour in supercritical water is reported. The influence of the homologous series of linear chain (C_1–C_8) carboxylic acids and alcohols in supercritical water was studied using a batch autoclave reactor. A reaction scheme was derived for the cracking mechanism in supercritical water which could explain the experimentally obtained product spectrum changes with increasing alkyl chain length. In addition, the influence of the number and positioning of -OH groups on the gasification behaviour in supercritical water is investigated.

Chapter 4, 5 and 6 are devoted to the catalyst screening studies for the reforming of aqueous waste at near critical conditions of water. Chapter 4 deals with the catalyst development for the reforming of ethylene glycol at near critical conditions of supercritical water (450 °C) using the continuous flow tubular reactor.[14] Several alumina supported mono- and bi-metallic catalysts based on Pt and Ni with different metal loadings were studied and a promising Pt-Ni bimetallic catalyst was identified.

In chapter 5, the catalytic performance of the Pt-Ni bimetallic catalyst, developed in chapter 4, was studied in detail for the catalytic reforming of glycerol. The influence of different operating parameters such as reaction temperature, initial feed concentration, location of the catalyst bed, nature of the feed stock (pure and crude glycerol) and weight hourly space velocity on the gasification behaviour of glycerol reforming in supercritical water is investigated. A reaction scheme is proposed for the decomposition of glycerol over Pt-Ni bimetallic catalyst in supercritical water. Additionally, catalyst characterization and stability tests (long durations up to ~85 h) of the catalyst were performed and analyzed in detail.

In Chapter 6, catalyst gasification is applied to realistic biomass derived feed streams. We report the production of hydrogen/methane from the catalytic hydrothermal reforming of two bio-liquids (here: glycerol and water soluble fraction of bio-oil also referred to as aqueous fraction) in the presence of commercially available nickel catalysts (promoted and un-promoted). The performances of these catalysts were studied by carrying long duration tests in the continuous flow reactor.

Different catalytically active metals and supports were studied for the hydrothermal gasification of aqueous fraction of bio-oil, thereby focussing on catalyst performance in terms of product distribution and carbon gasification efficiency. The performance of the best catalyst screened was optimised by varying different operating parameters such as temperature, feed concentration, reaction time and nature of the feed stock. This catalyst was then evaluated for its performance in a continuous flow reactor.

Lastly, an epilogue with final recommendations for future directions are presented that may lead to further development and make this process commercially available for the treatment of aqueous waste streams, in bio-refinery settings and beyond.

Chapter 2

Catalytic and non-catalytic supercritical water gasification of microalgae and glycerol[1]

[1] This chapter is an excerpt of paper published as:

Chakinala, A. G.; Brilman, D. W. F.; van Swaaij, W. P. M.; Kersten, S. R. A., Catalytic and non-catalytic supercritical water gasification of microalgae and glycerol. Industrial & Engineering Chemistry Research 2010, 49, (3), 1113-1122.

Chapter 2

2.1 INTRODUCTION

The rising population combined with the increased use of fossil fuels has led to the depletion of their sources at alarming levels and this has prompted exploration of alternate renewable and sustainable energy sources like wind, solar and biomass. As a consequence, there is a growing interest in harnessing the chemical energy from biomass which is more sustainable, is CO_2 neutral and can be converted in to high heating value fuels; either liquid or gaseous.

Microalgae are a plausible biomass energy source, as they are the fastest growing, sunlight driven cell factories that can convert atmospheric CO_2 into potential bio-fuels and chemicals.[36-37, 50-52] The growth rates of algae can be as much as ten times higher than for terrestrial plants, thereby minimizing the 'land-claim' for fuel production and avoiding direct competition with food-/feed production for arable land. Algae cells (with or without triglycerides included) are produced as 'wet biomass' for which conversion technologies like pyrolysis and 'dry' gasification compare unfavourably due to the high water content and the consequent high energy requirement to dry the biomass. Using water as a reaction medium for wet biomass conversion would eliminate the need for the drying process.

Supercritical water gasification (SCWG) is a probable technology for the conversion of wet biomass streams having a low overall heating value to produce high heating value product gases. At temperatures and pressures above the critical point ($T \geq 374$ °C, $P \geq 220$ bar), water undergoes significant changes in its physical properties with drastic decrease in dielectric constant, density, ionic product, viscosity and thermal conductivity.[8, 12, 15, 17-19, 40, 53-66] At such conditions, water behaves like an adjustable environmentally benign solvent with good transport properties, but also with a strong ability to breakdown hydrocarbons and carbohydrates, resulting in the production of pressurized gases mainly rich in H_2, CO, CO_2 and CH_4. The selectivity of the gas production towards H_2, syngas (H_2 + CO), or CH_4 can to some extent be steered by tuning the process conditions and by the use of catalysts.[12, 16-17, 54, 64]

The heat effects in SCWG related to water evaporation are marginal when compared with ambient conditions.[15, 17, 20, 60, 66] The use of an efficient counter-current heat exchanger between the feed streams and the reactor effluent can result in high thermal efficiencies, allowing to process low energetic aqueous (waste-) streams.[8, 15, 18, 20, 64, 66] The efficiency of this feed-product heat exchange is, however, crucial for the success of this process concept.

Generally, the feedstock for this type of process should either be homogenous liquid or pumpable slurry. A majority of the studies in the past have used synthetically made effluents (by dissolving biomass model compounds in water) to evaluate their gasification behaviour in SCW.[17, 40, 54-57, 62-65, 67] The extent of carbon conversion and the product gas distribution achieved

under these conditions may or may not be reproduced with real biomass, as these often contain variable amounts of compounds which can have significant influence on the gasification. For example, alkaline salts are known to intensify the gas yields, whereas *e.g.* proteins are reported to be difficult to gasify.[61-62, 65]

An associated advantage of using this process in an 'algae bio-refinery' is the option to integrate energy production with CO_2 capture and to re-use minerals retained in the process water by recycling them to the algae growth reactors/ponds ('closed nutrient loop').[16, 36-37, 50-52] At present the algae growth reactors are, however, considered to be too expensive[52], but the economics may be improved upon integrating the use of industrial waste effluents as feedstock for growth reactors (*e.g.* flue gas from power plants as source of CO_2 or utilizing wastewater streams as source of nutrients for algae production), by extracting the value added chemicals (*e.g.* proteins; amino acids; oil/lipids) as source of food- and feed ingredients and by upgrading the extracted algae oil for biodiesel production. Effluent streams from the latter separation step, but also the complete algae broth, can be gasified using SCWG to produce combustible gases. The product gas containing H_2, obtained from the SCWG, could be used for the hydrogenation of lipids extracted from the algae.

Antal[53] reported the gasification of macroalgae solutions (*Gracilaria*) of three different concentrations (0.1, 0.3 and 2.5 wt%) in SCW at 550 °C and 345 bar. He observed large variations in the product gas yields as well as in the carbon gasification efficiencies for the triplicates carried out and the nine test runs reported should be regarded as scouting experiments. Minowa and Sawayama[16] have proposed a new method of cultivation of microalgae in the recovered solution obtained from the low temperature (near-critical) catalytic gasification of algae. They performed three experimental runs with *Chlorella Vulgaris* at low temperature (350 °C) and in the presence of nickel catalyst and obtained a methane rich gas with carbon conversion ranging between 35 and 70%. Haiduc *et al.*[36] performed six tests of hydrothermal gasification of *Phaeodactylum tricornutum* at low temperatures (360–420 °C) aiming toward methane production in the presence and absence of ruthenium catalyst. For the un-catalyzed gasification the carbon conversion is in the range of 4 – 8%, while it was 34 - 74% with the catalyst and long reaction times (over 1h was required). Stucki *et al.*[37] reported 13 experimental runs of microalgae (*Spirulina platensis*) gasification in supercritical water at 400 °C in a small unstirred batch reactor system (30 mL) and in the presence of Ru/C and Ru/ZrO_2 catalysts. Complete conversion of algae to a methane rich gas was achieved at low concentrations (2.5 wt%) for 6 h reaction time and in the presence of a high catalyst to dry algae ratio of 8. Guan *et al.*[68] have studied the catalytic hydrothermal gasification of marine micro algae (*Nannochloropsis Sp*) with Ru supported on Carbon catalyst in a batch autoclave reactor. They reported complete conversion with a catalyst loading of 2 g/g at 410 °C and the

deactivation of catalyst is attributed to the catalyst poisoning due to sulphur and other elements such as Cl that are prevalent in the microalgae. Onduwili *et al.*[69] have reported the hydrothermal gasification of different species of micro algae (*Chlorella Vulgaris, Spirulina Platensis, Saccharina Latissima*) at 500 °C in a batch autoclave reactor in the presence of NaOH and/or Ni/Al_2O_3. High hydrogen yields were obtained in the presence of NaOH and with *Saccharina*, which is rich in carbohydrate content. The tarry liquid products after the reaction mainly consisted of phenols, alkyl benzenes, and polycyclic aromatic hydrocarbons as well as hetero cyclic nitrogen compounds.

Catalytic hydrothermal gasification of different strains of microalgae in a continuous flow reactor has been studied at relatively mild operating conditions in the presence of Ru/C catalyst by Elliott's group[70]. However, only 4 tests have been conducted in this continuous flow fixed bed reactor and they reported operational issues like plugging. The product gas consisted of methane and carbon dioxide in line with thermodynamic predictions. Guan *et al.*[71] developed a kinetic model for the gas formation from SCWG of microalgae following a reaction network comprising of two types of intermediates (fast and slow) that convert to gases. The type of intermediate that is most difficult to gasify under these conditions was found to be precursor that leads to char/coke formation. Several researchers till now have proven that algae can successfully be converted in SCW, however, an economic and energetic bottleneck for the production of synthetic natural gas from algal biomass is the growth of microalgae in artificial culture systems such as raceway ponds or photo-bioreactors.[72]

The aim of this work is to check the feasibility of microalgae gasification in SCW at high temperatures (above 550 °C) using quartz capillary micro reactors. This high-throughput screening technique for the conversion of biomass and model compounds at near- and supercritical conditions of water has been extensively used within our research group[17, 54-55, 59-60, 64] to study the effect of different process conditions like temperature, reaction time, concentration and screening of different catalysts to determine the product gas distribution and the gasification efficiency.

Algae form a complex feedstock, consisting of proteins, fats, carbohydrates, amino acids, lipids and minerals. The gasification of glycerol is used as a model system to study the influence of co-gasification of amino acids and alkali-salts on the gasification process. Glycerol is also relevant for algae gasification as it forms the backbone of lipids (present up to 40 wt% in algae) and, more general, glycerol is co-produced in the trans-esterification process for biodiesel making. Additionally, glycerol appears to be a suitable model compound as it decomposes in SCW without coke formation.[12, 17, 40, 64]

2.2 EXPERIMENTAL SECTION

2.2.1 MATERIALS

Microalgae (*Chlorella Vulgaris*) slurry was received from Ingrepro, The Netherlands. Nickel wire (thickness-0.25 mm) was obtained from Sigma Aldrich. Commercial catalysts Ru/TiO_2 (2 wt%), NiMo, CoMo, PtPd, and Ni wire were used as provided and their details are given in Table 2.1. The amino acids L-alanine, glycine and L-Proline were obtained from Sigma Aldrich. The composition of algae as provided by the supplier and those analyzed by us is given in Table 2.2.

Table 2.1: Characteristics of the catalysts.

Catalyst	Composition	BET (m^2/g)	Particle size (μM)
Ru/TiO_2 (Ru)	Ru (2%)	49	125
$NiMo/Al_2O_3$ (NiMo)	Ni (4%); Mo (21%)	182	125
$PtPd/Al_2O_3$ (PtPd)	Pd (0.68%); Pt (0.63%)	372	125
$CoMo/Al_2O_3$ (CoMo)	Co (5%); Mo (20%)	220	125
Inconel Powder	-	-	125
Ni wire	-	-	-

Table 2.2: Analysis of microalgae *Chlorella Vulgaris*.

Properties	
Moisture content (wt%)	92.7
Dry solid content (wt%)	7.3
Chemical composition (wt%)[a, b]	
Crude protein	50
Crude fat	13
Crude fibre	15
Ash	7
Carbohydrates	15
Mineral content (g/kg)[a, b]	
Ca	43
P	12.9
Na	1.1

K	7.1
Mg	6.1
Total amino acids (mg/Kg)[a]	246.2

[a] as given by supplier; [b] on a dry solid basis; [c] calculated by difference

2.2.2 QUARTZ CAPILLARIES

More details of preparation methods in quartz capillaries can be found in the literature.[17, 54-57] In short, quartz capillaries (ID: 0.2 cm; OD: 0.4 cm, L: 15 cm, V: ~0.5 cm^3) sealed at one end were loaded with algae slurry that corresponds to water density of 0.07 – 0.08 g/cm^3 (±240 bar) at respective temperature that is studied, flushed with argon and flame sealed at the other end and heated in a fluidized sand bed that is set to the desired experimental temperature. The heating time in the fluidized sand bed was ~30 s and the reaction time that is reported here includes the heating time. Gas analysis was done after rapid quenching of the capillaries in a water bath and by crushing it in a steel chamber (50 cm^3). The gases evolved are analyzed immediately using a gas chromatography attached to the crushing chamber. For catalytic experiments, a known amount of powdered catalyst was added to the capillary along with the biomass and is reacted in a fluidized sand bed after sealing and with no shaking. For the screening experiments with different catalyst, the ratio of catalyst to sample was maintained to be ~0.7 g/g and for excess catalyst it was ~2 g/g. For experiments with nickel wire, a 9 cm long nickel wire is inserted into the capillary along with the algae solution. For each single data point/experimental condition, four to six capillaries were used and the average value is reported.

2.2.3 CONTINUOUS FLOW TUBULAR REACTOR

A schematic diagram of the continuous flow tubular reactor used for the glycerol gasification is shown in Figure 2.1. The experimental set-up consists of two high performance liquid chromatography (HPLC) pumps from Lab Alliance that can deliver pressures of up to 400 bar. One pump was used to feed the water to supercritical conditions and it can deliver flow rates up to 0.1–24 mL/min. The second pump is used to pump the feedstock in to supercritical water at the mixing junction at a flow rate of 0.01–12 mL/min. All experiments were conducted using injection mode of operation, in which the glycerol solution is fed into SCW in the mixing chamber. The reactor tubing (ID: 0.2 cm, OD: 0.6 cm) is made of Inconel 600 having a composition of Ni (~ 72%), Cr (~ 15%), Fe (~ 8%) and is placed inside temperature controlled electrical heaters. The tube length in total is 143 cm and the reactor tube length after the mixing junction is 71.5 cm. Three electrical ovens were used for heating purposes and

these can be individually controlled and monitored (Eurotherm). As it was difficult to fix the thermocouples (type K) inside the reactor tube, they were placed outside the reactor wall and the outside temperature profile is logged using PICO software. The system pressure was controlled by a back pressure regulator (TESCOM) and the exit gas mixture from the reactor was cooled using a water cooled double pipe heat exchanger. The gas-liquid mixture was separated using a phase separator and the exit gas flow rate was measured using a wet gas meter (G1.6 Gallus 2000). The product gas composition was determined with an online sampling gas chromatograph (Varian 450-GC). The liquid phase product collected in the gas-liquid separator was then analyzed for the carbon content using the CHNS-O elemental analyzer (EA 1108, Fisons Instruments). Before and after each experiment the reactor was cleaned by pumping water alone to supercritical conditions for about 2 h to flush any remaining solids present in the reactor.

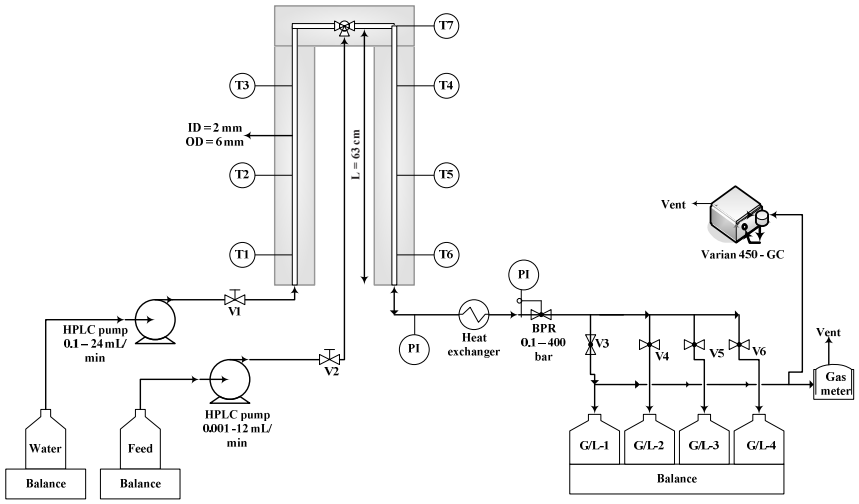

Figure 2.1: Schematic diagram of the continuous flow apparatus for SCWG of biomass.

2.2.4 ANALYSIS

The dry matter content of the algae slurry received was determined by drying at 80 °C in an oven and it was found to be ~ 7.3 wt%. The ultimate analysis of the dry and wet algae slurry was carried out using an Elemental Analyzer (EA 1108, CHNS-O, Fisons instruments).

Product gases from capillaries were analyzed using a gas chromatograph (GC) (Varian, CP-4900) after crushing them in the steel chamber which is connected to the GC. Continuous

analysis of the gaseous products with the continuous set-up was analyzed using a refinery GC (Varian, 450 - GC).

2.2.5 TERMS AND DEFINITION

In discussing the results, the following definitions are used.

The yield (Y_i) of product gas is defined as given below:

$$Y_i = \frac{N_i}{N_{feed}}$$

The gasification efficiency (GE) (or) carbon - gas conversion is defined as the degree of conversion of carbon in the feed to permanent gases:

$$\text{Gasification efficiency}, GE(\%) or (X) = \frac{\sum_i N_{c,i}}{N_{c,feed}} \times 100$$

The residence time (τ) in the continuous flow tubular reactor is calculated as follows:

$$\tau = \left[\frac{V * \rho_{T,p}}{\phi * \rho_{STP}} \right]$$

Where, V is the volume of the reactor, $\rho_{T,P}$ is the density of water reaction temperature and pressure, ρ_{STP} is the water density at ambient conditions, and ϕ is the total volumetric flow rate (STP).

2.2.6 CHEMICAL EQUILIBRIUM

Chemical equilibrium calculations were obtained using an in-house developed Matlab program that calculates according to the Gibbs minimization method[73] and the fugacity coefficients were calculated with the modified Soave-Redlich-Kwong equation of state.[74] The parameters for the modified Soave-Redlich-Kwong equation of state were obtained from Bertucco and Soave.[75-76] Thermodynamic properties were obtained from NIST-JANAF source. The equilibrium program calculates the yield (mol gas/mol feed) of permanent gases (H_2, CO, CO_2 and CH_4) and the yields of C_2-C_3 compounds are neglected in this program as their values are considered to be very small and it is only valid for glycerol experiments reported in this study.

2.3 RESULTS AND CONCLUSION

The results of SCWG of microalgae in quartz capillaries and glycerol gasification in SCW using a continuous flow tubular reactor are discussed in the subsequent sections. The decomposition of organics in SCW in to H_2, CO, CO_2 and CH_4 can be considered to proceed through the following set of reactions:

Steam reforming

$$C_xH_yO_z + (2x\text{-}z)\ H_2O \rightarrow xCO_2 + (y/2+2x\text{-}z)\ H_2$$

Water gas shift reaction

$$CO + H_2O \leftrightarrow CO_2 + H_2$$

Methanation reaction

$$CO + 3H_2 \leftrightarrow CH_4 + H_2O$$

The list of possible reactions is not complete; many other side reactions can- and will occur, like cracking, chain-rearrangements, condensation and polymerisation reactions. The underlying reaction mechanisms are not fully resolved, but there is consensus about ionic reactions being dominant in the subcritical region and free radical reactions prevailing in the supercritical region.[18-20, 40, 61-63, 65] The more complex the (biomass) feedstock, the more complex is the chemistry involved. The focus of this work on the gasification of a complex feedstock like algae is therefore not to resolve the reaction networks, but to identify the feasibility of the (complete) formation of gaseous products and to get a first impression of the reaction rate. Coke and tar formation is here seen as loss of gasification efficiency.

2.3.1 EFFECT OF TEMPERATURE ON MICRO-ALGAE GASIFICATION USING QUARTZ CAPILLARIES

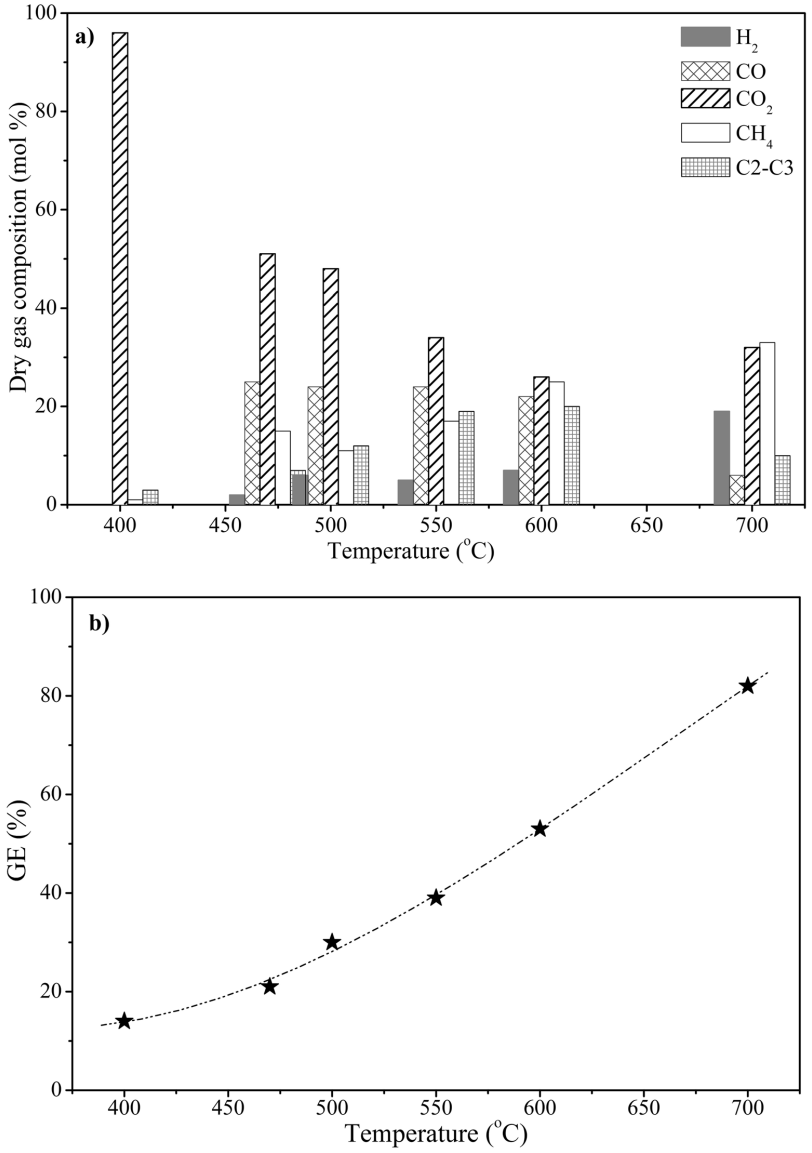

Figure 2.2: Effect of temperature on dry gas composition (a) and gasification efficiency (b) of algae gasification in quartz capillaries. Experimental conditions: Reaction time – 2 min; algae – 7.3 wt%; Pressure: ± 240 bar.

To ascertain the influence of the gasification temperature on product gas composition and gasification efficiency of non-catalytic SCWG of microalgae (7.3 wt%), a series of gasification experiments were conducted at different temperatures of 400, 470, 500, 550, 600 and 700 °C. For the reaction time of 2 minutes, the results are presented in Figure 2.2. As expected, temperature has a significant influence on the product gas composition, total gas yield and the gasification efficiency (GE). The GE increased as a function of temperature from 14% to 82% with increasing temperature from 400-700 °C respectively (Figure 2.2b). At lower temperatures, decarboxylation reactions[58, 62] are more dominant (similar trends have been observed in *e.g.* fast pyrolysis and torrefaction) and as a result, CO_2 is the main product obtained at 400 °C (Figure 2.2a). At higher temperatures (~ 600 °C and above), SCW becomes a more powerful oxidant and free radical reactions prevail.[19, 40, 58, 61-62, 65] Accompanied by an increased gas phase reactivity for the water gas shift reaction and methanation, this finally result in the formation of a mixture of gases containing H_2, CO_2, CO, CH_4 and some C_2-C_3 compounds. Visual observations of the capillaries after the reaction indicated coke formation as the reactor walls are coated to a more or lesser extent by black solid products. The colour of reactor walls was less intensive (gray color) at higher temperatures (above 600 °C) indicating a reduced coke formation. Similar observations of less coating of the reactor walls has been reported for glycine gasification at 500 °C in the presence of a nickel catalyst when compared with uncatalyzed gasification.[67]

2.3.2 EFFECT OF REACTION TIME ON MICRO-ALGAE GASIFICATION USING QUARTZ CAPILLARIES

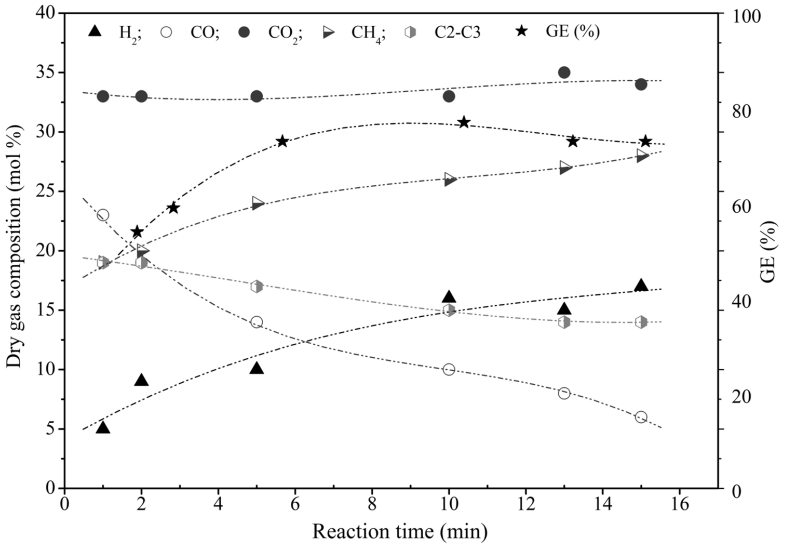

Figure 2.3: Effect of reaction time on gas composition and gasification efficiency for SCWG of algae. Experimental conditions: algae – 7.3 wt%; Temperature: 580 °C; Pressure: ± 240 bar.

Throughout the reaction time range studied (1 – 15 min) the distribution of gas yield and GE for the uncatalyzed SCWG of algae at 580 °C in quartz capillaries is as shown in Figure 2.3. After 5 min of reaction time, the carbon conversion reached the maximum value (73%) and further increasing the reaction time had no influence on the carbon conversion but the product gas distribution was changed. The H_2 and CH_4 content in the gas phase increased with reaction time at the expense of CO and C_2-C_3 fractions which, can be attributed due to the reforming of C_2-C_3 components to methane and hydrogen production via water-gas shift reaction. The CO_2 content was found to be independent of the reaction time within the range studied. Similar findings of no further increase in the carbon conversion after a certain reaction time for glucose gasification at 600 °C were reported earlier.[17, 54] The limited (maximum) gasification efficiency thus seems to be caused by either a fraction of the biomass being resistant against SCWG conditions or by an irreversible 'kinetically determined' selectivity towards coke/tar formation, which on its turn cannot be gasified under the conditions studied. The latter is the most probable, as non-first order behaviour is also observed for glucose.[60] Amino acids, and possibly proteins as they are formed from amino acids, are suspected to

cause difficulties in gasification.[12, 61-62, 65, 67] The large fraction of proteins in the algae studied (around 30 wt%) may have caused the incomplete gasification and hence, the effect of adding (some) amino acids on SCWG was investigated (see section 2.3.5). To confirm this, additional tests with L-alanine and L-proline (5 wt%) as model compounds in the quartz capillaries at 600 °C and 2 min reaction time were done and for this (uncatalyzed) system indeed hardly any carbon to gas conversion was noticed (results not presented).

2.3.3 EFFECT OF ALGAE CONCENTRATION ON MICRO-ALGAE GASIFICATION USING QUARTZ CAPILLARIES

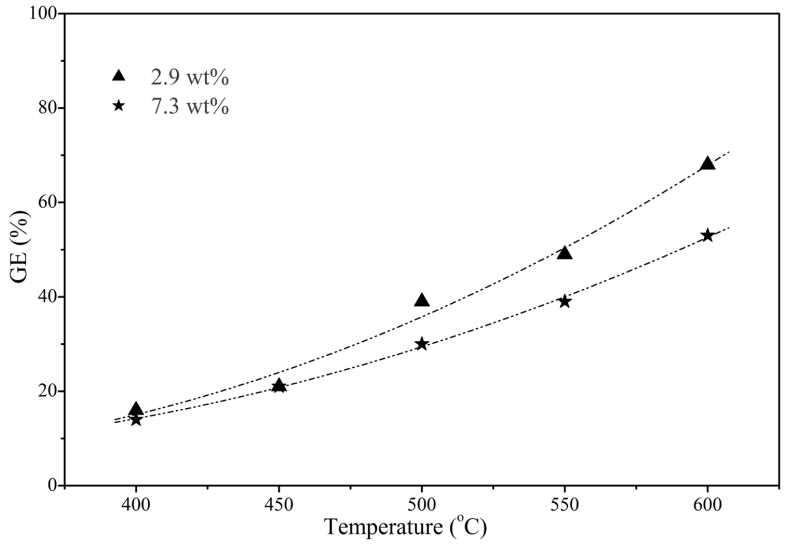

Figure 2.4: Influence of algae concentration (2.9 & 7.3 wt%) on gasification efficiency at different temperatures. Experimental conditions: Reaction time – 2 min; P – ± 240 bar.

Generally, the initial concentration of a reactant is an important parameter for many reaction systems. For SCWG it is often found to have a significant influence on the gasification rate and, moreover, on the extent of gasification in supercritical water.[17, 20, 54, 63] Knezˇevic´ *et al.*[60] have recently shown that the reaction rate for glucose conversion in hot compressed water is found to be first order with respect to gas formation while it was variable order (n>1) for char formation. The influence of two different algae concentrations (2.9 and 7.3 wt%) on the gasification efficiency at different temperatures after two minutes of reaction time is shown in Figure 2.4. It is obvious that higher carbon to gas conversion is achieved at the lower algae concentration (2.9 wt%). For the systems studied, maximum conversions are obtained at 600

°C and it was 68% and 53% with algae concentrations of 2.9 wt% and 7.3 wt% respectively. From a few scouting experiments with even more diluted algae solutions, the conversions seems to increase even further (up to complete conversion) with increasing dilution. However, the reproducibility of these experiments with quartz micro capillaries proved to be poor due to the small amounts of products formed and, hence, no values are reported here.

The product gas composition showed similar composition and change in composition with increasing the temperature for both the 7.3 wt% and the 2.9 wt% algae concentration series. High CO yields were obtained with 2.9 wt% algae concentrations at all temperatures when compared with 7.3 wt% concentration. In addition to H_2, CO, CO_2, and CH_4 there is always some C_2 (C_2H_4, C_2H_6) and C_3 (C_3H_6, C_3H_8) compounds produced at all temperatures and concentrations, independent of the initial algae concentration (data not shown).

2.3.4 EFFECT OF CATALYSTS ON MICRO-ALGAE GASIFICATION USING QUARTZ CAPILLARIES

Although higher temperatures and longer residence times are favourable for higher gas production, from a process point of view it is more economical to work at lower temperatures and shorter residence times. The need for catalysts arises to achieve higher gasification efficiencies and equilibrium gas yields. An effective catalyst for the production of H_2 in SCWG of biomass should facilitate the scissioning of C-C, and C-H bonds and, preferably, favour the water gas shift reaction.[77] Different catalysts were screened for the SCWG of algae in the quartz capillaries at 600 °C and two minutes of reaction time. The dry gas compositions obtained and the carbon-based GE are shown in Figure 2.5 a & b and are compared with uncatalyzed gasification of algae. It is clear from the figures that the total gas yields and compositions can be significantly different with different catalysts (for a given reaction time). Complete gasification was not achieved for these conditions and significantly longer reaction times, lower algae concentration and/or higher gasification temperatures are required to achieve this.

The catalytic wall effect of metal reactors on gasification behaviour and its tendency to promote water-gas shift activity in hot compressed water has been clearly established.[12, 17, 55] To try to mimic the reactions in metal reactors while using quartz capillary reactors we used Inconel powder and nickel wire acting as pseudo catalysts. High gas yield, GE of 84% and CH_4 yield (12 mol/kg algae) was obtained in the presence of Inconel powder acting as a pseudo catalyst, even when compared to other actual catalysts. From the results, it is obvious that metal reactor walls exhibit a significant catalytic effect and enhance the water-gas shift activity

and possibly the methanation reaction (as evidenced by the high methane content, see Figure 2.5 a).

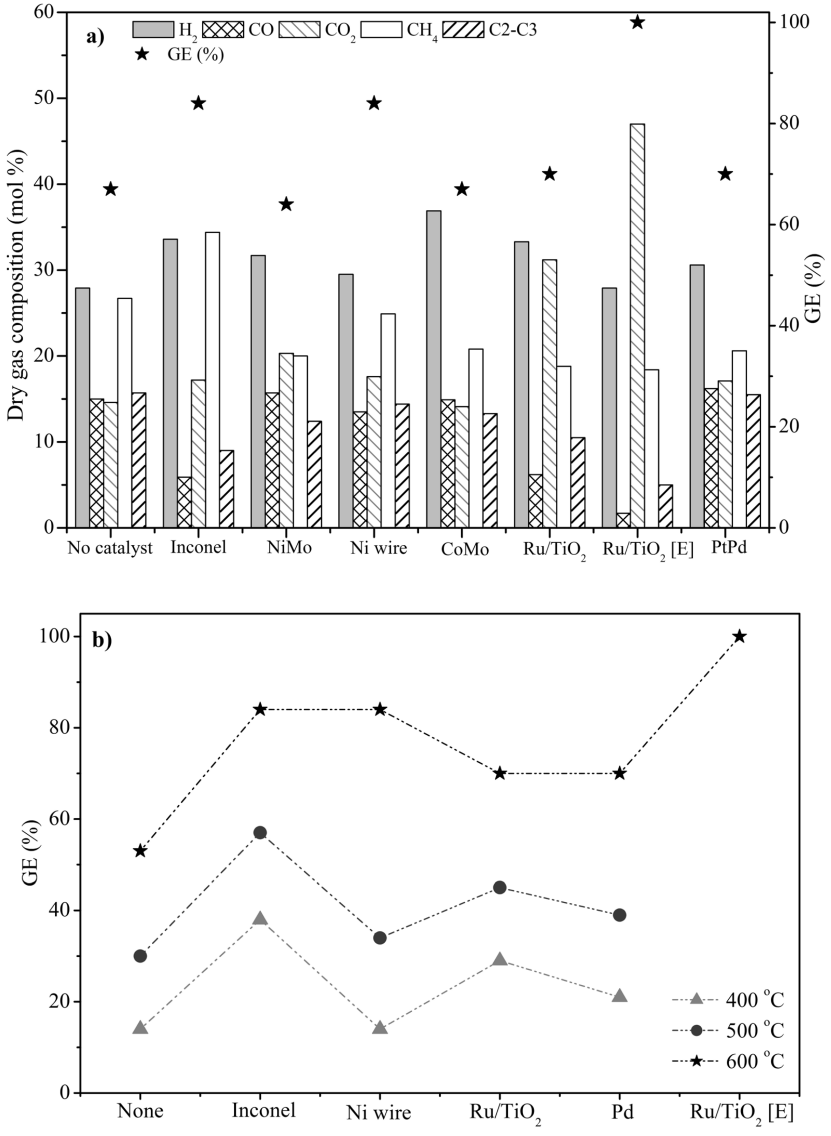

Figure 2.5: The influence of different catalysts on a) product gas distribution and GE of microalgae at 600 °C b) GE at different temperatures. Experimental conditions: Concentration – 7.3 wt%; Reaction time – 2 min; P – ± 240 bar; Catalyst/Sample – 0.7 g/g for Ru/TiO_2 (E) it was 2 g/g, (E) is excess.

The activity of catalysts with respect to the gasification efficiency of algae in SCW at 600 °C decreases in the order of Inconel ~Ni >Ru>PtPd>CoMo>NiMo. Higher H_2 yields (10 mol/kg algae) were obtained with Ru/TiO_2 catalyst and the activity of catalysts for high H_2 yields is in the order of Ru>NiMo>Inconel>Ni>PtPd>CoMo. Complete gasification was achieved with hydrogen rich product gas with Ru/TiO_2 at 700 °C and 2 min reaction time. Complete algae GE was also obtained at 600 ºC and 2 min reaction time with an excessive amounts of Ru/TiO_2 catalyst (cat/sample: 2 g/g). Complete gasification with excessive amounts of catalyst and incomplete conversion in the earlier runs both at 600ºC can be attributed due to poor contacting of the catalyst and reaction medium, catalyst poisoning, and also sintering at these conditions. A proper mixing of the catalyst and the biomass can however slightly improve the GE. The same will be case of poor contact with the catalyst and the reaction mixture can also implies for reactions done in the metal batch reactors if no proper shaking or mixing has been done that has been reported so far in the literature. However, the contact limitation of the catalyst and the reaction media is not pertinent for the experiments reported with nickel wire.

2.3.5 GLYCEROL GASIFICATION IN CONTINUOUS FLOW TUBULAR REACTOR

In this section, we present the results of glycerol gasification in the continuous flow reactor shown in Figure 2.1 with the aim to look at the influence of the presence of different additives like amino acids (here: L-alanine, glycine and L-proline) and alkali salt (here: K_2CO_3) on the product gas composition and carbon conversion to gaseous products. The continuous set-up was validated by five test runs with 10 wt% glycerol gasification in SCW at 600 °C, 250 bar and 5 s residence time carried on different dates for about an hour. The results showed good reproducibility and repeatability attaining complete carbon closure both from liquid and gas phase analysis and the gasification efficiencies obtained were 63, 64, 66, 66 and 66%. For glycerol experiments, the effluent was colourless and no evidence of coke formation also from the balance was noticed.

2.3.5.1 Influence of process conditions (temperature and residence time)

Figure 2.6 shows the comparison of gas yields and gasification efficiencies obtained experimentally and with the predicted equilibrium values at different temperatures of glycerol gasification (10 wt%) in SCW. From thermodynamics perspective, complete gasification is attained at all temperatures and the product gas of glycerol gasification in SCW mainly consisted of H_2, CO_2, & CH_4 with smaller amounts of CO (less than 1 vol%). The predicted yields of H_2 increases and the CH_4 yield declines as temperature increases. A marginal increase

in CO_2 and CO yield is expected at higher temperatures. The calculated CO yield was relatively very small (0.0795 mol/mol feed at 650 °C) for 10 wt% glycerol gasification.

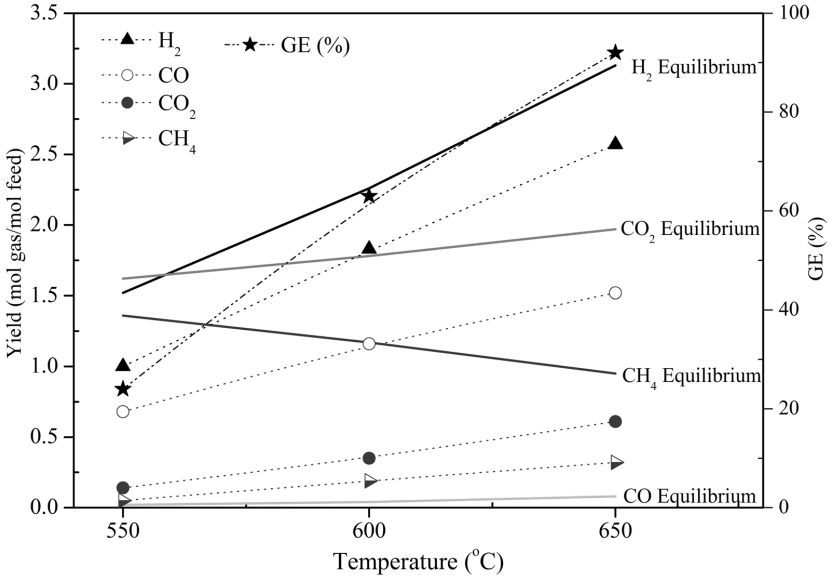

Figure 2.6: Comparison of the equilibrium gas yields with the experimental values at different temperatures for glycerol gasification. Experimental conditions: Concentration- 10 wt%; Residence time – 5 s; P- 250 bar.

It is evident from Figure 2.6 that the experimentally measured values are not in line with the equilibrium values. The equilibrium yields predicted for H_2, CH_4 and CO_2 were higher than the experimentally measured values. The CO yield obtained experimentally exceeds the equilibrium values, indicating that glycerol decomposition probably proceeds predominantly via the formation of CO and H_2. The experimentally obtained gasification efficiencies increased almost linearly as a function of temperature and it was 24%, 63% and 92% at temperatures 550, 600 and 650 °C respectively. With a raise in temperature from 550 °C to 650 °C, the total gas yield increased from 1.88 to 5.16 mol gas/mol feed and the product gas was mainly rich in H_2 and CO with less CO_2 and CH_4 yields over the temperature range studied. Additionally, a slight increase in the molar fraction of C_2-C_3 compounds (0.73 – 2.82 vol%) was noticed with increasing the temperature from 550 - 650 °C (results not in graph).

The decomposition profile for glycerol conversion over a range of residence time (4 – 11 s) at different temperatures (550, 600 and 650 °C) is shown in Figure 2.7. The carbon conversion increases linearly with increasing residence time over the temperature range that is studied. An

apparent pseudo first order kinetics for glycerol decomposition in SCW is fitted based on the gasification efficiency and the activation energy (E_a) was found to be 111 kJ/mol which is in close agreement with the value reported in the literature.[40] Maximum gasification efficiencies of 52%, 85% and 96% are achieved at 550, 600 and 650 °C and at longer residence times (11, 10 and 8 s) respectively.

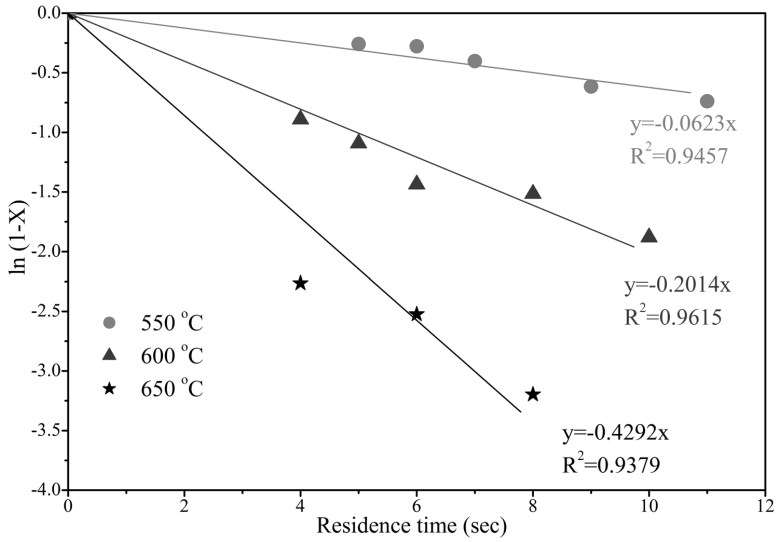

Figure 2.7: Normalized decomposition profile for 10 wt% glycerol conversion at 250 bar and three different temperatures.

2.3.5.2 Influence of amino acids & alkali salts

A few studies[61-62, 65, 67] have pointed out the possible influence of proteins and amino acids on SCW gasification. Di Leo *et al.*[67] examined the gasification of phenol and glycine (an amino acid) as model compounds for plants and protein biomass respectively in SCW and reported solids deposition on the quartz reactor wall for glycine at 500 °C in the presence and absence of nickel wire as a catalyst. They found that glycine was more resistant to gasification then phenol and the addition of a nickel wire catalyst assisted glycine gasification and reduced char formation, as evidenced by less char coating on the reactor wall. Kruse *et al.* studied the influence of proteins on hydrothermal gasification and liquefaction of real biomass feed stock (zoo mass[61]) and with model compounds (glucose[62]). They noticed a reduction in the glucose gasification efficiency in the presence of proteins/amino acids.

A set of experiments with glycerol gasification in SCW has been performed in the presence of three different amino acids (glycine, L-alanine & L-proline) and an alkali salt (K_2CO_3). Table 2.3 illustrates the influence of additives on the gas composition, gas yields and gasification efficiency under different conditions studied.

At 600 °C, no significant change in the product gas distribution of glycerol (10 wt%) gasification in SCW was observed in the presence of amino acids. It is noteworthy to mention that at 600 °C enhanced GE was observed with the addition of 0.5 wt% glycine and with the addition of 0.5 wt% L-alanine, when compared with no additives. However, the GE and total gas yield decreased significantly in the presence of L-proline (again 0.5 wt%). The reported GE values refer to the complete C-gasification efficiency of the total mixture; hence including the C introduced via the amino acids and or alkali salts (total C out via gas phase over total C in via glycerol and amino acids). On the other hand, at 550 °C no or a minor effect on the GE was observed in the presence of glycine and L-alanine and, again, no change in product gas distribution was noted.

A more clear effect of the presence of amino acids was observed with respect to coke formation. As indicated above, no coke formation was observed during SCWG of with glycerol alone. However, when cleaning the reactor after each experiment with glycerol and amino acid mixtures, the formation of some black solid particles (coke) was noticed. Unfortunately, we were not able to quantify the coke that is formed after these experiments. Coke formation was most pronounced when using the glycerol-proline mixture. This suggests a lower reactivity of glycine and alanine when compared to L-proline.

The coke observed is either directly produced from the amino acids added or from reaction products of the amino acids (or their decomposition intermediates/products) with glycerol (or its decomposition intermediates/products). In literature indeed an indication was found for a relatively high reactivity of L-proline, especially towards glucose.[78]

In the glycerol SCWG experiments without additives, the reactor effluent was colourless but in the presence of amino acids the effluent colour changed with respect to the type of amino acid used. The effluent colour in case of the glycine-addition was light yellow, while with L-alanine it turned into a dark yellow in colour. According to literature[78-81] this can indicate the formation of Maillard intermediates during the reaction. Surprisingly, the effluent color with L-proline was completely different to what is found with the other amino acids as it was chocolate brown in color and contained oily material. No oily matter was found in the effluent with either glycine or L-alanine. It is noteworthy to mention that also in the case of the addition of K_2CO_3 to the glycine-glycerol mixture at 500 °C an oily like substance in the effluent was noticed.

Several researchers[8, 11, 19, 20] have already reported the significant influence of alkali salts on biomass gasification, leading to higher gas yields by improving the water-gas shift activity. The behaviour of alkali salts in combination with amino acids on glycerol gasification was studied by adding K_2CO_3 and glycine (Table 2.3). The addition of K_2CO_3 induced an (essentially) complete conversion of glycerine and intensified the H_2 yield by promoting the water-gas shift. Remarkably, the addition of glycine (0.5 wt%) along with K_2CO_3 (0.5 wt%) reduced the GE of glycerol at 600 °C again below completion when compared with to the situation without amino acid. Alternatively, one could state that adding K_2CO_3 to the glycerol-glycine system increased the GE, although not (yet) to completion.

Table 2.3: Influence of the additives on 10 wt% glycerol gasification at 5 sec residence time.

Condition	**None**	**Glycine (0.5 wt%)**	**Alanine (0.5 wt%)**	**Proline (0.5 wt%)**	**None**	**Glycine (0.5 wt%)**	**Alanine (0.5 wt%)**	**K_2CO_3 (0.5 wt%)**	**K_2CO_3 (0.5 wt%) + Glycine (0.5 wt%)**
T, (°C)	600	600	600	600	550	550	550	600	600
P, (bar)	250	250	250	250	250	250	250	250	250
GE%	66	69	73	57	24	24	22	100	89
Dry gas composition (mol%)									
H_2	52	51	51	50	54	54	54	55	53
CO	34	32	32	31	30	29	31	1	1
CO_2	8	10	9	11	11	14	12	30	28
CH_4	4	5	5	5	2	2	2	5	6
$^*C_2$-C_3	2	2	3	4	2	2	2	9	13
Yield (mol gas/mol glycerol)									
H_2	2.05	2.09	2.22	1.59	0.77	0.82	0.74	2.69	2.61
CO	1.36	1.32	1.42	0.98	0.43	0.44	0.42	0.04	0.03
CO_2	0.30	0.39	0.39	0.34	0.16	0.21	0.16	1.48	1.40
CH_4	0.16	0.20	0.24	0.15	0.03	0.03	0.03	0.25	0.28
$^*C_2$-C_3	0.07	0.10	0.11	0.14	0.03	0.03	0.02	0.44	0.63
Dissolved carbon in effluent (wt%)	1.2	1.3	1.3	2.4	2.3	2.6	3.1	-	0.3
Effluent colour	Colorless	Light yellow	Dark yellow	Brownish color	Colorless	Light yellow	Dark yellow	Colorless	Light yellow

2.4 DISCUSSION

Protein biomass (like algae) generally contains a significant portion of proteins, which are made of amino acids that act as building blocks. The various amino acids present in the proteins have different chemical structures and hence different reactivity, but they all can undergo similar decarboxylation to produce carbonic acid and amines and de-amination reactions to produce ammonia and organic acids.[12, 78-80]

An incomplete carbon conversion of algae could potentially be ascribed due to the presence of these proteins/amino acids, as they have been reported to be quite recalcitrant during gasification and also due to the presence of carbohydrates.[15, 18-19, 61-62, 67, 78-80]

In the experiments with the continuous flow reactor, having a catalytically active Inconel wall, the gasification of glycerol was, however, not affected, if not enhanced, by the presence of L-alanine and glycine. This seems, at first glance, in contradiction with results presented by Kruse *et al.*[62] who noticed a reduction in the glucose gasification efficiency in the presence of proteins/amino acids. They suggested a mechanism in which the formation of relatively stable free radical anions (or nitrogen containing aromatics) generated via the Maillard reaction of proteins and carbohydrates result in a radical scavenging effect. As free radical chain reactions are considered highly relevant for gas formation, this then results in a reduction of the gasification efficiency. Probably Maillard-type reactions seem less prevalent in the case of glycerol gasification in the presence of glycine, L-alanine but more dominant with the L-proline.

The apparent reducing effect of L-proline on the gasification efficiency is therefore not likely due to this type of reactions, but more probable related to a direct radical scavenging effect, for which in recent years evidence was found.[78, 81] Proline is also known to accumulate in plant tissues during abiotic oxidative stresses, most likely for its radical scavenging properties. In line with the findings reported in this study, Kaul *et al.*[81] have also indicated that, in contrast to the radical scavenging effect of proline, glycine does not to interact with free radicals.

Our findings of enhanced coke formation are confirmed by the few experiences reported in literature. Kruse *et al.*[62] not only observed an increase in coke formation but also extensive nickel leaching due to corrosion in the presence of amino acids. Antal *et al.*[12] have also reported extensive corrosion and leaching of reactor walls during the tests with real biomass (potato waste) gasification in SCW.

Table 2.4 illustrate the comparison of gasification behaviour of algae with other model compounds and real biomass. Lignocellulosic biomass (as pine-wood) mainly comprises of cellulose, hemicellulose and lignin and minor amounts of other ingredients as minerals. Protein

biomass, such as algae, consists of proteins, carbohydrates, fats and other minerals. The composition of the biomass dictates the gasification behaviour and the product gas distribution. From Table 2.4, it is obvious that for the lignocellulosic biomass the lignin is the most difficult fraction to convert. Algae seem to be a promising feedstock for the conversion in SCW, not only considering the exceptional growth rates, but also due to the fact that they seem to be more readily converted via SCWG.

Table 2.4: Comparison of algae results in SCW with other reported studies using quartz capillaries.

References→	**This work**	**Potic[10]**	**Kersten *et al.*[7]**	**Resende *et al.*[12]**	**Resende *et al.*[13]**	**Sricharoenchaikul[28]**
Feedstock	Algae	Wood	Glucose	Lignin	Cellulose	Black liquor
Reaction time (min)	2	1	1	45	5	1
Pressure (bar)	240	300	300	310	310	300
Temperature (°C)	600	600	600	600	600	650
Concentration (wt%)	7.3	10	10	9	9	10
			Dry gas composition (mol %)			
H_2	7	1	12	11	15	10
CO	22	20	60	16	24	10
CH_4	25	12	13	35	18	14
CO_2	26	59	9	37	43	8
C_2-C_3	20	8	6	-	-	36
GE (%)	53	47	69	19	35	66

2.5 CONCLUSIONS

Initial studies were carried out with real biomass slurries (here: micro algae) in quartz capillary reactors and we found that for the uncatalyzed reaction, the results of microalgae conversion were more or less in-line with the lingo-cellulosic biomass conversion and the gasification efficiency increased with high temperatures and low initial feed concentrations. However, in the presence of excessive amounts of heterogeneous Ru catalyst complete conversion was obtained. The incomplete conversion of micro algae in the absence of any catalyst was found to be due to the presence of proteins. Further, the role of amino acids (building blocks of proteins) was studied in a continuous reactor on the glycerol gasification behaviour in supercritical water. We found that L-alanine and glycine are inert or even slightly enhanced the gasification, especially L-proline was found to suppress the gasification efficiency possibly by free radical scavenging. The presence of amino acids led in all cases to significant coke formation and colourization of the reactor effluent, possibly due to reaction products from Maillard-type reactions. The addition potassium carbonate enhanced the glycerol gasification and promoted the H_2 formation via water gas shift reaction. Algal biomass was found to be easily gasified in supercritical water. However the coke formation at high feed concentrations and the need for catalyst development to achieve complete gasification at technically and economically more favourable reaction conditions prompted us to study the chemistry and catalyst development.

Chapter 3

Supercritical water gasification of organic acids and alcohols: The effect of chain length[2]

[2] This chapter is an excerpt of paper published as:

Chakinala, A. G.; Kumar, S.; Kruse, A.; Kersten, S. R. A.; van Swaaij, W. P. M.; Brilman, D. W. F., Supercritical water gasification of organic acids and alcohols: The effect of chain length. The Journal of Supercritical Fluids 2013, 74, (0), 8-21.

Chapter 3

3.1 INTRODUCTION

Supercritical water (SCW), water heated under pressure to above its critical point (T>374 °C, P>220 bar), is attracting attention as a medium for chemical reactions.[42, 44, 82] Supercritical water gasification (SCWG) has been growing as a promising technology in converting (residual) organics present in aqueous biomass/waste streams with a high water content (80%) to high heating value product gases (*e.g.* H_2, CH_4, CO) and clear water.[4–7] A key advantage of the SCW is the possibility of tuning the properties of the reaction medium by varying the pressure and temperature and thus optimizing the reaction conditions.[4, 8] The water content in the aqueous biomass streams serves the purposes of reaction medium, being a reactant and act as a catalyst for the enhanced degradation rates of the organics in the biomass. However, the decomposition pathways of real biomass differs in sub– and supercritical water (ionic– vs. radical reactions being dominating) and is influenced by several variables such as feed characteristics (type of organics, solids/dry matter like cell walls etc.,) and process conditions (temperature, pressure, initial feed concentration, reaction time, heating up rate, pH).[82-83]

Several intermediate compounds are formed during the course of reaction when biomass is heated up under hydrothermal conditions, the majority of the stable intermediate compounds being similar to the compounds found in the hydrothermal liquefaction.[83] These intermediate compounds constitute of alcohols, acids, aldehydes, diols, ketones, phenols, furfurals and several other compounds.[83] Some of these compounds convert readily into gases (desired reaction), but additionally some of these compounds may also undergo polymerization reactions, leading to the formation of less reactive char/coke, which ultimately reduces the gas yield and can even result in reactor plugging.[32]

From earlier reports and our own unpublished data it is known that some compounds (for *e.g.*, methanol) are not very reactive in SCW in the absence of any catalyst and do not lead to char/tar formation.[11–14] However, other, often larger, compounds such as glucose and biomass feed containing sugar compounds are more reactive, and rapidly lead to char/tar formation (*via* HMF).[32, 82] It is therefore essential to understand more of the chemistry of biomass gasification in supercritical water in terms of the gasification behaviour; *e.g.* on the role of different functional groups and chain length effects. For future development this may help to minimise the char/tar formation and increase the carbon to gas conversion/gas yield, and where possible, to optimize/tune the product gas towards either H_2 or CH_4 rich gas.

The objective of this chapter is therefore to contribute to the understanding of the chemistry of biomass gasification in supercritical water by elucidating the relationship between molecular structures (chain length, functional groups) on the gasification behaviour. Carboxylic acids and alcohols are most frequently observed intermediate products from the hydrothermal

gasification of a wide variety of organic compounds, wastes and biomass, and were therefore chosen for systematic study.[33, 84] The goal of this work was to investigate experimentally if and how the chain length of linear alcohols and acids affects the product distribution during SCWG of these compounds. In this chapter the following series of experiments were carried out to study:

- The influence of chain length of linear organic acids ranging from C_1 to C_8 compounds on the gasification behaviour in terms of product gas yields and carbon to gas conversion.
- The influence of chain lengths of n–alcohols ranging from C_1 to C_8 on the gasification behaviour.
- The effect of increasing number of –OH groups and the positioning of these groups.

3.2 EXPERIMENTAL SECTION

3.2.1 MATERIALS, EXPERIMENTAL SET-UP AND PROCEDURE

All chemicals used in this study were obtained from Sigma Aldrich with a high purity. The experiments were carried out in a batch autoclave reactor (Inconel alloy:~ 72% Ni, 15% Cr and (~ 8% Fe) having an internal volume of 45 mL and a schematic diagram of the set–up is shown in Figure 3.1. For safety reasons, the reactor set–up was placed in a high pressure room and is controlled from outside the room during the experiments. The reactor is equipped with two orifices, one for a thermocouple and the other to connect to a pressure indicator and gate valve. The pressure and the temperature of the reactor is recorded and monitored using Pico Log software. With the help of a pneumatic arm, the autoclave can be immersed into– and removed out of the fluidized sand bed after the reaction. This sand bed was heated by an electric oven (with preheated fluidization gas).

The experimental procedure is as follows: In a typical run, the calculated amount of aqueous feed solution is loaded into the reactor and screwed tightly and connected to the pneumatic arm of the set–up. The final reactor pressure reached is an outcome of the initial amount of water added to the reactor which is calculated based on the density of water at the experimental conditions to be investigated. The line with the pressure reader was connected to the autoclave and flushed with nitrogen several times to remove any oxygen present in the system. The reactor was then pressurized with 20 bar of nitrogen which served the purpose for leak test. The line connecting to the autoclave was removed and the high pressure room was closed and the remainder of the experiment was monitored from outside. Using the pneumatic arm, the autoclave is positioned on the fluidized sand bed and then the reaction was initiated

by immersing the autoclave with the help of a piston into the preheated fluidized sand bed which had a temperature of ~30 °C higher than the desired reaction temperature. All the experiments were carried out at 600 ± 10 °C, 260 ± 30 bar and 15 min of reaction time. After the desired reaction time, the reactor was lifted and quenched in a cold water bath.

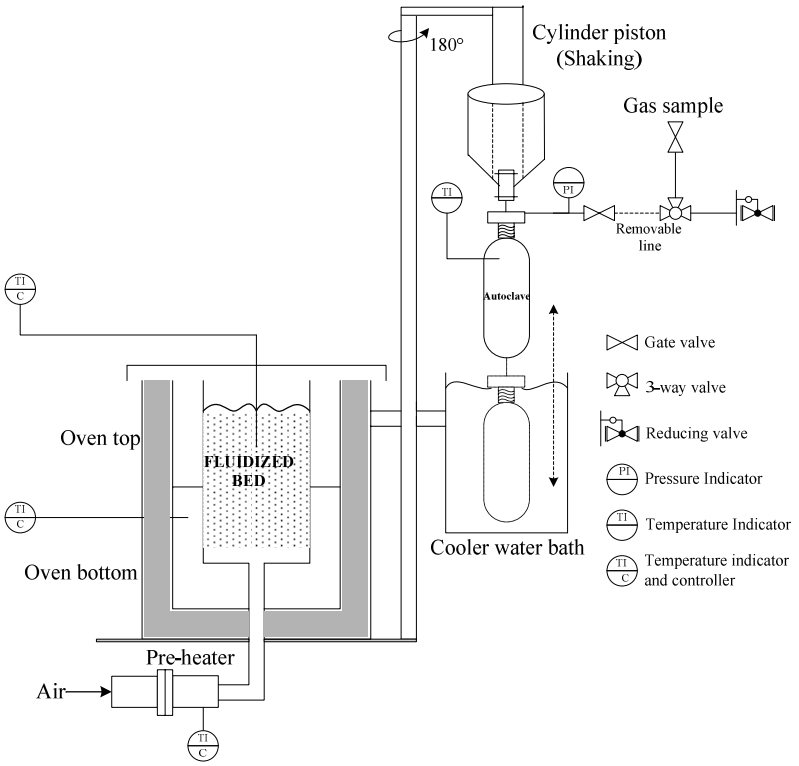

Figure 3.1: Schematic diagram of the experimental batch autoclave reactor set–up.

Gas samples were taken in a syringe and analyzed with an off–line gas chromatography. With the gas composition, the final pressure and temperature inside the reactor, the amount of each gas produced was calculated. After the reactor was cooled, it was depressurized and the autoclave was disconnected from the arm and opened. The remaining product (liquid and solids in suspension) was then collected in a glass bottle and the reactor was rinsed with acetone to remove any water–insoluble deposits. The aqueous phase was analyzed for dissolved organic carbon with an elemental analyzer (Fisions Instruments 1108 EA CHN–S).

Gas chromatography–mass spectrometry (GC–MS) analysis was performed with an Agilent GCMS 6890N to identify the intermediate compounds present in the liquid after the reaction.

3.2.2 TERMS AND DEFINITIONS

The gasification efficiency (GE) or carbon to gas conversion is defined as the degree of conversion of carbon in the feed to "C" containing gases.

$$\text{(Carbon) Gasification efficiency, C\_GE (\%)} = \frac{\sum_i N_{c,i}}{N_{c,feed}} \times 100$$

$$\text{Hydrogen Gasification efficiency, H\_GE (\%)} = \frac{\sum_i N_{H,i}}{N_{H,feed}} \times 100$$

$$\text{Oxygen Gasification efficiency, O\_GE (\%)} = \frac{\sum_i N_{O,i}}{N_{O,feed}} \times 100$$

The yield (Y_i) of product gas is defined relative to the carbon content by: $Y_i = \frac{N_{c,i}}{N_{c,feed}}$

Where, $N_{c,feed}$, $N_{H,feed}$, $N_{O,feed}$ are the number of moles of carbon, hydrogen and oxygen in the feed.

Whereas, $N_{c,i}$, $N_{H,i}$ and $N_{O,i}$ are the number of moles of carbon, hydrogen and oxygen atoms respectively in product gas (i=CO, CO_2, CH_4, C_2H_4, C_2H_6, C_3H_6, C_3H_8).

3.3 RESULTS AND DISCUSSION

Series of experiments are carried out to determine the influence of increasing the chain length of organic acids and alcohols, the number of OH groups and the positioning of OH groups on the gasification behaviour in SCW.

The postulated reaction pathways, under the assumption of radical reactions being dominant, for the decomposition of acids and alcohols in SCW are based on our experimental observations and from literature studies. As the complexity increases for higher chain lengths of carbon atoms, only for acids and alcohols with one, two and three carbon atoms the reaction schemes are presented and focus on the formation of permanent (product–) gases from these oxygenated model compounds.

The mechanisms proposed are formulated, on basis of a competitive scheme for the three parallel base–type reactions; being C–O, C–H and O–H bond scission. For higher carbon chain atoms, additionally the C–C bond breaking is taken into consideration. This competition of bond scissioning dictates the product distribution. It is tried to identify on basis of experimentally determined product distributions obtained in this work to derive from this preferred, or dominating, reaction paths.

3.3.1 GASIFICATION OF ORGANIC ACIDS

The influence of different chain lengths of organics acids and alcohols ranging from C_1 to C_8 on the gasification behaviour in SCW is studied.

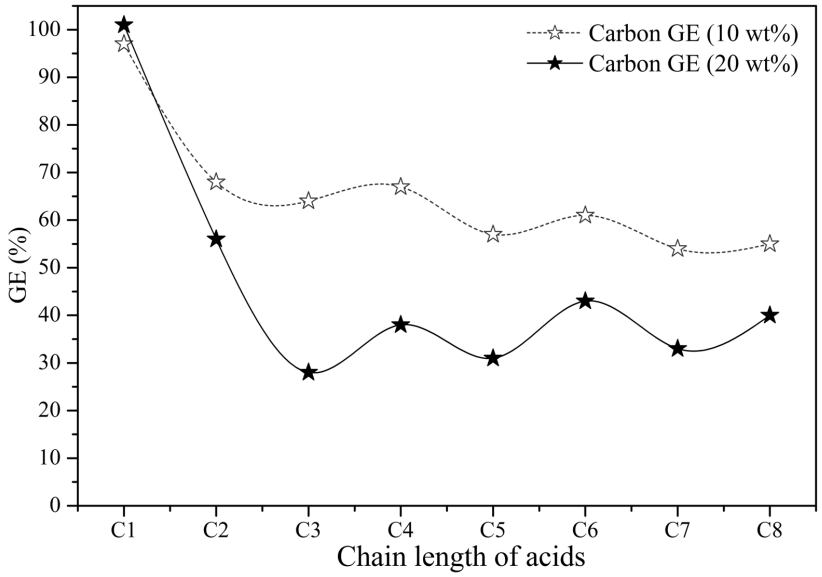

Figure 3.2: The carbon to gas conversion of different chain lengths of organic acids.

Figure 3.2 illustrates the trend in the carbon to gas conversion for two different concentrations (10 & 20 wt%) of a homologous series of linear organic acids, having carbon chain lengths from C_1 (formic acid) to C_8 (octanoic acid). It is evident from the Figure 3.2 and 3.3, that among all the acids, formic acid decomposes completely and rapidly into gases. The carbon GE decreases initially rapidly with increasing chain length after formic acid, but more slowly from C_3 onwards. The gasification efficiency trend shows a remarkable, damped oscillatory behaviour. Organic acids with an even number of carbon atoms were found to have higher

GE than those with an odd number of carbon atoms in the hydrocarbon chain. This trend is persistent, even for higher organic acids, and is visible for both the 10 wt% and the 20 wt% series. The initial feed concentration has a significant impact on the carbon GE. This is possibly due to ionic polymerisation reactions occurring during the initial phase of the reaction and leading to enhanced polymerization and subsequent increased tar and char forming reactions with increasing feed concentration. A polymerization has a higher reaction order than degradation; therefore it is always favoured at higher concentrations.[85] Visual observations of the reactor after the experiments reveal/confirm some char and tar formation with higher acids (after C_2).

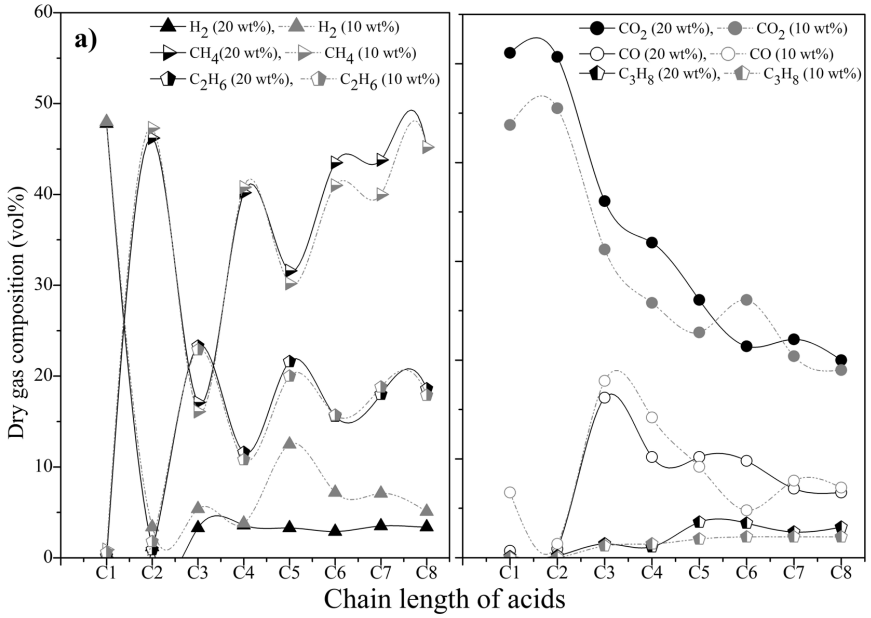

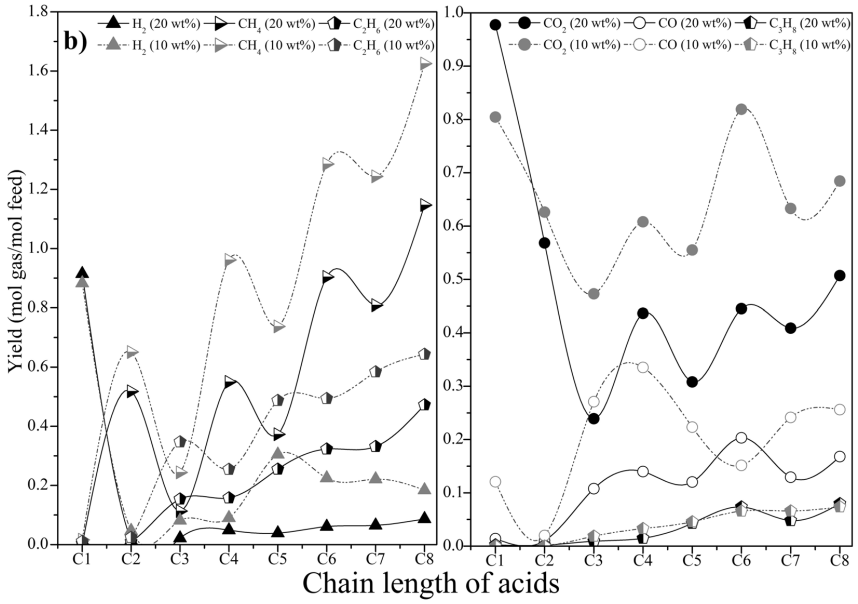

Figure 3.3: The influence of different chain lengths of organic acids on a) dry gas composition (vol%) b) product gas yields (mol/mol). Dark and thick symbols corresponds to 20 wt% organic concentration, light and dotted trend lines represent 10 wt% organic concentration.

The dry gas composition and product gas yields with increasing carbon chain length of organic acids with concentrations of 10 and 20 wt% are shown in Figure 3.3 a & b respectively. It is clear from Figure 3.3 a that there is hardly any influence of the initial feed concentration on the dry gas composition which suggests that the gas formation mechanism remains unaltered with initial feed concentration (Figure 3.3 a). This is in accordance with the assumption, that the polymerisation is a competitive parallel reaction.[85] The trends of product gas yields (mole/mole) are similar for both 10 and 20 wt% concentration. Higher gas yields are obtained for the less concentrated feed stocks, as expected from the gasification efficiency results discussed earlier (Figure 3.3 b).

3.3.1.1 Formic acid

Formic acid is an often reported intermediate product in the hydrothermal oxidation of a wide variety of organic compounds and wastes. The smallest of all carboxylic acids decomposes rapidly in SCW via two parallel paths, decarboxylation (forming CO_2 and H_2) and dehydration (into CO and H_2O).[86-89] The postulated free-radical mechanism for the formic acid decomposition in SCW is shown in Figure 3.4.

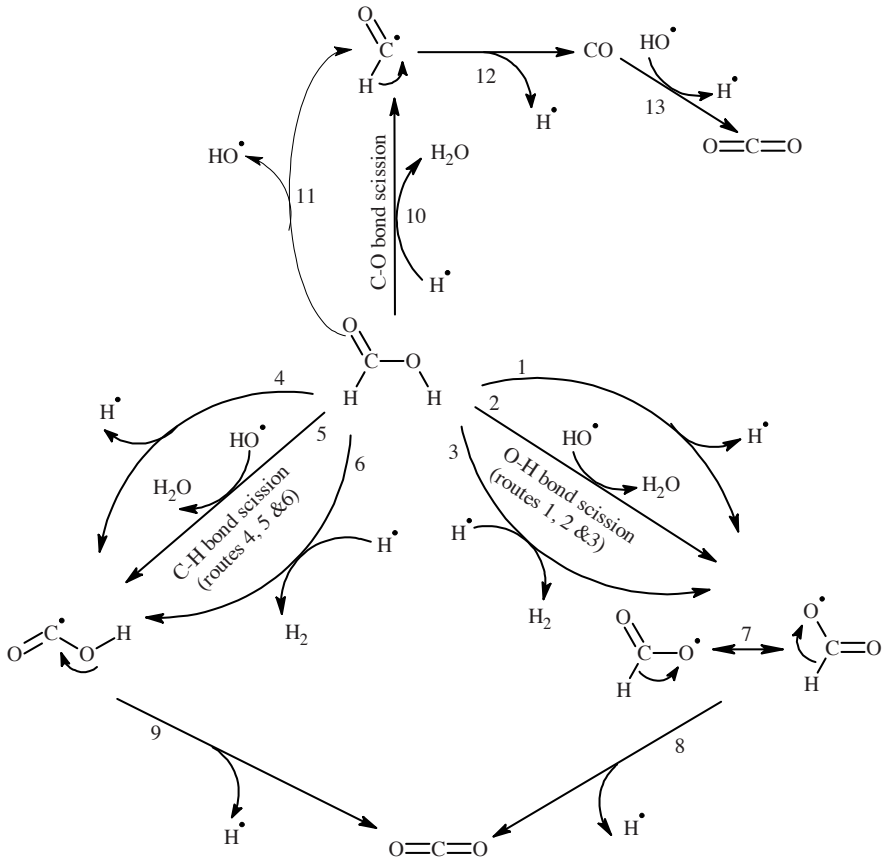

Figure 3.4: Postulated reaction mechanism of formic acid decomposition in SCW (reactions are indicated with numbers).

This free radical mechanism is discussed here because of the rather high temperature and low density (70.8 kg m^{-3}) in the experiments discussed here. High temperature and low densities should promote free radical reactions.[40] In addition this mechanism is used as basis for the free-radical mechanism used for the higher carboxylic acids. On the other hand a molecular mechanism catalysed by water has to be considered, explaining the preference of decarboxylation at neutral conditions.[86, 90-91]

Routes 1, 4 and 11 are initiation reactions for the free radical chain mechanism. By this reaction but mainly via the reactions with free-radical inside the chain, the bond breaking of O–H, C–H, and C–O occurs. Water is able to serve as transfer medium: Free radicals reacting

with water leads also to $H^{\bullet}$ and $OH^{\bullet}$ free radicals taking part in the chain. For this no influence on the chemical reaction rates is found.[43] On the other hand the solvent nature of SCW seems to have a significant influence, also in the free-radical mechanism.[92-93] Routes 1 and 4 are thermolytic scissioning of a bond, releasing $H^{\bullet}$. Routes 2 and 5 are induced by $OH^{\bullet}$, while Route 3, 6 and 10 are initiated by $H^{\bullet}$ radicals. In principle also other, carbon-containing free radicals, not only $OH^{\bullet}$ and $H^{\bullet}$, would lead to the same products. But these would not lead to new and independent reaction pathways, because the reactions of carbon containing free radicals are already considered. Routes 1–3 are abstraction of acidic hydrogen at the oxygen atom, leading to the formation of $HCOO^{\bullet}$ radicals which are stabilised by resonance effects (delocalization of electron). The $HCOO^{\bullet}$ radicals further decomposes into CO_2 and releases one $H^{\bullet}$ (route 8). Route 4–6 are the abstraction of hydrogen at α–carbon atom that leads to formation of $OC^{\bullet}OH$ radical which further decomposes into CO_2 and releases one $H^{\bullet}$ (route 9). Route 10, is a dehydration route where $H^{\bullet}$ reacts with OH group present in the compound and forms water and CO and releases one $H^{\bullet}$. CO can be further converted into CO_2 via the WGS reaction.

In the mechanism shown here, *e.g.* in Figure 3.4, the WGS reaction is shown as a free radical reaction. As mentioned above also a molecular mechanism via formic acid is also discussed. In this case the activation energies for the two pathways, to CO and to CO_2, are nearly identical without water and the formation of CO_2 is preferred in the case of complex formation with water. Still in this case the difference is only around 31 kJ/mole.[90] In the case not CO is formed but formic acid, small difference in the reaction medium would change the preference to CO or CO_2. It is therefore not surprising that sometimes the preferred product determined changes with reaction conditions. Wakai *et al.*[94] studied the decomposition of formic acid (0.1 to 1 M) at temperatures between 275 °C and 350 °C in quartz tubes. The carbon-containing products were measured by NMR after around 10 min reaction time. At low concentration and 300 °C CO_2 was the main product. At higher concentration CO was the dominant product. This was explained by an autocatalytic effect. For the 1 M solution, CO was the main product in the whole temperature range and the CO concentration was only slightly decreasing with temperature. The addition of metal powder (SUS 316L, Hastelloy C-276, Inconel 625; all common high-pressure vessel materials) supports decarboxylation.

Singleton *et al.*[95] in their experiments at low temperature found that the dominant interaction of the $OH^{\bullet}$ radicals is with the acidic hydrogen of formic acid, rather than with the formyl hydrogen. Although at high temperatures, abstraction from the formyl hydrogen would be

expected to make a significant contribution because of its anticipated positive activation energy.[95] Hence, reactions 1–3 seem to be the major reaction pathways.

The overall reaction (decarboxylation) can be written as:

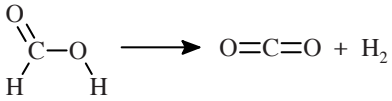

Although dehydration (reactions 10, 11) may occur to some extent, the above (decarboxylation) is therefore expected to be the major reaction pathway.

The experimental obtained gas composition, 51% CO_2 and 48% H_2, confirms that decarboxylation is dominant over dehydration. It could be argued that the dehydration reaction initially might have taken place, forming CO which further oxidizes into CO_2 via WGS reaction. Marginal amount (0.74%) of CO present in gas phase, indicates, however, a low extent of the dehydration reaction, as otherwise CO should have been present in significant amounts as seen in our gasification experiments using alcohols (discussed next section). It is very unlikely to convert CO to such a large extent (near to equilibrium) without the presence of any catalyst. The high CO_2 selectivity obtained is in–line with literature.[86] Remarkably, studies of formic acid decomposition in the gas phase[9, 13, 14] showed that the main reaction pathway in the gas phase was dehydration, which forms CO and H_2O, and that decarboxylation, which forms CO_2 and H_2, occurred to a lesser extent. However, based on literature[86, 90-91] and our experimental results above indicate that the main reaction under hydrothermal conditions is decarboxylation and that dehydration is insignificant.

3.3.1.2 Acetic acid

Acetic acid is one of the stable intermediate products that is often found during the degradation of several biomass wastes and is proven to be quite refractory in SCWG.[33, 42, 83-84] A postulated mechanism for acetic acid decomposition, again based on a radical reaction mechanism, is shown in Figure 3.5. Considering the gas phase composition found (46% CH_4 and 51% CO_2) it can be seen that the more significant reaction pathway is hydrogen abstraction from the carboxyl group (OH bond scission, path 1), as this leads to equimolar formation of CO_2 and CH_4.

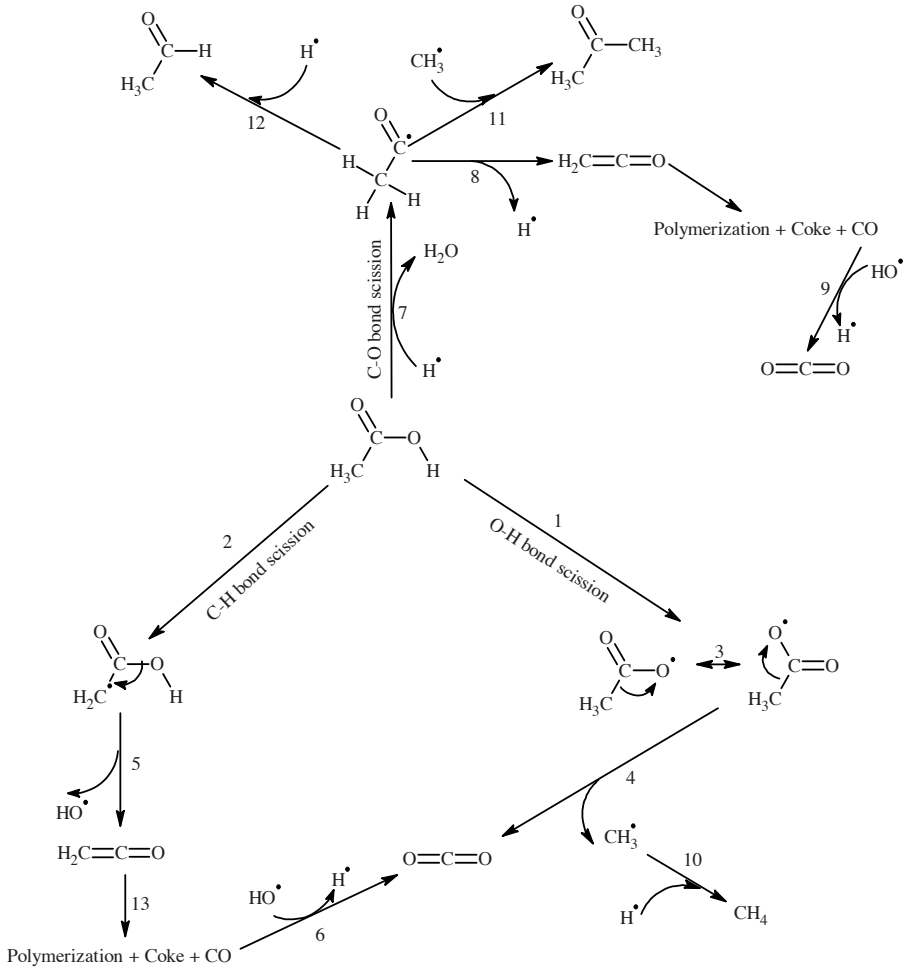

Figure 3.5: Postulated reaction mechanism of acetic acid decomposition in SCW (To keep the scheme simpler, C–H and O–H bond scission reactions are just indicated and the reaction pathways are analogous to those shown in Figure 3.4).

According to Meyer *et al.*[96] acetic acid does not decompose up to temperatures of 400 °C and it starts to decompose into CH_4 and CO_2 at above 450 °C. Watanabe *et al.* [97-98], found that acetic acid was very stable in the absence of any additive at 400 °C after 1 h of reaction time. They proposed two reaction schemes, monomolecular decarboxylation (CH_4 and CO_2) with the addition of KOH and bimolecular decarboxylation (acetone and CO_2) in the presence of ZrO_2.

The dissociation energies of different bonds present in acetic acid are as follows: D(CH_3COO–H) = 105.8±2 kcal/mole, D(H–CH_2COOH) = 98±2 kcal/mole (assumed to be the same as D(H–CH_2COCH_3).[99] Although D(CH_3COO–H) > D(H–CH_2COOH), the experimental data show that the O–H bond is more likely to break. In case of breaking of C–H bond breaking in H–CH_2COOH (path 2 and 4-6 in Figure 3.4), a ketene (CH_2CO) is formed (via dehydration). Generally, ketenes are very reactive and convert into polymeric compounds and gases: coke (carbon), resin, CO, CO_2.[100] However, no large fraction of coke was formed.

The overall reaction scheme for acetic acid considering COO–H bond breaking is:

$$CH_3COOH \rightarrow CH_4 + CO_2$$

The GC–MS analysis of the liquid samples indicated the presence of acetic acid in significant amounts. A minor amount of acetone is also detected in the liquid phase, for which the formation route is also shown in the proposed mechanism (Figure 3.5). The dominating pathway, however, proceeds via an O–H bond scission, resulting in the formation of equimolar amounts of CO_2 and CH_4 (Figure 3.3).

3.3.1.2 Propionic acid and other high molecular weight acids

For propionic acid decomposition a proposed mechanism is shown in Figure 3.6. The GC–MS analysis of the liquid phase product after the reaction identified propionic acid and acetone as main components (next to water) in the liquid phase. Very small amounts of acetic acid were detected in the liquid phase, indicating that breaking of C–C bond (pathway 16 followed by 17) now also occurs as initial step. Once acetic acid forms, it can produce acetone, CO_2 and water via bimolecular decarboxylation.[101] Small amount of benzene is also present in the liquid, pointing to the occurrence of aromatization reactions, leading to the formation of very stable aromatic compounds.

From the GC–MS analysis the major compound found in the liquid phase after the reaction was, however, the unconverted acid itself (> 95% of the organic compounds in the aqueous phase). Acetic acid was the major refractory compound that was identified in all the acid cases (except for formic acid decomposition), indicating the scissioning of C–C bonds leading to the formation of lower acids, which will then further undergo C–C cracking till acetic acid forms.

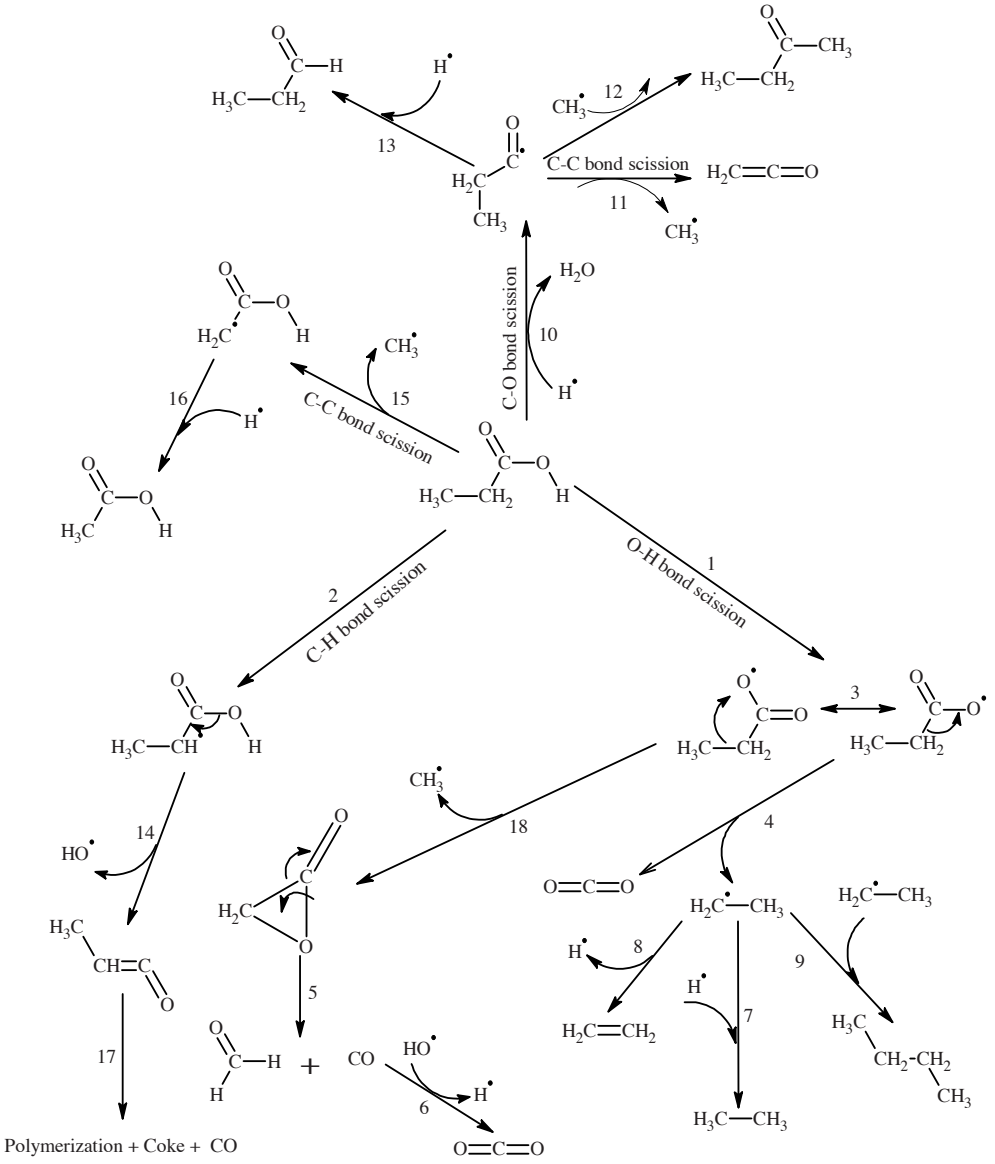

Figure 3.6: Postulated reaction mechanism of propionic acid decomposition in SCW (To keep the reaction scheme simpler, C–H and O–H bond scission reactions are just indicated and the reaction pathways are analogous to those shown in Figure 3.4).

Acetic acid may convert into acetone by bimolecular decarboxylation.[101] Acetic acid and acetone are the most stable compounds. For lower acids, up to C_4, acetic acid was present in small amounts while for higher acids, acetic acid was the most abundant compound in the liquid phase. That is in–line with concept that higher hydrocarbons are easier to crack.[102] Benzene and toluene were found in small amounts when gasifying higher acids, indicating the aromatization reactions. For higher acids we suspect that abstraction of α–hydrogen becomes significant, leading to the formation of ketene. Jin *et al.* have studied the oxidation reactions of high molecular weight carboxylic acid (stearic acid) in SCW and they proposed the reaction of high molecular weight carboxylic acids in SCW proceeds with the consecutive oxidation of higher molecular weight carboxylic acids to lower molecular weight carboxylic acids through several major pathways.[103]

Overall, it is found that the gasification of linear carboxylic acids in supercritical water starts predominantly with the scissioning of the O–H bond of the acid group. Subsequently, β scissioning is dominating in fractionation and gas formation, as argued below.

With this simple approach, the characteristic oscillatory behaviour of the gas product distribution with increasing alkyl chain length, as observed in Figure 3.3a, can be explained. In case of an even numbered carbon organic acids, initial acidic O–H bond scission followed by β scission leads to formation of CO_2 and a (n–1; hence odd number) alkyl radical. Continued β scission leads to significant C2 formation and ends by the formation of a CH_4 molecule (from CH_3 radical). For an odd numbered carboxylic acid, this process does not lead to the formation of a final CH_4 molecule.

Exact this oscillatory behaviour of the gas composition trend is seen in Figure 3.3 where more CH_4 and less C_2H_6 have been found in case of even numbered carbon organic acids. The oscillatory behaviour is super–positioned to another general trend that with increasing chain length more CH_4 is formed (Figure 3.3 b), most likely due to the increasing number of possible reactions and interactions between intermediates and apparently also resulting in more CH_4.

The oscillations in the GE trend (Figure 3.2) cannot be explained by this, but may be caused by constraints in the chemical analysis. When *e.g.* C_2H_5 radicals recombine with other alkyl radicals this leads to the formation of alkanes larger than butane which were not detectable by the installed GC. This may be the reason of our GE trend in which, in case of even numbered carbon acid GE is higher than for odd numbered carboxylic acids.

A simple model was developed to estimate the product gas distribution of different chain lengths of organic acids. Figure 3.7 is the model predictions of product gas distribution from different chain lengths of organic acids. Two assumptions were made for the model development that is complete conversion of acids to product gases and 75% conversion of C2

compounds that is initially formed via β scission as described earlier to methane formation according to following reaction given below.

$2C_2H_6 \rightarrow CH_4 + C_3H_8$

It is evident that the oscillatory behaviour of alkanes (CH_4 and C_2H_6) and the decreasing trend of H_2 and CO_2 from the experiments shown in Figure 3.3 are very well in line with model trends presented in Figure 3.7.

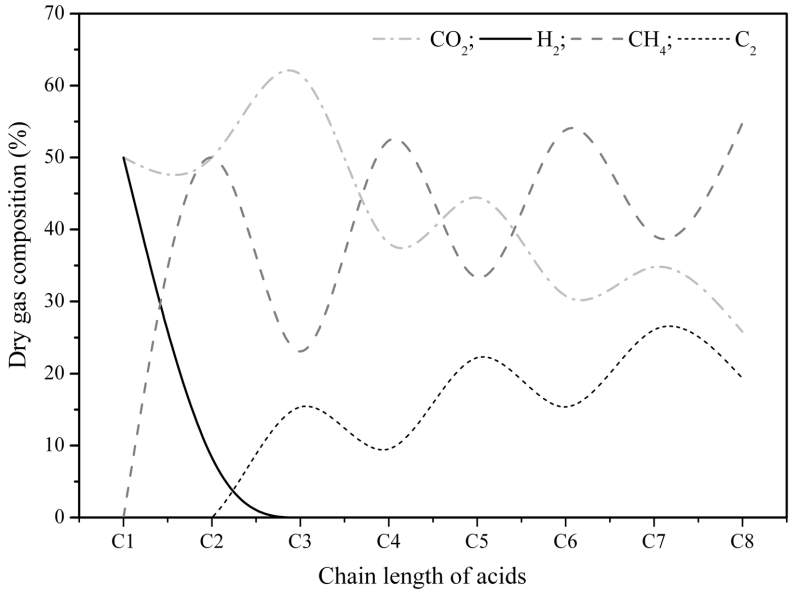

Figure 3.7: Model predictions of dry gas composition of different chain lengths of organic acids.

3.3.2 GASIFICATION OF ALCOHOLS

In this section results for a study on the influence of the alkyl chain lengths of linear n–alcohols ranging from C_1–C_8 on the gasification behaviour in supercritical water will be reported.

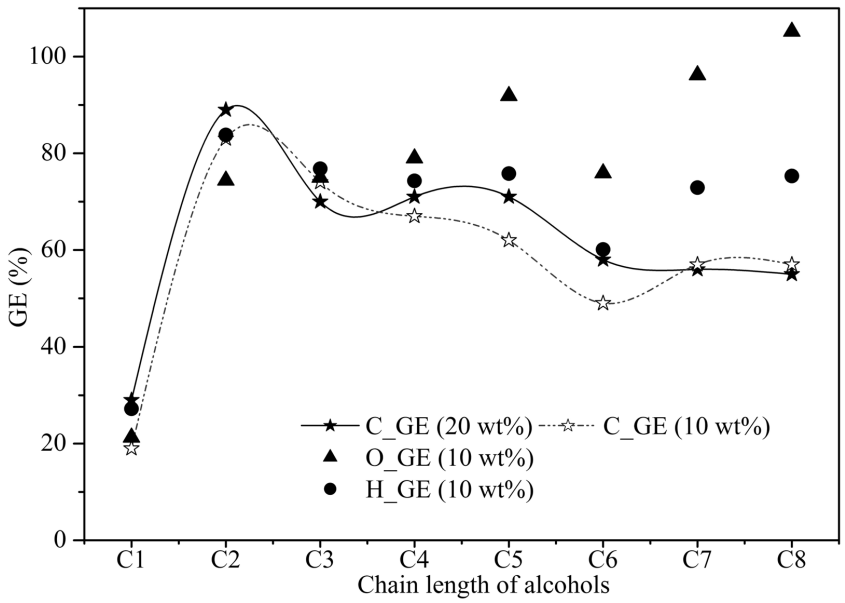

Figure 3.8: The gasification efficiencies of different chain lengths of alcohols (carbon GE was shown for 20 and 10 wt% feed concentration while the oxygen and hydrogen GE was shown for 10 wt% concentration).

The carbon GE trend for alcohols of different chain lengths, using 10 and 20 wt% solutions, is shown in Figure 3.8. It is evident from the figure that methanol has the lowest GE and ethanol the highest. After ethanol, a slight decrease in GE with increasing chain length is noticed. This can be attributed to the formation of intermediate compounds and their polymerization reactions leading to the formation of tar and char eventually reducing the GE. The alcohol concentration itself was found to have a minimal impact on the carbon GE, see Figure 3.8. This is in contrast with earlier findings for the gasification efficiency for organic acids of different chain lengths; see Figure 3.2 for comparison, where the concentration effect is significant.

The product gas composition (vol%) and yields (mole/mole) for different chain lengths of alcohols is shown in Figure 3.9 a and b respectively. From Figure 3.9 a, major differences in the gas composition is noticed until the C_3 compound and after C_3 (1–propanol), the dry gas composition doesn't change much with increasing chain length, except for carbon distribution over CO and CO_2. The dry gas composition on gasification of alcohols with increasing alkyl chain length shows opposite trends for CO and CO_2, for which no explanation was found. The sum ($CO+CO_2$) is however consistent and in line with the carbon to gas conversion and

also the oxygen balance (see Figure 3.8) shows a monotonous trend with chain length, despite the large variations in CO and CO_2 fraction.

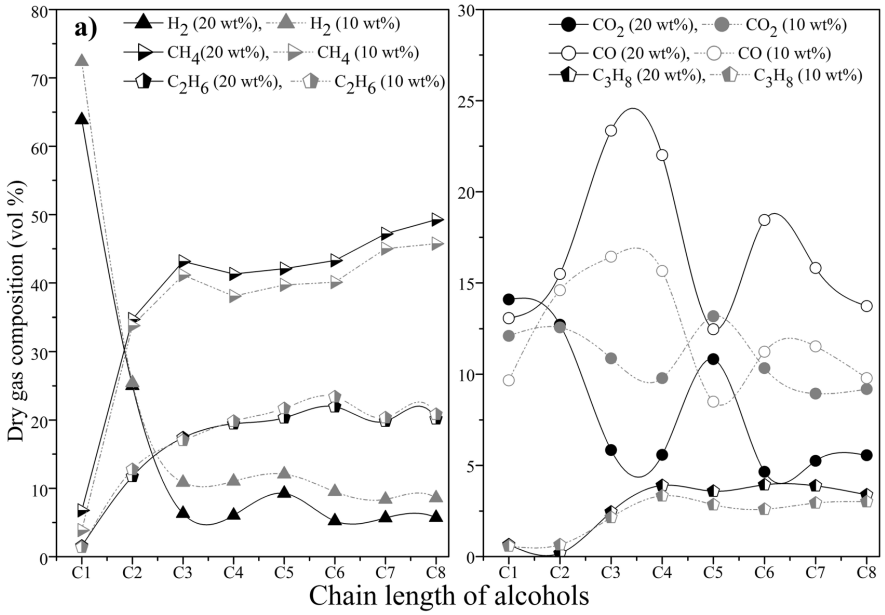

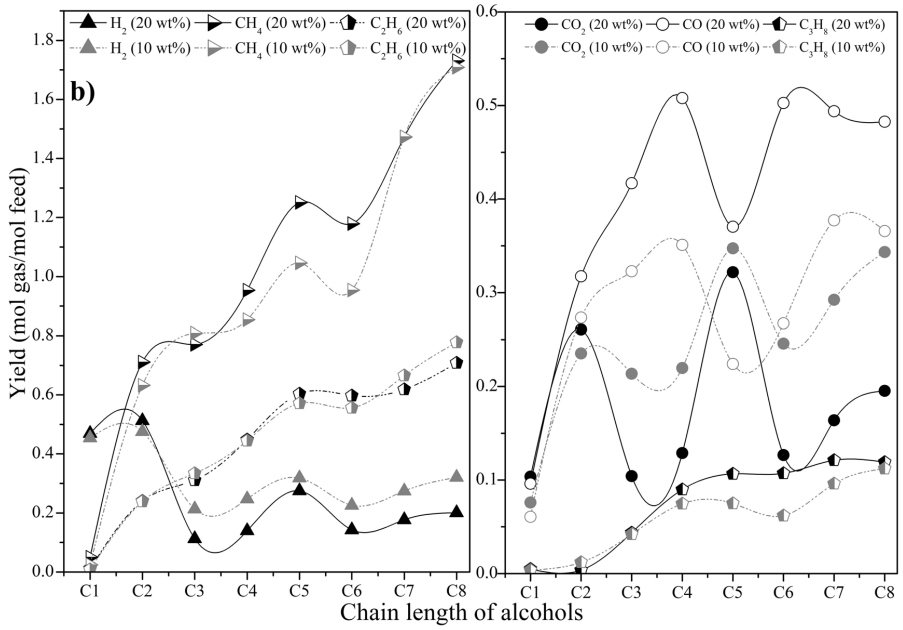

Figure 3.9: The influence of different chain lengths of organic alcohols on *a)* dry gas composition (vol%) *b)* product gas yields (mol/mol). Dark and thick symbols corresponds to 20 wt% organic concentration, light and dotted trend lines represent 10 wt% organic concentration.

The difference between the total moles of oxygen atoms in the ($CO+CO_2$) formed, being the oxygen–containing gases, and the moles of gasified (parent) organic alcohols will give an estimation of the moles of oxygen atoms that must have transferred to– or from water.

The oxygen and hydrogen gasification efficiencies for 10 wt% feed concentrations are higher than the carbon gasification efficiency after C2 compounds (Figure 3.8). From the oxygen–atom balance, the number of moles of oxygen atoms released equals the moles of organics gasified. A large fraction of that oxygen is recovered in the gas phase in the form of CO and CO_2 and the rest will be used to produce water via dehydration reaction. The opposite, more oxygen atoms in the gaseous products than released by the gasification of the organic molecules ('oxygen excess') is also possible. In that case, oxygen is obtained from the water phase and used to form CO_2 and additional hydrogen.

From the increase in the gap between CO and CO_2 with increasing organics concentration (Figure 3.9 a and b) it is suggested that this may have a large influence on the WGS reaction, as the water concentration is decreasing when going from the 10 wt% to the 20 wt% series.

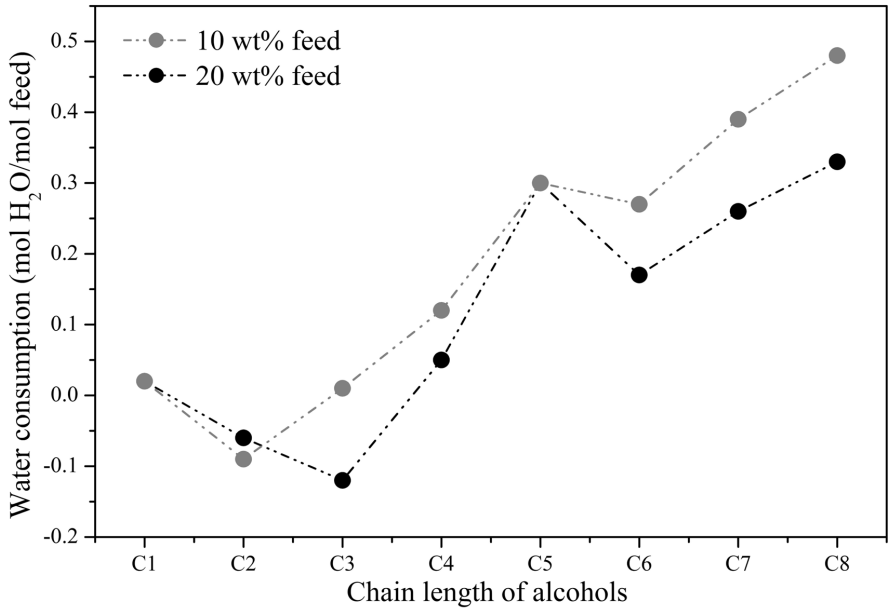

Figure 3.10: The extent of water consumption for different chain lengths of alcohols.

The calculated oxygen–based GE was found to be higher than the carbon–based GE from C_4–C_8 alcohols, suggesting the participation of water in the reaction. The number of moles of water consumed per mole of organics with increasing chain length for the alcohols can be appreciated from Figure 3.10. This implies that with increasing chain length the extent of dehydration reaction decreases, indicating that C–OH bond becomes more relatively more difficult to rupture in comparison to the other bonds and C–C bond cracking becomes dominant as we increase the chain length; which is in–line with findings for thermal cracking of hydrocarbons.[99, 104] Dehydration reactions become negligible after butanol and there is no significant influence of concentration on the extent of dehydration reaction.

3.3.2.1 Methanol

In the absence of any catalyst and at temperatures below 600 °C in SCW, methanol is confirmed in this work to be a stable compound.[105] The activation energies for pure methanol are reported as high as 191 kJ/mol, whereas the activation energy for ethanol was reported to be 145 kJ/mol.[106-107]

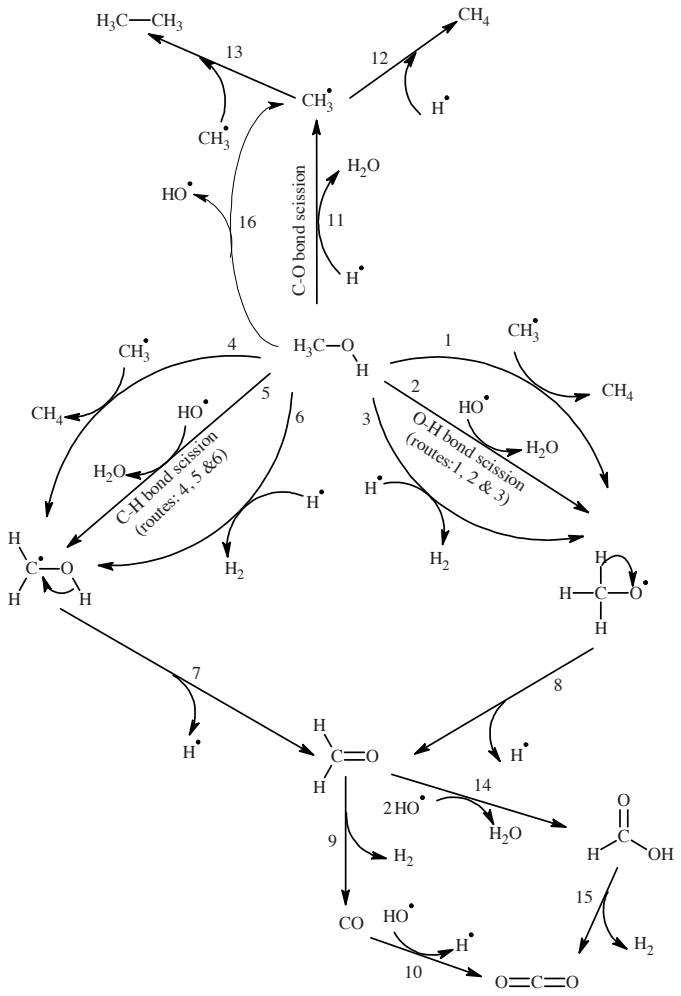

Figure 3.11: Postulated reaction mechanism of methanol decomposition in SCW (reactions are indicated with numbers).

A postulated mechanism for the methanol decomposition based on the experimental results and literature[97, 106-109] in SCW is shown in Figure 3.11. Routes 1–3 are the abstraction of acidic hydrogen at oxygen atom that leads to formation of $H_3CO^{\bullet}$ radical which decomposes into formaldehyde and releases one $H^{\bullet}$ (route 8). The formaldehyde that is formed can either decompose directly into CO and H_2 (route 9) or it can oxidise into formic acid which then further decompose to CO_2 and H_2. An alternative initiation reaction is the abstraction of the

hydrogen at the α–carbon atom (reaction 4–6), which may again lead to formaldehyde (route 7). The scission of the C–O bond, Route 11, is the dehydration route in which a $H^{\bullet}$ radical reacts with an OH group present in the compound and forms water and $CH_3^{\bullet}$, which will lead to methane formation. The methyl radical can further take part in many other routes, as shown in Figure 3.11. Considering the gas composition it can only be concluded that C–O bond breaking, leading to CH_4 formation, is the least favoured initiation pathway, since the CH_4 yield was found to be very low. The two other reaction pathways, C–H and O–H bond breaking, lead to a similar product composition ($CO+2H_2$).

The overall reaction stoichiometric for 20 wt% methanol concentration, as based on the experimental gas yields and methanol to gas conversion, can be written as:

$$29CH_3OH + 3H_2O \rightarrow 47.25H_2 + 5CH_4 + 11CO + 10.5CO_2 + 1.25C_2H_6$$

Traces of formic acid and formaldehyde were reported to be present in the effluent liquid of methanol decomposition in SCW[106, 108] using HPLC analysis and were also found in this study.

The relative low GE of Methanol (Figure 3.) in a metal reactor compared to other studies[110] show that the catalysis of the reactor wall is of minor importance here. Possible explanation is the relative low surface-to-volume ratio and perhaps passivation reducing the catalytic effect.

3.3.2.2 Ethanol

A postulated mechanism for the ethanol decomposition in SCW is shown in Figure 3.12. Considering the experimentally found gas composition it can be seen that all the three routes, C–O bond breaking, C–H, hydrogen abstraction and O–H, hydrogen abstraction are competing each other. Unlike the case of methanol where C–O bond cleavage was least favourable, here the presence of C_2H_6 in significant amounts indicates that C–O bond cleavage is also a significant reaction pathway. According to the scheme in Figure 3.10, the initiation by O–H bond scission and followed by C–C scission should results in around 50% carbon selectivity towards CH_4. The dry gas composition in Figure 3.9 b confirms therefore that this pathway is likely to dominate.

GC–MS analysis of the liquid phase showed that ethanol is the only significant product present in the liquid phase. Writing the reaction pathways for ethanol gasification in SCW in simple equations is given below:

C–O bond scission: $CH_3CH_2OH + H_2 \rightarrow CH_3CH_3 + H_2O$

O–H bond scission: $CH_3CH_2OH \rightarrow CH_4 + CO + H_2$

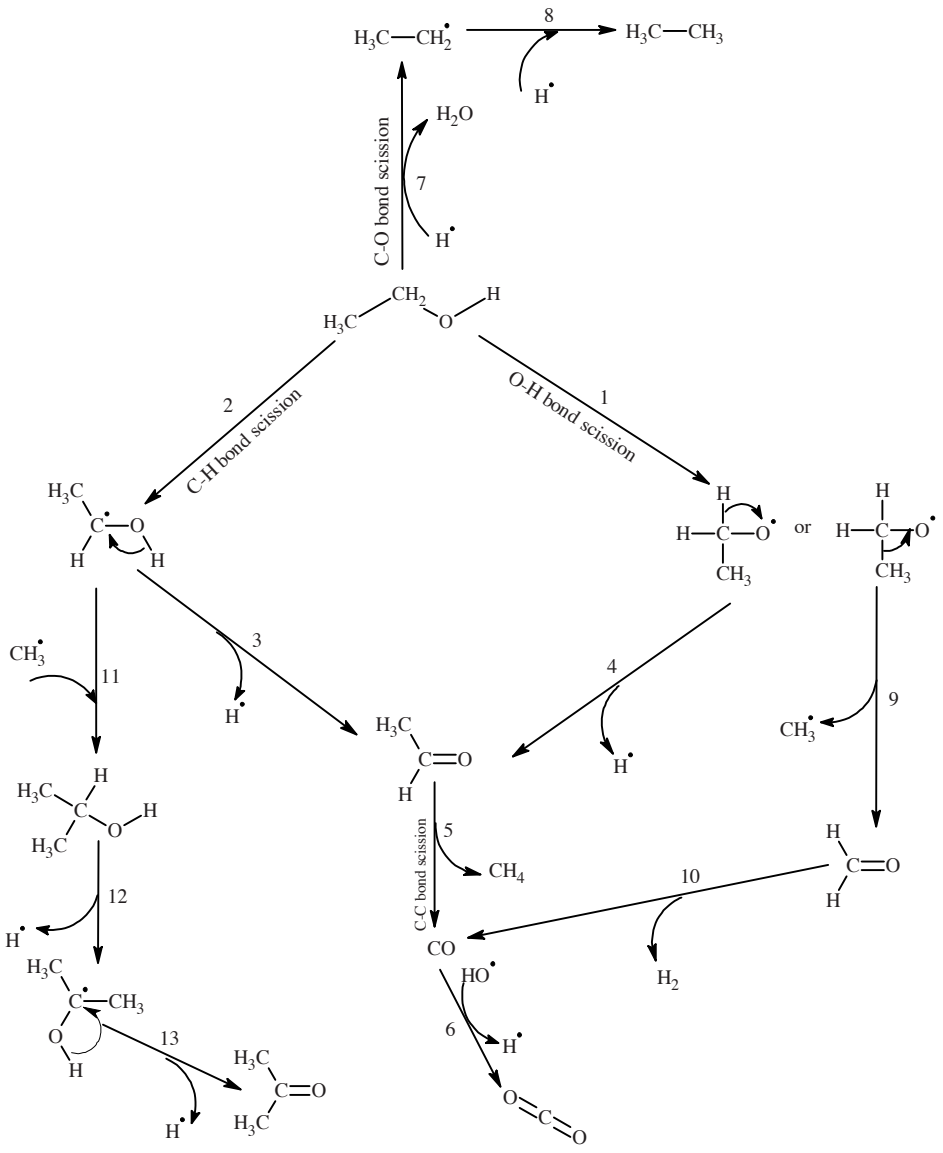

Figure 3.12: Postulated reaction mechanism of ethanol decomposition in SCW (To keep the reaction scheme simpler, C–O and C–H bond scission reactions are just indicated and the reaction pathways are analogous to those shown in Figure 3.10).

The overall reaction considering the experimental gas yields of 20 wt% ethanol to gas conversion can be written as:

$$89C_2H_5OH \rightarrow 49H_2 + 71CH_4 + 33CO + 26CO_2 + 24C_2H_6 + 4H_2O$$

Arita *et al.*[111] have reported the conversion of ethanol to hydrogen in supercritical water at 450–500 °C in a quartz reactor and proposed two reaction schemes, based on dehydrogenation and dehydration. Ethanol dehydrogenation was the major pathway that leads to acetaldehyde, which further decomposes to CH_4 and CO, which is in–line with our proposed scheme shown in Figure 3.12. The CO formed reacts via WGS to CO_2 and produces H_2. Acetaldehyde and trace amounts of methanol were detected in the effluent liquid of ethanol reforming in SCW.[112]

3.3.2.3 1–propanol and higher alcohols

A similar radical reaction mechanism is postulated for 1–propanol and is shown in Figure 3.13. It can be noticed that the schemes are rapidly gaining complexity going from methanol to ethanol to 1–propanol. The GC–MS analysis of the liquid phase after reaction showed the presence of significant amounts of unconverted 1–propanol in the liquid phase (as dominant compound). Small amounts of benzene and toluene are also detected in liquid phase, indicative for the occurrence of aromatization reactions. The GC–MS analysis of liquid phase products for other, higher alcohols (here: 1–butanol, 1–pentanol, 1–hexanol, 1–heptanol and 1–octanol) showed predominantly the presence of unconverted alcohols and some acetone and only very minor amounts of aromatic compounds derived from aromatization reactions. Kruse *et al.*[83] have studied the conversion of different C_4 compounds (1–butanol, 1–butanal, cis–butene–diol) in a batch reactor at 500 °C, 300 bar for 1 h and also reported the formation of aromatic rings (*e.g.*, phenol, benzene, toluene, alkylbenzenes, alkylphenols, phenylethanones) for each of the C_4 compounds studied.

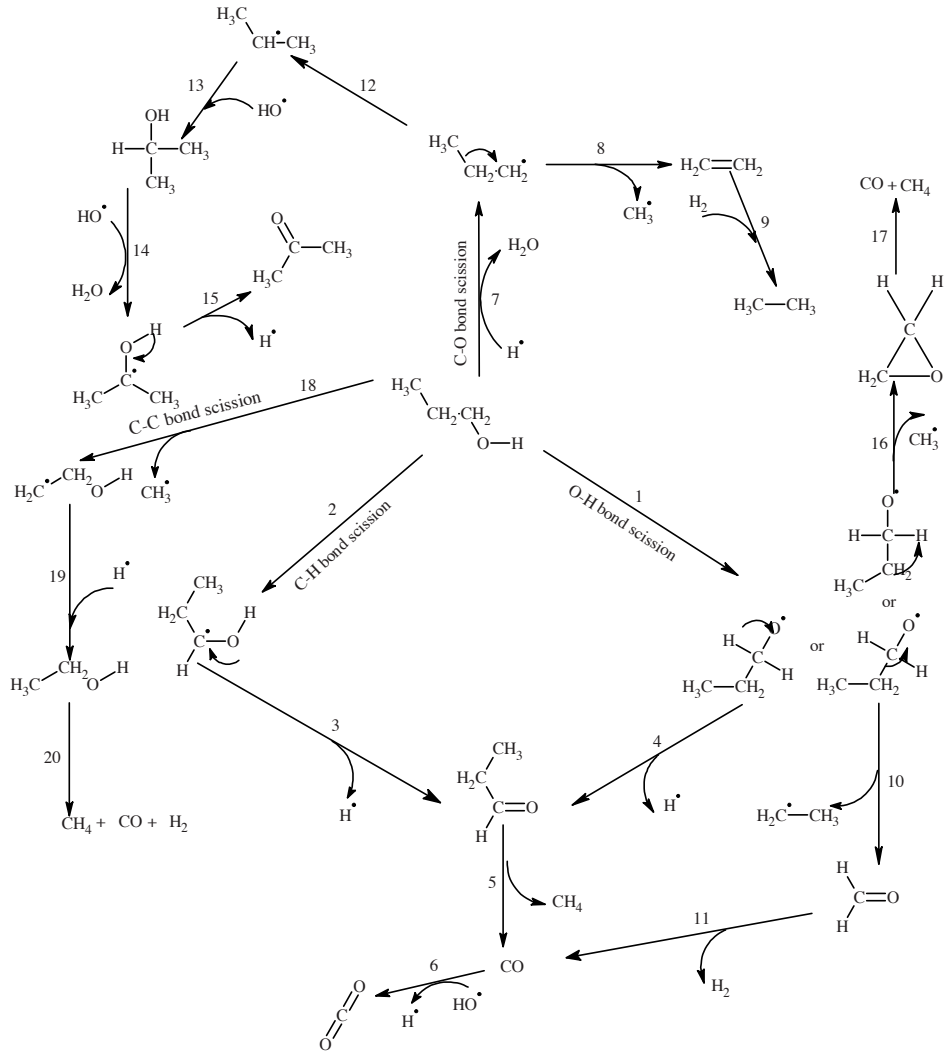

Figure 3.13: Postulated reaction mechanism of 1–propanol decomposition in SCW (To keep the reaction scheme simpler, C–O and C–H bond scission reactions are just indicated and the reaction pathways are analogous to those shown in Figure 3.10).

3.3.3 INFLUENCE OF OH GROUPS ON GASIFICATION

3.3.3.1 Number of OH groups

Additionally we studied the influence of the number of OH groups and their position within the molecule on the product gas composition and gasification yield. To study the influence of number of OH groups, we chose 1–propanol, 1, 2–propanediol and glycerol containing one, two and three OH groups respectively as model compounds.

To study the influence of positioning of the OH groups, we chose 1–propanol and 2–propanol having one OH group at different locations. Another set of compounds used was 1, 2–propanediol and 1, 3–propanediol having two OH groups located at different positions.

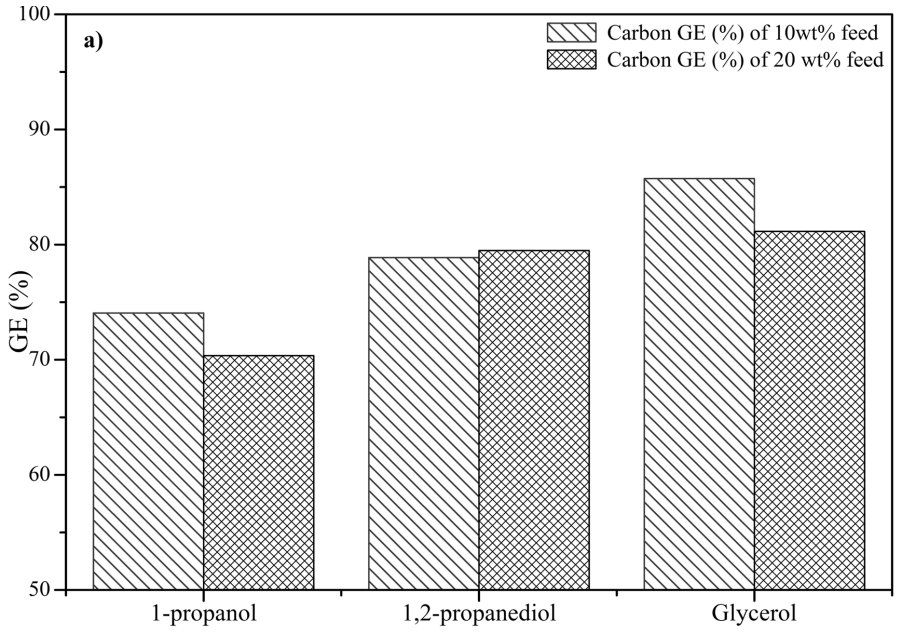

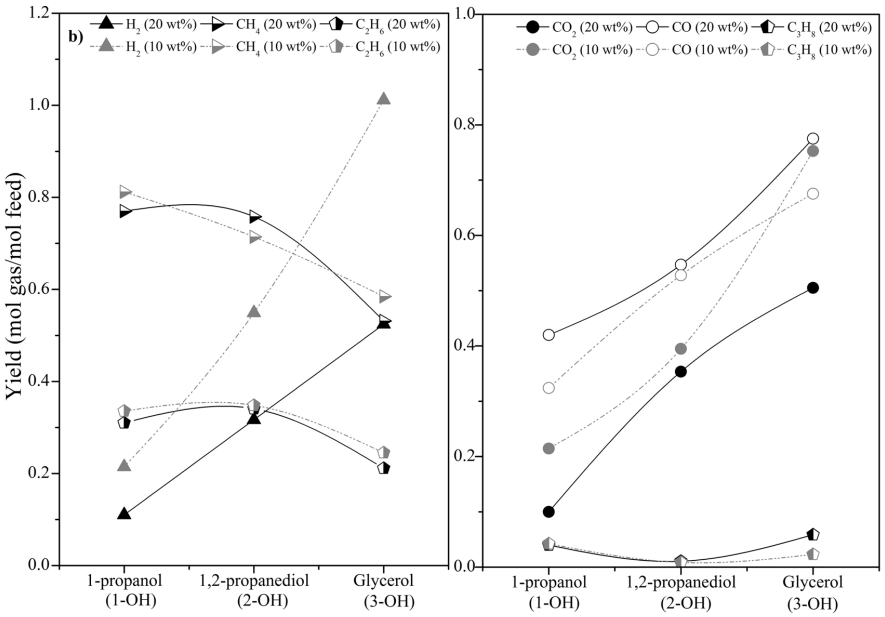

Figure 3.14: Influence of the number of OH groups on the gasification behaviour a) carbon to gas conversion b) product gas yields. Symbols with thick trend lines corresponds to 20 wt% organic concentration, symbols with dotted trend lines represent 10 wt% organic concentration.

The influence of number of OH groups on the GE and gas yields is shown in Figure 3.14 a and b. The initial feed concentration was found to have a minimal impact on the GE, which is in–line with the results of alcohols as discussed earlier. From Figure 3.14 a it is clear that the GE increases slightly with the number of OH groups in the compound. The number of hydroxyl groups in the alcohols also significantly affected the product gas yields which is evident from Figure 3.14 b. With increasing number of OH groups, the combined yield of CO and CO_2 increases about proportional, whereas the hydrogen yield increases clearly more than proportional. This latter effect may be related to an increased WGS activity, or an altered decomposition mechanism. The yield of alkanes decreases with an increase in the number of OH groups as more oxygen atoms are present in the reactant molecule and an increase in the number of sites that can be attacked by hydroxyl radicals with increase in number of OH groups. Additionally, an OH group stabilizes the intermediate radicals formed by its electron–releasing nature, easing the gasification process. As the number of OH groups increases, the intermediates that are formed become more and more stable.

3.3.3.2 Positioning of the OH groups

The influence of the positioning of OH groups at different locations in the molecular structure is studied with 1–propanol and 2–propanol, both having one OH group, and 1, 2–propanediol, 1, 3–propanediol, both having two OH groups, on the gasification efficiency and product gas yield is shown in Figure 3.15. It is clear from figure that the CH_4 yield is higher and less C_2H_6 is formed with 2–propanol than in case of 1–propanol. This can be explained assuming that β–scission is a significant (dominating) reaction pathway in the formation of gases. In case of 2–propanol, β–scission leads to mainly methane and CO, while in case of 1–propanol, β–scission leads to the formation of methane, ethane and CO.

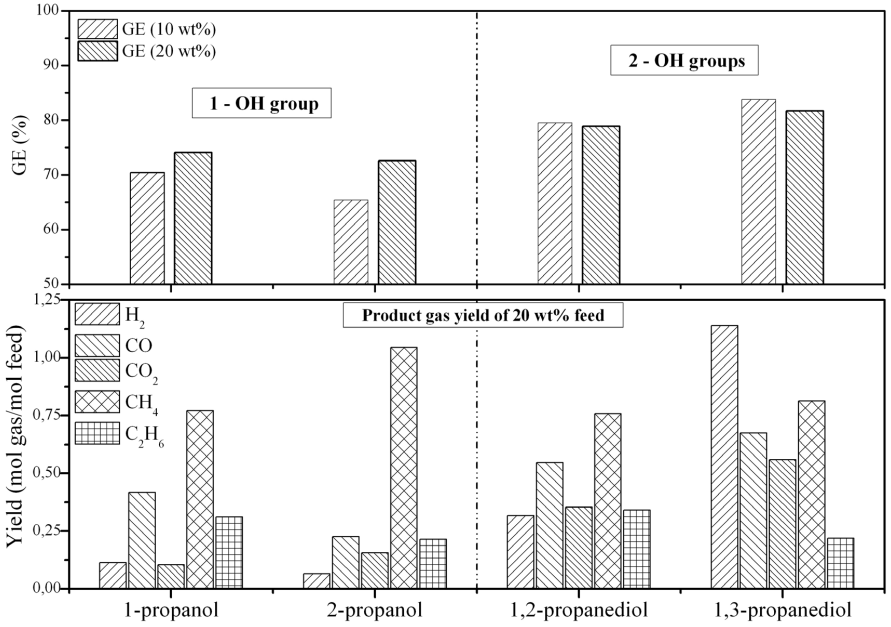

Figure 3.15: Effect of the positioning of OH group at different locations on the GE and product gas yields.

The hydrogen yield in case of 1, 2–propanediol is much lower than for 1, 3–propanediol and this clearly indicates the occurrence of dehydration reactions. The dehydration reaction is more favourable in case of 1, 2–propanediol than 1, 3–propanediol as explained below. In case of 1, 3–propanediol, there is only one available site for dehydration reaction to occur (*i.e.* extraction of the hydrogen atom present at second carbon atom followed by OH removal present at β position) and there are two factors that decelerate the dehydration route; steric hindrance

caused by the two OH groups that surrounds the hydrogen atom on the second carbon and the less stable radical formed in the absence of electron–releasing substituent, oxygen atom.

For dehydration reaction in case of 1, 2–propanediol there are three available sites where hydrogen can be extracted. Extraction of any hydrogen attached to carbon atom will lead to formation of a radical in which OH is present at β position and hence the chances of OH removal and hence dehydration reactions are much higher in case of 1, 2–propanediol than in case of 1, 3–propanediol.

3.4 CONCLUSIONS

The influence of alkyl chain length (C_1–C_8) for two homologous series of acids and alcohols as well as the number of OH groups and their position on a C_3 backbone on the gasification behaviour in supercritical water is studied. Alcohols were found to be easier to gasify than the corresponding acids. With increasing the chain length of acids from C_1–C_8, the gasification efficiency (GE) initially decreases drastically and then stabilises. While formic acid converts completely to gases, the rest of acids are quite prone to conversion. Also the initial acid concentration has a high impact on the gasification efficiency. Acids with an even number of carbon atoms were found to have high GE than the adjacent odd carbon atoms. A remarkable oscillating trend for the CH_4 and C_2 yield with increasing carbon number was noticed from the experimental data, but can be understood and explained on basis of the reaction mechanisms postulated in this work, characterized by an initiation step via O–H scissioning and subsequent β–scission reactions. Similarly, less C_2H_6 yields was observed with even numbered carbon atoms than for their adjacent odd numbered carbon atoms.

The carbon GE trend of alcohols was quite opposite to that of acids. Methanol was quite prone to gasify, while the other alcohols are easier to convert. The GE is however not strongly influenced by the alcohol concentration and marginal amounts of tar and char formation is noticed with higher alcohols. The electron donating nature of OH group increases the rate of gasification by stabilizing the intermediate radical formed and we found an increase in the GE with an increase in number of OH groups. Increase in the number of OH groups decreases the formation of hydrocarbons and increases CO formation, which subsequently leads to more CO_2 and H_2. The position of OH group has no influence on the gasification efficiency. The dehydration reaction was enhanced in case of adjacent OH groups.

Chapter3

Chapter 4

Hydrogen from ethylene glycol by supercritical water reforming using noble and base metal catalysts[3]

[3] This chapter is an excerpt of paper published as:

De Vlieger, D. J. M.; Chakinala, A. G.; Lefferts, L.; Kersten, S. R. A.; Seshan, K.; Brilman, D. W. F., Hydrogen from ethylene glycol by supercritical water reforming using noble and base metal catalysts. Applied Catalysis B: Environmental 2012, 111-112, 536-544.

Chapter 4

4.1 INTRODUCTION

Currently, hydrogen is mostly produced by the steam reforming of natural gas and other fossil feedstocks. Hydrogen is widely used in the ammonia industry, oil refining and food industry. It is foreseen that the demand for hydrogen will increase in the future for bio-refinery applications.[113-115] In order to meet the projected hydrogen demands more sustainably, hydrogen from bio-renewable organic sources is an elegant solution. This also helps mitigate the environmental concerns associated with the use of the depleting fossil fuel reserves.

The conversion of the aqueous bio/organic wastes (>80% water) into high heating value products such as hydrogen, syngas (CO/H_2) and methane using conventional reforming processes at lower pressures is energy intensive due to the need for the evaporation of water. Currently, two efficient ways of converting the low heating value aqueous wastes are reported.[116-118]

First is the so called "aqueous phase reforming" (APR) developed by Dumesic *et al.* [116, 119-120], in which the oxygenate feeds are reacted at mild temperatures in pressurized liquid water (225–265 °C, 29–56 bar) over supported metal catalysts. Supercritical water gasification (SCWG) is another process, wherein the properties of supercritical water are exploited for the reforming of organics in the aqueous stream into gaseous products.[8, 117, 121-122] At sub- and near critical conditions (T: 375 °C, P: 220 bar), thermodynamics favour selectivities towards alkanes in preference to hydrogen.[123] Higher temperatures above 600 °C are required to enhance hydrogen formation. Therefore, the need for catalyst arises to steer the product gas selectivities towards hydrogen and to achieve complete carbon to gas conversion at near critical conditions.

Catalysts for APR and SCWG should be active for C-C bond scission in order to be able to decompose the organic molecules and they should further enhance the water gas shift (WGS, $CO + H_2O \rightarrow CO_2 + H_2$) reaction to maximize hydrogen yields. Methanation ($CO_x + (2+x) H_2 \rightarrow CH_4 + xH_2O$) and Fischer Tropsch ($CO + 2H_2 \rightarrow -CH_2- + H_2O$) are undesired side reactions, as they consume the desired product, H_2. In order to suppress these reactions, catalysts should not be active for the scission of C–O bond.[124] Lower alkane selectivities are therefore expected for catalysts with low affinity towards C-O bond scission.

Davda *et al.*[124] reported the relative activities of different metals for C–C bond breaking, C–O bond activation, and WGS reaction. They reported that Ru, Ir and Ni showed high activities for C–C bond breaking, further Ru and Ni metals showed high activities for methane formation. Ir showed very low methanation activity but in contrast to Ru and Ni, almost no WGS activity was reported. Ir is a promising catalyst for breaking down oxygenated hydrocarbons via C–C bond scission. Adsorbed oxygenate fractions on the catalyst surface

resulting from C–C bond scission undergo dehydrogenation, yielding H_2 and CO.[124] Davda *et al.* [9]concluded that for the APR process, metals such as Pt, Pd and Ni–Sn alloys showed higher selectivities towards hydrogen when compared to Ni, Ru and Rh, which tend to make more alkanes and very less hydrogen.

Elliott *et al.*[125] tested several base and noble metal catalysts for the conversion of p-cresol in subcritical water (350 °C and ~200 bar) and identified Ni, Ru and Rh to be the most active metals for the reaction, but catalyst stability was a major problem. However, Ru was reported to be relatively stable catalyst for C–C bond breaking under hydrothermal conditions but almost complete conversion to methane rich gas was observed in the case of ethylene glycol.[9] Byrd *et al.*[126] also studied the catalytic properties of Ru/Al_2O_3 for supercritical reforming of glycerol at 750–800 °C and found full conversion using a 40 wt% glycerol solution, but also observed the formation of considerable amounts of undesired methane. Kersten *et al.*[54] observed full conversion for reforming of a 17 wt% glucose solution to methane rich product gas at 600 °C using a 3 wt% Ru/TiO_2 catalyst.

Ni based catalysts have been frequently explored for gasification of oxygenates (glucose, phenol, methanol) under supercritical conditions.[105, 117, 127-128] Ni based catalysts are generally active for gasification, but often tend to deactivate due to sintering and or coke formation.[105, 117] Selectivities to hydrogen and methane vary significantly in the studies reported and the choice of support seems to have a strong influence.[129] An unsupported Ni metal wire gave high hydrogen selectivities when methanol was used as reactant.[105]

Under subcritical conditions $Pt/\gamma\text{-}Al_2O_3$ is reported to be a stable catalyst showing high activity and selectivity towards hydrogen formation for APR of different model oxygenates namely methanol, ethylene glycol, glycerol and sorbitol.[116, 120, 124] One of the key steps in the APR reaction is the dehydration of oxygenates, which typically leads to hydrocarbon based species.[124]

Bio-liquids (aqueous phase of bio-oil for example) typically contain oxygenate concentrations in the range of 15–20 wt%. It was already reported that, under supercritical reaction conditions, the reforming of a solution containing at least 15 wt% oxygenate is required to be economically viable under supercritical conditions.[22] The target of this study is the development of an efficient catalyst for maximizing hydrogen yields during reforming of a typical oxygenate such as ethylene glycol taking advantage of the beneficial effects of high reaction rates in supercritical water. Catalyst design should take into account minimization of alkane selectivity which can be caused by dehydration of oxygenates as well as C–O bond

hydrogenolysis, *i.e.*, methanation. Further, minimizing coke formation and catalyst deactivation is of importance for practical applications.

Based on the information available for subcritical reforming and discussed above in terms of H_2/CH_4 selectivities and maximizing hydrogen yields, three monometallic catalyst systems Pt, Ir and Ni were chosen for the reforming of ethylene glycol as a model oxygenate in supercritical water. Development of a bimetallic Pt–Ni catalyst for the efficient production of hydrogen from ethylene glycol is discussed.

4.2 EXPERIMENTAL SECTION

4.2.1 CATALYST PREPARATION

Extrudates of γ-alumina (BASF AL-3992) were crushed and sieved to obtain particles within a size range of 300–600 μm and were used as catalyst support. $H_2PtCl_6 \cdot 6H_2O$, $IrCl_4$ and $Ni(NO_3)_2 \cdot 6H_2O$ precursors (analytical grade>99.9%) were obtained from Alfa Aesar. Mono- and bimetallic catalysts were prepared by wet (co) impregnation. The desired amount of precursor(s) was dissolved in water and added to the γ-alumina support (weight ratio H_2O/alumina = 1.8). The water was evacuated under vacuum at 100 °C. Catalysts made with Cl containing precursors were treated at 100 °C for 5 h (10 °C min^{-1}) under hydrogen (100 ml/min H_2 and 100 ml/min N_2) to remove any residual Cl.[130] Materials were finally calcined at 500 °C for 15 h (10 °C min^{-1}) under air (200 ml/min).

4.2.2 CATALYST CHARACTERIZATION

Metal loadings on the γ-alumina support were determined using a Philips X-ray fluorescence spectrometer (PW 1480). Surface areas of the catalysts were measured applying the BET method on an ASAP 2400 (Micromeritics). Metal dispersions were determined with pulse CO chemisorption at room temperature on 100 mg of catalyst using a Micromeritics Chemisorb 2750. CO/M ratios of 1 were assumed for all the catalysts. Before pulsing, the catalyst was reduced in H_2 at 400 °C for 1 h and cooled down in helium to room temperature subsequently. Average metal particle sizes for monometallic catalysts were calculated based on dispersion values, assuming hemispherical particle shape. X-ray diffraction (XRD) patterns were collected over the range 2θ = 20–75° on a Philips X'pert device using Cu Kα1 radiation source. X-ray spectra obtained were compared with the JCPDS/ICDD database. Spent catalysts were analyzed by TGA-MS to determine any coke deposits on the surface. Argon with 1 v/v% O_2 was flown over the catalyst while the temperature was increased from 25 to 800 °C. The weight of the catalyst was monitored by TGA and the composition of the gas output was

analyzed by MS. TEM imaging and temperature programmed reduction (TPR) was further used to characterize the catalysts. Catalysts (100 mg) studied by TPR were first heated up to 500 °C in oxygen (5% O_2/95% He) and then cooled down to room temperature in argon to remove any moisture from the surface. TPR experiments were carried out in a 10 ml/min hydrogen flow (5% H_2/95% Ar) and the temperature was increased to 10 °Cmin^{-1}. Consumption of hydrogen was taken as measure of reduction and plotted as function of temperature.

4.2.3 CATALYTIC TESTING

Figure 4.1 shows the schematic diagram of the continuous flow supercritical water reformer used in this study. A 2 ml/min flow of ethylene glycol (≥99% Sigma Aldrich) solution (typical concentrations in the range of 5–30 wt% are used depending on the experiment) was preheated to 450 °C at a pressure of 250 bar. After preheating, the solution entered a 63 cm long reactor (ID = 7 mm) in which 1.0 g of catalyst was placed. The reaction was performed at 450 °C and 250 bar. Under these conditions water is in the supercritical regime. The reactor effluent was cooled down to room temperature with a counter-current heat exchanger and pressure was reduced by a back pressure regulator to atmospheric pressure. A 500 ml glass bottle was used to allow the separation of gas and liquid products. The amount of gas produced was measured with an Actaris Gallus 2000 gas meter and the gas composition was analyzed with a Varian CP4900 micro-GC equipped with a MS5 and PPQ column. Carbon content analysis of the feed solution and the liquid product was conducted using an Interscience Flash 2000 Organic Elemental Analyzer. Elemental analyzer was used to determine the unconverted carbon content and HPLC analysis was done to identify the intermediate compounds present in the liquid. The flow rate of the feed stream and the amount of liquid product formed were monitored using balances under the respective glass vessels. Weight hourly space velocities (WHSV, g of ethylene glycol per g of catalyst per h) of EG for reforming of 5 and 15 wt% ethylene glycol solutions were, respectively, 5.9 and 17.8 h^{-1} and the residence time in the catalytic bed was 1.3 sec (density of water at reaction conditions (here: T = 450 °C and P=250 bar) is 109 kg/m^3).

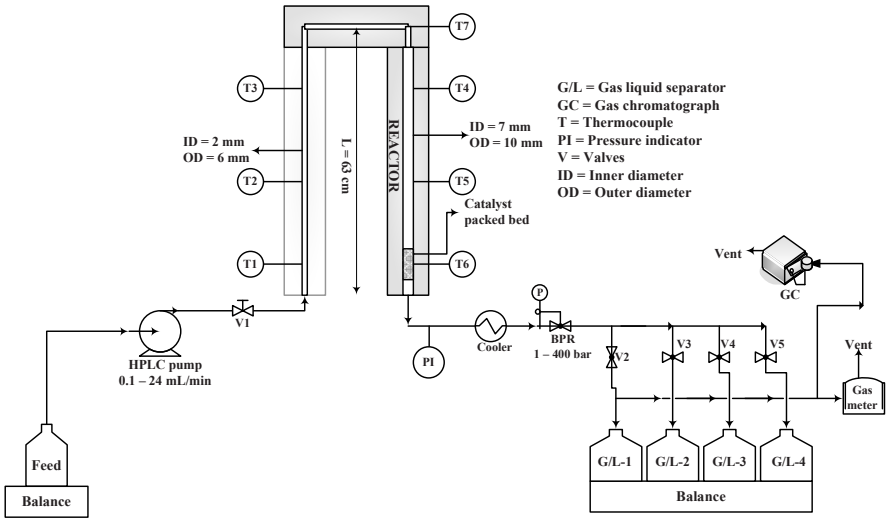

Figure 4.1: Schematic representation of the continuous flow supercritical water reformer.

Carbon balance was calculated taking into account the carbon-content in gas and liquid phases. The catalyst performance is presented in terms of selectivities to carbon containing products in gas phase (CO, CO_2, CH_4 and C2+) calculated based on distribution of carbon in these molecules. The carbon to gas conversion calculated have an error margin of ±4%. The maximum amount of hydrogen that can be theoretically obtained includes both reforming and WGS reaction. For ethylene glycol (EG) this maximal reforming ratio (RR) of H_2/CO_2 is 5/2.

$$C_2H_6O_2 \rightarrow 3\ H_2 + 2\ CO \text{ (optimal reforming)}$$

$$2CO + 2\ H_2O \rightarrow 2\ CO_2 + 2\ H_2 \text{ (WGS)}$$

$$C_2H_6O_2 \rightarrow 5\ H_2 + 2\ CO_2 \text{ (overall optimal reaction)}$$

% H_2 selectivity = (H_2 moles produced/C atoms in gas phase) (1/RR) ×100

% Selectivity of *i* = (C atoms in species *i*)/(C atoms in gas phase) ×100, where species *i* = CO, CO_2 or CH_4

% Gasification Efficiency, GE (or) carbon to gas conversion = (C atoms in gas phase) / (Total C atoms in feed stock) ×100

Turn over frequencies (TOF) were calculated for the monometallic catalysts based on the metal dispersions and is defined as the number of respective molecules produced/reacted per active catalytic site per minute.

4.3 RESULTS AND DISCUSSION

4.3.1 CATALYST CHARACTERIZATION RESULTS

Characteristics of the catalysts studied are given in Table 4.1. All fresh catalysts had surface areas of ±200 m^2/g, similar to that for the alumina used. All catalysts showed decrease in surface areas to ±20 m^2/g during the reaction. This decrease was found to happen during the initial stage of the reaction (within the first 15 minutes) and also occurred when only water (without organic reactants) was used. The decreasing surface area can be attributed to phase change of the γ-Al_2O_3 to boehmite as can be seen from the XRD patterns of the fresh and spent 1.15-0.35 wt% Pt–Ni/γ-Al_2O_3 catalysts as shown in Figure 4.2. Due to sensitivity issues of XRD, only metal loadings above 5 wt% can be identified. Hence, this technique is used only for identifying transformation of the phase change of γ-Al_2O_3 in supercritical water. For the fresh catalyst, diffraction peaks appear at $2\theta = 45.8°$ and 66.8° which corresponds to γ-Al_2O_3. Multiple peaks emerged for the spent catalyst after exposure to supercritical water and these correspond to the dominant phase of boehmite indicating hydrolysis of the support. Weaker reflections of alpha phase are also noticed. Similar observations of the phase change of γ-Al_2O_3 in supercritical water was reported by many authors.[126, 131-132] The phase change occurred during start-up of the reaction and therefore the reactions were performed in the presence of stable catalysts. It was reported earlier by Wawrzetz *et al.*[133] that the phase changes from γ-Al_2O_3 to boehmite did not cause blocking or deactivation of the catalytic sites.

Metal dispersions measured with CO chemisorptions were low for the Ir and Ni catalysts implying large particle sizes of 7.2 nm and 78 nm, respectively. TPR experiment showed that the most dominant Ni species on the support was $NiAl_2O_4$ (no TPR profile presented). A temperature of around 800–1000 °C was necessary to reduce this species under hydrogen at atmospheric pressure. These high reduction temperatures can be the reason for the low Ni dispersions measured, as the $NiAl_2O_4$ could not be reduced under the conditions used for the chemisorption experiment.

Table 4.1: Catalyst characterization results for fresh catalysts.

Catalyst supported on γ-alumina	Loading (%)	Dispersion (%)[a]	Average particle size (nm)	Surface area (m^2/g)
Ni	1.31	1	78	196
Ir	1.41	15	7.2	195
Pt	1.45	68	1.6	196
Pt	0.60	85	1.3	199
Pt	0.30	87	1.2	197
Pt–Ni	1.17–0.33	n.d.	n.d.	198
Pt–Ni	0.60–0.20	n.d.	n.d.	197
Pt–Ni	0.30–0.10	n.d.	n.d.	200

[a]Determined by CO chemisorption; n.d – not determined

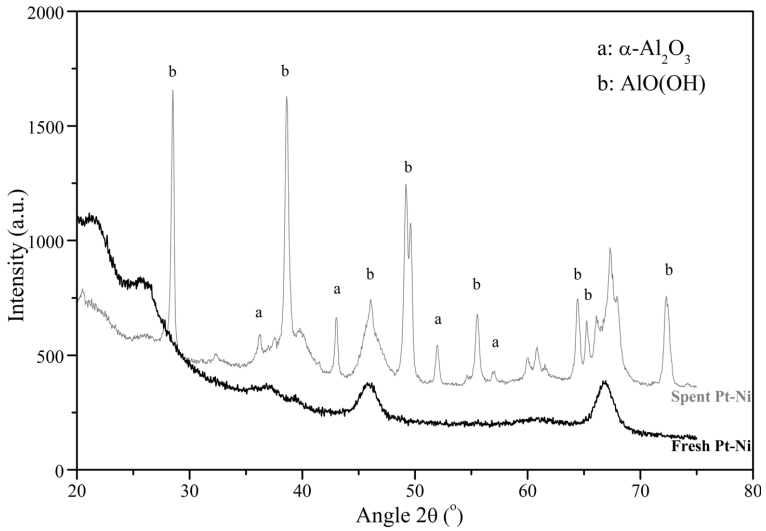

Figure 4.2: XRD spectra of fresh Pt–Ni (Pt-1.15% and Ni-0.35%) bimetallic catalyst (below) *vs.* spent Pt–Ni catalyst.

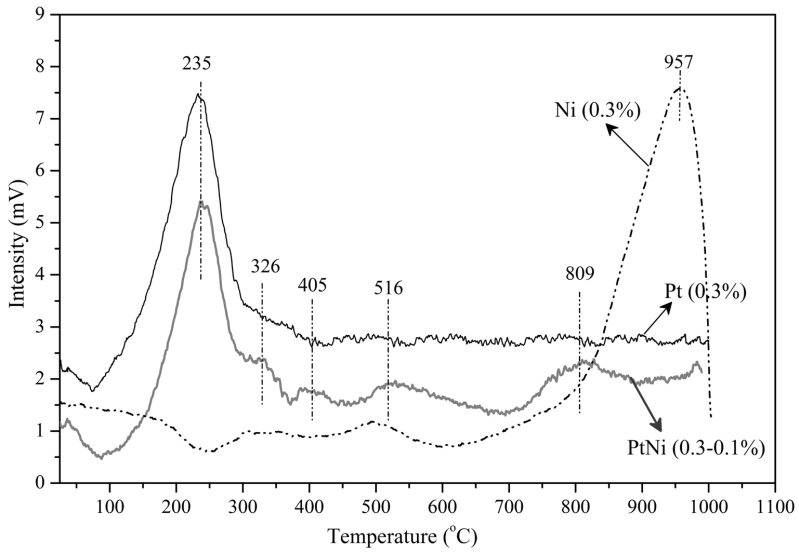

Figure 4.3: TPR profiles of fresh catalysts: a) Pt (0.3%), b) Ni (0.3%) and c) Pt–Ni (0.3–0.1%).

The nature of the interactions between Pt and Ni on the bimetallic Pt–Ni catalysts was studied by TPR. Mutual influences between Pt and Ni can vary from (*i*) no interactions – Pt and Ni are not situated near each other-, (*ii*) weak interactions – Pt and Ni are close together- and (*iii*) strong interaction – Pt–Ni alloy formation. The TPR profiles of the 0.3 wt% Pt/Al_2O_3, 0.3 wt% Ni/Al_2O_3 and 0.3–0.1 wt% Pt/Al_2O_3 are shown in Figure 4.3. Pt/Al_2O_3 showed only one reduction peak at 227 °C which can be attributed to the reduction of $Pt^{IV}(OH)_xCl_y$ to metallic Pt.[134] Ni/Al_2O_3 showed a large reduction peak between 800 °C and 1000 °C which can be attributed to $NiAl_2O_4$.[135] In the case of the Pt–Ni catalyst, reduction temperatures of 235, 326, 405, 516 and 809 °C were observed. The reduction peak at 809°C is attributed to $NiAl_2O_4$[135], indicating that some of the added Ni was inactive during the reaction due to strong interaction with the alumina support. Reduction peaks at 405 and 516 °C indicate large and smaller NiO particles, respectively.[136] The Pt reduction shifted to a higher temperature of 235 °C when Ni was present on the catalyst. This shift is assigned to interactions between Pt and Ni. However, the strength of this interaction is unknown. Also a reduction peak around 326 °C was observed and this is assigned to Ni that is strongly interacting with Pt as Pt is reported to lower the reduction temperature of NiO by facilitating dissociative hydrogen chemisorption which is necessary for the reduction of Ni.[137] Based on the TPR results it can be concluded that various degrees of interaction between Pt and Ni exist on the Pt–Ni catalyst, varying from no interaction to strong interaction.

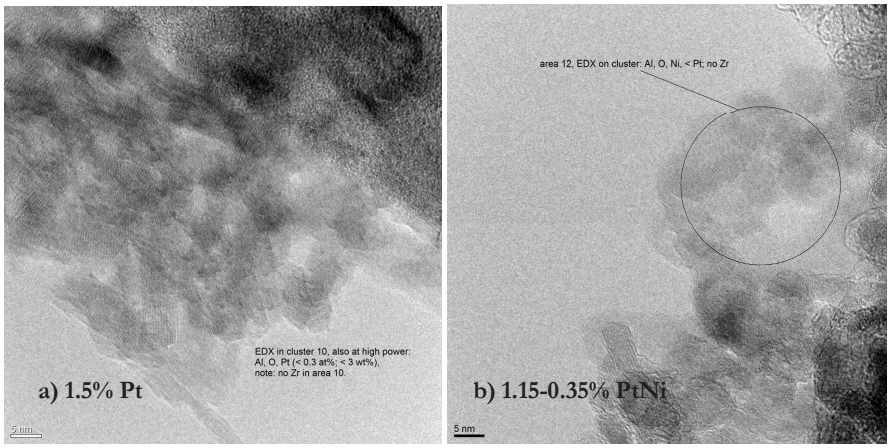

Figure 4.4: TEM images (5 nm scale) of fresh *a)* 1.5 wt% Pt/γ-Al_2O_3 and *b)* 1.15–0.35 wt% Pt–Ni bimetallic catalysts.

The monometallic Pt catalysts showed comparatively higher metal dispersion measured by CO chemisorption. A lower dispersion was found for the highest Pt loading, indicating larger particles for the highest Pt loading. Figure 4.4 a is a TEM image of the 1.5 wt% Pt on alumina catalyst. EDX confirmed the presence of Pt in this region and dark spots with a sub-nanometre diameter can be seen. These dark spots were not visible in areas were Pt was not indicated by EDX and are therefore attributed to the mass induced contrast between Pt and Alumina. In the case of bimetallic catalysts, determining dispersions separately for Pt and Ni is not straight forward and were not determined. A TEM image of the fresh 1.5 wt% Pt–Ni containing catalyst is shown in Figure 4.4 b. Again dark spots were observed on the alumina support. The size of these spots was also sub-nanometre in diameter and is also attributed to Pt or Pt–Ni particles. The presence of only Pt was observed in some areas but Ni was always found together with Pt and shows that Ni deposits in the neighbourhood of Pt, indicating interactions between Pt and Ni. TEM imaging indicates that the metal particles (Pt and Pt–Ni) on both catalysts are sub-nanometre in diameter.

4.3.2 CATALYTIC REFORMING RESULTS

Thermodynamic equilibrium gas composition[13] of different ethylene glycol concentrations at 450 °C and 250 bar is shown in Figure 4.5. Under the reaction conditions used in this study, CH_4 is the favourable product formed with a selectivity of 54% with 5 wt% EG and increases slightly with increasing the feed concentration at the expense of hydrogen.

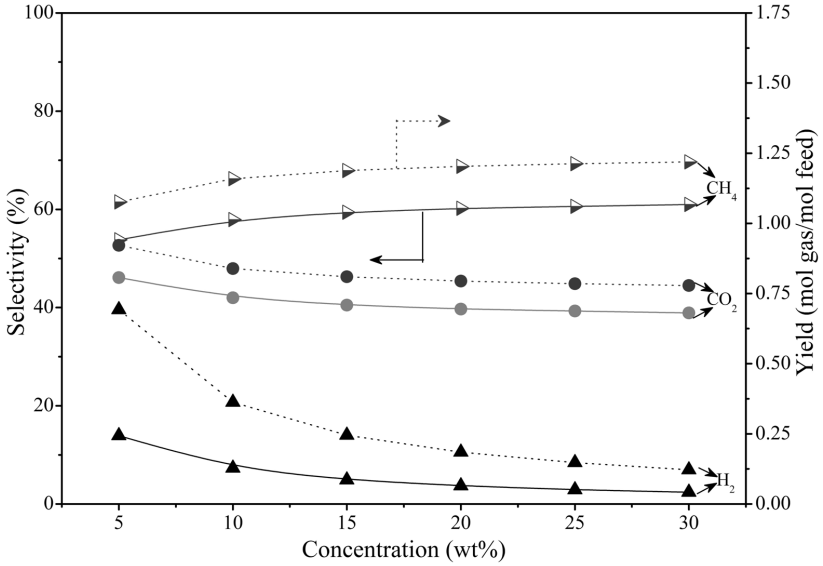

Figure 4.5: Thermodynamic chemical equilibrium composition for different feed concentrations ranging from 5 to 30 wt% of ethylene glycol reformed in supercritical water at 450 °C and 250 bar. Symbols with solid trend lines represent selectivity and dotted trend lines represent yield.

Table 4.2: Experimental data for the reforming of 5 wt% ethylene glycol (WHSV 5.9 h^{-1}) at 450 °C and 250 bar using 1.5 wt% Ni, Ir and Pt supported on γ-alumina.

	1.5 wt% Ni	**1.5 wt% Ir**	**1.5 wt% Pt**
Carbon to gas (%)	6	27	100
Carbon in liquid (%)	96	45	6
	Selectivity (%)		
H_2	26	35	87
CO_2	31	30	94
CO	55	40	1
CH_4	1	24	4
C2+	13	6	1
	Yield (mol gas / mol feed)		
H_2	0.08	0.61	4.24
CO_2	0.04	0.20	1.78
CO	0.06	0.29	0.01

CH_4	0.00	0.18	0.07
C2+	0.00	0.01	0.01

C2+ gases include C_2H_4, C_2H_6, C_3H_6 and C_3H_8.

Results of the catalytic experiments with 5 wt% EG for the alumina supported Ni, Ir, and Pt catalysts, are shown in Table 4.2. No reforming activity for EG was observed in a blank experiment (no catalyst) or with the alumina support only. In Table 4.2, carbon to gas (±5%) conversion and carbon remaining in liquid (±2%) indicate good carbon balances (102% and 106%), except for the Ir catalyst where ±30% is deposited on the catalyst as coke. Carbon to gas conversion is taken as measure for the gasification activity. Remaining carbon from the feed is either in coke or in the liquid product (EG, plus other carbon containing species). Results in Table 4.2 show that at comparable metal loadings, Pt was the most active.

The Ni based catalyst showed the lowest carbon to gas conversion of 6%. Ir catalyst gave a conversion of 27%. Pt catalyst showed near complete conversion of EG to gas phase products. These results are in line with Davda *et al.*[124], who also found Pt to be more active than Ir. In the case of Ni catalyst, we have used a low loading of 1.5 wt% for comparison with the other catalysts in the study. Other studies report usually much higher Ni loadings (~20 wt%). These catalysts were initially very active but underwent rapid catalyst deactivation. It is therefore difficult to compare our results with these studies.[117, 124]

In the case of Ni/Al_2O_3 catalyst, NiO clusters formed during calcination can undergo strong interaction with the alumina support, leading to the formation of stable $NiAl_2O_4$. Steam reforming and water gas shift activity is related to the presence of reduced Ni metal particles. The $NiAl_2O_4$ phase is stable under most reforming conditions and does not contribute to catalyst activity. A TPR experiment showed that the most dominant Ni species on the support was $NiAl_2O_4$. Since the Ni concentration is low in our catalyst, this is the only species to be expected. Catalysts containing larger amounts of Ni usually show both NiO and $NiAl_2O_4$ phases.[135] A temperature in the range of 800-1000 °C was necessary to reduce this species under hydrogen. Thus the low activity of the Ni compared to Ir and Pt catalysts is due to the presence of Ni in inactive $NiAl_2O_4$ phase, in this case.

Table 4.2 also give selectivities to the various gas products observed. The target in this study is to achieve a high selectivity towards hydrogen (*i*) by maximizing water gas shift and (*ii*) by minimizing methane formation. Both the Ni and Pt catalysts showed low selectivities for methane formation (<4%). Low methanation activity (CH_4 <4%) and high WGS activity (CO/CO_2 = 0.01) (see Table 4.2) results in the high selectivity for hydrogen (87%) as observed for the Pt catalyst. From Table 4.1 it is seen that metal dispersions for Pt is about 4 times

higher than Ir and this is also reflected in EG conversion. This implies similar intrinsic activities for both Ir and Pt for EG gasification. However, Ir catalyst showed the highest selectivity towards methane (24%) and also showed high amounts of carbonaceous deposits. Based on the results so far Pt/Al_2O_3 shows the best activity, highest selectivity to H_2 and minimal methane formation.

Optimizing the Pt loading without compromising the EG conversion is interesting from an environmental point of view and from the point of cost of Pt. Table 4.3 show the result of the influence of Pt loading on the catalyst performance for the reforming of 5 wt% EG. Characterization results of these catalysts are summarized in Table 4.1 as described in earlier section.

Table 4.3: Experimental data for the reforming of 5 wt% ethylene glycol (WHSV 5.9 h^{-1}) at 450 °C and 250 bar using 0.3, 0.6 and 1.5 wt% Pt supported on γ-alumina.

	0.3 wt% Pt	**0.6 wt% Pt**	**1.5 wt% Pt**
Carbon to gas %	95	99	100
Carbon in liquid (%)	4	2	6
	Selectivity (%)		
H_2	76	85	87
CO_2	84	87	94
CO	1	1	1
Alkanes (C_xH_y)	15	12	5

It can be seen from Table 4.3 that even using the lowest Pt loading resulted in near complete conversion of EG. Additional experiments with higher EG concentrations (15 wt%) and at higher space velocities (17.8 h^{-1}) were carried out. The results of these experiments are given in Table 4.4.

As expected, a lower overall conversion for the reforming of 15 wt% EG solution to carbon containing gaseous products was obtained, under comparable conditions. Interestingly, EG conversion levels were found to be in the same range (42-48%) for all the three Pt catalysts.

Hydrogen selectivities were lower in the case of experiments with higher EG concentration (15 wt%). Davda *et al.*[9, 124, 138] also reported that a shift towards CO and CH_4 is introduced with increasing ethylene glycol concentrations. Lower concentrations favour hydrogen, while at higher concentrations, increased levels of CO_x, and H_2 cause (hydrogen consuming) consecutive methane formation. This was observed for all the three catalysts. For the two catalysts, 0.3 and 0.6 wt% Pt, hydrogen selectivity is almost half of that for the experiments

with lower EG (5 wt%) concentration. The hydrogen selectivity decreases and methane selectivity increases for 15 wt% EG concentration when compared to 5 wt% EG using the catalyst with the lowest Pt loading (0.3 wt%). Interestingly, in the case of the 1.5 wt% Pt catalyst there is only a small increase in methane formation and hydrogen selectivity is unaffected for the higher EG concentration. HPLC analysis of the effluent obtained with catalyst with 0.3% Pt loading indicated the presence of ethylene glycol and other intermediates compounds such as acetaldehyde, formic acid and very little amount of ethanol.

Table 4.4: Experimental data for the reforming of 15 wt% ethylene glycol (WHSV 17.8 h^{-1}) at 450 °C and 250 bar using 0.3 Pt, 0.6 Pt and 1.5 Pt supported on γ-alumina.

	0.3 wt% Pt	**0.6 wt% Pt**	**1.5 wt% Pt**
Carbon to gas %	48	48	42
Carbon in liquid (%)	58	59	61
	Selectivity (%)		
H_2	42	51	80
CO_2	50	60	79
CO	20	14	14
Alkanes (C_xH_y)	30	26	7

Table 4.5: TOF's for the reforming of 15 wt% ethylene glycol (WHSV 17.8 h^{-1}) and hydrogen production.

Pt loading (%)	**Dispersion (%)**	**Average particle size (nm)**	**TOF EG 15 wt% EG (min^{-1})**	**TOF H_2 15 wt% EG (min^{-1})**
0.30	87	1.2	173	359
0.60	85	1.3	87	219
1.45	68	1.6	41	163

The intrinsic rates for reforming and hydrogen formation, in the case of experiments with 15 wt% EG, were calculated for the three monometallic Pt catalysts and are summarized in Table 4.5. Apparent TOF for the reforming of ethylene glycol was found to be more than four times higher for the 0.3 wt% Pt loadings compared to the 1.5 wt% Pt loading. The higher activity (TOF) of the former can be a consequence of (1) Pt particle structure effect (in this case smaller particles are more active) and (2) the higher Pt dispersion in bifunctional catalysts. It has been reported earlier [129] that the boundary between alumina and Pt is thought to be the active catalytic area for reforming since alumina also plays a role in the reforming reaction.

Reforming and WGS reactions involve oxidation with the oxygen present in the water molecule. This should involve splitting/activation of water molecules.[139] Pt is normally inert for water activation under typical gasification conditions.[140] Alumina, on the other hand is able to activate water by forming hydroxyl groups, which is necessary for the reforming reaction. Therefore reactive Pt sites should be in close proximity of alumina. Decreasing the particle size will increase the amount of Pt sites neighbouring alumina and therefore increasing the overall reforming activity.[139]

However, the increase in EG TOF is not proportional with the increase in H_2 TOF (4 *vs.* 2). Results in Table 4.4 seem to indicate that lower Pt loadings tend to favour methane formation. Lehnert and Claus[132] showed that, for the aqueous phase reforming of glycerol, the reaction was structure sensitive for Pt/Al_2O_3 catalysts. They observed that the selectivity towards CO and CH_4 increased with decreasing Pt particle size. They suggest that smaller particle sizes have more steps in the structure and this favours CO and CH_4 formation. C–C scission is suggested to occur on the face atoms while C–O scission is favoured on steps and edges.[132] Thus, in full agreement with the former, smaller Pt particle size can be responsible for the increase in methane formation.

Conditions during reforming in supercritical water are aggressive therefore, catalyst deactivation is a serious issue and lifetimes can be short due to leaching, sintering (Ostwald ripening) of metal particles and coking. The stability of the catalyst is therefore very critical for practical applications.

Table 4.6: Stabilities of Pt catalysts for the reforming of 15 wt% ethylene glycol (WHSV 17.8 h^{-1}).

Catalyst	Time (h)	Conversion (%)	Selectivity (%)				
			H_2	CO_2	CO	CH_4	C+
0.3 Pt	0.5	48	42	50	20	22	8
	9.0	31	72	57	36	5	3
0.6 Pt	0.5	48	51	60	14	19	7
	9.0	36	73	66	22	8	4
1.5 Pt	0.5	42	80	79	14	4	3
	9.0	42	82	80	15	2	3

The EG conversions to gas phase products and selectivities for the three monometallic Pt catalysts during a 9 h life test are shown in Table 4.5 for the reforming of 15 wt% EG. The Pt catalyst with the highest Pt loading (1.5 wt%) showed stable performances with respect to activity (42%) and selectivities (H_2 selectivity of 80%) during 9 h on stream. Lower Pt loadings

were less stable. For the lowest Pt loading (0.3 wt%) initially a conversion of 48% was obtained. The conversion however gradually dropped to 31% after 9 h on stream. With deactivation hydrogen selectivity improved at the expense of lower CH_4 formation.

One reason for deactivation can be the loss of metal from the catalyst by leaching. XRF analysis of the liquid products showed, however, no presence of metals. In addition metal loadings for the fresh and spent catalysts were found to be the same, verifying that leaching of Pt and alumina support during the reaction was unlikely.

Deactivation by coke deposition is also unlikely as oxidation and re-use of a spent 0.3 wt% Pt/Al_2O_3 catalyst showed. The catalyst was taken out of the reactor after 9 h on stream for the reforming of 15 wt% EG. The spent catalyst was re-oxidized in air at 500 °C for 5 h to burn off any coke species. After this treatment the catalyst was again used for the reforming of 15 wt% EG and no changes in activity or selectivities were observed compared to the properties after 9 h on stream. This indicates that deactivation was not induced by coke deposition. TGA-MS analysis of the spent Pt and Pt–Ni catalysts all showed 12 ± 1 % weight loss at 513 ± 3 °C. The gas stream showed that the weight loss was mainly due to the release of H_2O. For all catalysts, release of comparable quantities of water was observed. H_2O is probably formed during recombination of hydroxyl groups on the alumina support. Presence of coke on the catalysts was not indicated by the TGA-MS technique.

An indication for deactivation can be inferred from the selectivity data presented in Table 4.6. With deactivation the selectivity towards hydrogen improved and methane formation decreased. As discussed earlier[132] the Pt particle size is believed to influence the reforming activity and selectivity towards hydrogen and methane. Larger Pt particles tend to favour the formation of hydrogen, but are less active for EG reforming in contrast to smaller Pt particles that are very active for EG reforming but favour the formation of methane. In line with these arguments we suggest that the dominating deactivation mechanism is due to Pt particle growth. Initially the catalyst showed a high activity and a higher selectivity towards methane. During the reaction the Pt particles are believed to grow, resulting in a lower reforming activity and increased selectivity towards H_2. We can only suggest that the relatively large Pt particle size in the catalyst with the highest Pt loading is the reason for the stability with time.

From the results discussed so far we have shown that full conversion of a 5 wt% ethylene glycol solution to gas phase products could be achieved with high selectivity towards hydrogen using alumina supported Pt catalysts. At the higher EG concentrations (15 wt%) a loss of hydrogen was observed at the expense of more methane formation. Using lower Pt loadings showed a negative effect on the hydrogen selectivity for the reforming of 15 wt% ethylene glycol solution. In addition the catalyst with lower Pt loadings deactivated during the reaction.

The 1.5 wt% Pt/Al_2O_3 showed to be the best catalyst in terms of stability and hydrogen selectivity for the reforming of 15 wt% ethylene glycol. However, the intrinsic activity of the Pt active sites was still low.

Reforming of solutions with high EG concentrations and high hydrogen selectivities are economically interesting but this requires modification of the Pt catalysts as seen above. In case of the catalysts with lower Pt loadings the hydrogen selectivity and stability should be addressed. For the catalyst with the highest Pt loading the intrinsic activity should be improved. Ni/Al_2O_3 was not a very interesting catalyst with respect to EG conversions and H_2 yields, although Ni/Al_2O_3 showed the lowest CH_4 formation rate. Thus, Ni addition to monometallic Pt catalysts can be expected to improve hydrogen yields. Huber *et al.* [120] already reported that addition of Ni to a Pt/Al_2O_3 catalyst significantly increased the H_2 selectivity by suppressing CH_4 formation and at the same time also enhanced EG reforming activity. Furthermore, Ni is also an active metal for steam reforming and for the water gas shift reaction (necessary to enhance hydrogen yields) and is a cheaper substitute for Pt.[141-142] Possible synergetic effects of Ni addition to Pt catalysts were investigated for the reforming of ethylene glycol in supercritical water.

Table 4.7: Stabilities of Pt-Ni catalysts for the reforming of 15 wt% ethylene glycol (WHSV 17.8 h^{-1}).

Catalyst	Time (h)	Conversion (%)	Selectivity (%)				
			H_2	CO_2	CO	CH_4	C+
0.3 - 0.1 Pt–Ni	0.5	50	77	77	18	4	1
	9.0	50	79	78	17	3	1
0.6 - 0.2 Pt–Ni	0.5	63	84	88	8	3	1
	9.0	60	85	88	8	3	1
1.15 - 0.35 Pt–Ni	0.5	79	83	91	3	4	1
	9.0	77	86	90	5	4	1

Details of the Pt catalysts modified with Ni are given in Table 4.1. The conversions and selectivities for the three Pt–Ni bimetallic catalysts are shown in Table 4.6 for the reforming of 15 wt% ethylene glycol. Addition of Ni induced a significant improvement on the performance of the catalyst. In contrast to the 0.3 wt% Pt catalyst (Table 4.6) no deactivation was observed with the 0.3–0.1 wt% Pt–Ni catalyst during 9 h on stream. All Pt–Ni catalysts showed stable conversions and selectivities for the reforming of 15 wt% EG during 9 h on stream.

Another positive effect was observed on the hydrogen selectivity by addition of Ni. All tested Pt–Ni catalysts showed high H_2 selectivities with remarkably low CH_4 selectivities (maximum 3–4%). Addition of Ni to the catalyst with lowest Pt loading (0.3 - 0.1 Pt–Ni) almost doubled the hydrogen selectivity as a result of suppressing methane formation. In the case of Pt and Pt–Ni catalysts comparable initial concentrations of CO were observed. In case of Pt–Ni catalyst the CO_2 concentrations are much higher compared to the mono-metallic Pt catalyst. This is an indication that in presence of Ni, CO underwent a water gas shift reaction instead of a methanation reaction. The role of Ni in that case is to prevent hydrogenation of CO_x due to the intrinsic water gas shift activity of Ni.

Noble metals such as Pt are not capable of activating water for the water gas shift reaction and therefore require an active support material (in this case alumina) that provides the water activation. Ni however is capable of both activating water and CO in the water gas shift reaction without the need for a support. This occurs via NiO formation with water[143]. This intrinsic water gas shift activity of Ni might be the reason for the synergetic effect observed in bimetallic Pt–Ni catalysts.

Remarkably, from Table 4.7, it can be seen that 1.15–0.35 wt% Pt–Ni catalyst is two times as active as the monometallic counterpart (1.5 wt% Pt) with very high selectivity towards hydrogen (86%). The catalyst is also very stable. Based on calculations, Huber *et al.*[120] speculated that Pt–Ni catalysts have lower heats of H_2 and CO adsorption compared to pure Pt catalysts, causing lower surface coverage of adsorbed H_2 and CO and therefore minimize methanation of CO and allowing more sites to be accessible for the reactant to undergo reforming.

The carbon to gas conversion of 15 wt% EG and the hydrogen selectivities for the three monometallic Pt catalysts and three bimetallic Pt–Ni catalysts with different metal loadings during a 9 h reaction time are shown in Figure 4.6. It is evident from the figure that the bimetallic catalysts are shown to have higher conversions and stable hydrogen selectivities than the monometallic catalysts.

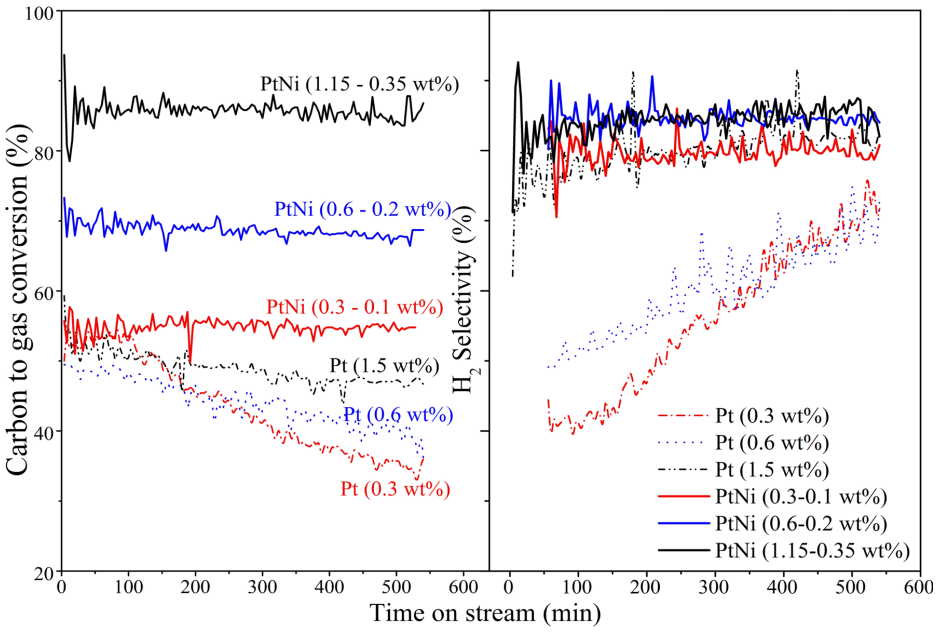

Figure 4.6: Activity and stability of monometallic Pt and bimetallic Pt–Ni catalysts for the reforming of 15 wt% EG at 450 °C and 250 bar.

The influence of EG concentration ranging from 5–30 wt% on the product gas selectivity and gasification efficiency with Pt–Ni (Pt – 1.15% and Ni – 0.35%) is shown in Figure 4.7. The carbon to gas conversion decreased from 100 to 60% with increasing concentration from 5 to 30 wt% suggesting that decreasing the space velocity (either by increasing the amount of catalyst or decreasing the feed flow) should give complete conversion at high EG concentrations. The H_2 and CO_2 selectivities decreased while the CO, CH_4 and C2+ selectivities increases with the EG concentration. However, with 30 wt% EG concentration, the carbon to gas conversions remained constant during 3h experimental run but the CO selectivity increased marginally indicating a decrease in water gas shift activity (Figure 4.8).

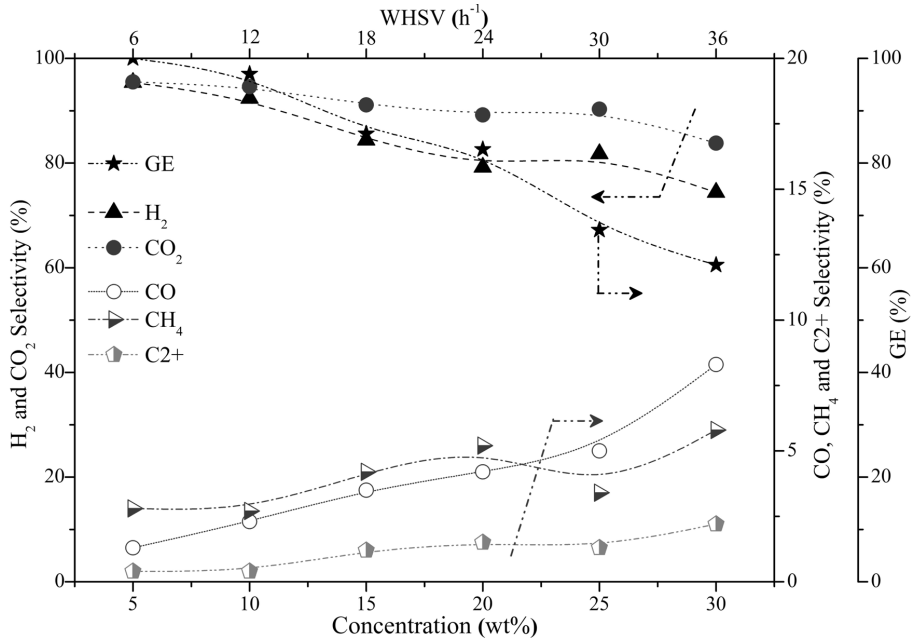

Figure 4.7: The influence of ethylene glycol concentration and its corresponding space velocities on the product gas selectivity and gasification efficiency in the presence of Pt–Ni (Pt-1.15 wt%, Ni- 0.35%) bimetallic catalyst at 450 °C and 250 bar (arrows indicate axis direction)

The bimetallic Pt–Ni/Al_2O_3 catalyst studied here, shows extremely good activity, is stable and very selective to hydrogen. This catalyst shows promise for practical applications. Supercritical water is Brønsted acidic and can be expected to help acid–base catalyzed reactions. This should enhance dehydration of oxygenates leading to reaction intermediates. The role for intermediates formed during dehydration and possible routes from them to hydrogen need to be established. The exact nature of interaction between Pt and Ni are under study in order to establish catalyst requirements.

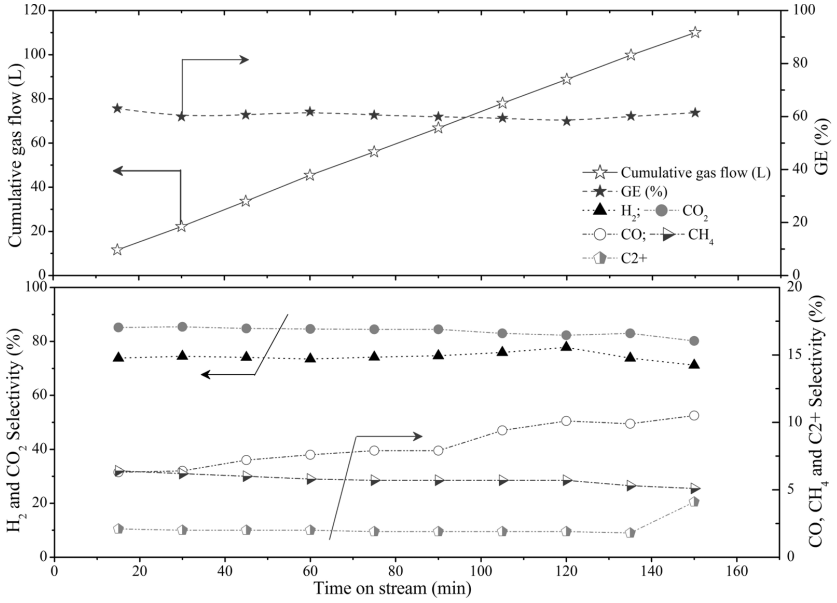

Figure 4.8: The gasification efficiency and the product gas selectivity of 30 wt% ethylene glycol concentration versus time with Pt–Ni (Pt-1.15 wt%, Ni-0.35%) bimetallic catalyst at 450 °C and 250 bar (arrows point towards axis direction).

4.4 CONCLUSIONS

In this chapter, the catalytic properties of alumina supported Pt, Ir and Ni catalysts for the reforming of ethylene glycol under supercritical conditions are studied. In the case of monometallic Pt catalysts, smaller Pt particles tend to give higher intrinsic activities. This is due to reforming being bifunctional over supported Pt catalysts, the support having the role of water activation. Thus the small particle sizes have larger interfacial (metal/support) area providing a higher activity. However, they yield also lower hydrogen selectivities due to increased methane formation. Methane can be formed by either dehydration of EG, and/or by the hydrogenation of CO_x. A new developed Pt–Ni bimetallic catalyst shows enhanced hydrogen yields by suppressing methane formation. Due to supposed lower CO coverage caused by the presence of Ni and an enhanced accessibility to Pt sites for reforming, the new Pt–Ni catalyst also shows two times more activity compared to a monometallic Pt catalyst. Moreover, the addition of Ni also prevented further sintering of Pt particles and stable performances were observed for the bimetallic Pt–Ni catalysts for the reforming of ethylene glycol even under supercritical conditions.

Chapter 4

Chapter 5

Catalytic reforming of glycerol in supercritical water over bimetallic Pt-Ni catalyst[4]

[4] This chapter is an excerpt of paper published as:

Chakinala, A. G.; van Swaaij, W. P. M.; Kersten, S. R. A.; de Vlieger, D.; Seshan, K.; Brilman, D. W. F., Catalytic Reforming of Glycerol in Supercritical Water over Bimetallic Pt–Ni Catalyst. Industrial & Engineering Chemistry Research 2013, 52, (15), 5302-5312.

Chapter 5

5.1 INTRODUCTION

It is imperative to explore ways of utilizing effectively the abundant and renewable biomass energy resources available to foster the production of new sources of energy and chemical intermediates, and reduce the fossil CO_2 emissions. The first generation bio-fuels and chemicals (*e.g.*, bio-diesel, bio-ethanol) produced nowadays is derived from sugars and vegetable oils. The production thereof, and their competition for land with food production, is subject to an ongoing debate. Therefore technologies (*e.g.* pyrolysis, gasification) are being explored to valorize the lignocellulosic ('second generation') biomass residues to value added products such as chemicals, liquids and gaseous fuels.

Today's research on biodiesel from lipids is focused in the direction of bio-refinery concepts (particularly for algae), in order to avoid any food chain conflict. The biodiesel process involves the transesterification of extracted fatty acids/lipids/vegetable oil with methanol in the presence of an alkali catalyst (KOH). Glycerol (glycerine or 1, 2, 3–propane tri-ol), is the major by-product of the biodiesel process. For every 100 kg of biodiesel around 11 kg of crude glycerol is produced.[144] It is forecasted that there will be an enormous increase in bio-diesel production in the future if the algae bio-refinery concept succeeds. This may create a glut of crude glycerol, becoming available as a feedstock at relatively low cost.

Although, pure glycerol has several applications (in *e.g.* cosmetics, pharmaceuticals, chemicals), the impurities (as methanol, water, alkali salts, free fatty acids, methyl esters, untreated mono-, di- and tri-glycerides in varying proportions) present in the crude glycerol, limit its usage.[145] Removal of the impurities or purification of the crude glycerol is an energy-intensive and expensive step. As a consequence there is significant scope for the direct conversion of crude glycerol from biodiesel processing to value added products.[144, 146]

Thermochemical processes that are presently available and under development for glycerol conversion include steam reforming[147], aqueous phase reforming[148-149] and hydrothermal gasification (sub- and supercritical water conditions).[126] In this study the focus is on the catalytic hydrothermal reforming of glycerol to hydrogen and alkanes.

Few studies have already been reported on the catalytic and non-catalytic reforming of glycerol at sub- and supercritical conditions of water. Complete gasification can be achieved in both cases, but the non-catalytic route requires much higher temperatures (min. 650 °C) and longer residence times.[13, 40, 54, 106, 126, 145, 150-151] Batch experiments with high glycerol concentrations (30 wt%) studied over a temperature range of 300–430 °C have shown that the highest rate of coke formation was observed at subcritical temperatures between 350 and 370 °C.[152]

The product gas from the non-catalytic supercritical water gasification of glycerol consists mainly of hydrogen, carbon monoxide and -dioxide and trace amounts of methane and higher alkanes.[13, 106] For the non-catalytic supercritical water gasification of glycerol activation energies have been reported, ranging from 104–196 kJ/mol[13, 40, 106, 151] for pure glycerol and up to 183 kJ/mol[106] for crude glycerol. The addition of alkali salts promotes the water-gas shift reaction by steering the product gas composition towards H_2 and CO_2 and accelerates the carbon to gas conversion. Guo *et al.*[151] studied the influence of different alkali salts (K_2CO_3, Na_2CO_3, KOH, NaOH) on glycerol gasification in SCW and as expected the product gas mainly consisted of H_2 and CO_2. The hydrogen yields with respect to alkali salts are as $NaOH>Na_2CO_3>KOH>K_2CO_3$. They also noticed a rise of 10 °C in the presence of alkali which is attributed to the water gas shift reaction. However, no significant increase in the carbon gasification efficiency was observed with all the salts studied.

Xu *et al.*[153] reported complete conversion of glycerol to a hydrogen rich gas with and without carbon-catalyst at 600 °C and 345 bar. Byrd *et al.*[126] achieved complete conversion for glycerol feed concentrations of up to 40 wt% into hydrogen, carbon dioxide and methane at 800°C, using a Ru/Al_2O_3 catalyst. At lower feed concentrations the hydrogen yield approached the theoretical yield (7 mole H_2 / mole glycerol), but no information on the catalyst stability was reported. May *et al.*[145] studied the conversion of 5 wt% glycerol at 510–550 °C, 350 bar with a Ru/ZrO_2 catalyst. They obtained higher gasification efficiencies with increasing residence times in the range up to 8.5 s and also with increasing reaction temperatures within the range studied. However, the reported carbon balance closure for their experiments was only between 60–80%. The organic compounds in the aqueous effluent primarily consisted of acetic acid, acetaldehyde and hydroxyacetone. Further, minor amounts of allyl alcohols, propionaldehyde, acrolein and acrylic acid were reported. The product gas mainly consisted of hydrogen, carbon dioxide and methane. Catalyst screening for the reforming of 10 wt% glycerol in SCW (375-700 °C and 8–87 sec) was carried out in a continuous flow reactor obtaining complete conversion with all the catalysts studied.[154] However, visual observations of catalyst after the reaction (max 3 h run time) revealed significant amounts of coke formation particularly with Ni/ZrO_2 and $Pt/CeZrO_2$, which is considered to have led to catalyst deactivation (noticed in terms of drop in gas flow rate).

To summarize: for the catalytic reforming of glycerol in SCW, so far expensive active catalysts like Ru were used, at very high reaction temperatures[126] and with incomplete[126, 145] conversion. Nearly complete conversion of aqueous glycerol solutions was only achieved at higher temperatures (above 600 °C)[40, 54, 126, 150, 155] or/and low concentration.[145] Glycerol (both pure and

crude forms) as a feedstock is extensively studied in this thesis both in terms of chemistry and catalysis aspects.

In the previous chapter, we have shown that platinum based bimetallic catalysts (Pt–Ni/Al_2O_3) are very promising. Initial tests for ethylene glycol reforming, at a temperature as low as 450 °C and at 250 bar, showed high activity, in terms of complete carbon to gas conversion, as well as a high selectivity in steering the product gas selectivities towards hydrogen and carbon dioxide (instead of methane production, as dictated by the thermodynamic equilibrium).[14]

The objective of this chapter is to explore the feasibility of bimetallic Pt–Ni/Al_2O_3 catalyzed gasification of glycerol in supercritical water at near critical conditions (here: 450 °C & 250 bar) by varying different operating parameters. Furthermore, the influence of impurities in glycerol on the gasification process is investigated.

5.2 EXPERIMENTAL SECTION

5.2.1 MATERIALS

Glycerol was obtained from Sigma Aldrich and crude glycerol[147] in neutralized form from BioMCN, the Netherlands. The elemental composition of the neutralized crude glycerol was determined using CHNS elemental analyzer (EA 1108, Fisons Instruments) and the water content was estimated using Karl Fisher (KF) titration (titrant: Hydranal composite 5, Metroohm 787 KF titrino). The water content of the crude glycerol was found to be 11%. The crude glycerol also consisted of organics (1.78 wt%) and inorganics (4.22 wt%). The organics in the crude glycerol mainly consisted of diglycerides (0.78%), triglycerides (0.5%), FAME (0.3%), free fatty acids (0.2%), methanol (0.01%) and trace amounts of citric acid and acetic acid. The inorganics in the crude glycerol consisted of 4.3% sodium chloride, 0.09% magnesium sulphate, 0.01% calcium sulphate. The elemental carbon and hydrogen as measured using the elemental analyzer was found to be 31.9 and 8.6 wt% respectively. The oxygen content was 59.5% and is calculated by difference.

5.2.2 CATALYST PREPARATION AND CHARACTERIZATION

Catalytic reforming of glycerol and other model compounds in supercritical water were performed over Pt–Ni (Pt–1.2 wt%, Ni–0.4 wt%) catalysts supported on γ–alumina. The catalysts were prepared by incipient wet impregnation of γ–alumina with H_2PtCl_6 $6H_2O$ solution and the method description is provided in the earlier chapter.[14]

5.2.3 EXPERIMENTAL SET-UP

The experimental details of the set-up used in this study are described in the earlier chapter.[14] All experiments were carried out in a premixed mode, where a diluted glycerol solution of desired concentration was constantly fed with an HPLC pump into the reactor, maintained at supercritical conditions of water. The tubular reactor was made of Inconel (inner diameter of 6.8 mm and length of 63 cm) and loaded with 1 g of catalyst, placed in the middle of the reactor. All the experiments are carried out with the catalyst bed located at 40 cm from the top of the reactor (unless otherwise stated). To check the influence of the bed location the catalyst bed was placed at 20 and 60 cm from the top of the reactor. Thermo-wells were welded to the reactor tube at different locations to measure the temperature profile over the reactor length. The temperatures reported here refer to the wall/reactor oven temperature. The inside temperature of the reactor tube was ~40–50 °C lower than the outside wall/oven temperature at the catalyst bed location (40 cm from top of the reactor). The effluent from the reactor was cooled with a double pipe heat exchanger, located after the back pressure regulator, and the condensate is collected in a gas-liquid separator.

The product gas flow rate was measured using a wet gas meter and analysed for its composition continuously with a GC (Varian 450–GC). The liquid effluent collected in the gas-liquid separator was analyzed for its elemental carbon content. The intermediate reaction compounds (glycerol, 1, 2-propanediol (1, 2-PD), 1, 3-propanediol (1,3-PD), ethylene glycol (EG), acetaldehyde, ethanol) present in the liquid were quantified off-line with a high performance liquid chromatography (HPLC, Agilent). The method for quantifying the liquid products using HPLC was adapted from the literature.[106, 145] In brief, a Biorad Aminex HPX-87H column was used and the mobile phase constituted of an aqueous solution of sulphuric acid (5 mM) set to a flow rate of 0.5 mL/min and maintaining the column temperature at 60 °C.

Thermogravimetric analysis (TGA) of the spent catalysts was carried out in an aluminium crucible using a NETZSCH STA 449 F3 Jupiter instrument. The samples were heated from room temperature to 850 °C at a heating rate of 10 °C/min in a stream of flowing air (30ml/min). The samples were held at 850 °C for 30 min to completely oxidize the carbonaceous deposits. The initial mass of the samples was determined using an external weighing balance. The mass rate loss is defined as

$$r_{wt} \equiv \frac{dX}{dT} = -\frac{(m_\tau - m_{\tau+1})}{m_0(T_\tau - T_{\tau+1})}\left(1/{}_oC\right)$$

Where τ and τ+1 are logged time, T (°C) is the temperature of the sample cup and m_o (mg) is the initial amount of sample, as weighed with the external balance. XRD analysis of the catalyst samples was performed using a Bruker D2 phaser instrument. Raman spectroscopy analyses of the catalysts were carried out using a Bruker (Senterra) instrument.

5.3 RESULTS AND DISCUSSION

5.3.1 EQUILIBRIUM GAS COMPOSITION AND NON-CATALYTIC GASIFICATION OF GLYCEROL

The equilibrium gas composition as a function of initial glycerol concentration (up to 30 wt%) at different reaction temperatures (400, 450 and 500 °C) and 250 bar was calculated and is shown in Figure 5.1. Thermodynamics predict methane formation at lower temperatures and high feed concentrations. High hydrogen yields are expected only at low feed concentrations and high reaction temperatures.

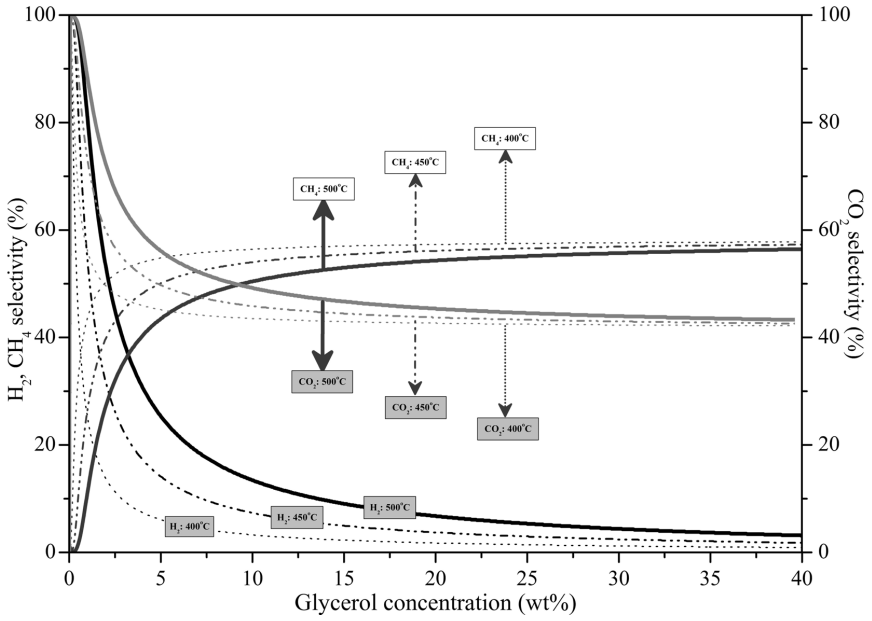

Figure 5.1: Calculated equilibrium gas yields of hydrogen, methane and carbon dioxide as a function of glycerol concentration and reaction temperature.

Non-catalytic gasification of 15 wt% of pure and crude glycerol was carried out at different operating temperatures and the product gas distribution is shown in Table 5.1. It is evident

from the table that the GE increased by raising the temperature. A maximum conversion of around 50% was obtained at 550 °C and only a very low degree of conversion (1%) at 450 °C. The product gas mainly constitutes of H_2, CO, CO_2 and minor amounts of CH_4 and C2+ compounds. Comparing the conversion of crude glycerol with that of pure glycerol, the GE is quite comparable but significant differences in the product distribution is noticed. The H_2 and CO yields decreased while the CO_2, CH_4 and C2+ yields increased with crude glycerol when compared to pure glycerol. Also from an operating point of view there was a large difference; as for the crude glycerol feed, the reactor was plugged after 2h of run time. From the table, it is apparent that the carbon closure was not 100% and this is related to the observation that the liquid effluent obtained was not a homogeneous liquid phase, but consisted of two phases, an aqueous (bottom) phase and oily phase on top. Due to the sampling issues with the elemental analyser only the carbon content of the aqueous phase is reported and therefore the carbon balance could not be closed.

Table 5.1: Non-catalytic gasification of pure and crude glycerol in supercritical water.

	15 wt% pure glycerol			**15 wt% crude glycerol**
Oven temperature (°C)	450	500	550	550
Pressure (bar)	250	250	250	250
Residence time (min)	1.37	1.13	0.98	0.98
Total run time (h)	2.5	2.5	3.0	2.0
Carbon to gas (%)	1.0±0.2	17.9±2.4	48.9±2.1	44.6±3.0
Carbon in aqueous phase (%)	82	63	21	17.8
	Yield (mol gas/mol feed)			
H_2	0.014	0.42±0.16	0.83±0.04	0.45±0.05
CO_2	0.008	0.18±0.03	0.34±0.02	0.44±0.05
CO	0.016	0.29±0.03	0.75±0.03	0.37±0.04
CH_4	0.001	0.03±0.01	0.17±0.02	0.21±0.02
C2+	0.001	0.02±0.00	0.09±0.02	0.13±0.02
	Dry gas composition (vol%)			
H_2	35.7	43.7±6.6	38±1.5	28.2±3.3
CO_2	21.0	19.7±1.6	15.8±1.3	27.3±3.0
CO	38.8	31.7±4.7	34.4±0.8	23.4±2.8

CH_4	1.6	3.2±0.2	7.7±1.1	13.0±1.2
C2+	2.9	1.7±0.3	4.0±0.7	5.4±0.5

5.3.2 REPRODUCIBILITY OF THE EXPERIMENTS

The reproducibility of the experiments was checked by performing several experiments under identical conditions and the details of the experiments and their results are presented in Table 5.2 and 5.3 respectively. From Table 5.2, it is evident that the first 3 experiments (Expt. 1, 2 and 3) are carried out at a feed flow rate of 1 ml/min, two experiments are carried out at 1.5 ml/min (Expt. 4 and 5) and last 2 experiments (Expt. 6 and 7) are carried out with 10 wt% glycerol at 2 ml/min). Table 5.3 presents the experimental gas yields and carbon to gas conversion of the experiments shown in Table 5.2. The results obtained under identical conditions are fairly close to each other indicating a good reproducibility of the experiments in this study.

Table 5.2: Experimental details carried out to check the reproducibility.

Sl. No.	Date	Catalyst, g	Glycerol, wt%	Flow, ml/min	Oven Temperature, °C	Pressure, bar	Time on stream, h
1	25-May-10	1	15	1.0	450	250	5
2	08-May-10	1	15	1.0	450	250	7
3	04-May-10	1	15	1.0	450	250	7
4	28-Sep-10	1	15	1.5	450	250	4
5	12-Apr-11	1	15	1.5	450	250	3
6	17-May-11	1	10	2.0	450	250	3
7	05-Nov-11	1	10	2.0	450	250	3

Table 5.3: Product gas yields (mol/mol) and GE (%) of the experiments carried out to check reproducibility.

Sl. No.	GE (%)	H_2	CO_2	CO	CH_4	C_2H_6	C_3H_8
1	99	2.894	1.911	0.043	0.547	0.219	0.011
2	97	2.486	1.775	0.030	0.487	0.279	0.017
3	98	2.824	1.890	0.036	0.551	0.202	0.024
4	100	2.114	1.641	0.021	0.474	0.392	0.012

5	94	3.017	1.877	0.028	0.632	0.103	0.011
6	77	2.884	1.689	0.020	0.486	0.059	0.003
7	76	2.512	1.610	0.034	0.483	0.080	0.002

5.3.3 INFLUENCE OF THE CARBON CHAIN LENGTH OF DIFFERENT OXYGENATED COMPOUNDS

Initial experiments (Table 5.3) showed that with the bimetallic Pt–Ni/Al_2O_3 catalyst (near) complete conversion of glycerol was achievable at a comparably low temperature (450 °C), in combination with a high selectivity towards hydrogen. To provide a frame of reference for the catalytic gasification, the efficacy of the process is compared with that for compounds as ethylene glycol, methanol, 1, 2-PD and sorbitol.

Figure 5.2 illustrates the influence of product gas selectivities and the GE for the selected oxygenated compounds. Complete carbon to gas conversion was obtained for methanol, ethylene glycol and glycerol, but not for propane-diol, glucose and sorbitol (6 carbon atoms). A strong decrease in the hydrogen selectivity was found for the series methanol > ethylene glycol >> glycerol > sorbitol, hence with increasing the number of carbon atoms, whereas the alkane selectivity increases with increasing number of carbon atoms. The hydrogen and alkane selectivity trends obtained are in line with the earlier published reports.[116] However, with glucose, being more susceptible to coke formation, only 30% carbon to gas conversion was obtained, even at a feed concentration as low as 1.5 wt%. For glucose reforming in supercritical water, the hydrogen and alkane selectivity were 50% and 16% respectively. The shift in hydrogen and alkane selectivities with increasing carbon number of the feed molecules is most probably related to the increased possibilities for intermediate compounds to undergo undesired side reactions and the occurrence of hydrogen consuming reactions.[9, 116]

Selectivity issues needs to be addressed for the production of H_2 from renewable biomass sources. Hydrogen production from oxygenated compounds would require an effective catalyst that promotes reforming reactions via C-C bond scissioning followed by water-gas shift reaction and simultaneously inhibits the formation of alkanes via C-O bond scissioning followed by hydrogenation step. Alkanes are formed from subsequent reaction of H_2 and CO_2 via methanation and Fisher-Tropsch reactions. Pt is known to exhibit reasonable C-C bond scission activity and low activity for C-O scission reactions and the series methanation and Fisher-Tropsch reactions. Nickel based catalysts exhibits relatively high activities towards C-C bond scissioning and methanation reaction.[9, 116] Thus, alloying of inexpensive Ni to Pt leads to more catalytic sites each with higher activity than Pt.[120]

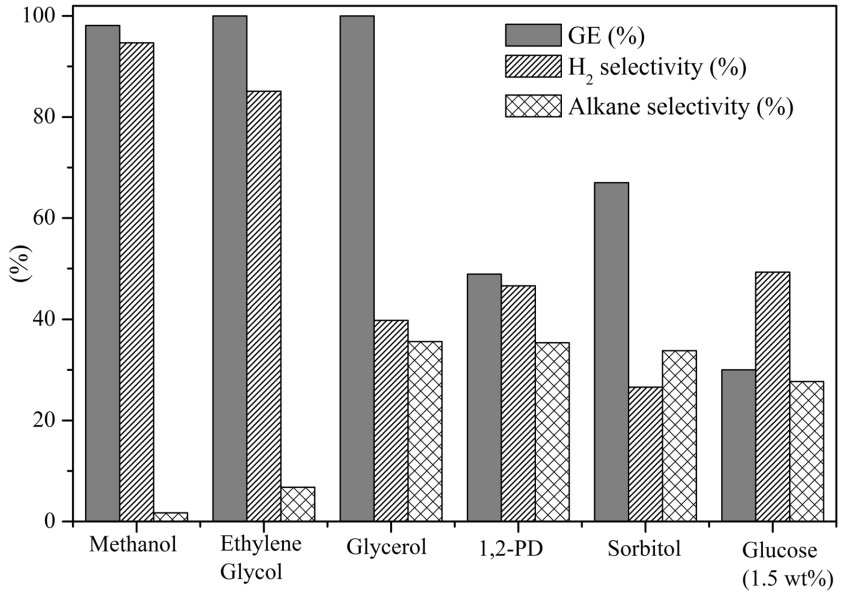

Figure 5.2: The influence of different chain lengths of carbon containing oxygenated compounds on the product gas selectivities in the presence of a bimetallic Pt–Ni/Al2O3 catalyst. Experimental conditions: Feed concentration – 15 wt%, Oven temperature–450 °C, P–250 bar, WHSV- 8.93 h^{-1}.

5.3.4 EFFECT OF TEMPERATURE

The effect of temperature on the carbon to gas conversion and product gas selectivity of 15 wt% glycerol reforming in SCW is studied over a temperature range of 380–500 °C. Figure 5.3 shows the cumulative gas production as a function of time and the gasification efficiencies based on gas analysis and liquid phase analysis. The cumulative gas production increased linearly with time for all reaction temperatures studied (Figure 5.3a), suggesting that the catalyst activity (and selectivity to gas) did not degrade during the experimental run. Earlier, we have shown that this Pt–Ni bimetallic catalyst was also very active and stable during a 9 h experimental run for the reforming of ethylene glycol.[14]

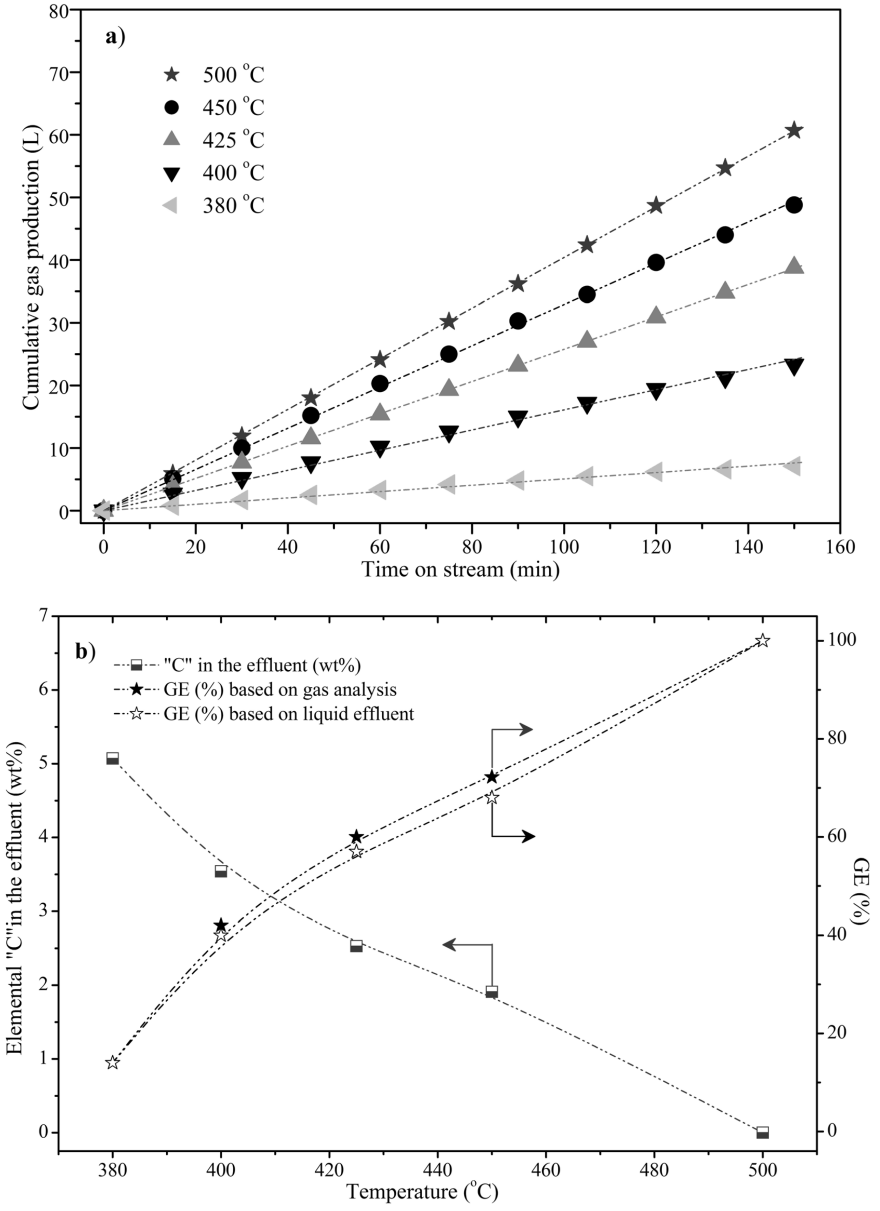

Figure 5.3: The influence of oven temperature on *a)* the cumulative gas production rate *b)* gasification efficiencies based on produced product gas and liquid analysis at different temperatures.

Increasing the reaction temperature generally favours the carbon to gas conversion. An increase in the gasification efficiency with temperature raise was obtained and is shown in Figure 5.3 b. The carbon content of the liquid effluent decreases with increasing temperature. Note that the carbon to gas conversions based on the gas yield and on the liquid analysis of the effluent after the reaction are more or less similar, indicating good closure (100%) of the (carbon) mass balance and thus no-, or at least very little-, coke formation.

The product gas selectivities, obtained from reforming the 15 wt% glycerol as a function of temperature, are displayed in Figure 5.4. In contrast to the equilibrium calculations, which predict methane to be the dominating product, the product gas obtained mainly consists of CO_2 and H_2. Though the temperature has a strong effect on the carbon to gas conversion, only marginal changes in the product gas selectivities were noticed. The CO selectivity found was always below 2.5% at all temperatures studied and only a slight decrease in the CO_2 selectivity from 77.7% to 62.1% is noticed. The methane selectivity increased from 12.8% at 380 °C to 19.4% at 500 °C and the hydrogen selectivity increased from 31.7% at 380 °C to 48.5% at 450 °C and then decreased to 39.4% on further raising the temperature to 500 °C.

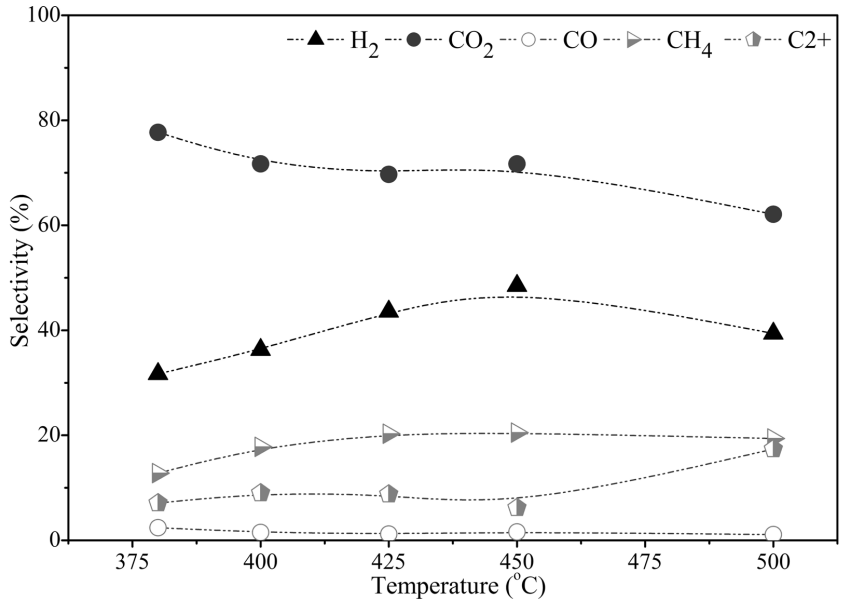

Figure 5.4: The influence of oven temperature on the product gas selectivities of glycerol reforming in supercritical water. Experimental conditions: Glycerol – 15 wt%; Pressure – 250 bar; Pt–Ni/Al_2O_3 – 1 g; Feed flow rate – 2 mL/min, WHSV – 17.86 h^{-1}.

The temperature had a notable influence on the concentration of intermediate compounds present in the liquid effluent (Figure 5.5). At low reaction temperatures, unconverted glycerol is the major compound identified in the liquid phase among the intermediate products such as 1, 2-PD, ethanol, acetaldehyde and ethylene glycol. High yields of the liquid products were identified at lower temperatures and with raising the temperature the yields of these species decreased due to higher reforming activity leading to an enhanced ethane yields. These results indicate that reforming of glycerol at near critical conditions of water, catalyzed by an acid (γ-Al_2O_3) and metal-functionality of the catalyst (here Pt–Ni), results in 1, 2-PD as the main liquid product, in line with results from Wawrzetz *et al.*[133]

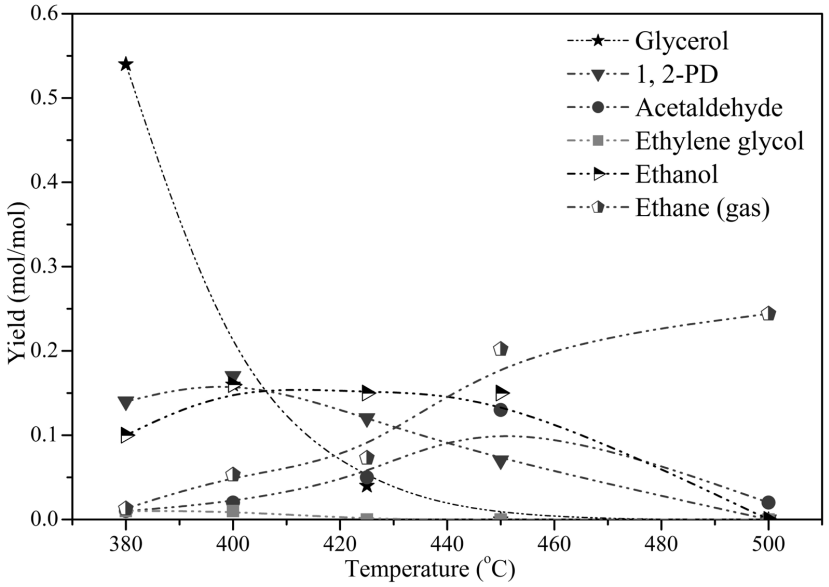

Figure 5.5: The influence of 15 wt% of glycerol reforming in supercritical at various oven temperatures on the product distribution of the intermediate compounds present in the liquid effluent. Experimental conditions: Glycerol – 15 wt%; Pressure – 250 bar; Pt–Ni/ Al_2O_3 – 1 g; Feed flow rate – 2 mL/min.

5.3.5 EFFECT OF CONCENTRATION

High feedstock concentrations are beneficial from both process efficiency and economic perspectives.[22] On the other hand, for some compounds it has been noticed in earlier studies that *e.g.* coke formation and other undesired side reactions are enhanced at higher feed concentrations. To study this effect for glycerol, the initial glycerol concentration was varied from 2.6 to 20 wt% to see its influence on the gasification behaviour and product selectivities

at a fixed catalyst loading (1g), see Figure 5.6. The increase in feed concentration at a fixed catalyst loading corresponds to increase in WHSV.

The gasification efficiency decreases steadily from 99% to 46% with increasing the feed concentration. Remarkably, the GE started reducing at a significantly lower level (around 5 wt%) than the concentration for which the C2+ selectivity started increasing (around 15 wt%). The CO selectivity increased marginally to 2.5% at high glycerol concentration, but was always very low. The hydrogen selectivity, on the other hand, decreased more strongly from 59.2% to 32%, whereas the CO_2 and CH_4 selectivities remained more or less constant ~73% and 20%, respectively.

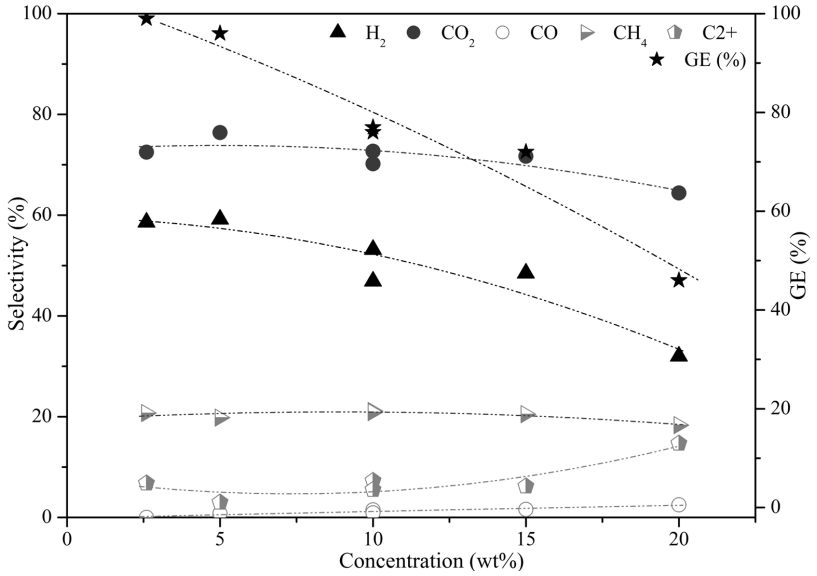

Figure 5.6: Effect of glycerol feed concentration on the product gas selectivities when reformed in SCW at oven temperature set to 450 °C and 250 bar in the presence of Pt–Ni catalyst.

The major liquid intermediate components present in the liquid effluent mainly consists of unconverted glycerol, 1, 2-PD, 1, 3-PD, acetaldehyde and ethanol. The yields of the liquid intermediates increased at higher glycerol concentrations (shown in Table 5.4). Trace amounts of 1, 3-PD in the liquid phase were observed at high glycerol concentrations and its formation route is shown in the proposed reaction pathway (Figure 5.10). Higher selectivities to 1, 3-PD and also 1, 2-PD can be achieved by modifying the supported Pt catalysts with W or Re modifiers.[156] By altering the Pt catalysts it is therefore possible to selectively tune the

dehydrogenation and dehydration activity and thereby controlling the reforming routes to either towards 1,2-PD or 1,3-PD.

Table 5.4: Quantification of the liquid intermediate compounds obtained at reforming of different concentrations of glycerol in SCW.

Feed (wt%)	Intermediate products in the liquid (mol/mol feed)			
	Glycerol	1, 2 PD	Acetaldehyde	Ethanol
20	0.22	0.14	0.09	0.11
15	-	0.07	0.13	0.15
5	-	-	0.01	0.29

5.3.6 EFFECT OF SPACE VELOCITY

To identify the optimum conditions at which maximum conversion to the desired products could be achieved, the effect of reaction time has been varied by changing the WHSV by varying the feedstock flow rate.

The WHSV used in this study ranged from 8.93–44.6 h^{-1} and was varied by raising the feed flow rate (15 wt% glycerol) from 1 to 5 ml/min. The influence of the WHSV on the gasification efficiency and the product gas yields is shown in Figure 5.7 a and b and in Figure 5.8 for the products identified in the liquid phase. The gasification efficiencies based on gas yields and also liquid effluent elemental analysis closely matches, indicating almost complete mass balance closure. The gasification efficiency decreased significantly from 100 to 20% with increasing WHSV, due to the shorter residence time within the catalyst (packed-) bed. A similar behaviour of gasification efficiency trend is observed and discussed earlier when the feed concentration was increased, while keeping the catalyst loading and reactant flow rate constant. The CO selectivity was always very low (<2%) at all the space velocities studied. At higher space velocities, the higher alkane selectivity decreased from 17.7 to 2.8%, while the methane selectivity remained constant (~18%) and the CO_2 selectivity increased from 63% to 79%. The hydrogen selectivity increased from 39.8% at 8.9 h^{-1} and reached a maximum of 48.5% at 17.9 h^{-1}. At further increasing the space velocity, the hydrogen selectivity returned to the initial selectivity of 39.5% at 44.6 h^{-1}.

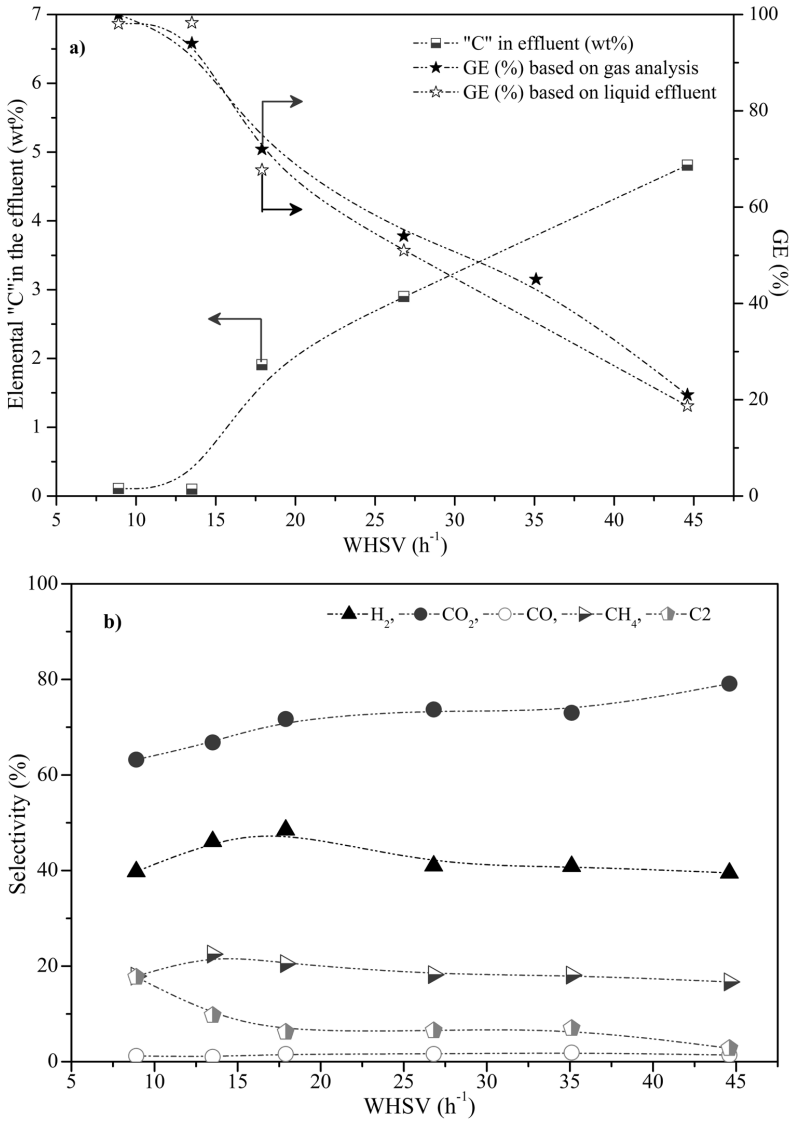

Figure 5.7: Effect of different WHSV on the a) gasification efficiency and elemental C present in the effluent b) product gas selectivities. Experimental conditions: Glycerol–15 wt%; Oven temperature–450 °C; Pressure–250 bar; Pt–Ni/Al_2O_3–1 g.

The yields of liquid reaction intermediates at different space velocities are shown in Figure 5.8. At higher space velocities, the unconverted glycerol is the major product present in the liquid

and it increased with increasing the space velocity. The yield of 1, 2–PD increased to 0.2 mol/mol at 26.8 h^{-1} and remained stable at higher space velocities. Acetaldehyde yield increased to 0.13 at 17.9 h^{-1} and further increasing the space velocity led to decreased yields. The yields of ethanol and ethylene glycol were lower than for the other components. The ethane yield decreased with increasing the space velocity. Ueda *et al.*[157] obtained similar products in the liquid phase in their study of the hydrogenolysis of glycerol over Pt-modified Ni catalyst. The C-O hydrogenolysis to 1, 2-PD was the main reaction and further hydrocracking reaction leads to ethylene glycol. In our case the yields of 1, 2-PD are higher than the ethylene glycol which means that the hydrocracking of 1,2-PD is relatively slow. The reaction of 1, 2-PD produces ethanol and methane. At higher conversions achieved at high reaction temperatures, long residence time and low feed concentrations, the yields of the liquid products decreased significantly, while the yields of product gases increased notably, which indicates that all the liquid products undergo further reactions to gaseous products via analogous reaction pathways, as discussed in later sections.

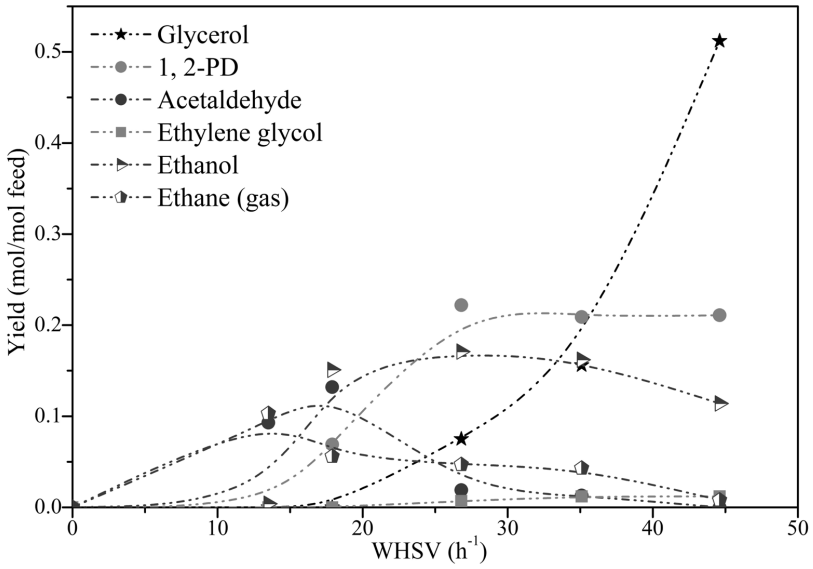

Figure 5.8: Effect of WHSV on the intermediate compounds present in the liquid after glycerol reforming in SCW. Experimental conditions: Glycerol – 15 wt%; Oven temperature–450 °C; Pressure–250 bar; Pt–Ni/Al_2O_3–1 g.

5.3.7 CRUDE GLYCEROL REFORMING

The results obtained with the pure and the crude glycerol feed stocks are noticeably different. The cumulative gas production and the gasification efficiency of both crude and pure glycerol are shown in Figure 5.9 a. It can be noticed from the figure that the gasification efficiency of the pure glycerol remains stable during the run, whereas for the crude glycerol the gasification efficiency declines drastically and the cumulative gas production trend has a non-linear behaviour with time (decreasing slope), suggesting deactivation of the catalyst. Consequently, a similar trend of decreasing gas yields for crude glycerol reforming at 450, 475 and 500 °C is shown in Figure 5.9 b, where the hydrogen and CO_2 yields drop significantly with time. This decrease in the gas yields and gasification (or, in other words, deactivation of the catalyst) can be attributed to coke formation and also may be associated with the presence of impurities such as chlorides, methyl esters and trace amounts of biodiesel present in the crude. A similar behaviour of catalyst deactivation was reported for the steam reforming of crude glycerol.[147] In section 5.3.11 the post-mortem analysis of the catalyst is discussed.

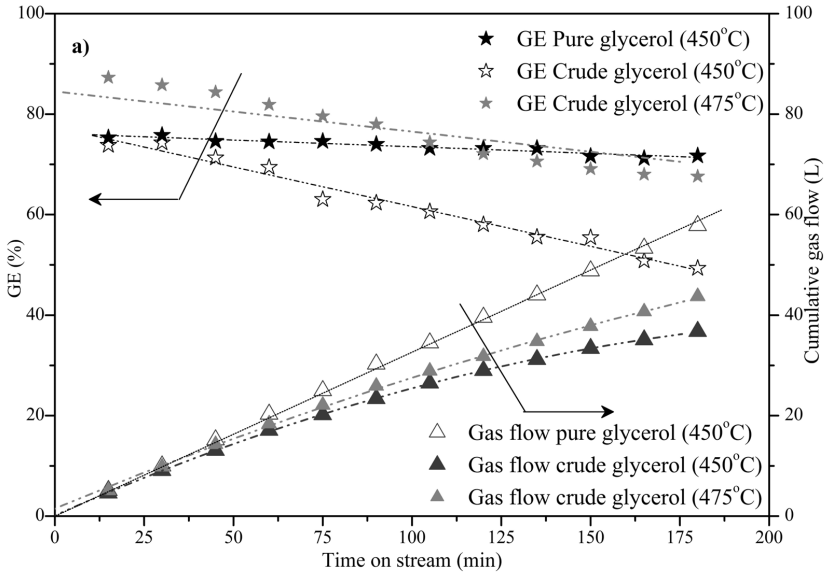

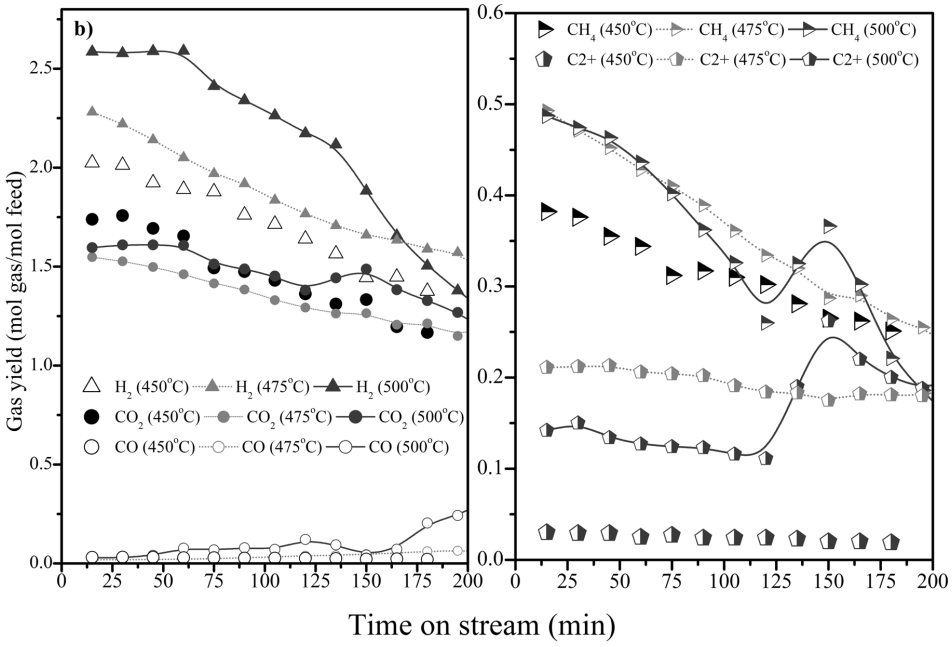

Figure 5.9: The product gas yields and the GE of glycerol reformed in SCW a) comparison of the GE and cumulative gas production with time on stream for crude and pure glycerol b) Product gas yields with time on stream for crude glycerol. Experimental conditions: Glycerol concentration– 15 wt%; Oven temperature – 450, 475 and 500 °C; Pressure – 250 bar; Pt-Ni–1 g.

5.3.8 MECHANISTIC IMPLICATIONS OF GLYCEROL REFORMING ROUTES OVER PT-NI CATALYST IN SUPERCRITICAL WATER

Glycerol is a saturated compound having a higher O/C ratio than any other commodity chemicals. Reforming of glycerol over platinum catalysts leads to hydrogen production via dehydrogenation. The hydrogen produced can immediately initiate hydrogenolysis; a reduction step in which the chemical bonds of an organic molecule are dissociated by simultaneous addition of hydrogen to the resulting molecular fragments. Typical reaction products of glycerol hydrogenolysis include 1, 2-PD, 1, 3-PD, 1-Propanol, 2-Propanol and Ethylene glycol. Formation routes for these compounds based on the literature[156, 158] and our experimental data are collectively presented in a proposed reaction network scheme, which is shown in Figure 5.10.

The three major steps in the catalytic reforming of glycerol at low temperatures in supercritical water are dehydrogenation-dehydration-hydrogenation mechanisms, all presented in the

scheme. The primary route for the formation H_2 and CO_2 proceeds via glyceraldehyde as a major product. The main precursors for the CO_x formation are the aldehyde and carboxylic groups. The formation of liquid intermediates from glycerol reforming in supercritical water can be explained by three different routes. The top route shows the dehydration of glycerol to 2-hydroxyacetone and its further hydrogenation to 1, 2-PD formation. The second route to the formation of 1, 2-PD is via dehydrogenation of glycerol leading to glyceraldehyde which in the subsequent process undergoes dehydration reactions producing acetol (hydroxy acetone) and its successive hydrogenation to the production of 1, 2-PD. In this study, the acidic functionality of the γ-Al_2O_3 plays a role in the dehydration reaction and the hydrogenation reactions are catalyzed by the active Pt–Ni metal. The third route to the formation of 1, 3-PD proceeds in a similar fashion as 1, 2-PD by the dehydration of glycerol to 3-hydroxypropanal (thermodynamically less stable than acetol) and its hydrogenation. Since, only very low concentration of 1, 3-PD is obtained when compared to high concentrations of 1, 2-PD, this route has very less contribution when compared to above two routes described and therefore this route was considered to be unimportant.

It is further reported that 1, 3-PD has a high reactivity[146], comparable to that of glycerol, whereas (and in contrast-) 1, 2-PD was found to have a lower reactivity than glycerol. Hence, high yields of 1, 2-PD were obtained due to its low reactivity in subsequent gasification reactions and only trace amounts of 1,3-PD were obtained due to its high reactivity. The successive hydrogenolysis of 1, 2-PD and 1 3-PD leads to the formation of 1-Propanol and 2-Propanol, but these products are not found in our study. The formation of ethylene glycol can be explained either by decarbonylation of glyceraldehyde or by retro-aldol condensation of glyceraldehyde yielding glycolaldehyde and formaldehyde and their hydrogenation to produce ethylene glycol. Additionally, acetaldehyde and ethanol are other major liquid products formed and the plausible route to the formation of these compounds is via decarbonylation of glyceraldehyde forming ethanediol which subsequently dehydrates to acetaldehyde and in turn can be hydrogenated to ethanol.[133] The presence of lower alkanes (CH_4 and C_2H_6) can be attributed to the over hydrogenolysis of the degraded intermediate products or can result from the decarbonylation or decarboxylation of intermediate products.[133, 156] Glycerol reforming in supercritical water with Pt-Ni catalyst mainly leads to gases (H_2, CO_2, CH_4, C_2H_6 and C_3H_8), liquid intermediate products which at high reaction temperatures also reform to lower alkanes (CH_4 and C_2H_6).

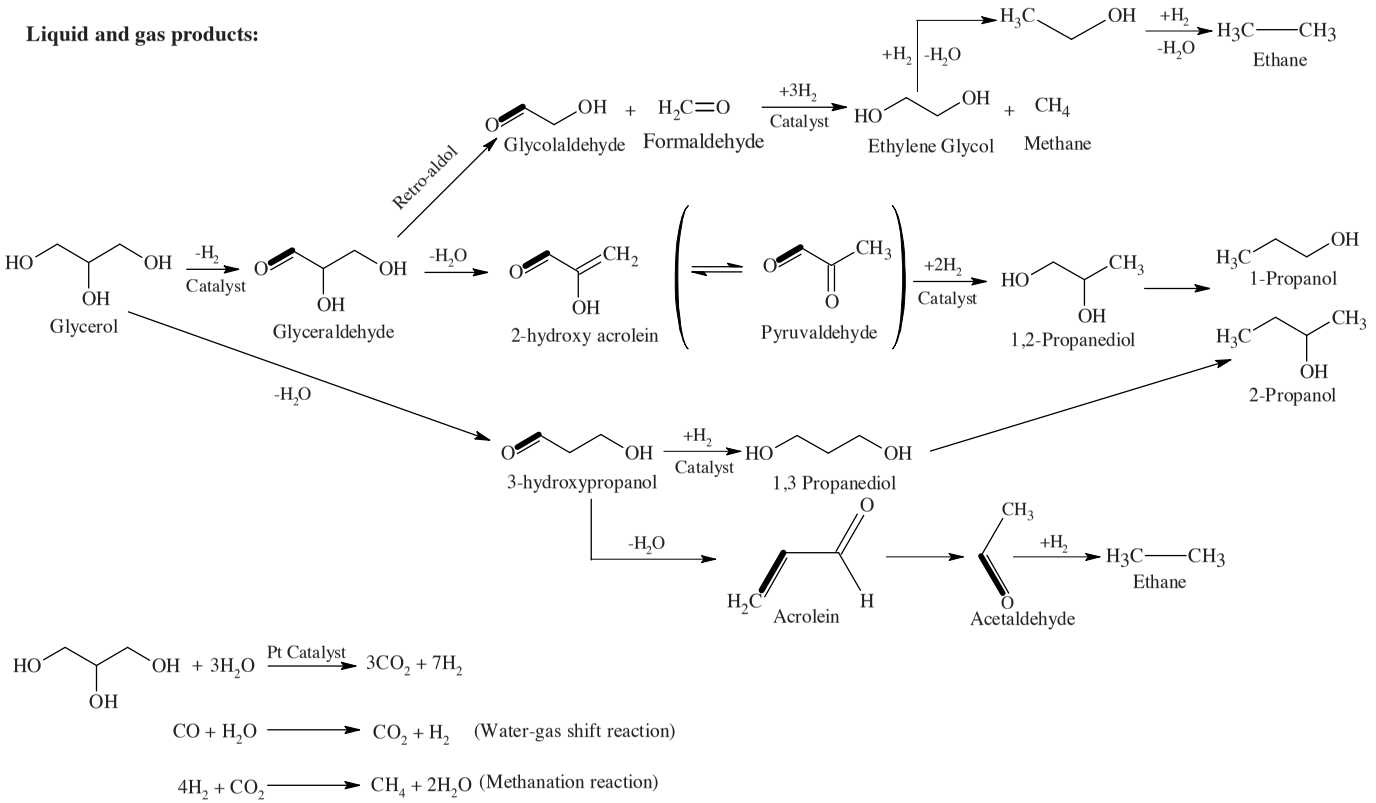

Figure 5.10: Possible reaction pathways of glycerol reforming in supercritical water towards liquid and gaseous products in the presence of bimetallic Pt–Ni catalyst.

5.3.9 STABILITY TEST

The stability of the catalyst is of utmost importance for its viability in the further development of an application or conversion process. The long term stability test of the bi–metallic catalyst for converting (at 500°C) an aqueous feed containing 20 wt% of glycerol is shown in Figure 5.11. Notable changes in the carbon to gas conversion and product selectivities of H_2 and C2+ are seen during the initial 5 h. The propane selectivity showed a noticeable decrease, probably due to deactivation of the hydrogenation sites. Due to the high initial activity of the catalyst complete conversion was initially obtained and then decreased slightly. However, stable conversion and a nearly constant product distribution are obtained through the remaining 80h of the run. The CO selectivity was less than 2% throughout the run time. After 85h the run had to be stopped due to problems with the feed pump, not related to the gasification process itself. Although, apparently the catalyst performance did not suffer from any leaching during the test run, it underlines the need for applying more stable supports (*e.g.* ZrO_2) which doesn't change its crystalline structure unlike γ-Al_2O_3.

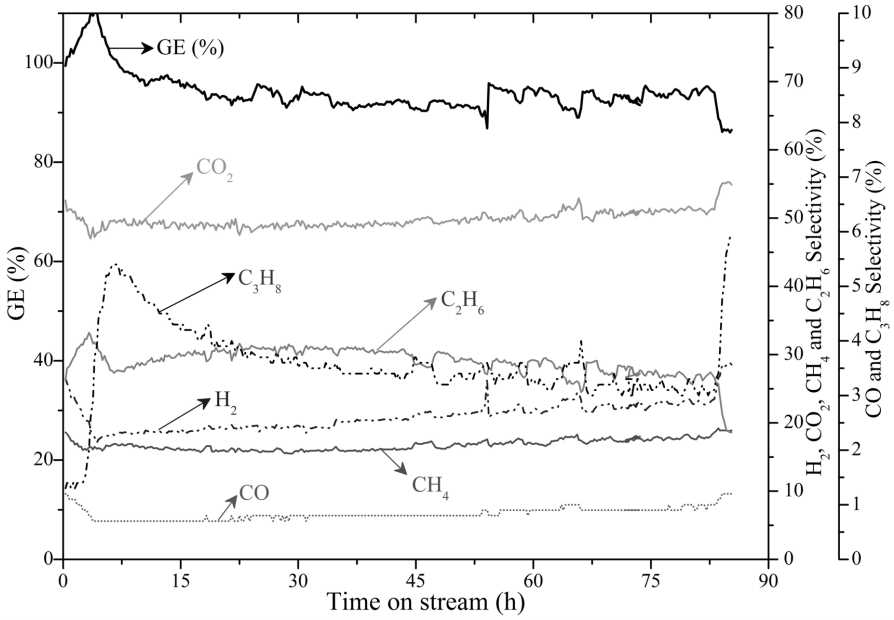

Figure 5.11: Long term stability test of the Pt–Ni bi–metallic catalyst carried out with reforming of 20 wt% glycerol in supercritical water at oven temperature set to 500 °C, 250 bar and at a space velocity of 4.0 h^{-1}.

5.3.10 INFLUENCE OF THE CATALYST BED LOCATION

Catalyst coking is one of the major issues in any reforming process and one of main reasons is due to the formation of intermediate species that are more prone to coke formation. In this study we investigated the possible influence of the position of the catalyst bed in the lab scale reactor used, in order to minimize the coke formation in the supercritical water reforming process. The hypothesis was that some reaction intermediates formed in the absence of a catalyst (directly at the point of feed injection) may form coke precursors, which are then difficult to convert, even in the presence of a catalyst. In that case, the longer the distance between the catalyst bed and the feed entrance, the lower the gasification efficiency expected. To evaluate this, the gasification efficiency and product gas selectivities are determined for different situations in which the reactor ovens were set at 450 °C and for which the catalyst bed is placed at three different locations: 20, 40 and 60 cm from the top of the reactor where the (premixed-) feed enters. The gasification efficiencies and the product distribution obtained when the catalyst was placed at 20 and 60 cm are quite comparable, but the values are significantly different from the values obtained at 40 cm, see Table 5.5. This significant difference in the conversion and product distribution could (in hindsight) be correlated well to the (later determined) temperature gradient inside the reactor tube. It was found that there is (on average) a temperature difference of some 50 °C from the wall to the inside of the reactor, and, more importantly, the temperatures measured at the three different locations are also significantly different (respectively 380 °C, 400 °C and 375 °C at 20 cm, 40 cm and 60 cm from the top of the reactor). Maximum conversion was achieved when the catalyst was placed in the middle of the reactor tube (at 40 cm from the top), where the maximum temperature was reached. The distance from feed injection to catalyst bed itself does not seem to be an important factor in the coke formation nor gasification reduction.

Table 5.5: Product distribution of 15 wt% glycerol reforming in supercritical water (oven set-point 450 °C), 250 bar and 8.93 h^{-1} in the presence of Pt–Ni catalyst placed at different bed locations.

Catalyst bed location	Inside reactor Temp. °C	GE (%)	Selectivity (%)				
			H_2	CO_2	CH_4	CO	C2+
20 cm	380	78	32.0	59.8	15.9	1.1	23.2
40 cm	400	98	41.0	64.0	18.6	1.2	16.2
60 cm	375	72	30.8	62.1	15.0	1.1	21.8

5.3.11 CATALYST CHARACTERIZATION

The stability of heterogeneous bi-metallic catalyst applied under the hydrothermal test-conditions was evaluated by the BET and XRF analysis of the catalysts before and after the reaction. The XRF analysis of the fresh and spent catalysts indicated no leaching of metals under the conditions studied. However, a significant loss in the surface area of the spent catalyst (25 m^2/g) is ascribed to the phase change of γ-Al_2O_3 (194 m^2/g) to boehmite and the results are in agreement with earlier studies.[2, 7, 16, 17]

Table 5.6: Catalyst characterization results of fresh and spent samples.

Catalyst ID	XRF analysis (wt%)	BET surface area (m^2/g)
Fresh catalyst	Pt-1.2; Ni-0.42	194
Spent catalyst – 500 °C, 250 bar	Pt-1.2; Ni-0.42	25

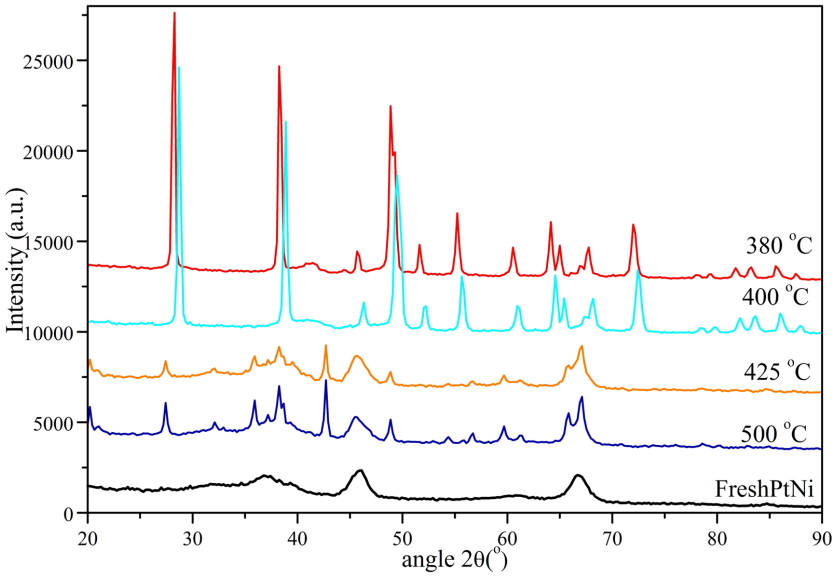

Figure 5.12: XRD spectra of the fresh and spent catalysts obtained at different reforming temperatures (380, 400, 425 and 500 °C) in supercritical water.

Post mortem analysis of the fresh and spent catalyst by means of X-ray diffraction revealed the phase change of γ-Al_2O_3 to boehmite (Figure 5.12). The fresh γ-Al_2O_3 peak consisted of two

peaks at 45.6° and 66.7°, while the spent catalysts obtained at different reforming temperatures have multiple peaks which correspond to boehmite and α-Al_2O_3. This phase change of alumina from gamma to alpha/boehmite is in-line with the BET surface areas given in Table 5.6.

Figure 5.13 shows the morphological changes of the fresh and spent catalyst obtained after reforming of glycerol at 400 °C in supercritical water. It is evident from the figure that significant morphological changes in the crystalline structure of the spent catalyst are obtained after exposure to supercritical water at different reaction temperatures. The spent catalyst consisted of agglomerates of sharp crystals when compared to the fresh catalyst.

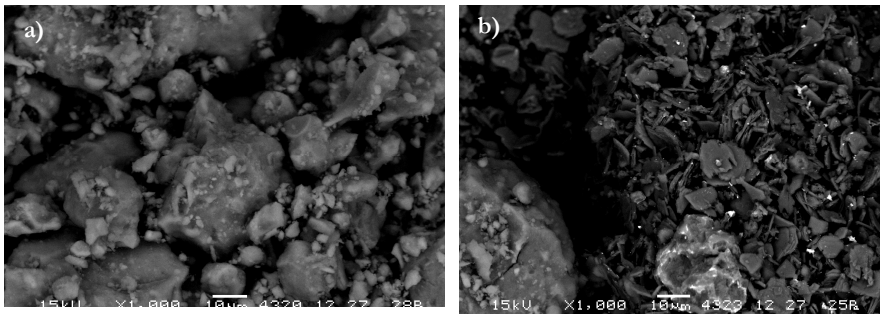

Figure 5.13: Scanning electron micrographs of a) fresh and b) spent catalyst of glycerol reforming carried out at 400 °C (oven temperature) and 250 bar.

Carbonaceous deposits on the Pt-Ni catalyst used for glycerol reforming were studied by Raman spectroscopy. Raman spectra of the spent Pt-Ni catalyst used for glycerol reforming and blank experiment (exposure to supercritical water only) are depicted in Figure 5.14. The Raman spectrum of the Pt-Ni catalyst that was exposed to supercritical water in the absence of organic reactants showed five absorption bands in the range of 0–4000 cm^{-1}. As discussed in a previous study, these bands are attributed to the boehmite phase[159-160] which is formed as a result of the phase change of the catalyst γ-Al_2O_3 support when subjected to supercritical water.[14, 161] In case of the catalyst used for glycerol reforming, no boehmite absorption bands are visible in the Raman spectrum. However, the spectrum showed two characteristic carbon bands in the range of 1300–1700 cm^{-1},[162-164] indicating coke deposition. The absence of any boehmite absorption bands can be explained by the fact that Raman spectroscopy is a surface technique and coverage of the catalyst surface by coke makes the boehmite invisible. The nature of the coke is further investigated by TGA up to a temperature of 850 °C.

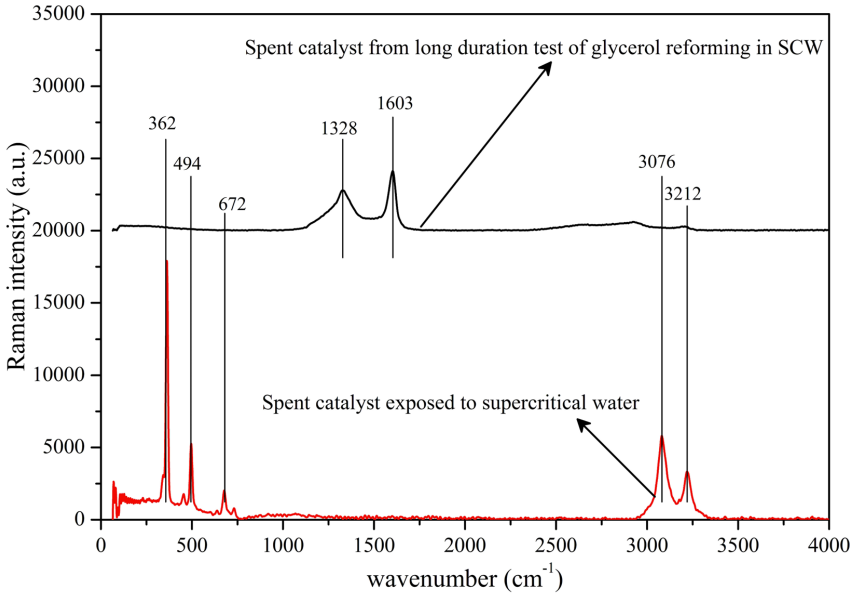

Figure 5.14: Raman spectra of spent Pt-Ni catalysts *a)* exposed to supercritical water (red) *b)* long duration test (85 h) of glycerol reforming (black).

TGA analysis of the fresh and spent catalysts of glucose, glycerol and 1, 2-PD reforming in SCW is shown in Figure 5.15. Peaks arising after 300 °C indicate the presence of carbonaceous deposits on the spent Pt-Ni catalysts. For crude glycerol reforming at 475 °C, a wide peak which represents the coke conversion on the spent catalyst is observed in the temperature range of 300–600 °C, while for 1, 2-PD it is observed in the temperature range of 500–600 °C. Comparatively a small peak is also noticed with 1.5 wt% glucose reforming at 450–600 °C. A large peak is observed in case of long duration test with glycerol reforming representing significant amount of coke formation during the test. Despite the coke formation the catalyst did not show any deactivation during 85 h time on stream, indicating that the formation of coke did not pose a problem on the catalyst activity in supercritical water. The high tendency of supercritical water to dissolve organic species, including carbonaceous deposits[165] is believed to help clean the catalytic surface of any coke deposits to ensure accessibility of reactants to the catalyst. However, with crude glycerol catalyst deactivation was seen very quickly due to the presence of impurities (both organic and inorganic). XRF analysis of the spent catalysts from crude glycerol indicated the presence of several inorganic impurities particularly chlorides (22%) on the catalysts and we believe this could be one of the prime reasons for immediate catalyst deactivation in case of crude glycerol. We also believe that there could be an increase

in the crystallite size after the reaction but we couldn't able to assess the extent of metal sintering in this study.

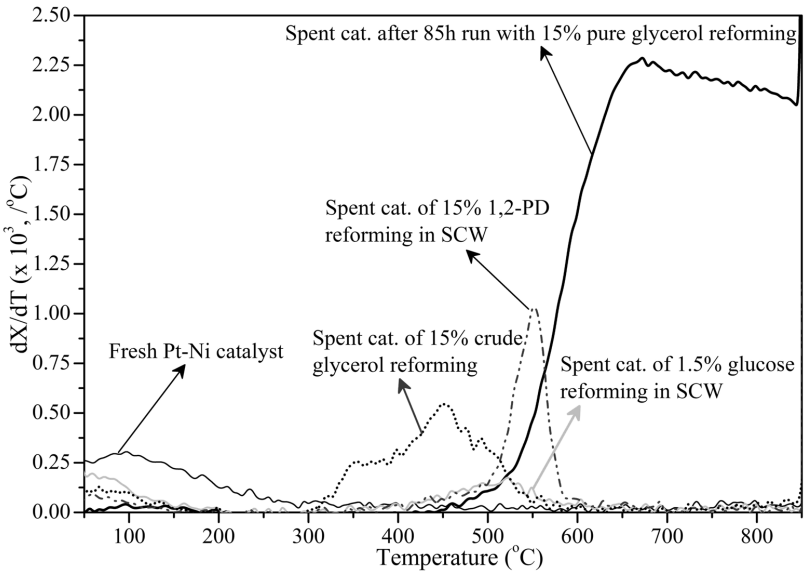

Figure 5.15: TGA analysis of *a)* fresh Pt-Ni catalyst *b)* spent catalyst of 15 wt% 1, 2-PD reforming in SCW *c)* spent catalysts of 1.5 wt% glucose reforming *d)* spent catalyst of crude glycerol reforming and *e)* spent catalysts of 15 wt% glycerol reforming for 85 h in SCW.

5.4 CONCLUSIONS

Catalytic reforming of glycerol in supercritical water was studied over Pt–Ni/Al_2O_3 bi-metallic catalyst at near critical conditions of water (around 400 °C reaction temperature). The influence of different processing parameters such as temperature, space velocity, feed stock concentration and the nature of feed stock on the conversion and gas yields was investigated. The main gas products in the glycerol reforming are H_2, CO_2, CH_4, C2+ and minor amounts of CO. The liquid phase products of the glycerol reforming mainly consisted of acetaldehyde, 1, 2-propanediol and ethanol. Complete conversion of glycerol was achieved at the moderately low temperatures of 400-450 °C studied. The product gas showed high hydrogen gas yields, in contrast to the thermodynamic equilibrium composition.

High reaction temperatures accompanied with low space velocities and low feed stock concentrations favours high conversion and maximum hydrogen selectivity. At high feed concentrations, low reaction temperatures and high space velocity the GE decreased and liquid

effluent after the reaction mainly consisted of unconverted glycerol and other liquid intermediate compounds such as acetaldehyde, 1, 2-propanediol, ethanol, ethylene glycol. At high reaction temperatures these liquid intermediates are catalytically reformed to product gases and enhanced yields of higher alkanes were noticed.

A comparison of the reforming activity of the catalyst and process with respect to the feedstock characteristics was made by comparing the carbon to gas conversion and product distribution of pure and crude glycerol. The catalyst was more prone to immediate deactivation with crude glycerol, although initial conversion and product distribution are similar to those obtained with pure glycerol. The catalyst deactivated rapidly with crude glycerol, while for the pure feedstock the catalyst showed stable performance for a long duration run, demonstrated up to 85 h.

Chapter 6

Experimental studies of hydrothermal gasification of bio-liquids in a continuous reactor

Chapter 6

6.1 INTRODUCTION

Supercritical water gasification (SCWG) is a technology that is proposed to convert wet biomass streams to a high heating value gas product. At temperatures and pressures above critical point (T> 374 °C; P> 221 bar), water serves both as a solvent and participates as a reactant in the process. In this chapter, we studied the catalytic reforming of two aqueous waste streams, namely the water soluble fraction (also referred as aqueous fraction) of pyrolysis oil and glycerol, a by-product in biodiesel production.

Pyrolysis is a thermo-chemical process to convert solid biomass into liquid oil, which is a mixture of oxygenated compounds and water. In this process, relatively dry biomass is rapidly heated to temperatures around 450–500 °C in the absence of oxygen.[166-167] During pyrolysis, dry wood is converted into liquid, with a typical yieldof 65-70%. The heating value of pyrolysis oil (HHV ~ 17 MJ/kg) is low compared to fossil fuels (HHV ~ 45 MJ/kg) due to high water content, which is typically about 15-25%. Pyrolysis oil has a higher volumetric energy density compared to the original biomass. However, the high water content, oxygen content and acidic nature of the pyrolysis oil prevents its application in a standard refinery. Separating pyrolysis oil into a water soluble (aqueous phase) and a water-insoluble fraction (heavy oil phase) is one way to deal with above mentioned issues with pyrolysis oil to integrate with existing refineries. Two possible applications of the heavy phase are it can be used as a substitute for phenol-formaldehyde formulations[118] or it can be upgraded to fuels[3].

For the aqueous phase of pyrolysis oil a few studies have reported on the production of H_2 by catalytic steam reforming. However, steam reforming of such highly diluted aqueous waste streams is an energy intensive step. Though, SCWG is a promising technology for such aqueous waste streams, remarkably only a very limited number of studies have reported on the reforming of the water soluble fraction of pyrolysis oil in supercritical water. A literature overview of the catalytic and non-catalytic reforming of water soluble fraction of bio-oil in supercritical water is reported elsewhere.[31]

Another feedstock investigated in this study is glycerol. Crude glycerol is a by-product of biodiesel production. At present there are several applications for pure glycerol. However, the presence of impurities in crude glycerol limits its suitability for these applications. Therefore, there is a need for direct valorisation of crude glycerol without any purification.[144, 146] Recently, the production of synthesis gas via hybrid steam reforming of glycerol and methane carried out at different process conditions and in the presence of commercial steam reforming catalysts has been reported.[147] Steam reforming of pure glycerol was found to be much easier than that of the neutralised crude glycerol at 800 °C and the loss of catalytic activity with crude glycerol was attributed to the presence of organic and inorganic impurities.

Catalytic reforming of glycerol in supercritical water is now attracting a great deal of applied research interest. A brief summary of the catalytic and non-catalytic reforming of glycerol in supercritical water is summarized in our earlier work.[155] Complete conversion of glycerol in supercritical water, with a product gas composition in agreement with thermodynamic equilibrium, was reported in the presence of alumina supported Ruthenium catalyst at high temperatures (800 °C). It is noteworthy that Byrd *et al.*[126] noticed reactor plugging with continued operation at 700 °C and 241 bar, even at low glycerol concentrations (5 wt%). Incomplete conversion of glycerol reforming in supercritical water with Ru/ZrO_2 catalyst was reported at moderate temperatures (500 °C), but the catalyst was reported to be stable for 25 h.[145]

In contrast, we have recently shown that Pt-Ni bimetallic catalysts are more stable and very active in supercritical water for the reforming of (pure) glycerol at relatively low temperatures and high space velocity.[155] Complete conversion of glycerol in supercritical water was already obtained at relatively low temperature (450–500 °C) and the product gas distribution with Pt-Ni catalyst completely differed from equilibrium values. Reforming of crude glycerol was, however, found to be difficult, leading to catalyst deactivation probably due to the presence of several impurities.

Conventional nickel based catalysts are used for the production of synthesis gas via methane steam reforming. To improve upon their coking tendency, intensive research efforts are made devoted at improving both the performance and life time of Ni-based catalysts by doping with several alkali (Mg, Ca, Li, Na, K) based promoters.

Very few studies have reported about the catalyst stability in reforming biomass, or model compounds representing it, in supercritical water. Waldner *et al.*[122] reported that the skeletal nickel catalysts are initially active but prone towards rapid sintering, while Ruthenium supported on carbon catalysts were shown to be active and stable up to 220 h in the reforming of 20 wt% synthetic liquefied wood (prepared by mixing different components like formic acid, acetic acid, ethanol, phenol and anisole having different concentrations) in supercritical water at 400 °C and 300 bar.

The objective of this chapter is to study the catalytic hydrothermal reforming of the aqueous fraction of pyrolysis oil and glycerol, in the presence of commercially available nickel catalysts and to investigate the influence of promoting agents (K) on the coking resistance.

6.2 EXPERIMENTAL SECTION

6.2.1 FEED STOCKS

High purity (>99%) glycerol was obtained Sigma Aldrich. The water soluble fraction (hereafter called as aqueous fraction) of bio-oil was prepared by diluting the pyrolysis oil (obtained from VTT, Finland) with water in a 1:2 mass ratio and mixed thoroughly. The mixture is then phase-separated in a funnel and allowed to phase-separate overnight. The heavy phase of oil settles at the bottom and the water soluble fraction on top. The aqueous fraction is then filtered to remove any remaining particles. This liquid was then diluted by water addition to the desired concentration of organics. Elemental composition (on dry basis) and the water content of the aqueous fraction of bio-oil are shown in Table 6.1.

Table 6.1: Elemental composition (on dry basis) and the water content of aqueous fraction.

Feed	Organics (wt%)	Water (wt%)	C (wt%)	H (wt%)	O (wt%)
Aqueous fraction	15.4	84.6	51.43	6.75	41.82

6.2.2 REACTOR SET-UP

The experimental details of the set-up used in this study were described in earlier work/previous chapter.[14, 155] All experiments were carried out in a premixed mode, in which the aqueous fraction of pyrolysis oil or the diluted glycerol solution of desired concentration is constantly fed with an HPLC pump into a preheated stream of water at supercritical conditions. The tubular reactor (having an inner diameter of 7 mm and length of 63 cm) was made of Inconel and was loaded with the desired amount of catalyst, located at the middle of reactor tube. The effluent from the reactor was cooled with a double pipe heat exchanger. After the back pressure regulator, the condensed liquid is collected in a gas-liquid separator and the gas phase sent to the ventilation system and for on-line gas phase analysis. The weight hourly space velocity (WHSV) is defined as the gram of organics per gram of catalyst per hour $g_{organics}$ $(g_{catalyst}\ h)^{-1}$.

The catalyst reduction and regeneration were carried out in the same reactor *in-situ*. The catalyst was reduced in a stream of Hydrogen flow at 500 °C for 30 min prior to the start of the experiment. When the catalyst is completely coked or in other words, deposited with carbon, it is then regenerated at 600 °C in a stream of air flow for 30 min followed by reduction with hydrogen for another 30 min before the continuation of experiment.

6.2.3 LIQUID AND GAS PHASE ANALYSIS

The product gas flow rate was measured using a wet gas meter and is analysed online continuously with a GC (Varian 450-GC). The liquid effluent collected in gas-liquid separator was analyzed for its elemental carbon content using an elemental analyser (EA 1108, Fisions Instruments).

6.2.4 CATALYST CHARACTERIZATION

Four different catalysts *a*) Raney Nickel, *b*) Nickel-I (Ni-I), *c*) Nickel-II (Ni-II) and *d*) Pt–Ni were used in this study for the reforming of glycerol and aqueous fraction. A commercially available Raney Nickel (Raney 2800) catalyst in slurry form was purchased from Sigma Aldrich. Commercial (alumina-supported) steam reforming Ni catalyst (unpromoted Katalco-23 referred as Ni-I; NiO~18%) was used in this study. Potassium was impregnated on the Ni-I catalysts using a wet impregnation method and is referred to as Ni-II. The elemental composition of the fresh Pt–Ni/γ-Al_2O_3, supported (Ni-I and Ni-II) and unsupported (Raney-Ni) nickel catalysts are shown in Table 6.2 More details of the Pt–Ni bimetallic catalyst used in this study is reported elsewhere.[14, 155]

Table 6.2: XRF analysis of the fresh catalysts.

Catalyst	Ni (wt%)	K (wt%)	Pt (wt%)
Raney-Ni	N.A.	N.A.	0
Ni – I	18	0	0
Ni – II	17.2	6.2	0
Pt–Ni	0.35	0	1.15

N.A – Not available

6.3 RESULTS AND DISCUSSION

In this section, we discuss the results of glycerol and water soluble fraction of pyrolysis oil reforming in supercritical water in the presence of commercial Ni catalysts.

6.3.1 GLYCEROL REFORMING WITH NICKEL CATALYST IN SUPERCRITICAL WATER

Figure 6.1 illustrates the gasification efficiency and the product gas yields for reforming of 15 and 31 wt% glycerol solutions over Raney Nickel (unsupported metallic) catalyst in supercritical water. Complete conversion of glycerol to gases was obtained, even at the higher concentration level (31 wt%) and stable product gas yields were obtained for the continuous runs over the full 3 h of operation. The gas composition is in close agreement with the thermodynamic equilibrium. Complete gasification of glycerol, at a temperature of max. 450 °C, with production of a gaseous product at equilibrium composition is thus very well possible.

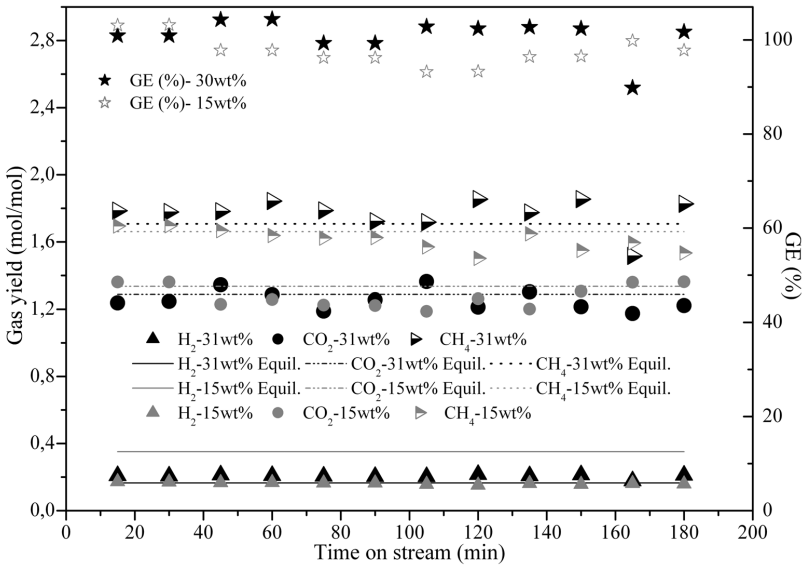

Figure 6.1: The gasification efficiency and product gas yields of 15 and 31 wt% glycerol in supercritical water with Raney Nickel catalyst. Experimental conditions: Oven temperature – 450 °C, P–250 bar, Raney-Ni catalyst, WHSV–1.44 h^{-1} (15 wt% glycerol) and 3.14 h^{-1} (31 wt% glycerol).

Raney-Ni is a highly active catalyst due to its large surface area and is widely used for industrial application in hydrogenation reactions. Since it is relatively cheap and highly active catalyst, this catalyst is studied under supercritical conditions. However, several authors have reported earlier that though Raney –Ni has high initial activity it was found to be rapidly deactivated due to sintering in hydrothermal conditions.[122, 168-169] Therefore, commercially available Nickel supported alumina catalysts which are commonly used for industrial methane reforming are investigated.

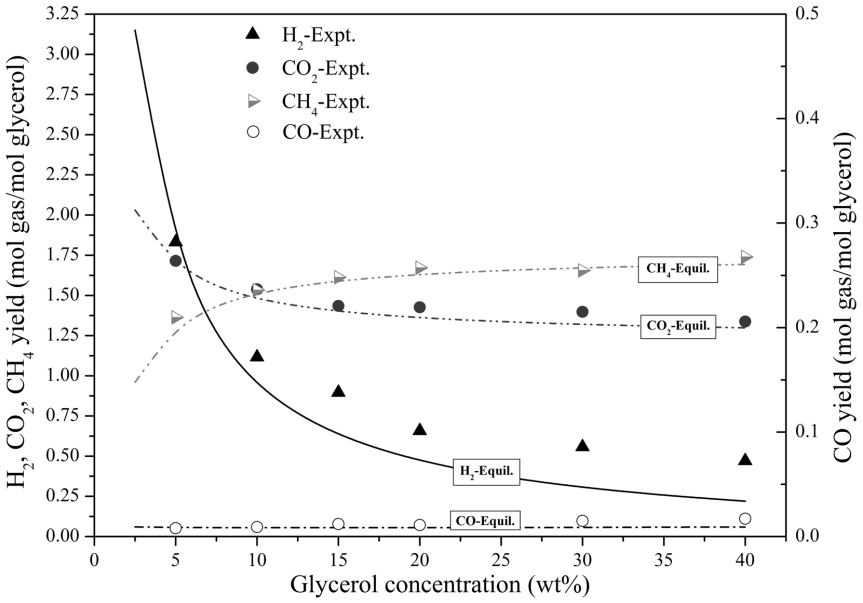

Figure 6.2: Effect of concentration on the product gas distribution of glycerol reforming in supercritical water. Experimental conditions: Oven temperature – 500 °C, P – 250 bar, Catalyst–Ni-II (3 g), Run time - ~1.5 h, Lines indicate the equilibrium gas composition and symbols corresponds to the experimental values.

Subsequently, the effect of glycerol concentration on the product distribution was studied in the range of 5–40 wt% for a commercial steam reforming catalyst (Ni on alumina support; Ni-I). Figure 6.2 illustrates that for this catalyst increasing the feed concentration leads to a decrease in hydrogen yield, accompanied with increasing methane yield and marginal drop in CO_2 yield. Still, also for this catalyst, complete carbon to gas conversion was obtained at the feed concentration studied. It is also evident from the figure that the experimental gas yields are in line with the calculated equilibrium values. Above 5 wt% glycerol concentration, the experimental hydrogen yields are higher than the thermodynamic values which can be attributed to the sensitivity of analytical measurement technique. Byrd *et al.*[126] reported similar gasification behaviour of glycerol in supercritical water at 800 °C with Ruthenium catalyst, in which they observed, at increasing concentration, also somewhat higher H_2 and CO_2 yields than calculated at thermodynamic equilibrium values.

The influence of temperature was studied by raising the oven temperature from 450 to 550 °C and the product gas distribution is shown in Figure 6.3. The lines represent equilibrium values in case of complete conversion. It is evident from the figure that the yields of H_2, CO_2, CO and CH_4 roughly follow the trends predicted by the equilibrium calculations although the

individual values deviate somewhat. The hydrogen yield increases significantly with temperature and is associated with a slight decrease in the methane yield. Complete carbon to gas conversion of glycerol was achieved in the temperature range studied, except at 450 °C, for which the carbon to gas conversion was ~65% and the liquid effluent showed a light yellowish colour. In earlier work[13-14, 155] we have already shown the good reproducibility/repeatability of the experiments with the set-up used in this study. The single experiment at 450 °C was carried out in duplicate to confirm this at the end of the measurement series. The results obtained at 450 °C are far from equilibrium due to in complete conversion (65%) but still much higher than without catalyst (~ 1% conversion with no catalyst see Table 5.1, Chapter 5) and limited methanation activity. However, we do see a very high hydrogen yield and low methane yield and this suggests that methane is not a primary product but is formed from CO_x and hydrogen. Similar observations of gas composition were observed for non-catalytic results (see Chapter 5) with hydrogen as a dominant product.

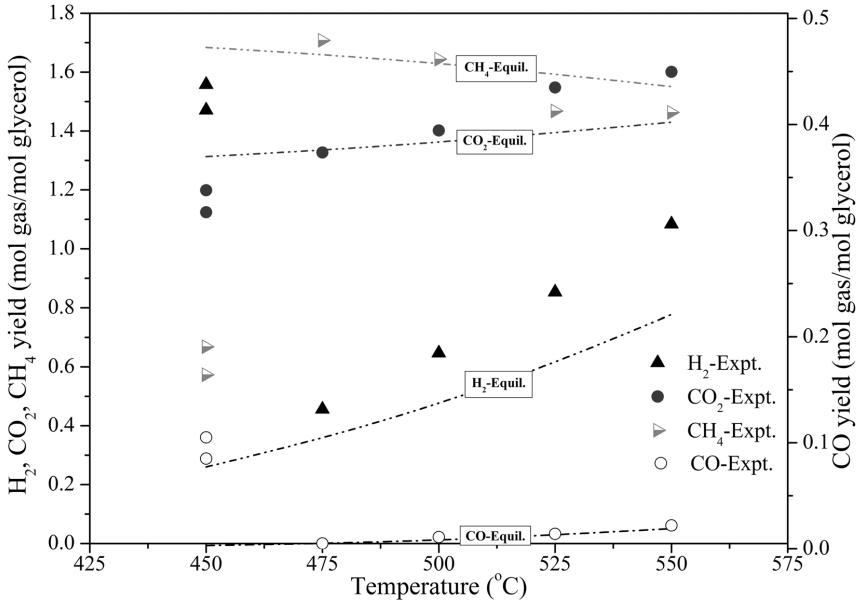

Figure 6.3: Effect of reaction temperature on the product gas distribution of glycerol reforming in supercritical water. Experimental conditions: P – 250 bar, glycerol concentration – 20 wt%, Catalyst– Ni-I (3 g), WHSV– 5.8 h^{-1}, Lines indicate equilibrium gas composition and symbols corresponds to the experimental values.

The high gasification efficiency (Figure 6.2) and apparently stable operation during further testing, led to the initiative of further testing the stability of the system in a duration test for several days of operation. The results thereof are presented in Figure 6.4 and discussed below.

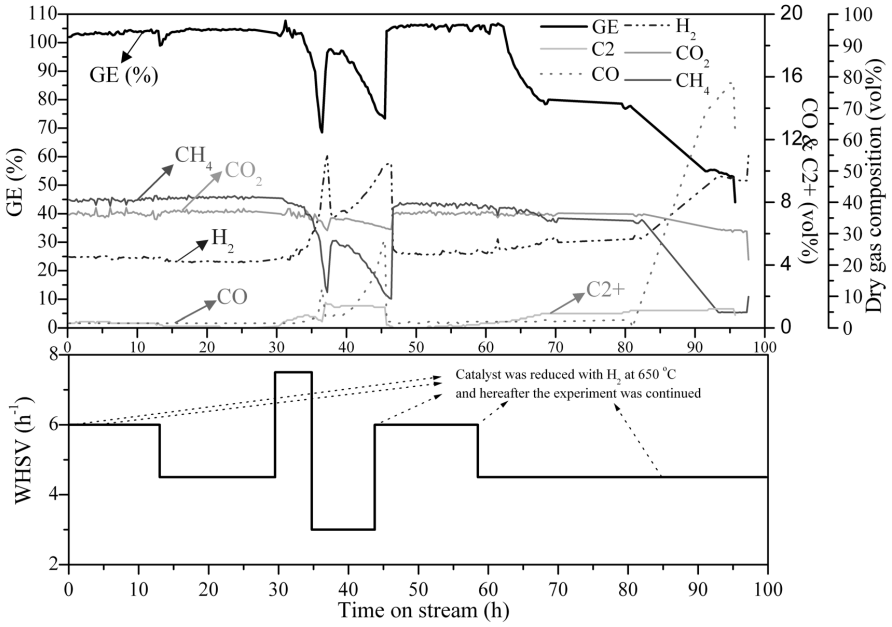

Figure 6.4: Catalytic reforming of glycerol in supercritical water. Experimental conditions: Glycerol concentration – 15 wt%, Oven temperature – 500 °C, P – 250 bar, Catalyst–Ni-I (3g).

The gas composition and the GE of 15 wt% glycerol reforming in supercritical water as a function of time and WHSV are shown in Figure 6.. The experimental campaigns carried out over a period of time, defined by changing the space velocity (by changing feed flow rate) and by regenerating and reducing the catalyst are also shown in Figure 6.4. The catalyst was reduced in-situ with hydrogen prior to the start of experiment and again after 6, 43.5, 58 and 85 h of operation on stream. The catalyst was regenerated by burning off the coke deposited on the catalyst in a stream of flowing air for 30 min at 600 °C followed by reducing the catalyst with hydrogen stream for another 30 min prior to continuation of experiment at 43.5 and 58 h. The gas composition and the GE remain unchanged when the space velocity was reduced from 6 to 4.5 h^{-1} during the initial 30 hours. But when the WHSV is suddenly raised to 7.5 h^{-1} after 30 h, a significant drop in the GE and changes in the product spectrum is noticed. The observed gas composition is indicative for incomplete conversion which was earlier observed at low temperatures (450 °C) with decrease in methane and increase in hydrogen. This might be due to the methanation reactions are much slower than the gasification to primary gaseous products. Reducing the space velocity to 3 h^{-1} partly restored the GE, but immediately started to drop gradually due to catalyst deactivation, most likely via coke formation. After

regenerating the catalyst by oxidizing the coke and reducing the catalyst with hydrogen, complete conversion was obtained but then it started to deactivate rapidly after 65 h and even further reducing the catalyst was not sufficient to regenerate the catalyst and deactivation continued. Since we weren't able to measure the completeness of regeneration in this experiment it could be due to this reason that the deactivation of the catalyst continued. In Chapter 5, we have shown that Pt-Ni bimetallic catalysts are active and stable for up to 85 h while coke was formed. However, in this study supported Ni catalysts deactivate due to coke formation this indicates that Pt-Ni has better coke gasification and reforming properties compared to supported Ni catalysts.

The catalytic behaviour of the bare Ni/Al_2O_3 catalysts in the gasification behaviour of glycerol reforming in supercritical water at 500 °C in terms of carbon to gas conversion and product gas distribution versus reaction time is illustrated in Figure 6.5. The catalyst was stable and active for 17 h which is evident in terms of complete conversion and stable product gas distribution. The product gas distribution closely matches the thermodynamic equilibrium values. The conversion drops significantly after 17 h and changes in product gas spectrum is shown in the figure. The H_2, CO and C2+ concentration increases significantly with loss in catalytic activity, whereas the methane yield decreases significantly from 44.4% to 11.5%. Only a marginal decrease in CO_2 concentration is noticed. The loss of catalytic activity after 17 h of reaction time is primarily due to coking of the bare Ni catalyst. Visual observation inside the reactor and catalyst particles after the experiments indicated coke formation.

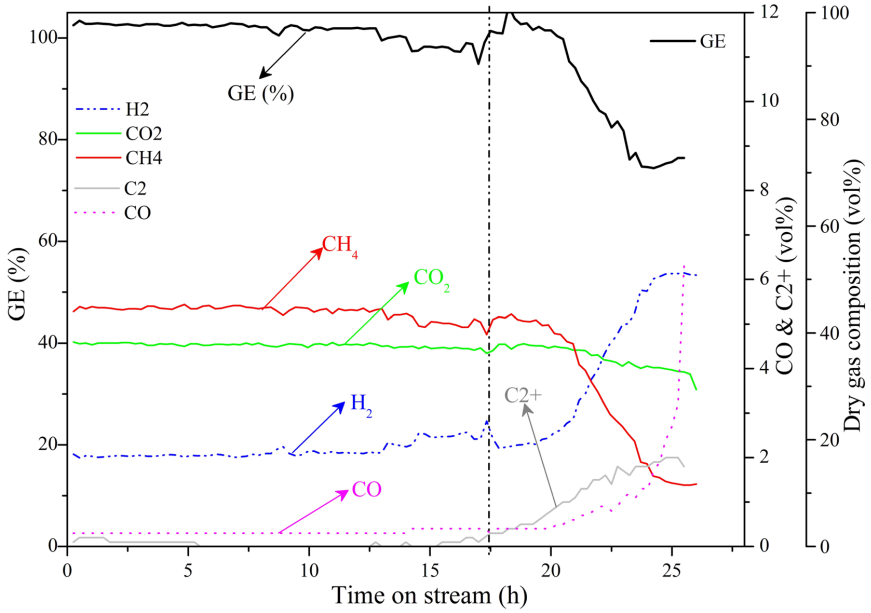

Figure 6.5: Carbon to gas conversion and product gas distribution of glycerol reforming in supercritical water. Experimental conditions: Glycerol concentration –20 wt%, Oven temperature –500 °C, P– 250 bar, Catalyst– Ni-I (3 g), WHSV– 6.15 h^{-1}.

The gasification behaviour of the K-doped Ni/Al_2O_3 catalysts on the glycerol conversion and product gas composition is shown is Figure 6.6. The catalyst was found to be more stable and active for 34h of time on stream, showing (near-) complete conversion and stable product gas distribution. Hence, the addition of K to the bare Ni catalysts increased the catalyst lifetime by a factor two. However, also the K-doped Ni catalysts deactivated very slowly. This was hypothesized and subsequently proven to be related to the leaching of K from the Ni catalysts. XRF analysis of the spent catalysts revealed very less or no K on the spent catalysts, indicating the loss of the impregnated K from the catalysts at supercritical conditions. The residual liquid collected during the gasification was analyzed in terms of Ni content (HACH spectrophotometer, measurement range 0.05 to 1 mg/l) which indicated no leaching of nickel (below 0.05 mg/l). Comparing Figures 6.5 and 6.7, it is also evident that methane composition decreases as the GE decreases due to catalyst deactivation and consequently hydrogen yield increases.

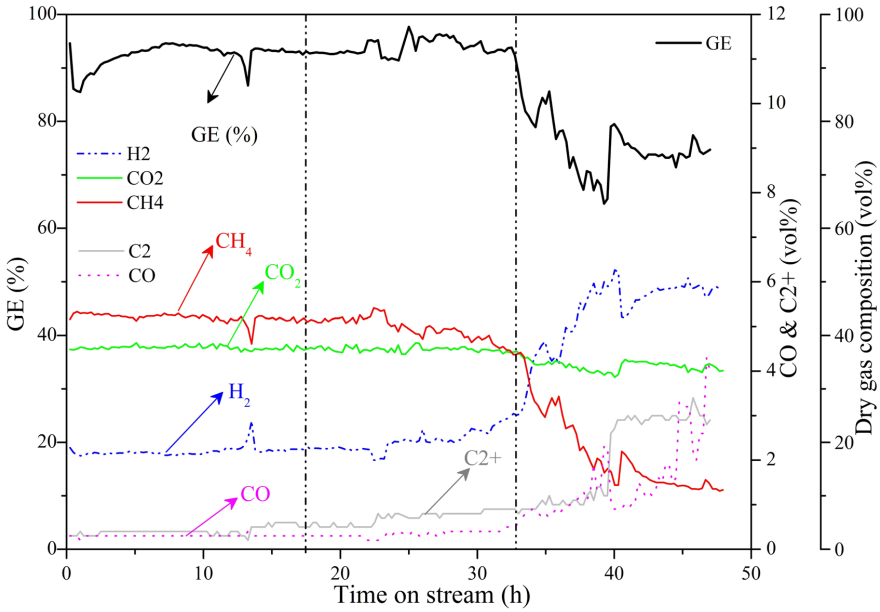

Figure 6.6: Carbon to gas conversion and product gas distribution of glycerol reforming in supercritical water. Experimental conditions: Glycerol concentration – 20 wt%, T – 500 °C, P – 250 bar, Catalyst–Ni-II (3 g), WHSV – 6.15 h^{-1}.

Long term stability of the catalyst at 550 °C and 15 wt% glycerol with Ni-I catalyst is shown in Figure 6.7. The catalyst was stable for almost 97 h with stable product gas distribution and complete carbon to gas conversion. The same catalyst was stable for less than 20 h when 20 wt% glycerol was reformed at 500 °C, see Figure 6.5. Remarkably, raising the oven temperature by 50 °C and decreasing the feed concentration to 15 wt% increased the catalyst stability over 95 h. This increase in stability is accompanied by less coke formation and a higher reforming activity of the catalyst at these conditions. It could be hypothesised that by these changes in operating conditions the gasification rate of coke precursors (intermediates in the gasification reaction network) is fast enough to keep up with the rate of their formation. The experiment was forced to stop after 97 h due to some technical problems related to the pump (and hence not related to catalyst deactivation).

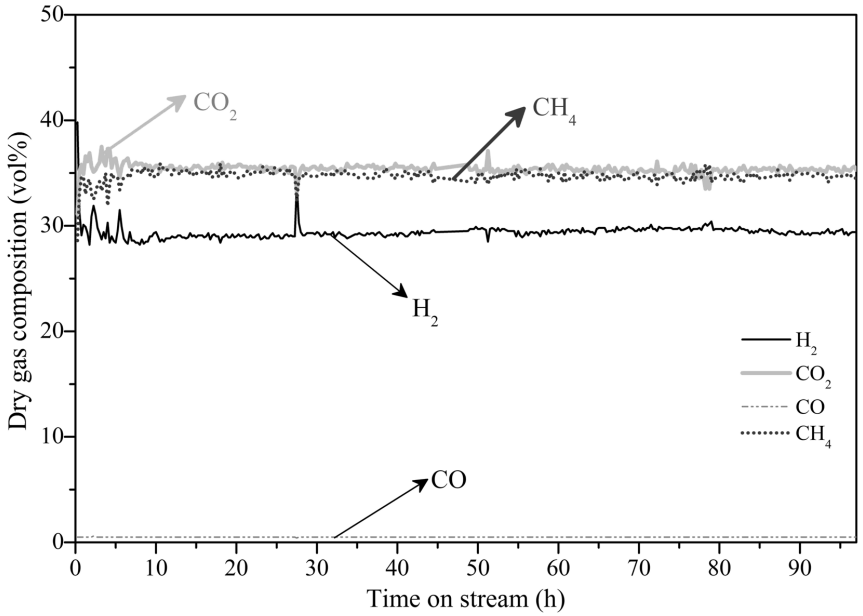

Figure 6.7: Carbon to gas conversion and product gas distribution of glycerol reforming in supercritical water. Experimental conditions: Glycerol concentration –15 wt%, T – 550 °C, P – 250 bar, Catalyst–Ni-I (3 g), WHSV – 4.5 h^{-1}.

Table 6.3: Comparison of the gas composition (vol%) and GE of glycerol reforming with different catalysts at 250 bar.

Catalyst	Conc. (wt%)	WHSV (h^{-1})	Run time, h	Oven Temp. (°C)	GE (%)	H_2	CO_2	CO	CH_4	C2+
Pt–Ni	20	4.2	24.5	500	98	35.3	38.5	0.6	12.8	12.8
Ni–I	20	6.2	14.25	500	100	17.5	37.8	0.3	44.4	0.05
Ni–II	20	6.2	4.25	500	100	15.2	38.3	0.2	45.8	0.5
Equilibrium	20			500	100	13.6	39.2	0.2	46.9	0

Table 6.3 presents the results of 20 wt% glycerol reforming in supercritical water 500 °C and 250 bar with three different catalysts along with the equilibrium composition. It is clear from the table that almost complete conversion was achieved with all the catalysts, but the product gas composition significantly varied. The product gas composition with supported nickel catalysts (Ni–I and Ni–II) are more or less the same and in accordance with the equilibrium

values. However, with the Pt–Ni catalyst, high hydrogen, C2+ yields and less methane yields were obtained. Apparently this catalyst is much less active for the methanation reaction, CO undergoing water gas shift reaction instead of methanation reaction. Huber *et al.*[120] reported that Pt-Ni catalysts have lower heats of H_2 and CO adsorption causing lower surface coverage of adsorbed H_2 and CO and therefore minimize methanation of CO and allows more sites to be accessible which enhance the reforming activity.

A remarkable observation was made from the XRF analysis of the potassium content in the spent catalyst, as obtained after the duration test, which is shown in Figure 6.8. It is evident that the potassium content in the spent catalyst decreases with increasing time on stream and this can be attributed to the leaching of potassium from the catalyst surface. From Figure 6.5, 6.6 and 6.8 it suggests that the addition of potassium clearly enhanced the catalyst lifetime by promoting simultaneous coke gasification.

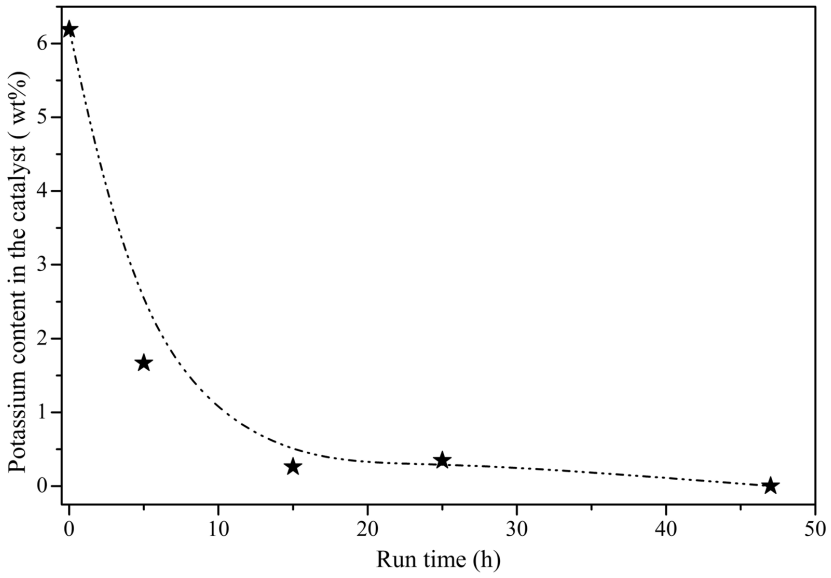

Figure 6.8: XRF analysis of potassium content in the spent Ni-II catalysts carried out at different time on stream. Experimental conditions: Glycerol concentration –20 wt%, T – 500 °C, P – 250 bar, Catalyst–Ni-II (3 g).

6.3.1 REFORMING OF PYROLYSIS OIL AQUEOUS FRACTION IN SCW USING NICKEL BASED CATALYSTS

Till date, very few studies have been carried out on the reforming of water soluble fraction of bio-oil and, to the best of our knowledge, there are no reports which show complete conversion for continuous operation. Figure 6.9 shows the reforming of 5 wt% aqueous fraction over Raney Nickel catalyst in supercritical water at 600 °C and 250 bar for over 10 h duration. The space velocity was kept constant for over 7 h at 0.23 h^{-1} and after that the feed flow rate was increased which led to an increase in the space velocity up to 0.46 h^{-1}. It is clear from the figure that complete carbon to gas conversion was obtained during the entire time on stream of 10 h. The gas flow rate, gasification efficiency and the product distribution remained stable for over 7 h and with increase in the space velocity (by an increased gas flow rate) a significant change in the product distribution is noticed, which seems to restore over a time period much longer than the initial time (less than 0.5 h) needed to achieve state. The hydrogen yield initially decreased rapidly upon switching the flow and increased slowly afterwards to the original concentration and similarly the methane yield increased and then decreased to the original concentration. The product gas mainly consisted of hydrogen, carbon dioxide and methane and the composition obtained matches closely the equilibrium values.

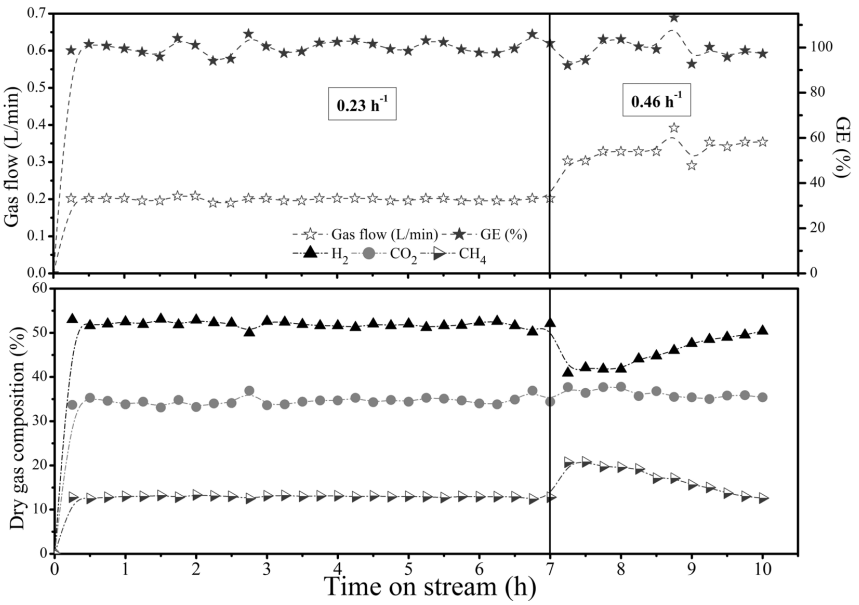

Figure 6.9: The product gas yields of catalytic hydrothermal reforming of 5 wt% aqueous fraction of bio-oil. Experimental conditions: Oven temperature = 600 °C, P = 250 bar, Catalyst = Raney Ni, WHSV = 0.23 and 0.46 h^{-1}.

Figure 6.10 illustrates the influence of space velocity and feed concentration on the carbon to gas conversion, gas flow rate and dry gas composition of aqueous fraction reforming in supercritical water at 450 °C and 250 bar. Up to 4 h of time on stream experiment was carried out with ~5 wt% aqueous fraction and the space velocity was changed after 150 min of reaction time. After 4 h, the feed concentration of aqueous fraction of bio-oil was increased to ~15 wt%. Complete conversion was obtained with 5 wt% feed concentration. However, with the 15 wt% feed concentration the catalyst deactivated rapidly due to coke formation after 2 h of reaction time, evidenced by decreasing GE and significant changes in the product gas distribution (decreasing methane and increasing hydrogen composition). Since, the aqueous fraction of bio-oil consists of several unknown compounds which could have led to significant deactivation of the catalyst by coke formation. After 8 h experimental run, coke combustion was carried out at 650 °C with a stream of flowing air for 2 h. After coke combustion, the catalyst was re-reduced with hydrogen. When the experiment continued, the deactivation was however also continuing.

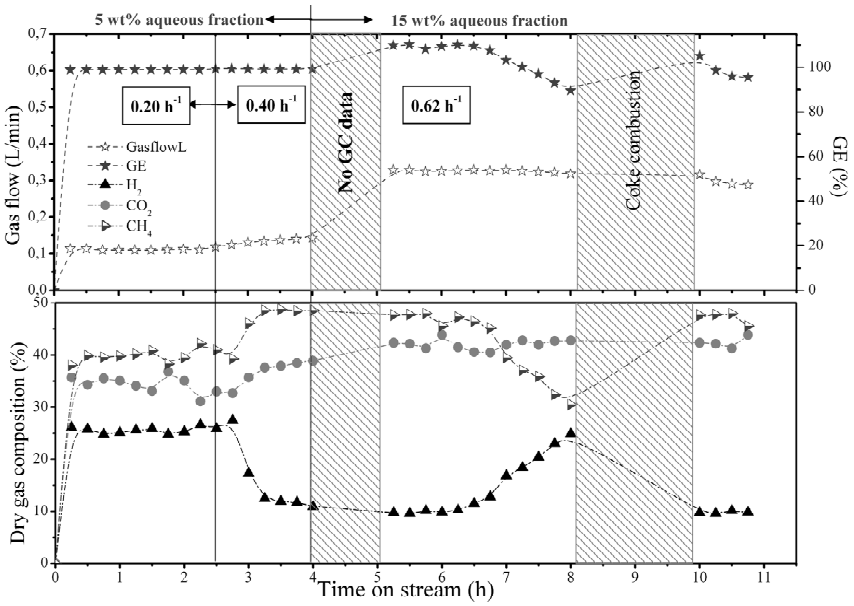

Figure 6.10: Concentration of product gases during the catalytic hydrothermal gasification of aqueous fraction of bio-oil. Experimental conditions: Catalyst: Raney Nickel, Oven temperature = 450 °C, P = 250 bar, WHSV = 0.20, 0.40 and 0.62 h^{-1}.

Reforming of the aqueous fraction of bio-oil was carried out with Ni-I and Pt–Ni catalysts and the results are presented in Table 6.4.

Table 6.4: Reforming of aqueous fraction of bio-oil with Ni-I and Pt–Ni catalysts.

Parameter	**1**	**2**	**3**
Oven temperature (°C)	550	550	575
Pressure (bar)	250	250	250
Feed concentration (wt%)	7.7	7.7	7.7
Catalyst	Pt–Ni	Ni–I	Ni–I
Catalyst amount (g)	5	5	5
WHSV (h^{-1})	1.39	1.38	0.86
Run time (h)	2.5	1.5	1.5
GE (%)	74.4	47.4	74.3

Carbon in feed (wt%)†	4.03	4.03	4.03
Carbon in aqueous phase (%)	16.6	16.5	13.7
Carbon in aqueous phase (wt%)†	0.67	0.667	0.553
Dry gas composition (vol%)			
H_2	29.9	34.6	36.8
CO_2	44.6	41.8	36.7
CH_4	18.6	13.7	26.1
CO	0.2	6.3	0.4
C_2H_6	3.3	1.4	0
C_2H_4	0	0.5	0
C_3H_6	0.1	1.1	0
C_3H_8	3.3	0.5	0

†Carbon in the aqueous phase analyzed with an elemental analysis.

In our previous study/early chapters[14, 155] we have shown that the Pt–Ni bimetallic catalyst was active and stable for long durations tested with model compounds like ethylene glycol and glycerol. This motivated us to evaluate this catalyst in the reforming of aqueous fraction of bio-oil. A maximum conversion of 74% was obtained with the Pt–Ni catalyst at 550 °C and at 575 °C with Ni-I catalyst. The Ni-I catalyst deactivated very rapidly (within 1 h), when compared to the more stable Pt–Ni catalyst. This Pt–Ni bimetallic catalyst was earlier shown to be active and stable for 85 h in case of glycerol reforming. The liquid effluent after the reaction consisted of an oily phase on top of the aqueous phase. Due to sampling issues with this inhomogeneous system, complete carbon balance closure could not be achieved. In addition, reforming of aqueous fraction of bio-oil led to significant amount of coke formation, which is not directly quantifiable. Visual observations of all the spent catalysts showed the presence of coke. This is further confirmed by TGA analysis of the fresh- and of spent Pt–Ni catalyst after reforming with aqueous fraction, as presented in Figure 6.11. The fresh catalyst did not show a significant mass loss in the range of 300–650 °C, but for the spent catalyst a peak arises in the temperature range of 300–650 °C, indicating the presence of carbonaceous deposits on the catalyst surface

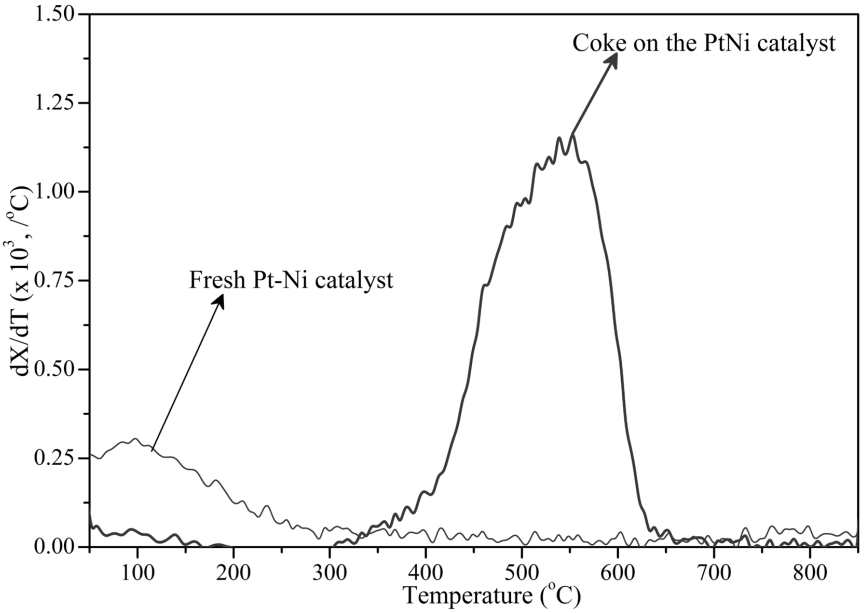

Figure 6.11: TGA analysis of the fresh and spent Pt–Ni catalyst obtained from the reforming of aqueous fraction of bio-oil at 550 °C and 2.5 h run time.

6.4 CONCLUSIONS

In this chapter, we evaluated the catalytic reforming of glycerol and water soluble fraction of pyrolysis oil with commercial nickel catalysts (supported and unsupported) in supercritical water. Complete conversion of glycerol with initial concentrations ranging from 5–40 wt% was achieved at 500 °C and 250 bar in the presence of nickel catalysts with product gas yields in-line with the thermodynamic equilibrium values.

The influence of oven temperature was studied in the range of 450-550 °C for 20 wt% glycerol reforming with alumina supported nickel catalyst (Ni-I). A minimum temperature of 475 °C is needed for complete conversion. At incomplete conversion (when operating at lower temperature or during catalyst deactivation) it was found that the product gas composition deviates from equilibrium and shows that methane is a secondary product.

With the alumina supported Ni catalysts, there are two options for enhanced catalyst lifetime. The competition between coke formation and gasification of coke precursors can be driven

towards gasification either by operating at somewhat higher temperatures (here: 550 *vs.* 500 °C for glycerol gasification) and low feed concentrations.

For the pyrolysis oil aqueous phase complete conversion of a 5 wt% and 15 wt% aqueous fraction was obtained with skeletal Raney-Ni catalyst in supercritical water at very low space velocities (high catalyst loading) at relatively low temperature (450 °C). With supported catalyst the maximum gasification efficiency obtained was 74% at 575 °C with Ni–I catalyst and with Pt–Ni catalyst at 550 °C. The Raney-Ni catalyst has a high initial activity but deactivated very rapidly due to sintering and coke formation.

The supported Ni catalyst deactivated rapidly with the Ni–I within the short duration test due to severe coke formation, as observed in terms of decreasing carbon to gas conversion and changes in the product gas spectrum. The Pt–Ni catalyst was stable for almost 2.5 h. Visual observations of the spent catalysts for both glycerol and aqueous fraction reforming indicated that coke formation was the primary reason for catalyst deactivation. This suggests that coke formation cannot be avoided during the process. However, the catalyst activity and lifetime can be enhanced if the coke production equals the coke gasification during the process.

Finding the operating conditions (T, WHSV) where the gasification rate can keep up with the rate of formation of coke precursors is essential for long term, stable operation.

Appendix-1

Catalyst screening for the hydrothermal gasification of aqueous phase of bio-oil[5]

[5]This appendix is an excerpt of paper published as:

Chakinala, A. G.; Chinthaginjala, J. K.; Seshan, K.; van Swaaij, W. P. M.; Kersten, S. R. A.; Brilman, D. W. F., Catalyst screening for the hydrothermal gasification of aqueous phase of bio-oil. Catalysis Today 2012, 195, (1), 83-92.

Appendix-1

A.1 INTRODUCTION

In this appendix, bio-oil obtained from pyrolysis of lignocellulosic biomass was phase-separated into an aqueous and a non-aqueous fraction by addition of water. The aqueous fraction of bio-oil thus obtained was catalytically reformed in supercritical water using a batch autoclave reactor.

The aim of this work is to find or develop an efficient catalyst to completely convert the aqueous phase of bio-oil (~18% organics) in SCW. The design criteria for the catalyst development are to achieve *i*) complete carbon to gas conversion *ii*) tune the product gas selectivity towards hydrogen and *iii*) minimise char/coke formation that usually leads to reactor plugging in a continuous flow reactor. Catalyst screening involved studying the influence of different metals, supports and also reaction parameters (*e.g.*, temperature, feed concentration, residence time, feed nature) on the gasification behaviour.

A.2 EXPERIMENTAL SECTION

A.2.1 MATERIALS

γ-Alumina (γ-Al_2O_3, BASF), Activated carbon (AC, Norit ROX 0.8), Silica (SiO_2, Evonik), Zirconia (ZrO_2, Evonik), Titania (TiO_2, Evonik) were used as catalyst supports. Cerium nitrate hexahydrate was also used as catalyst deposited on Zirconia support. Acetylacetonate salts comprising of Pt, Pd, Ru, Rh and Ni were used in the preparation of respective metal catalysts.

A.2.2 CATALYST PREPARATION AND CHARACTERIZATION

The catalyst supports were pulverized to a particle size ranging between 300 - 600 μm. Organic phase wet impregnation was used to deposit the active metal on the surface of the support using the respective metal acetylacetonate precursor dissolved in toluene. The supports were immersed in toluene, containing the proper amount of metal precursor dissolved, in a round bottomed flask of a vacuum rotary evaporator. The flask was immersed in silicon oil bath maintained at a temperature of 45 °C. Toluene was completely evaporated by slowly applying vacuum and leaving behind the metal precursor deposited on the support. The respective catalysts were obtained by decomposing the metal precursor deposited on supports by calcination in air at 300 °C (ramp of 5 °C/min) for 2 h and at 600 °C (ramp of 5 °C/min) for 1h and subsequently the samples were reduced at 600 °C for 1 h and then cooled to room temperature. Similar conditions were followed for all the catalysts except for the preparation of Pd supported on activated carbon, where the sample was calcined at 250 °C (ramp of 5

°C/min) for 2 h and then reduced at 550 °C (ramp of 5 °C/min) for 1 h and then cooled to room temperature.

In the preparation of metal (Ru, Pd) supported Ceria-Zirconia (here after denoted as Ce-ZrO_2) catalysts, the required amounts of Cerium nitrate hexahydrate precursor were dissolved in water and then dispersing Zirconia particles in the solution, in a round bottomed flask of a vacuum rotary evaporator. The flask was immersed in silicon oil bath maintained at a temperature of 75 °C. Water was completely evaporated by slowly applying vacuum and leaving behind the Ceria precursor deposited on the Zirconia particles. The support was then calcined in air at 600 °C (ramp of 5 °C/min) for 6 h and then cooled to room temperature at ramp of 10 °C/min. The Ce-ZrO_2 support was then deposited with respective metal acetylacetonate precursor by following the procedure mentioned above.

Table A.1: Characteristics of the fresh catalysts used in the experiments.

Catalyst type	**Metal loading (wt%)**	**Active particle size (nm)**	**BET surface area (m^2/g)**
Pt/γ-Al_2O_3	3.32	3	199
Ni/γ-Al_2O_3	2.92	221	199
Rh/γ-Al_2O_3	2.32	N.D.	199
Pd/γ-Al_2O_3	2.51	5	199
Ru/γ-Al_2O_3	2.41	111	199
Pd/TiO_2	1.27	36	44
Pd/ZrO_2	1.93	11	45
Pd/SiO_2	1.80	7	166
Pd/AC	1.88	174	1146
Pd/Ce-ZrO_2	Pd=1.57 Ce=7.77	N.D	45
Ru/Ce-ZrO_2	Ru=0.97 Ce=10.7	N.D.	45

N.D. – Not determined

Table A.1 presents the details of all the catalysts used in this study. It is clear from the table that activated carbon possess the highest surface area among all the supports and the order of the support with respect to BET surface area is AC>γ-Al_2O_3>SiO_2>ZrO_2~TiO_2~Ce-ZrO_2.

X-ray fluorescence spectroscopy (XRF) (Phillips PW 1480 spectrometer) was used to determine the catalyst composition. The active metal particle size was determined by CO chemisorption. The BET surface area and porosity of all the catalysts were determined using with nitrogen adsorption-desorption at -196 °C in a Micromeritics TriStar instrument. The crystal structures of the fresh and spent catalysts were analysed by powder X-ray diffraction (XRD) performed on a Philips X'pert device with CuKα as the radiation source. Step scans were taken in the range 2θ from 15–75°. Due to the limitations of XRD sensitivity, a minimum of ~5 wt% metal loading sample is needed for identification and quantification of the crystallite size using the Scherrer equation. Thermogravimetric analysis (TGA) of the spent catalysts was carried out in aluminium crucible using NETZSCH STA 449 F3 Jupiter instrument.

A.2.3 FEED STOCK ANALYSIS

Three different feedstocks *i*) made-up fraction, *ii*) pyrolysis condenser fraction[170-171] and) hydro-deoxygenation fraction (HDO)[3] were used in this study. The feedstocks characteristics are given in Table A.2.

Table A.2: Feedstock characteristics.

Aqueous fraction ID	Organics (wt%)	H_2O** (wt%)	Elemental composition (wt%)*		
			C	H	O♣
Made–up–I	18.4	81.6	8.72	10.10	81.18
Made–up–II	51.5	48.5	24.40	7.20	68.40
Pyrolysis condenser	17.5	82.5	11.0	9.79	79.22
Hydro–deoxygenation	23.0	77.0	8.93	9.79	81.28

♣Calculated by difference, * Analyzed using elemental analyzer, ** Analyzed with Karl Fisher titration

The made-up organic fraction-I and II was prepared by mixing pyrolysis oil[3, 172] and water in 1:2 and 1:1 ratios respectively to induce phase separation and to obtain a desired organic concentration. The pyrolysis oil and water mixture was phase separated over night in a conical funnel and the water soluble fraction of organics in the bio-oil was filtered with a Whatman filter paper and used for experiments. The pyrolysis condenser fraction was obtained from our pyrolysis plant (second condenser) which is described elsewhere.[171] The aqueous HDO fraction was obtained from our HDO experiments which was described elsewhere.[173] Karl-Fischer titration was used to determine the water content of the feedstocks. The elemental

composition was analyzed using the CHNO elemental analyzer (Fisions Instruments 1108 EA CHN-S).

A.2.4 EXPERIMENTAL SET-UP AND PROCEDURE

The catalytic hydrothermal gasification of the aqueous fraction of bio-oil was conducted in the batch autoclave reactor which is described in our earlier chapter (Chapter 3).

In a typical run, ~4.5 g of aqueous feed solution and 0.5 g of catalyst (depending on the experimental condition) was loaded into the reactor and carried out the experiment. The elemental composition of the aqueous fractions of bio-oil is given in Table A.2. After the experiment, the remaining products (liquid and solids in suspension) were collected in a glass bottle and the reactor was rinsed with acetone to remove any water-insoluble deposits. The aqueous phase was analyzed for dissolved organic carbon with an elemental analyzer.

Gas samples were taken in a syringe and analyzed using a micro gas chromatography (Varian CP 4900; 10 mmol sieve 5A Ar, 10 mmol sieve 5A He, 10 m PPQ He, 8 m Sil-5CB He) used to detect H_2, O_2, N_2, CH_4, CO, CO_2, C_2H_4, C_2H_6, C_3H_6 and C_3H_8. With the gas composition, the final pressure and temperature inside the reactor, the amount of each gas produced was calculated. After the reactor was cooled, it was depressurized and the autoclave was disconnected from the arm and opened.

A.2.5 CONTINUOUS SET-UP

Details of the continuous set-up used for the catalytic reforming of aqueous fraction of bio-oil are described in a previous publication.[14]

A.3 RESULTS AND DISCUSSION

Here we present the results of the influence of different noble metals, supports and parametric evaluation such as temperature, residence time, feed stock concentration and different kinds of feeds on the carbon to gas conversion and product gas selectivities. Finally, post-mortem analyses of the spent catalyst characterization results are discussed.

A.3.1 EFFECT OF DIFFERENT NOBLE METAL CATALYSTS

The carbon gasification efficiency and product gas selectivities (H_2, CH_4, higher alkanes) of aqueous bio-oil gasification in SCW at 500 °C and 280 bar for 15 minutes of reaction time and in the presence of various transition metal (Pt, Ru, Pd, Rh, Ni) catalysts supported on γ-Al_2O_3, is shown in Figure A.1. The product composition and the gasification efficiencies were

significantly different with different metals. All the catalysts except Ni showed reasonable carbon to gas conversions. The highest gasification efficiency was achieved with Ru catalyst and the order of the catalysts in terms of conversion is Ru>Pt>Rh~Pd>Ni. Palladium catalyst showed higher selectivity towards H_2 and the order of the catalysts in terms of H_2 selectivity are Pd>Ru~Rh>Pt>Ni. Ru catalyst showed significantly high selectivity towards methane. The two plausible reactions for the formation of alkanes can be due to the dehydration reaction of the oxygenated compound or via methanation reaction. The order of the catalysts in terms of CH_4 selectivity is Ru>Rh>Pt>Pd>Ni. These trends suggest that an effective catalyst for the reforming of oxygenated compounds would be based on metals that generally possess high activities towards C-C bond breaking,[9, 124] which is required to obtain gaseous "C" specie (in the form of CO, CO_2, CH_4) from the oxygenated compound and high water-gas shift activity.

The presence of active metals not only influences the carbon to gas efficiencies but also affects the product gas distribution. High H_2 selectivity is favoured upon the active metals which show low methanation activity and low hydrogenation activity. The high methanation activity of Ru found is in agreement with the literature.[9, 124] For Pd and Pt reasonable GE and hydrogen selectivity are obtained. Davda *et al.* [9, 124] also reported high H_2 selectivity over Pd catalysts for the aqueous phase reforming of ethylene glycol. Ni based catalysts are very attractive as they are readily available and cost effective when compared to noble metal catalysts, despite their methanation activity and least stability in the SCWG process. The Nickel catalyst was found to be least active among all the catalysts studied which is due to very less metal loading, leading to the formation of stable $NiAl_2O_4$ during the calcination process. Catalysts with higher Ni loadings usually present in two phases, NiO accompanied with stable $NiAl_2O_4$. The NiO phase is easily reducible with the in-situ generated hydrogen during the reforming process. While, the stable $NiAl_2O_4$ phase do not contribute to any reforming activity unless it is reduced with hydrogen at high temperatures (~800 °C).[174] Thus, the low activity of the Ni catalysts compared to other catalysts is due to the presence of Ni in inactive and stable $NiAl_2O_4$ phase, in this case.

To conclude Pd catalysts showed reasonable gasification efficiencies with high H_2 and low alkane selectivity, while Ru catalysts exhibited higher conversion with low H_2 and high alkane selectivities. In view of these observations further catalyst screening studies have been performed with Ru and Pd metal catalysts.

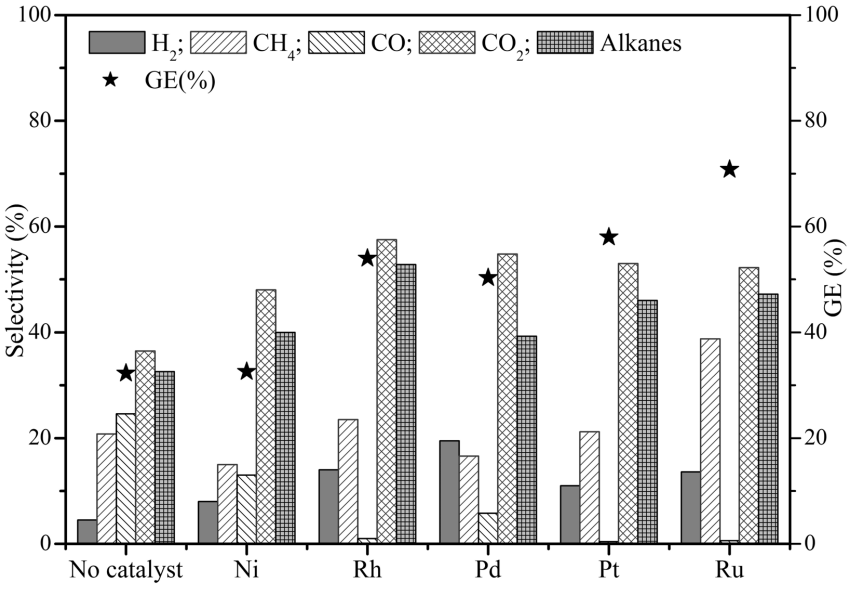

Figure A.1: The influence of different noble metal catalysts supported on alumina on the carbon to gas conversion and product gas selectivities of aqueous bio-oil (Made–up–I) reforming in SCW at 500 °C, 300 bar, 15 min reaction time and a catalyst loading of 0.6 ($g_{organics}/g_{dry\ organics}$).

A.3.2 EFFECT OF DIFFERENT SUPPORT MATERIALS

In view of the reforming activity of Pd supported on alumina catalyst (high H_2 and low alkane selectivities) when compared to other metal catalysts as discussed earlier, various Pd catalysts were prepared to study the influence of the support materials on the activity and the hydrogen production selectivity by reforming the water soluble fraction of bio-oil in supercritical water. Figure A.2 illustrates the effect of various supported Pd catalysts on the GE and product gas selectivities of aqueous fraction of bio-oil (18% organics) reforming at 500 °C, 280 bar and 15 min of reaction. For the Pd/support combinations studied, all catalysts showed similar GE. Both ZrO_2 and Al_2O_3 supported Pd catalysts showed high selectivity towards H_2. γ-Al_2O_3 is widely used as a catalyst support for a variety of process including the SCWG applications, owing to its high specific surface area, high thermal stability and low cost. Water gas shift activity is essential to increase the H_2 selectivity. However, noble metals cannot readily perform the WGS reaction as the water molecule is thermodynamically too stable to be activated on noble metals. It was reported that supports with red-ox properties such as TiO_2, ZrO_2 and CeO_2 can effectively enhance the shift activity.[175] Basic supports are shown to be more stable

than γ-Al_2O_3 and have a higher selectivity towards hydrogen than alkanes in biomass gasification.[176] Altering the red-ox properties of the support and surface oxygen mobility is a way to enhance the catalyst performance. Ceria is as an oxide support possessing high red-ox properties and the mobility of surface oxygen/hydroxyl groups. Reduction of Ce^{4+} to Ce^{3+} aids in the formation of bridging hydroxyls, which are claimed to be active for WGS reaction.[175] Mixed oxides of Ce-ZrO_2 promote the red-ox properties of the support and are shown to have improved the catalyst performance in the WGS reaction.[175, 177-178] In this study, among the Pd based catalysts, Ce-ZrO_2 support indeed showed high selectivity towards H_2, which makes it a promising support for effective shift activity under these conditions. For the reforming of switch grass bio-crude in SCW a lower GE was observed for the Titania supported catalysts whereas a high hydrogen selectivity was reported with ZrO_2 supported catalysts.[34] Several researchers have studied the influence of support on the catalytic activity in hydrothermal gasification of biomass.[125, 179-180] Minowa and Ogi[176] have studied the hydrothermal gasification of cellulose in a batch autoclave reactor using reduced nickel catalysts with different supports and they report a strong influence of supports on the catalytic activity in terms of product gas selectivities which is attributed to the acidity/basicity of the supports but also depended on the overall catalyst size (BET surface area) and active metal particle size (nickel crystallite size).

Apparently, Ce-ZrO_2 is a promising support due to the aforementioned reasons in terms of enhanced WGS activity as well as high stability to withstand under hydrothermal conditions. Therefore, further optimisation studies have been carried out using this support material combined with either Pd or Ru metal catalysts.

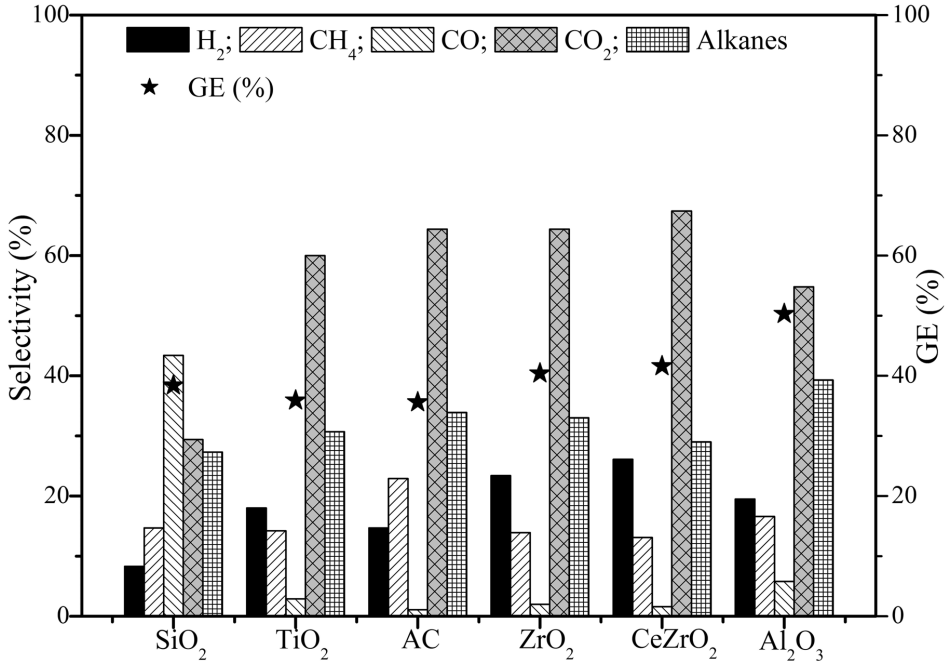

Figure A.2: The influence of different palladium supported catalysts (silica, titania, activated carbon (AC), zirconia, ceria-zirconia, γ-alumina) on the carbon to gas conversion and product gas selectivities of aqueous bio-oil (Made–up–I) reforming in SCW at 500 °C, 300 bar, 15 min reaction time and a catalyst loading of 0.6 ($g_{organics}/g_{dry\ organics}$).

A.3.3 EFFECT OF TEMPERATURE

It is well known that higher temperatures enhance the gasification efficiency and according to equilibrium calculations hydrogen selectivity is favoured. The effect of temperature ranging from 450–580 °C on the activity and product gas selectivities of 18 wt% organics at 300 bar and 15 min of reaction time with Ru and Pd supported on Ce-ZrO_2 is shown in Figure A.3. Both the catalysts (Ru and Pd) show considerable increase in the GE with increase in temperature. Ru showed better GE over Pd at all temperatures. CH_4 selectivity with both the catalysts increases with the increase in temperature. Higher alkane (C_2, C_3) selectivity increases with temperature over Pd and Ru. Methanation activity of both the catalysts increases with temperature, however, Pd shows low methanation activity as compared to Ru. At high temperature Pd showed high H_2 selectivity and reasonably high activity. The selectivity towards CO was very low with both the catalysts.

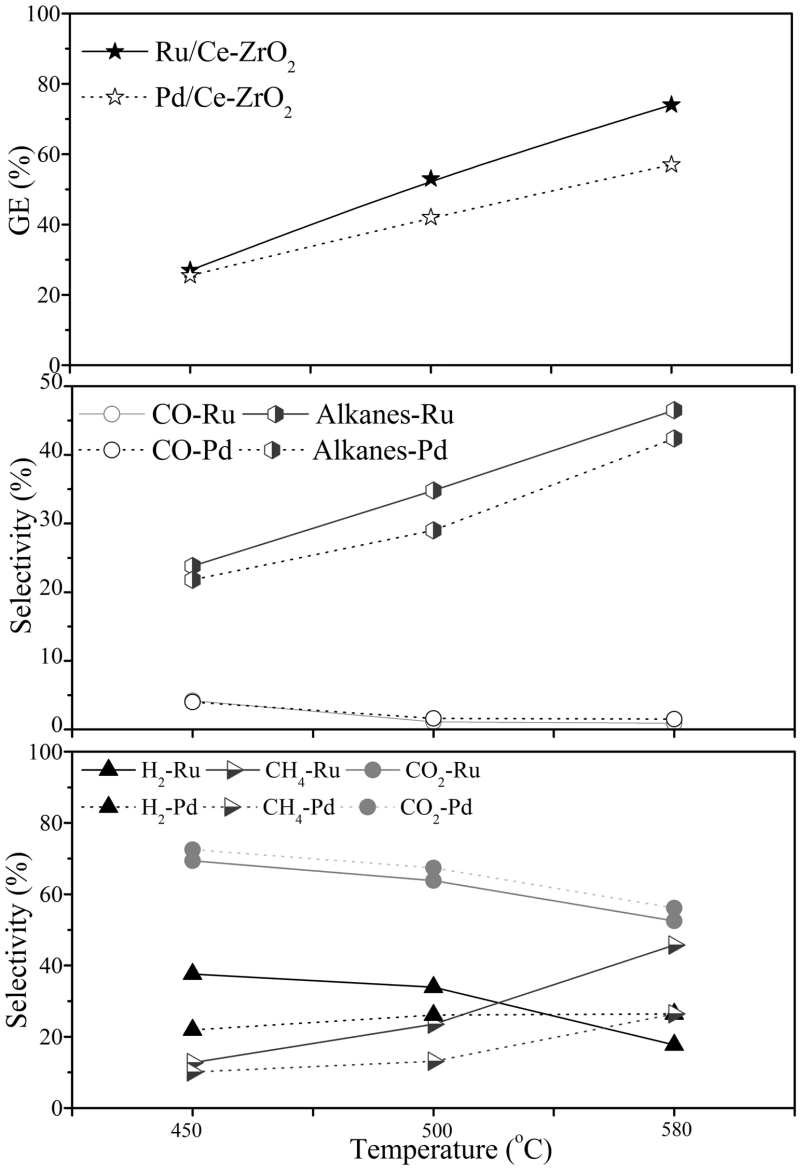

Figure A.3: The influence of different temperatures on the carbon to gas conversion and product gas selectivity of aqueous bio-oil (Made–up–I) reforming in SCW at 300 bar, 15 min reaction time, catalyst loading of 0.6 ($g_{catalyst}/g_{dry\ organics}$), Ru/Ce-$ZrO_2$ (solid trend lines), Pd/Ce-ZrO_2 (dotted trend lines).

A.3.4 EFFECT OF REACTION TIME

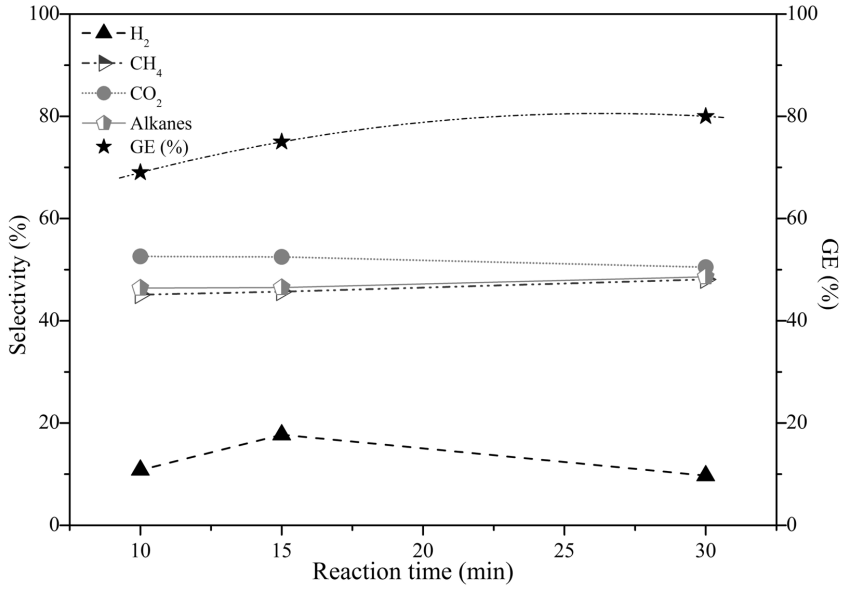

Figure A.4: The influence of reaction time on the carbon to gas conversion and product gas selectivity of aqueous bio-oil (Made–up–I) reforming in SCW at 580 °C, 300 bar, catalyst loading of 0.6 ($g_{catalyst}/g_{dry\ organics}$) of Ru/Ce-$ZrO_2$.

Generally, increasing the contact time or residence time of the reactant with the catalyst increases the conversion and steer the product gas selectivity towards equilibrium. The effect of residence time on the activity of Ru supported on Ce-ZrO_2 and product gas selectivities of 18% organics aqueous bio-oil feed at 580 °C is shown in Figure A.4. It is evident from the figure that an increase in the reaction time led to slight increase in the GE. No significant changes in the product gas selectivities are observed except for marginal changes in the hydrogen selectivity which decreases slightly after 15 min of reaction time.

A.3.5 EFFECT OF CATALYST LOADING

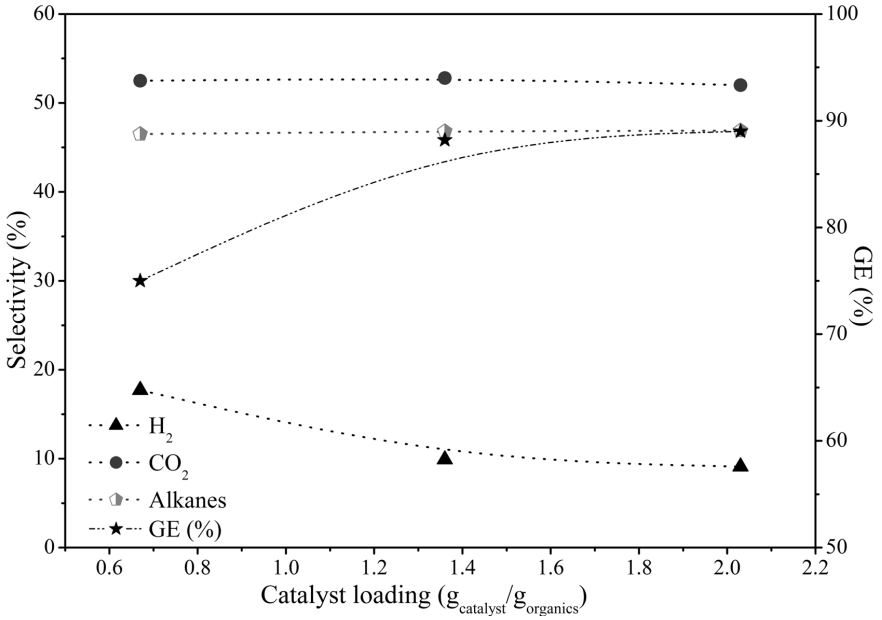

Figure A.5: The influence of Ru/Ce-ZrO_2 catalyst loading on the carbon to gas conversion and product gas selectivity of aqueous bio-oil (Made–up–I) reforming in SCW at 580 °C, 280 bar and 15 min reaction time.

High catalyst loadings generally increase the rate of reaction due to the availability of large number of active metal particles that accelerates the carbon conversion. The influence of three different Ru/Ce-ZrO_2 catalyst loadings ($g_{cat}/g_{organics}$) on the activity and H_2, CH_4 selectivities at 580 °C and 15 min reaction time is shown in Figure A.5. H_2 selectivity decreased with increasing catalyst loading while no significant change in the alkane selectivity was noticed. Maximum carbon to gas conversion was observed at the highest catalyst loading, but a further increase in catalyst loading is expected to have little effect (Figure A.5). Elemental analysis of the liquid effluent after the reaction at higher conversions indicated almost no carbon present and this incomplete carbon balance closure can be attributed to the formation of coke either during the heating up period or the reaction.

A.3.6 EFFECT OF ORGANIC CONCENTRATION

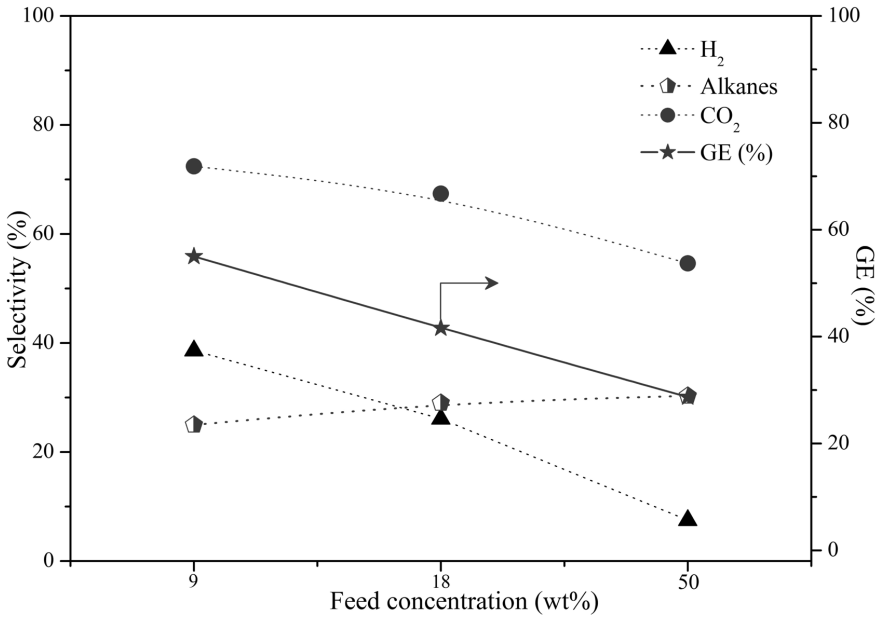

Figure A.6: The influence of different feed concentrations of aqueous bio-oil on the carbon to gas conversion and product gas selectivities in supercritical water at 500 °C, 280 bar, 15 min reaction time and Pd/Ce-ZrO_2 catalyst (0.5 g).

High feed stock concentrations are beneficial both from process and economics point of view and it is shown that the net process energy efficiency of the SCWG improves with high feed stock concentration of biomass.[22, 181] The influence of three different concentrations of aqueous fraction of bio-oil (9, 18 and 50 wt%) on the reforming activity of the selected Pd/Ce-ZrO_2 catalyst at 500 °C and 15 min reaction time is depicted in Figure A.6. In line with trends reported earlier, the GE decreased significantly with increasing feed concentration. Maximum conversion was achieved at the lowest concentration (9 wt% feed concentration). The H_2 and CO_2 selectivities decreased with increasing feed concentration, while a marginal increase in alkane selectivity was noticed.

A.3.7 NATURE OF FEED

Generally, the characteristics of feedstocks have a significant influence on the gasification behaviour in supercritical water. The influence of different feedstocks (refer to Table A.2) was tested with the Pd/Ce-ZrO_2 catalyst at 580 °C and 15 min reaction time and the results are

shown in Figure A.7. Notable differences in GE and product gas selectivities are noticed for the different feedstocks. These differences in the GE can be due to the organic compounds present in the feedstocks. This is likely to be due to the presence of dissolved sugars (levoglucosan) and refractory components that are present in the phase separated made up fraction and not in the fast pyrolysis condensate and the HDO fraction. These sugar-compounds are very reactive and lead to char formation and simultaneously reduce the gas production and are hence liable for a lower carbon to gas conversion. Comparatively, less GE was obtained with the made-up bio-oil fraction than with the other two feed stocks.

Even though, the HDO fraction has the highest feed concentration of organic material, it has the highest conversion, primarily due to the nature of the organic compounds. During the HDO process, the sugars originally present in the pyrolysis oil are hydrogenated in the presence of a catalyst to their respective sugar alcohols (polyols), which are easier to reform have less tendency towards coke formation.[182] The H_2 and CO_2 selectivity were reduced while the alkane selectivity increased with the fast pyrolysis fraction and the HDO fraction in comparison with the bio-oil made up fraction.

Figure A.8 presents the gasification efficiency and the product gas selectivities of catalytic reforming of the made-up fraction and the fast pyrolysis condenser fraction in supercritical water using a continuous flow reactor. It is evident from this figure that 100% GE was obtained with the pyrolysis condenser fraction during the 3 h run with stable product gas composition. A somewhat lower conversion was obtained with the made-up fraction and the selectivity towards C2 compounds is noticeable after 2 h. Simultaneously, the liquid effluent turned to a light yellowish colour indicating catalyst deactivation. A significant amount of coke was deposited on the catalyst with the made-up fraction when compared to the pyrolysis condenser fraction.

One way of processing aqueous wastes containing sugars while minimising char/coke formation and achieving complete carbon to gas conversion with a high H_2 selectivity is to do first a pre-treatment step by catalytic hydrogenation at lower temperatures (300 °C), thereby converting all the sugars to respective polyols. In a subsequent step, this product is comparatively easy to reform with much lesser operating problems than the original sugar compounds. Part of the hydrogen generated at high pressures from the reforming of polyols can be used for the initial catalytic hydrogenation step.[182]

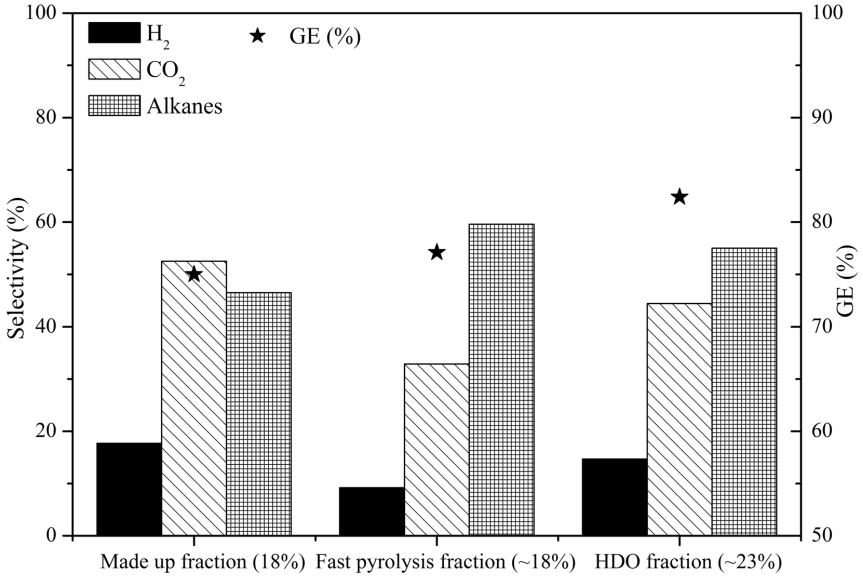

Figure A.7: The influence of different aqueous bio-oil feedstocks on the gasification behaviour in supercritical water at 580 °C, 280 bar, 15 min reaction time and Pd/Ce-ZrO_2 catalyst.

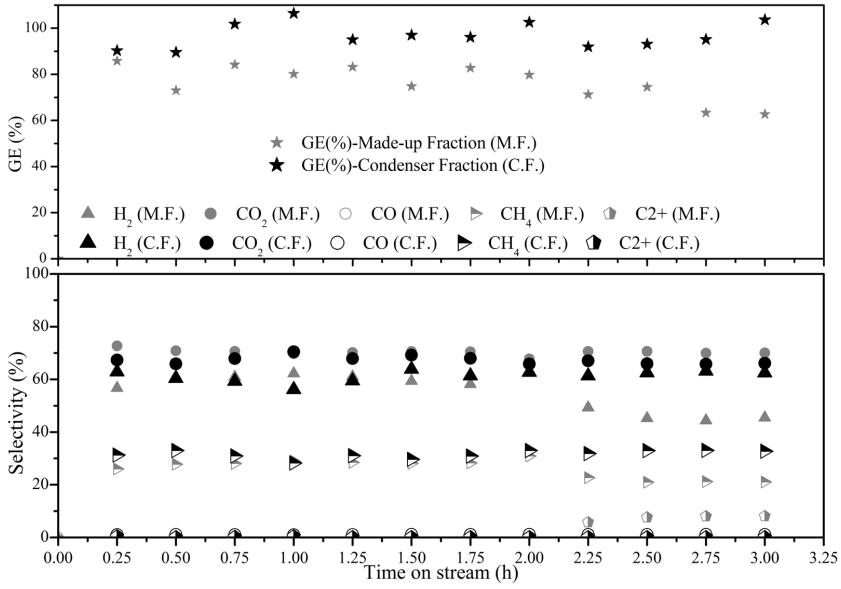

Figure A.8: Catalytic reforming of the aqueous fraction of bio-oil in supercritical water using a continuous flow reactor. Experimental conditions: Feed– Made-up-I and Pyrolysis condenser fraction, Feed concentration–5 wt% , T – 600 °C, P – 250 bar, Ru/Ce-ZrO_2 catalyst – 6 g, Flow – 2 mL/min.

A.3.8 CATALYST CHARACTERIZATION RESULTS

Thermo-gravimetric analysis of the internal coke deposited on the catalysts having different supports is shown in Figure A.9. Very less or almost no internal coke deposition on the γ-Al_2O_3 supported catalyst is noticed. The internal coke deposited on the activated carbon supported catalyst could not be quantified as the support started to completely oxidise in the temperature range of 400–700°C. Maximum internal coke formation is observed with Ti supported catalysts. It is evident from Figure A.9, that two different cokes are formed on the supports. Low temperature coke conversion in the range of 300–450 °C is observed for TiO_2, Ce-ZrO_2 and ZrO_2 supported catalysts. Comparatively, high temperatures in the range of 400–600 °C, are needed for the conversion of coke on silica supported catalysts.

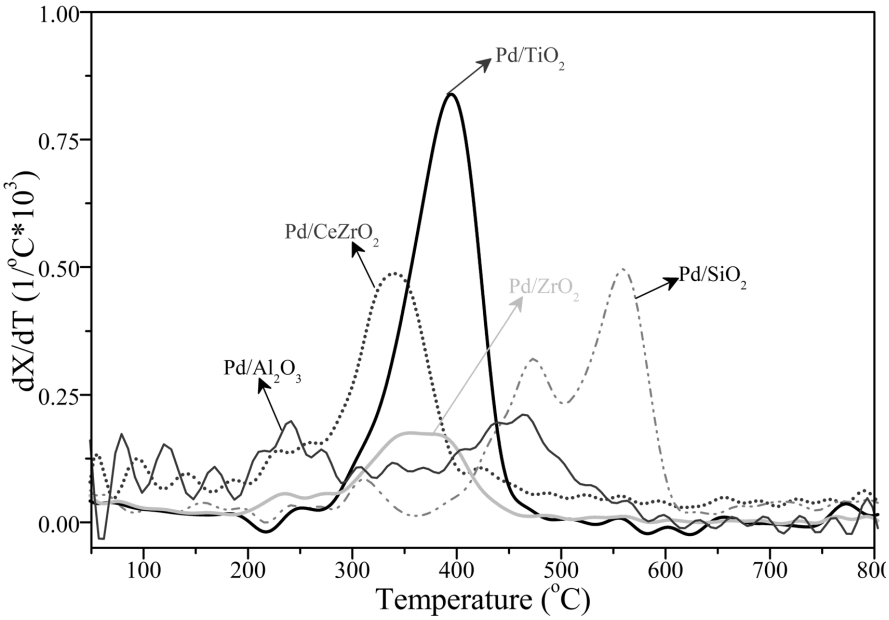

Figure A.9: Thermo-gravimetric analysis of the internal coke deposited on the catalysts after the reaction at heating rate of 10 °C/min in stream of flowing air (30 ml/min).

The crystalline structures of the fresh and spent catalysts are verified by XRD analysis and are shown in Figure A.10. As can be seen from the figure, fresh γ-Al_2O_3 has two peaks at 2θ=45.8° and 66.8°. The transformation of γ-Al_2O_3 increases with increasing temperature to corundum followed by sequence of γ →δ→θ→α, the surface area decreases with each step and the final transition to the alpha phase is associated with the greatest decrease.[183] Elliott *et al.* [179-180] have reported that after the exposure of γ-Al_2O_3 in sub or supercritical water at 350 °C and 200 bar, δ- and γ-Al_2O_3 were completely hydrolyzed to give boehmite, while η-Al_2O_3 formed a mix of boehmite and α-Al_2O_3 leading to loss of surface area. XRD analysis verified that the fresh Ti support was found in a mix of both rutile and anatase form.

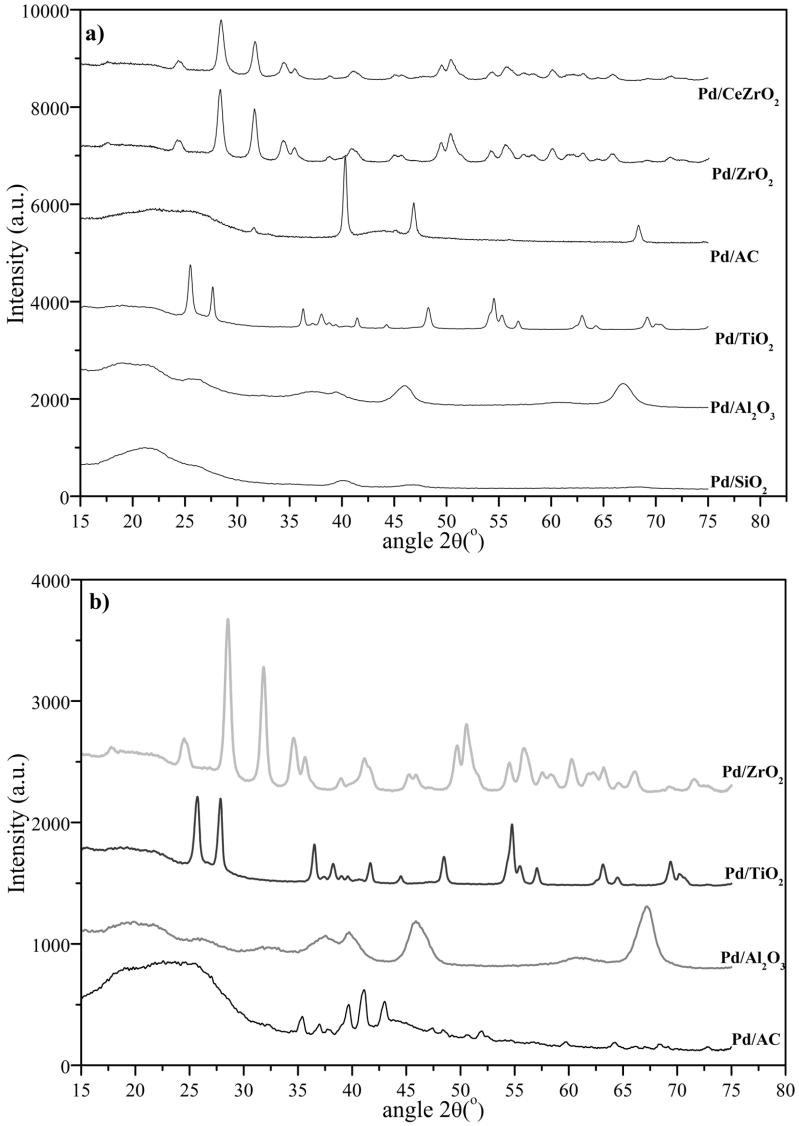

Figure A.10: XRD analysis of the fresh (a) and spent catalysts (b).

The percentage reduction of the BET surface area is defined as the ratio of final surface area after the reaction to the initial surface area. The loss in surface area due to phase change is shown in terms of BET surface area reduction is illustrated in Figure A.11. Significant loss in

the surface area is observed for silica and activated carbon supports. A slight increase in the surface area of the catalyst is noticed with ZrO_2, TiO_2 and Ce-ZrO_2 after the reaction. This gain in the surface area after the reaction can be associated due to the deposition of internal coke in the catalyst. The loss in surface area may differ in realistic conditions when tested in a continuous flow reactor.

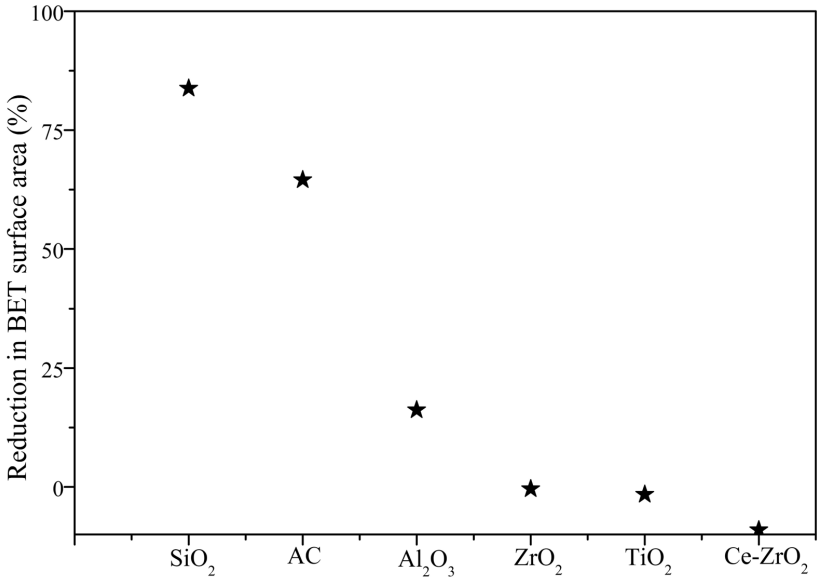

Figure A.11: Percentage reduction of catalyst surface area loss after 15 min of reaction time.

A.4 CONCLUSIONS

Catalytic supercritical water gasification is an attractive process to processing wet biomass streams but also appears to be applicable for wastewater treatment produced from biomass pyrolysis and upgrading processes in a wood-based (ligno-cellulosic) bio-refinery system. The main scope of this process is to completely convert the organics present in the water soluble fraction of bio-oil to combustible gases in the presence of a catalyst. The present study provides a quantitative evaluation of the reforming activity of several catalysts, support materials and different operating parameters on the conversion and product gas selectivities of water soluble fraction of bio-oil. Ru was found to be the most active catalyst in terms of gasification efficiency as well as alkane selectivity. The catalyst supports tested had a negligible effect on the conversion, but a prominent effect on the product gas distribution. Titania supported catalysts were found to have a high amount of internal char deposition when

compared to other supports. Though carbon supported catalysts have high specific surface area they are prone to gasification in supercritical water. Stable support materials identified for the hydrothermal gasification of biomass include ZrO_2, Ce-ZrO_2 and TiO_2. High temperatures, low feedstock concentrations, high catalyst loadings and longer residence time favoured high conversion. The aqueous wastewater from the HDO process was more easily converted than the aqueous fraction obtained from the condenser fraction and the made-up waste stream. A more complete gasification and stable product gas composition was obtained with the condenser fraction, when compared to the (made-up) bio-oil fraction. This significant difference between the two feeds is primarily due to the presence of sugars components in the made-up fraction, which lead to more coke formation and incomplete conversion due to catalyst deactivation.

Chapter 7

Epilogue

Biomass gasification in supercritical water is a complex process as it involves scissioning of larger molecules to gaseous products under the influence of free radical reactions, which are dominant at high temperatures (above 600 °C). It should be noted that this technology, though promising, is still immature, despite extensive research at the laboratory scale. There has been only a limited number of pilot scale set-ups established around the world. The major issues associated with the gasification of aqueous biomass slurries in SCW are pumping feedstocks to high pressures, dealing with char/coke formation during heating, coke on catalyst and the handling the presence of impurities like salts and minerals in the real feeds which can lead to severe fouling and even reactor plugging and corrosion issues. Additional efforts are required in areas such as design of an efficient heat exchanger, handling the solid and liquid by-product, ash removal and mixing inside the reactor, in order to pave the way towards realization of SCWG in actual practice.

Understanding the chemistry of biomass gasification is a challenging task. From activities undertaken for realistic feedstocks (glycerol, algae and pyrolysis oil aqueous phases) and the systematic variation of molecular chain length for n-alcohol and n-carboxylic acid gasification some insights could be obtained on the reaction paths. From the alcohol/acid series the intriguing oscillations in methane selectivity with increasing chain length could be understood on basis of postulated reaction mechanisms based on (*i*) initiation of cracking by H abstraction from the functional group and (*ii*) followed by β-scission of the alkyl chain. A further noticeable observation is the dependency of gasification yield on carboxylic acid feed concentration, whereas for alcohols there is no such effect. This suggests that side-reactions limiting the gasification yield may predominantly be ionic in nature and active during the heating up trajectory.

For glycerol the role of dehydration was clearly shown by comparing product composition vs. gasification efficiency. The reaction mechanism has been elucidated and, considering the low coke-tendency of the feed, the technology for purified glycerol can be considered to be almost ready for scale-up to large-scale demonstration and commercial application. A possible concern may be the handling of the salt content of crude glycerine from biodiesel production.

The addition of amino acids (as protein building block) to a glycerol feed showed significant reduction in gasification efficiency as well as strong coloring (from colorless to 'chocolate-brown') of the liquid effluent; an indication of strong interaction of decomposition intermediates via *e.g.* Maillard reactions. This illustrates the difficulty in fundamental studies for complex feedstocks in comparison with a more well-defined and essentially single compound (*e.g.* feedstock as pure glycerol in water). For more complex feed streams a pilot plant study is

therefore an unavoidable step in the process development trajectory towards large scale operation.

Catalyst development showed significant progress considering the tested catalysts with model compounds. Often the gasification temperature for (near-) complete gasification could be reduced from 650-700 °C to 550 °C or below, and for some feedstocks (like ethylene glycol even close to 400 °C). Stability of catalyst and -support needs more attention, in combination with the targeted feed. Relatively cheap nickel-based (reforming-) catalyst, with- and without second metal co-catalyst, gave promising results for duration runs as long as 85 h. During catalyst development attention was focused on the active metal component and to a lesser extent to the support material. Based on the (limited) experiences now obtained carbon, titania and zirconia supports are superior to the γ-Al_2O_3 support often used, also in this work, and should be preferred for further work in this field.

Applying the catalysts to 'real' biomass as slurries of micro-algae and the aqueous phase of pyrolysis oil showed that indeed catalyst lifetime remains an issue. In situ rejuvenation of the catalyst and stable, non-leaching catalyst support materials need to be developed. There is an outlook to complete gasification of microalgae, however due to the reaction of intermediate products described above, more catalyst- and process development (*e.g.* implementing hydrothermal liquefaction as pre-treatment) is needed.

For understanding the chemistry – and catalysis aspects for complex feedstocks, it is realized that these cannot be mimicked perfectly with a single model compound! Hence, developing gasification in supercritical water, for *e.g.* algae slurries or pyrolysis oils aqueous phases, should start with selecting- and focusing on a targeted feed stream. To turn it into a working system, operating for many hours, much more work, also in the fundamentals, is needed before the technology is ready for up-scaling and commercialization. The activities required comprise catalyst development and handling (regeneration!) as well as process development issues, before a reliable system can designed and build at significant scale. It is recommendable to conduct this process development directly on the foreseen application (biomass feed stream), in view of possible system-specific complications. Only for somewhat simpler applications, as gasification of pure glycerine or methanol, up-scaling and commercial application is within reach, albeit that the presence of impurities in the feed may require some additional (process-) development work.

Chapter 7

BIBILIOGRAPHY

1. U.S. Energy Information Administration In Annual Energy Review 2011: Vol. DOE/EIA-0384(2011), September 2012.
2. Renewable energy outlook. In Agency, I. E., Ed. 2012; pp 211-240.
3. De Miguel Mercader, F. Pyrolysis oil upgrading for co-processing in standard refinery units. University of Twente, Enschede, 2010.
4. Waldner, M. H. Catalytic hydrothermal gasification of biomass for the production of synthetic natural gas. ETH Zurich, Zurich, Switzerland, 2007.
5. Huber, G. W.; Iborra, S.; Corma, A., Synthesis of transportation fuels from biomass: Chemistry, catalysts, and engineering. *Chemical Reviews* **2006,** 106, (9), 4044-4098.
6. Westerhof, R. J. M. Refining fast pyrolysis of biomass. University of Twente, Enschede, 2011.
7. Rossum, v. G. Steam reforming and gasification of pyrolysis oil. University of Twente, Enschede, 2009.
8. Matsumura, Y.; Minowa, T.; Potic, B.; Kersten, S. R. A.; Prins, W.; van Swaaij, W. P. M.; van de Beld, B.; Elliott, D. C.; Neuenschwander, G. G.; Kruse, A.; Antal, M. J., Biomass gasification in near- and super-critical water: Status and prospects. *Biomass & bioenergy* **2005,** 29, (4), 269-292.
9. Davda, R. R.; Shabaker, J. W.; Huber, G. W.; Cortright, R. D.; Dumesic, J. A., A review of catalytic issues and process conditions for renewable hydrogen and alkanes by aqueous-phase reforming of oxygenated hydrocarbons over supported metal catalysts. *Applied Catalysis B: Environmental* **2005,** 56, (1-2), 171-186.
10. Huber, G. W.; Dumesic, J. A., An overview of aqueous-phase catalytic processes for production of hydrogen and alkanes in a biorefinery. *Catalysis Today* **2006,** 111, (1-2), 119-132.
11. Komula, d. http://www.virent.com/wordpress/wp-content/uploads/2011/08/Virent-Article-in-Bioplastics-Magazine.pdf (04-September-2013),
12. Antal, M. J.; Allen, S. G.; Schulman, D.; Xu, X. D.; Divilio, R. J., Biomass gasification in supercritical water. *Industrial & Engineering Chemistry Research* **2000,** 39, (11), 4040-4053.
13. Chakinala, A. G.; Brilman, D. W. F.; van Swaaij, W. P. M.; Kersten, S. R. A., Catalytic and non-catalytic supercritical water gasification of microalgae and glycerol. *Industrial & Engineering Chemistry Research* **2010,** 49, (3), 1113-1122.
14. de Vlieger, D. J. M.; Chakinala, A. G.; Lefferts, L.; Kersten, S. R. A.; Seshan, K.; Brilman, D. W. F., Hydrogen from ethylene glycol by supercritical water reforming using noble and base metal catalysts. *Applied Catalysis B: Environmental* **2012,** 111-112, 536-544.
15. Peterson, A. A.; Vogel, F.; Lachance, R. P.; Froling, M.; Antal, M. J.; Tester, J. W., Thermochemical biofuel production in hydrothermal media: A review of sub- and supercritical water technologies. *Energy & Environmental Science* **2008,** 1, (1), 32-65.
16. Minowa, T.; Sawayama, S., A novel microalgal system for energy production with nitrogen cycling. *Fuel* **1999,** 78, (10), 1213-1215.
17. Potic, B. Gasification of biomass in supercritical water. University of Twente, Enschede, The Netherlands, 2006.
18. Kruse, A., Supercritical water gasification. *Biofuels Bioproducts & Biorefining-Biofpr* **2008,** 2, (5), 415-437.

19. Kruse, A., Hydrothermal biomass gasification. *Journal of Supercritical Fluids* **2009,** 47, (3), 391-399.
20. Sricharoenchaikul, V., Assessment of black liquor gasification in supercritical water. *Bioresource Technology* **2009,** 100, (2), 638-643.
21. Yan, B.; Wei, C. h.; Hu, C. s.; Xie, C.; Wu, J. z., Hydrogen generation from polyvinyl alcohol-contaminated wastewater by a process of supercritical water gasification. *Journal of Environmental Sciences* **2007,** 19, (12), 1424-1429.
22. Nakamura, A.; Kiyonaga, E.; Yamamura, Y.; Shimizu, Y.; Minowa, T.; Noda, Y.; Matsumura, Y., Detailed Analysis of Heat and Mass Balance for Supercritical Water Gasification. *Journal of Chemical Engineering of Japan* **2008,** 41, (8), 817-828.
23. Nakamura, A.; Kiyonaga, E.; Yamamura, Y.; Shimizu, Y.; Minowa, T.; Noda, Y.; Matsumura, Y., Gasification of Catalyst-Suspended Chicken Manure in Supercritical Water. *Journal of Chemical Engineering of Japan* **2008,** 41, (5), 433-440.
24. D'Jesus, P.; Artiel, C.; Boukis, N.; Kraushaar-Czarnetzki, B.; Dinjus, E., Influence of educt preparation on gasification of corn silage in supercritical water. *Industrial & Engineering Chemistry Research* **2005,** 44, (24), 9071-9077.
25. D'Jesus, P.; Boukis, N.; Kraushaar-Czarnetzki, B.; Dinjus, E., Influence of process variables on gasification of corn silage in supercritical water. *Industrial & Engineering Chemistry Research* **2006,** 45, (5), 1622-1630.
26. Yanik, J.; Ebale, S.; Kruse, A.; Saglam, M.; Yuksel, M., Biomass gasification in supercritical water: II. Effect of catalyst. *International Journal of Hydrogen Energy* **2008,** 33, (17), 4520-4526.
27. Xu, X. D.; Antal, M. J., Gasification of sewage sludge and other biomass for hydrogen production in supercritical water. *Environmental Progress* **1998,** 17, (4), 215-220.
28. Gasafi, E.; Reinecke, M. Y.; Kruse, A.; Schebek, L., Economic analysis of sewage sludge gasification in supercritical water for hydrogen production. *Biomass & bioenergy* **2008,** 32, (12), 1085-1096.
29. Gasafi, E.; Meyer, L.; Schebek, L., Exergetic efficiency and options for improving sewage sludge gasification in supercritical water. *International Journal of Energy Research* **2007,** 31, (4), 346-363.
30. Idesh, S.; Kudo, S.; Norinaga, K.; Hayashi, J.-i., Catalytic hydrothermal reforming of water-soluble organics from the pyrolysis of biomass using a Ni/Carbon catalyst impregnated with Pt. *Energy & Fuels* **2012,** 26, (1), 67-74.
31. Chakinala, A. G.; Chinthaginjala, J. K.; Seshan, K.; Swaaij, W. P. M. v.; Kersten, S. R. A.; Brilman, D. W. F., Catalyst screening for the hydrothermal gasification of aqueous phase of bio-oil *Catalysis Today* **2012**, (Catbior Special Issue).
32. Penninger, J. M. L.; Rep, M., Reforming of aqueous wood pyrolysis condensate in supercritical water. *International Journal of Hydrogen Energy* **2006,** 31, (11), 1597-1606.
33. Di Blasi, C.; Branca, C.; Galgano, A.; Meier, D.; Brodzinski, I.; Malmros, O., Supercritical gasification of wastewater from updraft wood gasifiers. *Biomass and Bioenergy* **2007,** 31, (11-12), 802-811.
34. Byrd, A. J.; Kumar, S.; Kong, L. Z.; Ramsurn, H.; Gupta, R. B., Hydrogen production from catalytic gasification of switchgrass biocrude in supercritical water. *International Journal of Hydrogen Energy* **2011,** 36, (5), 3426-3433.
35. Brown, T. M.; Duan, P. G.; Savage, P. E., Hydrothermal Liquefaction and Gasification of Nannochloropsis sp. *Energy & Fuels* **2010,** 24, 3639-3646.

36. Haiduc, A.; Brandenberger, M.; Suquet, S.; Vogel, F.; Bernier-Latmani, R.; Ludwig, C., SunChem: an integrated process for the hydrothermal production of methane from microalgae and CO_2 mitigation. *Journal of Applied Phycology* **2009,** 21, (5), 529-541.
37. Stucki, S.; Vogel, F.; Ludwig, C.; Haiduc, A. G.; Brandenberger, M., Catalytic gasification of algae in supercritical water for biofuel production and carbon capture. *Energy & Environmental Science* **2009,** 2, (5), 535-541.
38. Matsumura, Y., Evaluation of supercritical water gasification and biomethanation for wet biomass utilization in Japan. *Energy Conversion and Management* **2002,** 43, (9-12), 1301-1310.
39. Water Phase Diagram. http://www.chemicalogic.com/Pages/DownloadPhaseDiagrams.aspx (August, 20),
40. Buhler, W.; Dinjus, E.; Ederer, H. J.; Kruse, A.; Mas, C., Ionic reactions and pyrolysis of glycerol as competing reaction pathways in near- and supercritical water. *Journal of Supercritical Fluids* **2002,** 22, (1), 37-53.
41. Akiya, N.; Savage, P. E., Roles of Water for Chemical Reactions in High-Temperature Water. *Chemical Reviews* **2002,** 102, (8), 2725-2750.
42. Bröll, D.; Kaul, C.; Kramer, A.; Krammer, P.; Richter, T.; Jung, M.; Vogel, H.; Zehner, P., Chemistry in supercritical water. *Angewandte Chemie - International Edition* **1999,** 38, (20), 2998-3014.
43. Kruse, A.; Ebert, K. H., Chemical reactions in supercritical water 1. Pyrolysis of tert-butylbenzene. *Berichte Der Bunsen-Gesellschaft-Physical Chemistry Chemical Physics* **1996,** 100, (1), 80-83.
44. Savage, P. E., Organic chemical reactions in supercritical water. *Chemical Reviews* **1999,** 99, (2), 603-621.
45. Adschiri, T.; Hakuta, Y.; Arai, K., Hydrothermal synthesis of metal oxide fine particles at supercritical conditions. *Industrial and Engineering Chemistry Research* **2000,** 39, (12), 4901-4907.
46. Loppinet-Serani, A.; Aymonier, C.; Cansell, F., Current and Foreseeable Applications of Supercritical Water for Energy and the Environment. *Chemsuschem* **2008,** 1, (6), 486-503.
47. Loppinet-Serani, A.; Aymonier, C.; Cansell, F., Supercritical water for environmental technologies. *Journal of Chemical Technology & Biotechnology* **2010,** 85, (5), 583-589.
48. Schmieder, H.; Abeln, J., Supercritical water oxidation: State of the art. *Chemical Engineering & Technology* **1999,** 22, (11), 903-908.
49. Gadhe, J. B.; Gupta, R. B., Hydrogen production by methanol reforming in supercritical water: Catalysis by in-situ-generated copper nanoparticles. *International Journal of Hydrogen Energy* **2007,** 32, (13), 2374-2381.
50. Ross, A. B.; Jones, J. M.; Kubacki, M. L.; Bridgeman, T., Classification of macroalgae as fuel and its thermochemical behaviour. *Bioresource Technology* **2008,** 99, (14), 6494-6504.
51. Yusuf, C., Biodiesel from microalgae. *Biotechnology Advances* **2007,** 25, (3), 294-306.
52. Sheehan, J.; Dunahay, T.; Benemann, J.; Roessler, P., A look back at the U.S. department of energy's aquatic species program-Biodiesel from algae. In DOE, Ed. NREL/TP-580-24190: US, 1998.
53. Antal, M. J. *Hydrogen production by gasification of glucose and wet biomass in supercritical water*; University of Hawaii: Hawaii, 1990.
54. Kersten, S. R. A.; Potic, B.; Prins, W.; Van Swaaij, W. P. M., Gasification of model compounds and wood in hot compressed water. *Industrial and Engineering Chemistry Research* **2006,** 45, (12), 4169-4177.

55. Potic, B.; Kersten, S. R. A.; Prins, W.; van Swaaij, W. P. M., A high-throughput screening technique for conversion in hot compressed water. *Industrial & Engineering Chemistry Research* **2004,** 43, (16), 4580-4584.
56. Resende, F. L. P.; Neff, M. E.; Savage, P. E., Noncatalytic gasification of cellulose in supercritical water. *Energy & Fuels* **2007,** 21, (6), 3637-3643.
57. Resende, F. L. P.; Fraley, S. A.; Berger, M. J.; Savage, P. E., Noncatalytic gasification of lignin in supercritical water. *Energy & Fuels* **2008,** 22, (2), 1328-1334.
58. Karayildirim, T.; Sinag, A.; Kruse, A., Char and coke formation as unwanted side reaction of the hydrothermal biomass gasification. *Chemical Engineering & Technology* **2008,** 31, (11), 1561-1568.
59. Knezevic, D.; Schmiedl, D.; Meier, D.; Kersten, S.; Van Swaaij, W., High-throughput screening technique for conversion in hot compressed water: Quantification and characterization of liquid and solid products. *Industrial & Engineering Chemistry Research* **2007,** 46, (6), 1810-1817.
60. Knezevic, D.; van Swaaij, W. P. M.; Kersten, S. R. A., Hydrothermal Conversion of Biomass: I, Glucose Conversion in Hot Compressed Water. *Industrial & Engineering Chemistry Research* **2009,** 48, (10), 4731-4743.
61. Kruse, A.; Krupka, A.; Schwarzkopf, V.; Gamard, C.; Henningsen, T., Influence of proteins on the hydrothermal gasification and liquefaction of biomass. 1. Comparison of different feedstocks. *Industrial & Engineering Chemistry Research* **2005,** 44, (9), 3013-3020.
62. Kruse, A.; Maniam, P.; Spieler, F., Influence of proteins on the hydrothermal gasification and liquefaction of biomass. 2. Model compounds. *Industrial & Engineering Chemistry Research* **2007,** 46, (1), 87-96.
63. Lu, Y.; Guo, L.; Zhang, X.; Yan, Q., Thermodynamic modeling and analysis of biomass gasification for hydrogen production in supercritical water. *Chemical Engineering Journal* **2007,** 131, (1-3), 233-244.
64. van Rossum, G.; Potic, B.; Kersten, S. R. A.; van Swaaij, W. P. M., Catalytic gasification of dry and wet biomass. *Catalysis Today* **2009,** 145, (1-2), 10-18.
65. Schmieder, H.; Abeln, J.; Boukis, N.; Dinjus, E.; Kruse, A.; Kluth, M.; Petrich, G.; Sadri, E.; Schacht, M., Hydrothermal gasification of biomass and organic wastes. *Journal of Supercritical Fluids* **2000,** 17, (2), 145-153.
66. Kersten, S. R. A.; van Swaaij, W. P. M.; Lefferts, L.; Seshan, K., Options for catalysis in the thermochemical conversion of biomass into fuels. In *Catalysis for Renewables*, Wiley-VCH Verlag GmbH & Co. KGaA: 2007; pp 119-145.
67. Dileo, G. J.; Neff, M. E.; Kim, S.; Savage, P. E., Supercritical water gasification of phenol and glycine as models for plant and protein biomass. *Energy & Fuels* **2008,** 22, (2), 871-877.
68. Guan, Q.; Wei, C.; Savage, P. E., Hydrothermal Gasification of Nannochloropsis sp with Ru/C. *Energy & Fuels* **2012,** 26, (7), 4575-4582.
69. Onwudili, J. A.; Lea-Langton, A. R.; Ross, A. B.; Williams, P. T., Catalytic hydrothermal gasification of algae for hydrogen production: Composition of reaction products and potential for nutrient recycling. *Bioresource Technology* **2013,** 127, 72-80.
70. Elliott, D. C.; Hart, T. R.; Neuenschwander, G. G.; Rotness, L. J.; Olarte, M. V.; Zacher, A. H., Chemical Processing in High-Pressure Aqueous Environments. 9. Process Development for Catalytic Gasification of Algae Feedstocks. *Industrial & Engineering Chemistry Research* **2012,** 51, (33), 10768-10777.
71. Guan, Q.; Wei, C.; Savage, P. E., Kinetic model for supercritical water gasification of algae. *Physical Chemistry Chemical Physics* **2012,** 14, (9), 3140-3147.

72. Brandenberger, M.; Matzenberger, J.; Vogel, F.; Ludwig, C., Producing synthetic natural gas from microalgae via supercritical water gasification: A techno-economic sensitivity analysis. *Biomass and Bioenergy* **2013**, (0), 1-9.
73. Kyle, B. G., Chemical and process thermodynamics. In Prentice Hall PTR: Englewood cliffs: New Jersey, 1999.
74. Soave, G.; Barolo, M.; Bertucco, A., Estimation of high-pressure fugacity coefficients of pure gaseous fluids by a modified SRK equation of state. *Fluid Phase Equilibria* **1993,** 91, (1), 87-100.
75. Bertucco, A.; Barolo, M.; Soave, G., Estimation of Chemical Equilibria In High-Pressure Gaseous Systems by a Modified Redlich-Kwong-Soave Equation of State. *Industrial & Engineering Chemistry Research* **1995,** 34, (9), 3159-3165.
76. Giorgio, S., Equilibrium constants from a modified Redlich-Kwong equation of state. *Chemical Engineering Science* **1972,** 27, (6), 1197-1203.
77. Kunkes, E. L.; Simonetti, D. A.; West, R. M.; Serrano-Ruiz, J. C.; Gartner, C. A.; Dumesic, J. A., Catalytic conversion of biomass to monofunctional hydrocarbons and targeted liquid-fuel classes. *Science* **2008,** 322, (5900), 417-421.
78. Moens, L.; Evans, R. J.; Looker, M. J.; Nimlos, M. R., A comparison of the Maillard reactivity of proline to other amino acids using pyrolysis-molecular beam mass spectrometry. *Fuel* **2004,** 83, (11-12), 1433-1443.
79. Sato, N.; Quitain, A. T.; Kang, K.; Daimon, H.; Fujie, K., Reaction kinetics of amino acid decomposition in high-temperature and high-pressure water. *Industrial & Engineering Chemistry Research* **2004,** 43, (13), 3217-3222.
80. Klingler, D.; Berg, J.; Vogel, H., Hydrothermal reactions of alanine and glycine in sub- and supercritical water. *Journal of Supercritical Fluids* **2007,** 43, (1), 112-119.
81. Kaul, S.; Sharma, S. S.; Mehta, I. K., Free radical scavenging potential of L-proline: evidence from in vitro assays. *Amino Acids* **2008,** 34, (2), 315-320.
82. Dinjus, E.; Kruse, A., Hot compressed water - a suitable and sustainable solvent and reaction medium? *Journal of Physics-Condensed Matter* **2004,** 16, (14), S1161-S1169.
83. Kruse, A.; Bernolle, P.; Dahmen, N.; Dinjus, E.; Maniam, P., Hydrothermal gasification of biomass: consecutive reactions to long-living intermediates. *Energy & Environmental Science* **2010,** 3, (1), 136-143.
84. Calvo, L.; Vallejo, D., Formation of organic acids during the hydrolysis and oxidation of several wastes in sub- and supercritical water. *Industrial & Engineering Chemistry Research* **2002,** 41, (25), 6503-6509.
85. Kruse, A.; Faquir, M., Hydrothermal biomass gasification - Effects of salts, backmixing, and their interaction. *Chemical Engineering & Technology* **2007,** 30, (6), 749-754.
86. Yu, J.; Savage, P. E., Decomposition of formic acid under hydrothermal conditions. *Industrial and Engineering Chemistry Research* **1998,** 37, (1), 2-10.
87. Saito, K.; Shiose, T.; Takahashi, O.; Hidaka, Y.; Aiba, F.; Tabayashi, K., Unimolecular decomposition of formic acid in the gas phase on the ratio of the competing reaction channels. *Journal of Physical Chemistry A* **2005,** 109, (24), 5352-5357.
88. Yu, J.; Savage, P. E., Decomposition of Formic Acid under Hydrothermal Conditions. *Industrial & Engineering Chemistry Research* **1998,** 37, (1), 2-10.
89. Honma, T.; Inomata, H., The role of local structure on formic acid decomposition in supercritical water: A hybrid quantum mechanics/Monte Carlo study. *Fluid Phase Equilibria* **2007,** 257, (2), 238-243.
90. Akiya, N.; Savage, P. E., Role of water in formic acid decomposition. *Aiche Journal* **1998,** 44, (2), 405-415.

91. Zhang, Y.; Zhang, J.; Zhao, L.; Sheng, C., Decomposition of Formic acid in supercritical Water. *Energy & Fuels* **2009,** 24, (1), 95-99.
92. Akiya, N.; Savage, P. E., Effect of water density on hydrogen peroxide dissociation in supercritical water. 2. Reaction kinetics. *Journal of Physical Chemistry A* **2000,** 104, (19), 4441-4448.
93. Mizan, T. I.; Savage, P. E.; Ziff, R. M., Fugacity coefficients for free radicals in dense fluids: HO_2 in supercritical water. *Aiche Journal* **1997,** 43, (5), 1287-1299.
94. Wakai, C.; Yoshida, K.; Tsujino, Y.; Matubayasi, N.; Nakahara, M., Effect of Concentration, Acid, Temperature, and Metal on Competitive Reaction Pathways for Decarbonylation and Decarboxylation of Formic Acid in Hot Water. *Chemistry Letters* **2004,** 33, (5), 572-573.
95. Singleton, D. L.; Paraskevopoulos, G.; Irwin, R. S., Rates and mechanism of the reactions of hydroxyl radicals with acetic, deuterated acetic, and propionic acids in the gas phase. *Journal of the American Chemical Society* **1989,** 111, (14), 5248-5251.
96. Meyer, J. C.; Marrone, P. A.; Tester, J. W., Acetic acid oxidation and hydrolysis in supercritical water. *Aiche Journal* **1995,** 41, (9), 2108-2121.
97. Watanabe, M.; Sato, T.; Inomata, H.; Smith, R. L.; Arai, K.; Kruse, A.; Dinjus, E., Chemical reactions of C-1 compounds in near-critical and supercritical water. *Chemical Reviews* **2004,** 104, (12), 5803-5821.
98. Watanabe, M.; Iida, T.; Aizawa, Y.; Ura, H.; Inomata, H.; Arai, K., Conversions of some small organic compounds with metal oxides in supercritical water at 673 K. *Green Chemistry* **2003,** 5, (5), 539-544.
99. McMillen, D. F.; Golden, D. M., Hydrocarbon Bond Dissociation Energies. *Annual Review of Physical Chemistry* **1982,** 33, (1), 493-532.
100. Olaj, O. F., Comprehensive Chemical Kinetics. Vol. 5. Decomposition and Isomerization of Organic Compounds. Von C. H. Bamford und C. F. Tipper Elsevier Publishing Company, Amsterdam—London—New York 1972. 1, Aufl., XVI, 779 S., zahlr. Abb. *Angewandte Chemie* **1974,** 86, (19), 712-712.
101. Watanabe, M.; Inomata, H.; Smith, R. L.; Arai, K., Catalytic decarboxylation of acetic acid with zirconia catalyst in supercritical water. *Applied Catalysis A: General* **2001,** 219, (1-2), 149-156.
102. Jia, N.; Moore, R. G.; Mehta, S. A.; Ursenbach, M. G., Kinetic modeling of thermal cracking reactions. *Fuel* **2009,** 88, (8), 1376-1382.
103. Jin, F.; Moriya, T.; Enomoto, H., Oxidation Reaction of High Molecular Weight Carboxylic Acids in Supercritical Water. *Environmental Science & Technology* **2003,** 37, (14), 3220-3231.
104. Abbot, J.; Dunstan, P. R., Catalytic cracking of linear paraffins: Effects of chain length. *Industrial & Engineering Chemistry Research* **1997,** 36, (1), 76-82.
105. DiLeo, G. J.; Savage, P. E., Catalysis during methanol gasification in supercritical water. *Journal of Supercritical Fluids* **2006,** 39, (2), 228-232.
106. van Bennekom, J. G.; Venderbosch, R. H.; Assink, D.; Heeres, H. J., Reforming of methanol and glycerol in supercritical water. *The Journal of Supercritical Fluids* **2011,** 58, (1), 99-113.
107. Hack, W.; Masten, D. A.; Buelow, S. J., Methanol and ethanol decomposition in supercritical water. *Zeitschrift fur Physikalische Chemie* **2005,** 219, (3), 367-378.
108. Vogel, F.; Blanchard, J. L. D.; Marrone, P. A.; Rice, S. F.; Webley, P. A.; Peters, W. A.; Smith, K. A.; Tester, J. W., Critical review of kinetic data for the oxidation of methanol in supercritical water. *The Journal of Supercritical Fluids* **2005,** 34, (3), 249-286.

109. Boock, L. T.; Klein, M. T., Lumping strategy for modeling the oxidation of C1-C3 alcohols and acetic acid in high-temperature water. *Industrial and Engineering Chemistry Research* **1993,** 32, (11), 2464-2473.
110. Boukis, N.; Diem, V.; Habicht, W.; Dinjus, E., Methanol reforming in supercritical water. *Industrial & Engineering Chemistry Research* **2003,** 42, (4), 728-735.
111. Arita, T.; Nakahara, K.; Nagami, K.; Kajimoto, O., Hydrogen generation from ethanol in supercritical water without catalyst. *Tetrahedron Letters* **2003,** 44, (5), 1083-1086.
112. Therdthianwong, S.; Srisiriwat, N.; Therdthianwong, A.; Croiset, E., Hydrogen production from bioethanol reforming in supercritical water. *The Journal of Supercritical Fluids* **2011,** 57, (1), 58-65.
113. Kalinci, Y.; Hepbasli, A.; Dincer, I., Biomass-based hydrogen production: A review and analysis. *International Journal of Hydrogen Energy* **2009,** 34, (21), 8799-8817.
114. Bleeker, M. F.; Kersten, S. R. A.; Veringa, H. J., Pure hydrogen from pyrolysis oil using the steam-iron process. *Catalysis Today* **2007,** 127, (1-4), 278-290.
115. Tanksale, A.; Beltramini, J. N.; Lu, G. M., A review of catalytic hydrogen production processes from biomass. *Renewable and Sustainable Energy Reviews* **2010,** 14, (1), 166-182.
116. Cortright, R. D.; Davda, R. R.; Dumesic, J. A., Hydrogen from catalytic reforming of biomass-derived hydrocarbons in liquid water. *Nature* **2002,** 418, (6901), 964-967.
117. Guo, Y.; Wang, S. Z.; Xu, D. H.; Gong, Y. M.; Ma, H. H.; Tang, X. Y., Review of catalytic supercritical water gasification for hydrogen production from biomass. *Renewable & Sustainable Energy Reviews* **2010,** 14, (1), 334-343.
118. Czernik, S.; French, R.; Feik, C.; Chornet, E., Hydrogen by catalytic steam reforming of liquid byproducts from biomass thermoconversion processes. *Industrial and Engineering Chemistry Research* **2002,** 41, (17), 4209-4215.
119. Shabaker, J. W.; Davda, R. R.; Huber, G. W.; Cortright, R. D.; Dumesic, J. A., Aqueous-phase reforming of methanol and ethylene glycol over alumina-supported platinum catalysts. *Journal of Catalysis* **2003,** 215, (2), 344-352.
120. Huber, G. W.; Shabaker, J. W.; Evans, S. T.; Dumesic, J. A., Aqueous-phase reforming of ethylene glycol over supported Pt and Pd bimetallic catalysts. *Applied Catalysis B: Environmental* **2006,** 62, (3-4), 226-235.
121. Yamaguchi, A.; Hiyoshi, N.; Sato, O.; Bando, K. K.; Osada, M.; Shirai, M., Hydrogen production from woody biomass over supported metal catalysts in supercritical water. *Catalysis Today* **2009,** 146, (1-2), 192-195.
122. Waldner, M. H.; Krumeich, F.; Vogel, F., Synthetic natural gas by hydrothermal gasification of biomass selection procedure towards a stable catalyst and its sodium sulfate tolerance. *Journal of Supercritical Fluids* **2007,** 43, (1), 91-105.
123. Vagia, E. C.; Lemonidou, A. A., Thermodynamic analysis of hydrogen production via steam reforming of selected components of aqueous bio-oil fraction. *International Journal of Hydrogen Energy* **2007,** 32, (2), 212-223.
124. Davda, R. R.; Shabaker, J. W.; Huber, G. W.; Cortright, R. D.; Dumesic, J. A., Aqueous-phase reforming of ethylene glycol on silica-supported metal catalysts. *Applied Catalysis B: Environmental* **2003,** 43, (1), 13-26.
125. Elliott, D. C.; Hart, T. R.; Neuenschwander, G. G., Chemical processing in high-pressure aqueous environments. 8. Improved catalysts for hydrothermal gasification. *Industrial and Engineering Chemistry Research* **2006,** 45, (11), 3776-3781.
126. Byrd, A. J.; Pant, K. K.; Gupta, R. B., Hydrogen production from glycerol by reforming in supercritical water over Ru/Al_2O_3 catalyst. *Fuel* **2008,** 87, (13-14), 2956-2960.

127. Furusawa, T.; Sato, T.; Sugito, H.; Miura, Y.; Ishiyama, Y.; Sato, M.; Itoh, N.; Suzuki, N., Hydrogen production from the gasification of lignin with nickel catalysts in supercritical water. *International Journal of Hydrogen Energy* **2007,** 32, (6), 699-704.
128. Lee, I. G.; Ihm, S. K., Catalytic Gasification of Glucose over Ni/Activated Charcoal in Supercritical Water. *Industrial & Engineering Chemistry Research* **2009,** 48, (3), 1435-1442.
129. Shabaker, J. W.; Huber, G. W.; Davda, R. R.; Cortright, R. D.; Dumesic, J. A., Aqueous-phase reforming of ethylene glycol over supported platinum catalysts. *Catalysis Letters* **2003,** 88, (1-2), 1-8.
130. Radivojević, D.; Seshan, K.; Lefferts, L., Preparation of well-dispersed Pt/SiO_2 catalysts using low-temperature treatments. *Applied Catalysis A: General* **2006,** 301, (1), 51-58.
131. Luo, N.; Fu, X.; Cao, F.; Xiao, T.; Edwards, P. P., Glycerol aqueous phase reforming for hydrogen generation over Pt catalyst - Effect of catalyst composition and reaction conditions. *Fuel* **2008,** 87, (17-18), 3483-3489.
132. Lehnert, K.; Claus, P., Influence of Pt particle size and support type on the aqueous-phase reforming of glycerol. *Catalysis Communications* **2008,** 9, (15), 2543-2546.
133. Wawrzetz, A.; Peng, B.; Hrabar, A.; Jentys, A.; Lemonidou, A. A.; Lercher, J. A., Towards understanding the bifunctional hydrodeoxygenation and aqueous phase reforming of glycerol. *Journal of Catalysis* **2010,** 269, (2), 411-420.
134. Lieske, H.; Lietz, G.; Spindler, H.; Völter, J., Reactions of platinum in oxygen- and hydrogen-treated $Pt/\gamma\text{-}Al_2O_3$ catalysts: I. Temperature-programmed reduction, adsorption, and redispersion of platinum. *Journal of Catalysis* **1983,** 81, (1), 8-16.
135. Li, C.; Chen, Y.-W., Temperature-programmed-reduction studies of nickel oxide/alumina catalysts: effects of the preparation method. *Thermochimica Acta* **1995,** 256, (2), 457-465.
136. Jerzy, Z., Morphology of nickel/alumina catalysts. *Journal of Catalysis* **1982,** 76, (1), 157-163.
137. Arenas-Alatorre, J.; Gómez-Cortés, A.; Avalos-Borja, M.; Díaz, G., Surface Properties of $Ni\text{-}Pt/SiO_2$ Catalysts for N_2O Decomposition and Reduction by H_2†. *The Journal of Physical Chemistry B* **2004,** 109, (6), 2371-2376.
138. Davda, R. R.; Dumesic, J. A., Catalytic reforming of oxygenated hydrocarbons for hydrogen with low levels of carbon monoxide. *Angewandte Chemie-International Edition* **2003,** 42, (34), 4068-4071.
139. Takanabe, K.; Aika, K.; Inazu, K.; Baba, T.; Seshan, K.; Lefferts, L., Steam reforming of acetic acid as a biomass derived oxygenate: Bifunctional pathway for hydrogen formation over Pt/ZrO2 catalysts. *Journal of Catalysis* **2006,** 243, (2), 263-269.
140. Grenoble, D. C.; Estadt, M. M.; Ollis, D. F., The chemistry and catalysis of the water gas shift reaction: 1. The kinetics over supported metal catalysts. *Journal of Catalysis* **1981,** 67, (1), 90-102.
141. Matas Güell, B.; Babich, I. V.; Lefferts, L.; Seshan, K., Steam reforming of phenol over Ni-based catalysts-A comparative study. *Applied Catalysis B: Environmental* **2011,** 106, (3-4), 280-286.
142. Lin, J.-H.; Biswas, P.; Guliants, V. V.; Misture, S., Hydrogen production by water–gas shift reaction over bimetallic Cu–Ni catalysts supported on La-doped mesoporous ceria. *Applied Catalysis A: General* **2010,** 387, (1-2), 87-94.
143. Rostrup-Nielsen, J. R., *Catalytic Steam Reforming.* Springer-Verlag 1984.
144. Viinikainen, T. S.; Karinen, R. S.; Krause, A. O. I., Conversion of Glycerol into Traffic Fuels. In *Catalysis for Renewables*, Wiley-VCH Verlag GmbH & Co. KGaA: 2007; pp 209-222.

145. May, A.; Salvado, J.; Torras, C.; Montane, D., Catalytic gasification of glycerol in supercritical water. *Chemical Engineering Journal* **2010,** 160, (2), 751-759.
146. Sels, B.; D'Hondt, E.; Jacobs, P., Catalytic Transformation of Glycerol. In *Catalysis for Renewables*, Wiley-VCH Verlag GmbH & Co. KGaA: 2007; pp 223-255.
147. Balegedde Ramachandran, R. P.; van Rossum, G.; van Swaaij, W. P. M.; Kersten, S. R. A., Preliminary Assessment of Synthesis Gas Production via Hybrid Steam Reforming of Methane and Glycerol. *Energy & Fuels* **2011,** 25, (12), 5755-5766.
148. Kunkes, E. L.; Simonetti, D. A.; Dumesic, J. A.; Pyrz, W. D.; Murillo, L. E.; Chen, J. G. G.; Buttrey, D. J., The role of rhenium in the conversion of glycerol to synthesis gas over carbon supported platinum-rhenium catalysts. *Journal of Catalysis* **2008,** 260, (1), 164-177.
149. Simonetti, D. A.; Rass-Hansen, J.; Kunkes, E. L.; Soares, R. R.; Dumesic, J. A., Coupling of glycerol processing with Fischer-Tropsch synthesis for production of liquid fuels. *Green Chemistry* **2007,** 9, (10), 1073-1083.
150. Xu, X. D.; Matsumura, Y.; Stenberg, J.; Antal, M. J., Carbon-catalyzed gasification of organic feedstocks in supercritical water. *Industrial & Engineering Chemistry Research* **1996,** 35, (8), 2522-2530.
151. Guo, S.; Guo, L.; Cao, C.; Yin, J.; Lu, Y.; Zhang, X., Hydrogen production from glycerol by supercritical water gasification in a continuous flow tubular reactor. *International Journal of Hydrogen Energy* **2012,** 37, (7), 5559-5568.
152. Mueller, J. B.; Vogel, F., Tar and coke formation during hydrothermal processing of glycerol and glucose. Influence of temperature, residence time and feed concentration. *Journal of Supercritical Fluids* **2012,** 70, 126-136.
153. Xu, X.; Matsumura, Y.; Stenberg, J.; Antal Jr, M. J., Carbon-catalyzed gasification of organic feedstocks in supercritical Water. *Industrial and Engineering Chemistry Research* **1996,** 35, (8), 2522-2530.
154. van Bennekom, J. G.; Kirillov, V. A.; Amosov, Y. I.; Krieger, T.; Venderbosch, R. H.; Assink, D.; Lemmens, K. P. J.; Heeres, H. J., Explorative catalyst screening studies on reforming of glycerol in supercritical water. *Journal of Supercritical Fluids* **2012,** 70, 171-181.
155. Chakinala, A. G.; de Vlieger, D. J. M.; Seshan, K.; Kersten, S. R. A.; Van Swaaij, W. P. M.; Brilman, D. W. F., Catalytic reforming of glycerol in supercritical water over bi-metallic Pt–Ni catalyst. *Industrial & Engineering Chemistry Research* **2012**.
156. Nakagawa, Y.; Tomishige, K., Heterogeneous catalysis of the glycerol hydrogenolysis. *Catalysis Science & Technology* **2011,** 1, (2), 179-190.
157. Ueda, N.; Nakagawa, Y.; Tomishige, K., Conversion of Glycerol to Ethylene Glycol over Pt-modified Ni Catalyst. *Chemistry Letters* **2010,** 39, (5), 506-507.
158. Torres, A.; Roy, D.; Subramaniam, B.; Chaudhari, R. V., Kinetic Modeling of Aqueous-Phase Glycerol Hydrogenolysis in a Batch Slurry Reactor. *Industrial & Engineering Chemistry Research* **2010,** 49, (21), 10826-10835.
159. Ruan, H. D.; Frost, R. L.; Kloprogge, J. T., Comparison of Raman spectra in characterizing gibbsite, bayerite, diaspore and boehmite. *Journal of Raman Spectroscopy* **2001,** 32, (9), 745-750.
160. Kiss, A. B.; Keresztury, G.; Farkas, L., Raman and IR-spectra and structure of boehmite (γ-AlOOH) - evidence for the recently discarded d-2h(17) space group. *Spectrochimica Acta Part a-Molecular and Biomolecular Spectroscopy* **1980,** 36, (7), 653-658.

161. Ravenelle, R. M.; Copeland, J. R.; Kim, W. G.; Crittenden, J. C.; Sievers, C., Structural changes of γ-Al_2O_3-supported catalysts in hot liquid water. *ACS Catalysis* **2011,** 1, (5), 552-561.
162. Vogelaar, B. M.; van Langeveld, A. D.; Eijsbouts, S.; Moulijn, J. A., Analysis of coke deposition profiles in commercial spent hydroprocessing catalysts using Raman spectroscopy. *Fuel* **2007,** 86, (7-8), 1122-1129.
163. Espinat, D.; Dexpert, H.; Freund, E.; Martino, G.; Couzi, M.; Lespade, P.; Cruege, F., Characterization of the coke formed on reforming catalysts by laser Raman-spectroscopy *Applied Catalysis* **1985,** 16, (3), 343-354.
164. Guo, J.; Lou, H.; Zheng, X. M., The deposition of coke from methane on a Ni/$MgAl_2O_4$ catalyst. *Carbon* **2007,** 45, (6), 1314-1321.
165. Savage, P. E., A perspective on catalysis in sub- and supercritical water. *Journal of Supercritical Fluids* **2009,** 47, (3), 407-414.
166. Hoekstra, E.; Hogendoorn, K. J. A.; Wang, X.; Westerhof, R. J. M.; Kersten, S. R. A.; van Swaaij, W. P. M.; Groeneveld, M. J., Fast pyrolysis of biomass in a fluidized bed reactor: In situ filtering of the vapors. *Industrial & Engineering Chemistry Research* **2009,** 48, (10), 4744-4756.
167. Westerhof, R. J. M.; Kuipers, N. J. M.; Kersten, S. R. A.; van Swaaij, W. P. M., Controlling the Water Content of Biomass Fast Pyrolysis Oil. *Industrial & Engineering Chemistry Research* **2007,** 46, (26), 9238-9247.
168. Vogel, F.; Waldner, M. H.; Rouff, A. A.; Rabe, S., Synthetic natural gas from biomass by catalytic conversion in supercritical water. *Green Chemistry* **2007,** 9, (6), 616-619.
169. Waldner, M. H.; Vogel, F., Renewable production of methane from woody biomass by catalytic hydrothermal gasification. *Industrial & Engineering Chemistry Research* **2005,** 44, (13), 4543-4551.
170. Westerhof, R. J. M.; Brilman, D. W. F.; Garcia-Perez, M.; Wang, Z.; Oudenhoven, S. R. G.; van Swaaij, W. P. M.; Kersten, S. R. A., Fractional Condensation of Biomass Pyrolysis Vapors. *Energy & Fuels* **2011,** 25, (4), 1817-1829.
171. Westerhof, R. J. M.; Brilman, D. W. F.; van Swaaij, W. P. M.; Kersten, S. R. A., Effect of Temperature in Fluidized Bed Fast Pyrolysis of Biomass: Oil Quality Assessment in Test Units. *Industrial & Engineering Chemistry Research* **2009,** 49, (3), 1160-1168.
172. De Miguel Mercader, F.; Koehorst, P. J. J.; Heeres, H. J.; Kersten, S. R. A.; Hogendoorn, J. A., Competition between hydrotreating and polymerization reactions during pyrolysis oil hydrodeoxygenation. *AIChE Journal* **2011,** 57, (11), 3160-3170.
173. De Miguel Mercader, F.; Koehorst, P. J. J.; Heeres, H. J.; Kersten, S. R. A.; Hogendoorn, J. A., Competition between hydrotreating and polymerization reactions during pyrolysis oil hydrodeoxygenation. *Aiche Journal* **2011**.
174. de Vlieger, D.; Chakinala, A. G.; Lefferts, L.; Kersten, S. R. A.; Seshan, K.; Brilman, D. W. F., Hydrogen from supercritical water reforming of ethylene glycol using alumina supported noble and base metal catalysts. *Applied Catalysis B: Environmental* **2011**.
175. Azzam, K. G.; Babich, I. V.; Seshan, K.; Lefferts, L., A bifunctional catalyst for the single-stage water-gas shift reaction in fuel cell applications: Part 2. Roles of the support and promoter on catalyst activity and stability. *Journal of Catalysis* **2007,** 251, (1), 163-171.
176. Minowa, T.; Ogi, T., Hydrogen production from cellulose using a reduced nickel catalyst. *Catalysis Today* **1998,** 45, (1-4), 411-416.
177. Ruettinger, W.; Liu, X.; Farrauto, R. J., Mechanism of aging for a Pt/CeO_2-ZrO_2 water gas shift catalyst. *Applied Catalysis B: Environmental* **2006,** 65, (1-2), 135-141.

178. Wootsch, A.; Descorme, C.; Duprez, D., Preferential oxidation of carbon monoxide in the presence of hydrogen (PROX) over ceria-zirconia and alumina-supported Pt catalysts. *Journal of Catalysis* **2004,** 225, (2), 259-266.
179. Elliott, D. C., Catalytic hydrothermal gasification of biomass. *Biofuels Bioproducts & Biorefining-Biofpr* **2008,** 2, (3), 254-265.
180. Elliott, D. C.; Sealock Jr, L. J.; Baker, E. G., Chemical processing in high-pressure aqueous environments. 2. Development of catalysts for gasification. *Industrial and Engineering Chemistry Research* **1993,** 32, (8), 1542-1548.
181. Withag, J. A. M.; Smeets, J. R.; Bramer, E. A.; Brem, G., System model for gasification of biomass model compounds in supercritical water - A thermodynamic analysis. *The Journal of Supercritical Fluids* **2012,** 61, (0), 157-166.
182. Vispute, T. P.; Huber, G. W., Production of hydrogen, alkanes and polyols by aqueous phase processing of wood-derived pyrolysis oils. *Green Chemistry* **2009,** 11, (9), 1433-1445.
183. Byrd, A. J.; Gupta, R. B., Stability of cerium-modified gamma-alumina catalyst support in supercritical water. *Applied Catalysis A: General* **2010,** 381, (1-2), 177-182.

JOURNAL PUBLICATIONS

1. Chakinala, A. G.; Brilman, D. W. F.; van Swaaij, W. P. M.; Kersten, S. R. A., Catalytic and non-catalytic supercritical water gasification of microalgae and glycerol. Industrial & Engineering Chemistry Research 2010, 49, (3), 1113-1122.

2. Chakinala, A. G.; Kumar, S.; Kruse, A.; Kersten, S. R. A.; van Swaaij, W. P. M.; Brilman, D. W. F., Supercritical water gasification of organic acids and alcohols: The effect of chain length. The Journal of Supercritical Fluids 2013, 74, (0), 8-21.

3. De Vlieger, D. J. M.; Chakinala, A. G.; Lefferts, L.; Kersten, S. R. A.; Seshan, K.; Brilman, D. W. F., Hydrogen from ethylene glycol by supercritical water reforming using noble and base metal catalysts. Applied Catalysis B: Environmental 2012, 111-112, 536-544.

4. Chakinala, A. G.; van Swaaij, W. P. M.; Kersten, S. R. A.; de Vlieger, D.; Seshan, K.; Brilman, D. W. F., Catalytic Reforming of Glycerol in Supercritical Water over Bimetallic Pt–Ni Catalyst. Industrial & Engineering Chemistry Research 2013, 52, (15), 5302-5312.

5. Chakinala, A. G.; Chinthaginjala, J. K.; Seshan, K.; van Swaaij, W. P. M.; Kersten, S. R. A.; Brilman, D. W. F., Catalyst screening for the hydrothermal gasification of aqueous phase of bio-oil. Catalysis Today 2012, 195, (1), 83-92.

ACKNOWLEDGEMENTS

The four years of research described in this thesis will always remain as a wonderful and memorable experience in my life. I take this opportunity to express my gratitude to all those who either directly or indirectly contributed towards the successful completion of this thesis. Culmination of this project led to this dissertation as well as sharpened many facets of both my personal and professional life in the Netherlands a worthwhile. Herewith, I wish to express my gratitude to all those wonderful people for making my life more enjoyable while away from home.

Foremost, I would like to express my gratitude to Prof.dr. Sascha R. A. Kersten and Prof.dr.ir. W. P. M. van Swaaij for giving me the opportunity to pursue my PhD in the TCCB (now SPT) group and also for their encouragement, support and invaluable suggestions. Next, I would like to extend my sincere gratitude to Dr.ir. D.W.F. Brilman, my mentor, for his wonderful guidance, long discussions, constant support and providing me the flexibility in leading the research in a right path. I learned a lot from you, particularly for initiating my quest to ask '*why*' at each stage of learning. My sincere thanks towards the endeavours you put in to achieve the best possible outcome of this work. I would like to extend my thanks to the Senter Novem for funding this industrially relevant project and also for organizing the project meetings which helped in the successful completion of this project.

The experimental work described in this research would never have been possible with out the help of skilled technicians. I would like to thank all the technicians (Benno, Karst, Robert) for their painstaking work in building the continuous set-up and providing quick-fix solutions with the set-up upset. I extend my thanks to Erna for her assistance in solving the GC issues and analyzing samples. Special thanks to Yvonne for arranging all the conference trips, deciphering Dutch documents and for all your administrative support in these last days.

I was fortunate enough to get excellent students and their valuable contribution was responsible for the successful completion of this project. Rens, was my first undergraduate student as well my paranymph, started his initial experimental work with micro algae gasification using quartz capillaries. This work was published in conference proceedings, journal publication and also won the second prize in the NPS poster presentation. Shushil, my paranymph, was the first master student who laid the foundation for studying the chemistry aspects of SCWG. Frank, thanks for your experimental work in the continuous reactor with the complex feedstocks. Thanks to Martin Bos and Sonia for working on heat transfer studies in supercritical water. Thanks to Erwin for your studies related to 'algae on chip' concept.

The close cooperation with different groups within the University had a synergistic effect in this research. I would like to express gratitude to the Catalytic Process and Materials (CPM) group, especially to Prof. K. Seshan, Prof. Leon Lefferts and Dennis de Vlieger for the joint collaboration. It was indeed a wonderful experience of collaborating with your group. Thanks to Louise (CPM group) for the catalyst analysis (BET & XRF). I would also extend my thanks to the Thermal Engineering group, particularly Prof.dr.ir. Gerrit Brem and Jan Withag for all the technical discussions during the EOS-LT project meetings. Special thanks to Prof. Andrea Kruse for the collaborative work and also for accepting to be part of my PhD committee. Thanks to Dr. Robbie Venderbosch for all the technical discussions during project meetings and for being part of my committee.

Thanks to my colleagues, Dragan, Mariken, Guus (for all the administrative support during my initial days of research), Roel, Pavlina, Ferran, Elly, Wei, Laura, Maria, Jithu, Jose, Samuel, Cindy, Stijn, Martin, Shushil, Rens and Ragav (For the lengthy technical discussions that covered most of the topics like energy from biomass, algae, supercritical water gasification *vs* steam reforming, catalysis and process economics. Other interesting discussions related to movies, cricket, conferences and for updating me with all the happenings (gossips) at the coffee machine).

Special thanks to the Indian community at the University for making my stay in Enschede a very memorable by organizing several events and activities. My heart felt gratitude to my friends, Vishnu (pully), Vijay (Ganti)-Ranjini, Arun-Gayatri, CP Suresh, Vishi, Jithin, Andy-Subhashini, Anand-Renuka, Seshan-Jayanthi, Jyothi-Kranti, Jithu-Lavanya, Giri-Varsha, Koti, Srikrishna-Gayatri, Kishore-Hema, Rajesh, Raja, Hrudya and Jigar.

I wish to express my gratitude to my family members particularly my uncle, aunt for taking care of my parents while I am away. Most of all I wish to express my deepest gratitude to my parents and sister. This would not have been possible without their love, sacrifices, encouragement, understanding, courage and support shown despite many testing times at their end. I would like to thank my Dad for his creative inputs in making this thesis cover page. My heartfelt gratitude to my wife (Nandana), for the support and encouragement you have shown to me. Special thanks for the efforts you have put in this thesis by giving critical comments (both technical and non-technical) which made this dissertation possible.

Anand Chakinala

December, 2013